



<https://theses.gla.ac.uk/>

Theses Digitisation:

<https://www.gla.ac.uk/myglasgow/research/enlighten/theses/digitisation/>

This is a digitised version of the original print thesis.

Copyright and moral rights for this work are retained by the author

A copy can be downloaded for personal non-commercial research or study,
without prior permission or charge

This work cannot be reproduced or quoted extensively from without first
obtaining permission in writing from the author

The content must not be changed in any way or sold commercially in any
format or medium without the formal permission of the author

When referring to this work, full bibliographic details including the author,
title, awarding institution and date of the thesis must be given

Enlighten: Theses

<https://theses.gla.ac.uk/>
research-enlighten@glasgow.ac.uk

The Geochemistry of the
Connemara Gneiss Complex,
Co. Galway, Ireland.

BARRY EDWARD KEELING

Thesis submitted for the Degree of Ph.D.

University of Glasgow

Department of Geology

December 1981

GLASGOW
UNIVERSITY
LIBRARY

Thesis
6472
Copy 1

ABSTRACT

An area of about 100 sq.km. immediately north of the Galway granite has been studied. The area encompasses the central part of the Connemara Gneiss complex, a syntectonic suite of basic, intermediate and acidic intrusives and migmatized Dalradian sediments. 50 rock samples from the complex have been analysed by X-Ray fluorescence methods for all major elements and up to 13 trace elements (Cr,Co,Ni,Rb,Sr,Y,Zr,Nb,Ba,La,Ce,Pb,Th). In addition, 41 of these rock samples have been analysed by neutron activation methods for up to 9 trace elements (La,Ce,Nd,Sm,Eu,Tb,Yb,Lu,Sc). These data together with microprobe analyses of 60 mineral grains from the samples, are presented and used to deduce the petrogenesis of the Gneiss complex.

The orthomagmatic rocks were intruded into the pelites, semipelites, and quartzites of the Dalradian Cashel Formation, during the period between the onset of the D2 deformation and the completion of the D3 deformation. The initial intrusions were basaltic in composition and they were intruded during D2 mainly as thick sheets and masses, which are conformable to the F2 foliation in the country rocks. These intrusions were then fragmented and, the rocks amphibolitised during the combined D3 deformation and M3 metamorphism. The cause of the M3 event was the intrusion of the intermediate magmas, which solidified to form the tonalitic orthogneisses. High degrees of partial melting occurred in the aureole zone of these intermediate magmas, forming the paragneiss. There is field evidence for large scale assimilation of paragneiss by the magma. The intrusion of small amounts of granitic magma, during the latter stages of D3, completed the magmatic phase.

From a microtextural analysis of metabasite rocks with a relict igneous mafic mineralogy of augite and hypersthene, it is shown that the amphiboles in these rocks are metamorphic in origin. Using the same microtextural criteria, the hornblende in the tonalitic orthogneiss is thought to be primary. The presence of skeletal andesine, and the absence of albitic plagioclase, in the granitic orthogneisses suggests that plagioclase was not stable in the granitic magma. In the melanosome residues in the paragneiss mobilisate, evidence of the high temperature reaction; biotite \longrightarrow sillimanite + ilmenite + melt component,

is preserved. These melanosomes are undoubtedly non-equilibrium mineral selvages since plagioclase varies between An_{21} - An_{42} in a single melanosome.

The majority of the samples have compositions which, to a close approximation, represent the compositions of the magmas from which they formed. The metabasite-orthogneiss rocks appear to be comagmatic on the basis of the continuous variation of major element abundances across the suite. Using simple Harker-type plots and more complex multicomponent graphical systems (Ab-An-Or-Q, and CMAS), a hypothesis is formulated which relates the total variation of composition across the metabasite-orthogneiss suite as the locus of compositions attained by a single parental basic magma undergoing fractional crystallisation. An early fractionation assemblage consisting of augite and hypersthene drove the basic magma along an Fe-enrichment, SiO_2 -depletion trend, until it was superseded by a low- SiO_2 fractionation assemblage of hornblende + plagioclase + Fe-Ti ore. The magma became markedly enriched in SiO_2 with further fractionation, evolving to tonalitic compositions. It is noted that the assimilation of siliceous paragneiss could help to produce this extreme SiO_2 -enrichment trend. As a first approximation, the hypothesis agrees well with experimental phase relations of the join; gabbro-tonalite-granite. The H_2O contents of the tonalitic and granitic magmas is estimated to be 6-8wt% and >10wt%, respectively. The experimental melting relations of biotite-plagioclase-quartz schists are used to describe the melting relationships in the paragneiss, and a peak temperature of c.900°C is estimated for the aureole zone around the tonalitic intrusions.

A continuous variation in trace element abundances from the most basic to the most acidic rocks of the metabasite-orthogneiss suite confirm the comagmatic nature of these rocks. This variation is qualitatively described in terms of mineral-melt distribution coefficients for a changing magma composition. The fractional crystallisation scheme proposed above, is generally confirmed, though the assimilation of metasediment appears to be much more important in the formation of the SiO_2 -rich magma than was first thought. The REE data are crucial in understanding the evolution of the magma that occurred after it had reached a tonalitic composition. It is evident that hornblende was a fractionation phase right across the tonalite-granite composition

range. Plagioclase fractionation slowed, and finally stopped in the tonalitic magma because of the build-up of H_2O in the magma. Orthite joined hornblende and quartz as a fractionation phase in the granitic magma.

Quantitative multicomponent least-square fitting of trace element abundances in selected metabasite and orthogneiss samples to a closed-system fractional crystallisation model, proves fairly successful. However, the results suggest that assimilation of paragneiss, by the Fe-rich, SiO_2 -poor basic magma, was critical in the initiation of the SiO_2 -enrichment trend of the magma.

The role of combined fractional crystallisation and assimilation in the formation of calc-alkaline magmas and anorthosites, from a broadly tholeiitic type of parental magma, is discussed.

ACKNOWLEDGEMENTS

I would like to thank Professor B. E. Leake for his supervision, involving days in the field, many periods of discussion and reading the manuscript.

My thanks are due to Drs. M. R. Giles, P. J. Treloar, C. M. Farrow and Mr. I. W. Fergusson for stimulating discussions on various aspects of the research.

Most of the geochemical analysis was carried out in the Geochemistry Unit of the Geology Dept., Glasgow University. I wish to thank Dr. C. M. Farrow for his considerable assistance in this part of the work. Rare Earth element determinations were carried out in the Scottish Universities Research and Reactor Centre, National Engineering Laboratories, East Kilbride. I am grateful to Dr. J. E. Whitley who allowed me considerable time on the analysis apparatus, and for the assistance that he, Dr. A. B. MacKenzie, and Mr. A. Wilson gave in the actual analysis.

I thank Dr. F. Albarede for his helpful correspondence pertaining to the computer program, which he supplied, for solving linear overdetermined multi-component systems. I would also like to thank Mr. D. A. Fildes and the other staff of the Glasgow University Computing Advisory Service for their assistance and advice.

For all photographic work I am grateful to Mr. D. MacLean, and for their assistance I thank Mr. R. Morrison and the rest of the technical staff of the Geology Dept.

The typing of chapters 2 and 3 and most of the tables was done by Miss. A. Inglis whose assistance is very much appreciated.

Finally, my thanks are due to my parents, Bob and Edith, and family and also to my fiancée, Alison, for their constant encouragement and support during this study.

This research was supported by a University of Glasgow, Faculty of Science, Research Grant.

TABLE OF CONTENTS.

Memorandum.	
Abstract.	
Acknowledgements.	
Table of contents.	
List of figures.	
List of plates.	
List of tables.	
List of abbreviations.	
Chapter 1. <u>Introduction.</u>	1
1.1 The geological setting - a summary of previous work.	1
1.1.1 The Dalradian rocks.	1
1.1.2 The syntectonic intrusive complex.	2
1.2 The aim of this work.	4
1.3 The area studied in this work.	4
Chapter 2. <u>The Petrography and Field Relations of the Rocks of the Intrusive Complex.</u>	6
2.1 Metabasites.	6
2.1.1 Field relations.	6
2.1.2 Petrography.	7
2.2 Orthogneisses.	11
2.2.1 Field relations.	11
2.2.2 Petrography.	12
a melanocratic tonalitic orthogneiss.	14
b leucocratic tonalitic orthogneiss.	14
c granodioritic and granitic orthogneiss.	15
2.3 Paragneiss.	16
2.3.1 Field relations.	16
2.3.2 Petrography.	18
2.4 Conclusions.	20
Chapter 3. <u>Major Element Geochemistry of the Rocks of the Intrusive Complex.</u>	21
3.1 The metabasite and orthogneiss samples - do they represent cumulate or magma compositions?	21
3.2 Harker-type diagrams.	23
3.3 The AFM diagram and other major element classification diagrams.	26

3.4	The Ab-An-Or-Q system.	27
3.5	The CMAS system.	29
3.5.1	Minerals in the CMAS system.	30
3.5.2	Rocks in the CMAS system.	31
3.6	Phase relations across the join gabbro-tonalite-granite.	35
3.7	Phase relations in the anatexis of metapelitic rocks.	38
3.8	Conclusions.	40
Chapter 4.	<u>Trace Element Geochemistry of the Rocks of the Intrusive Complex.</u>	42
4.1	Trace element distribution theory.	42
4.1.1	Trace element mineral-melt distribution coefficients.	42
4.1.2	Trace element variation in terms of bulk distribution coefficients.	44
4.2	Trace element distributions in the rocks of the intrusive complex.	46
4.2.1	Trace element (ppm) versus SiO ₂ (wt%) plots of the metabasite-orthogneiss rocks.	46
	a The incompatible trace elements:-Rb,Ba,Pb,Th.	47
	b The transitional D elements:-Zr,Y,Nb,Ce.	49
	c The compatible elements:-Cr,Ni,Co,Sc,Sr.	50
4.2.2	Trace element variations in the paragneiss rocks.	51
4.3	The Rare Earth element (REE) distributions in the rocks of the intrusive complex.	52
4.3.1	The geochemical properties of the REE.	52
4.3.2	REE mobility during alteration.	54
4.3.3	Chondrite-normalised REE patterns of the rocks of the intrusive complex.	55
	a Metabasite REE* patterns.	57
	b Tonalitic orthogneiss REE* patterns.	60
	c Granodioritic and granitic orthogneiss REE* patterns.	63
	d Paragneiss REE* patterns.	66
4.4	Tectonic setting of the metabasites from their Zr, Ti, and Y contents.	68
4.5	Conclusions.	69

Chapter 5. <u>Trace Element Modelling of the differentiation of the metabasite-orthogneiss magmas.</u>	70
5.1 Mathematical models of trace element mass balance in a magma undergoing fractional crystallisation.	70
5.2 Simple fractionation vectors and their comparison with the metabasite-orthogneiss trend.	73
5.3 Quantitative modelling of the total equilibrium fractional crystallisation process to the trace element variations in the metabasite-orthogneiss series.	75
5.3.1 The computation of the equilibrium fractionation process.	76
5.3.2 Presentation and discussion of the results of the modelling.	79
a Fractionation within the metabasite group.	80
b Fractionation from a highly fractionated metabasite magma type to a melanotonalitic orthogneiss magma type.	86
c Fractionation from the melanotonalitic orthogneiss magma type to the leucotonalitic orthogneiss magma type.	88
d Fractionation from the leucotonalitic orthogneiss magma type to the granitic orthogneiss magma type.	90
5.4 Conclusions of the trace element modelling.	91
Chapter 6. <u>Discussion of the results, and general conclusions.</u>	93
6.1 Discussion of the results.	93
6.2 General conclusions of this work.	98
6.3 Suggestions for further research.	99
References.	101
Appendix 1. Rock Analyses.	
Appendix 2. Mineral Analyses.	
Appendix 3. Details of computing used in this work.	
Appendix 4. List of Sample Localities.	

List of figures.

Fig.		preceding page
1.1	Sketch map of the geology of Connemara, Western Ireland.	1
1.2	The geology of the field area.	4
2.1	Major element v. SiO_2 (wt%) plots of the amphiboles.	13
2.2	Modal QAP plot of the orthogneisses.	13
3.1	N.C.I v. N.P.C. plot.	21
3.2	$(\text{MgO} + \text{tFeO} - \text{TiO}_2)$ (wt%) v. Al_2O_3 (wt%) plot of the metabasite rocks.	22
3.3	Major element (wt%) v. SiO_2 (wt%) plots.	24
3.4	Major element (wt%) v. Solidification Index plots.	24
3.5	$(\text{Na}_2\text{O} + \text{K}_2\text{O})$ (wt%) v. SiO_2 (wt%) plot.	26
3.6	AFM (wt%) diagram.	26
3.7	Al_2O_3 (wt%) v. Normative plagioclase composition.	26
3.8	Normative corundum v. SiO_2 (wt%) plot.	26
3.9a	Projections of the gneissic rocks in the normative Ab-An-Or-Q system.	27
b	Schematic view of phase relations in the normative Ab-An-Or-Q system.	27
3.10	CMAS projections of the minerals.	30
3.11	Simple magma evolution models.	31
3.12	CMAS projections of the rocks and minerals.	32
3.13	A 3-D summary of the CMAS distribution of the igneous rocks and their minerals.	33
4.1	Trace element (ppm) v. SiO_2 (wt%) plots.	46
4.2	Ba/Rb v. Cr.	47
4.3	Sr v. Cr.	47
4.4	tFeO/MgO v. Cr.	47
4.5	Metabasite REE* patterns.	57
4.6	Tonalitic orthogneiss REE* patterns.	60
4.7	Granodioritic and granitic orthogneiss REE* patterns.	65
4.8	REE geochemistry of a hornblende-aplite.	65
4.9	Evolution of the *Eu anomaly.	65
4.10	Kf-rich tonalitic orthogneiss REE* patterns.	66
4.11	Paragneiss REE* patterns.	66
4.12	REE K_D 's for the common magmatic phases.	67

	preceding
Fig.	page
4.13 Ti-Zr-Y discrimination diagram.	68
4.14 A qualitative summary of the differentiation of the metabasite-orthogneiss magmas.	68
5.1 Fractionation vectors applied to the metabasite-orthogneiss series.	73
6.1 A quantitative summary of the differentiation of the metabasite-orthogneiss magmas.	95

List of tables.

Fig.		preceding page
2.1	Pyroxenes and their metamorphic products.	9
4.1	Mineral-melt distribution coefficients.	44
4.2	REE chondrite normalising values.	55
4.3	REE characteristics of the metabasite-orthogneiss series.	56
4.4	Hornblende/Aplite K_D 's.	64
5.1	Fractionation from BK102 to BK138.	80
5.2	Fractionation from BK138 to BK406.	86
5.3	Fractionation from BK406 to BK403 and from BK403 to BK401.	88

List of plates.

Chapter 2.

Plates 1-9. The various xenolith types and morphologies present in the paragneiss.	16
---	----

LIST OF ABBREVIATIONS

An	- Anorthite	HYP	- Hypersthene
Ab	- Albite	AUG	- Augite
Or	- Orthoclase	Bte, BTE	- Biotite
Q	- Quartz	K-feld	- Potash feldspar
ILM	- Ilmenite	Woll	- Wollastonite
Px, PX	- Pyroxene	Ky	- Kyanite
Opx, OPX	- Orthopyroxene	En	- Enstatite
Cpx, CPX	- Clinopyroxene	sill	- Sillimanite
PLAG	- Plagioclase	musc	- Muscovite
HBE	- Hornblende	tFeO, FE*O	- total Fe as Fe ²⁺

Chapter 1.

Introduction.

1.1 The geological setting - a summary of previous work.

Connemara lies at the south-western limit of the Dalradian outcrop in western Ireland (fig.1.1). The Dalradian rocks of Connemara were strongly deformed and metamorphosed in the Caledonian orogeny. In the south of Connemara, these rocks were also intruded by syntectonic gabbroic, tonalitic, and granitic magmas. The metamorphic grade is high over most of Connemara and increases to high amphibolite grade in the south, a trend which can be directly attributed to the emplacement of the syntectonic magmas. Major post-tectonic intrusions, such as the Galway granite, were emplaced in the south and west of the region.

1.1.1 The Dalradian rocks.

The stratigraphy and structure of the Dalradian rocks of Connemara are now well understood. This state of knowledge has been arrived at after more than two and a half decades of field mapping, initiated by R.M.Shackleton and carried on by B.E.Leake and his co-workers.

In 1965, Kilburn, Pitcher and Shackleton recognised that the rocks of Connemara were Dalradian in age and that they could be directly correlated with the Dalradian of Donegal and Scotland. Since that time, Kilburn (unpublished work), Edmunds and Thomas (1966), Badley (1972,1976), Patrick (1967), Yardley (1974,1976), Treloar (1977) and Leake (unpublished work) have mapped the central, northern and eastern parts of Connemara. Cruse and Leake (1968) described the ground to the north-west and Cobbing (1969) and Tanner (1967) the region to the west. Leake has mapped much of the south-west of Connemara and also ground to the east in the Cashel district (1970,a), the intervening area being described by Evans (1959) and Bremner (1977). Harvey (1967) mapped in the extreme south in the Glinsk district and Senior (1973) the Shannavara district in the south-east.

A formal stratigraphy and structure for the whole of Connemara was first published by Badley (1976), which was only slightly modified by Yardley (1976). Recently, Tanner and Shackleton (1979) have presented a regional synthesis of the stratigraphy and

2

structure of central Connemara which includes both generalised geological and structural maps and structural sections. The Dalradian stratigraphical sequence of Connemara was proposed by Badley (1976) and Tanner and Shackleton (1979).

Since their deposition, these rocks have undergone four main deformational phases, the second and third of which were extremely intense and produced major F_2 and F_3 isoclinal folds. Major metamorphic events, M_2 and M_3 , accompanied the D_2 and D_3 deformations, respectively, with the M_3 event probably producing the highest regional temperatures, in the Dalradian rocks. The fourth deformation produced large scale open folds and one of these, the eastward-plunging Connemara Antiform, controls the geology of central Connemara.

The Lower and Middle Dalradian succession outcropping in the core of this F_4 fold is flanked to the south and north by the Dalradian Cashel and Kylemore Formations, respectively, but is separated from them by major tectonic breaks. North of the Cashel Formation is the 'steep belt', a zone of F_3 folds and slides, and south of the Kylemore Formation is the Renvyle-Bofin slide (Cruse and Leake, 1968). The Cashel and Kylemore Formations lie structurally above the central Connemara succession and are presumed to be younger than it, however, the stratigraphic relations between all three are uncertain due to the nature of their mutual contacts. Morris and Tanner (1977) tentatively correlate the Kylemore and Cashel Formations because of their roughly analogous structural positions, their similar lithologies and the fact that they are both intruded by ultrabasic and basic rocks. Tanner and Shackleton (1979) postulated that the Ballynakill Formation, (the youngest rocks to occur structurally below the slide surfaces and found only in western Connemara), is the stratigraphical equivalent of both the Kylemore and Cashel Formations but decided that the present evidence was insufficient to formally correlate the three formations.

1.1.2 The syntectonic intrusive complex.

The syntectonic intrusive complex of southern Connemara is composed of ultrabasic and basic rocks, tonalitic, granodioritic and granitic gneisses, and anatectic and quartz-feldspathised gneissic derivatives of the Cashel Formation.

Bounded to the south by the Galway granite batholith, the intrusive complex occurs in a narrow belt which runs eastwards for

at least 65 km from Slyne Head until it disappears below the Carboniferous cover.

The geology of the complex remained undescribed until an account of the Cashel-Lough Wheelaun intrusion appeared (Leake, 1958). This was followed by a study of the pelitic hornfelses and desilicated pelitic xenoliths associated with the intrusion (Leake and Skirrow, 1960). Evans (1964) later considered the trace element variations in the hornfelses and xenoliths.

Harvey (1967), working in the Glinsk district, recognised that the complex was composed of several different component rock groups. These he classified as:-

1. Massive ultrabasic and basic amphibolite.
2. Basic gneiss - a broad group of rocks including both metasomatically-altered sheared amphibolites and the coarse grained hornblende labradorite gneiss.
3. Biotite, quartz, plagioclase gneiss with minor hornblende.
4. Biotite, quartz, andesine gneiss.
5. Quartz, andesine, microcline, biotite gneiss.

Whilst Harvey recognised that some of the gneisses had an igneous origin, he favoured a metasomatic origin for the bulk of them. This, he reasoned, was the only possible explanation for the wide range in both their appearance and chemical compositions and for the gradational field boundaries that appear to exist between them.

In 1970, Leake published a major work describing in detail, both petrographically and petrologically, the various components of the complex in the Cashel district, an area which he described as 'a key area for the elucidation of the sequence of events in Connemara and the relationships of the metasediments, the basic and ultrabasic rocks and the orthogneisses'. In addition, he presented a geological map and structural interpretation of the area.

On the origin of the syntectonic intrusive suite, Leake, although acknowledging that major metasomatic activity did occur during its formation, proposed that this had only a modifying influence on what was essentially a magmatic rock series. Excepting the paragneisses, he concluded that the rocks were the products of the crystallisation of amphibole and calcic plagioclase from a basic magma containing a high volatile content. To account for the observed dissemination of each component rock group throughout the complex, he envisaged a dynamic situation in which fractionating basic magma, mantled by hornfelses Dalradian metasediment, was

repeatedly squeezed during D_2 and D_3 tectonic movements. This caused the complete disruption of the cumulate pile beneath it and the injection, into the country rocks, of differentiated magmas spanning the composition range gabbro, through diorite, quartz-diorite, to granodiorite. During consolidation of the granodiorite, late residual magma separated from it forming the relatively small bodies of microcline granite gneiss.

Senior (1973), working on the intrusive complex to the east, in the Shannavara district, came to virtually the same conclusions as Leake (1970) had previously. He also realised that the metasediments adjacent to the orthogneisses had undergone partial melting, but considered that there had been little or no assimilation of country rocks by the intruding magmas.

Recently, Leake and Senior (ms.) have considered the origin of the intrusive rocks in the complex using geochemical data gathered by both authors and also considering Harvey's contribution, this account being a summary of all previous work on this part of the complex.

Further west in the continuation of the syntectonic intrusive complex there lies a large ultrabasic and basic intrusion, the Roundstone complex, which has been studied by Morton (1964), and Bremner (1977). The amphibolites and hornblende gabbros previously described, are believed to be coeval with those of the Roundstone body (Leake and Senior (ms.), Bremner and Leake (1981)).

1.2 The aim of this work.

The aim of this work is to try to conclusively determine the origins of the various components of the syntectonic intrusive complex. This is attempted using:-

1. The framework provided by previous workers.
2. Field observations made in this study.
3. A petrographic study of the rock types.
4. New petrological data formulated during the tenure of this research, by myself, including major and trace element rock analyses, Rare Earth element analyses of rocks and a few mineral extracts, and microprobe mineral analyses.
5. Computer modelling.

1.3 The area studied in this work.

In order to carry out the aim of this work, an area in the

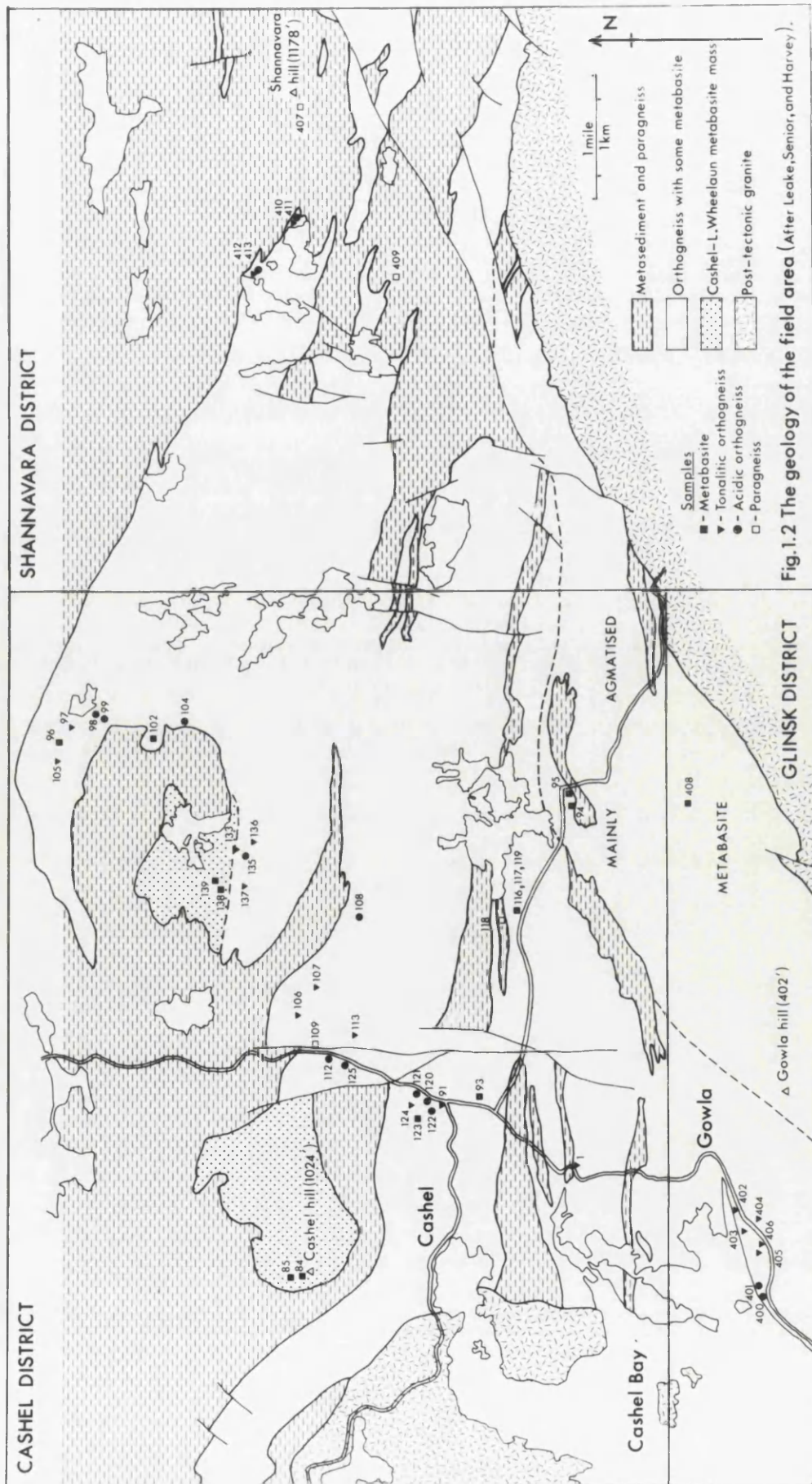


Fig. 1.2 The geology of the field area (After Leake, Senior, and Harvey).

in the south of Connemara, roughly 100 km² in areal extent, encompassing the Cashel, Shannavara, and Glinsk districts, has been examined (fig.1.2). Field work was carried out using both the uncountoured, six inch to one mile, Irish Ordnance Survey map sheet, 51 (Cashel district), and the geological maps of the Cashel, Shannavara, and Glinsk districts (Leake (1970a), Senior (1973, thss.), Harvey (1967, thss.)).

Cashel hill (1024') and Shannavara hill (1178') in the western and eastern parts of the field area, respectively, dominate the topography. Exposure is generally good on the higher ground in the Shannavara district and around Cashel hill. However, the ground below 200 feet, which encompasses much of the northern and central parts of the field area, is invariably poorly exposed, except around the lough shores, and the coast in the Glinsk district, due to extensive peat bogs and some drumlins. There is little correlation between the geology and the topography.

Geologically, the field area contains Cashel Formation metasediments and a major section of the syntectonic intrusive complex. It is bounded to the north by the Connemara Antiform and to the south by the Galway granite.

Chapter 2.

The Petrography and Field Relations of the Rocks of the Intrusive Complex.

The complex is composed of three component rock groups :-

1. metabasites
2. orthogneisses
3. paragneisses

2.1 Metabasites.

These metamorphosed basic and ultrabasic rocks have undergone considerable spatial disruption and amphibolitisation since their intrusion into the Dalradian of south Connemara. According to Leake (1970a), they were intruded during the D2 deformation as large masses and sheets which were subsequently fragmented in this and the later D3 deformation. The hornfelsed metasediments which must have mantled such intrusions now outcrop over a wide area in a rather patchy manner, and have suffered considerable metamorphic alteration.

2.1.1 Field Relations.

Throughout the area, metabasite occurs mainly as large intrusive masses (eg. the Cashel-Lough Wheelaun intrusion. Leake, 1970a), or as much smaller pods and lenses (< 40 metres in length), embedded in the Dalradian country rocks. It may also occur as 'pod-like' xenoliths in the orthogneisses, and is a common rock type constituting some 25% of the complex.

On weathering surfaces the metabasites are coloured pale to dark green and are speckled with white blebs of feldspar that stand out above the surface. Green patches of chlorite and epidote are common in these rocks and indicate the severity of their metamorphically retrogressed state. Hornblende occurs ubiquitously in the metabasites and, although usually less than 4mm in mean grain diameter, it may occasionally reach a much larger size. At one outcrop of the Lough Wheelaun metabasite mass in the Cashel district, hornblende occurs as megapoikiloblasts of up to 5cm in mean diameter and contains numerous plagioclase inclusions.

Ultramafic metabasites occur locally throughout the field area, notably in the southern side of Cashel Hill and in the area around Loughaunillaun to the east. They are massive rocks and are composed of up to 90% chloritised and epidotised hornblende and bronze-tarnished pyroxene.

Large areas of agmatized metabasite occur in the field area with individual blocks up to 2 metres across and separated by thin veins of quartz-rich pegmatite. Adjacent metasediments show no trace of agmatization and indicate that this process occurred while the metasediments were heated sufficiently so that they could deform in a plastic manner.

Igneous banding is found in the metabasite and consists of layers up to a metre thick, grading from mafic-rich at one boundary to relatively feldspar-rich at the other. However, the igneous banding is limited to a few exposures only and many of the larger metabasite masses in the area are devoid of any igneous banding.

Metabasite occurring as small pods (10-40m in length) in the metasediment, may be either schistose or massive. Very small lenses (1-2m in length) are commonly schistose. Metabasite-metasediment contacts are usually concordant and a clear example is seen on the western slope of Cashel Hill where an extremely sharp contact, between massive metabasite and the adjacent hornfelsed rocks, runs parallel to the main F2 foliation.

2.1.2 Petrography.

A typical metabasite has a granoblastic texture and contains anhedral and subeuhedral amphiboles (40-65%), saussuritised labradorite or bytownite (30-50%), up to 10% quartz and variable amounts of accessory opaque ore, apatite, prehnitised biotite, epidote and chlorite.

Two types of amphibole are present in the metabasites, one of them being a brown to dark green hornblende which is commonly poikilitic and the other a colourless to bright green actinolite. The hornblende, in exceptional circumstances, occurs as grains up to 4cm across, for example in parts of the Lough Wheelaun intrusion, Cashel district, but is usually between 0.3-1cm in mean grain diameter. Poikilitic varieties of the hornblende enclose small subeuhedral plagioclase and fragmented

euhedral opaque grains, and the proportion of inclusions may be as high as 65%. The actinolite occurs mainly as aggregates of small (1mm mean diameter) anhedral grains associated with quartz and fragments of opaque ore. Both types of amphibole tend to be variably chloritised. Representative microprobe analyses of both the hornblende and the actinolite are listed in Table 2.1.

Plagioclase occurs as subeuhedral grains, c 0.2-0.5mm in mean diameter, and is mainly labradorite, although bytownite does occur, especially in the ultrabasic rocks. Unaltered grains of plagioclase show excellent Carlsbad-Albite twinning, but these are scarce as the feldspar is, in most cases, strongly decomposed to saussurite and epidote.

Quartz occurs mainly in cusped-edged aggregates, up to 0.3mm in length, of strongly sutured grains and sub-grains, and exhibits strained extinction. Elsewhere quartz is present as irregular blebs intimately associated with actinolite clots. The opaque ore occurs as fragments, presumably formed in the D3 deformation, of originally euhedral and subeuhedral grains either at interstitial locations in the rock or as a common inclusion in both types of amphibole. In polished sections, viewed with reflected light, the ore fragments display an intricate microstructure, which proves to be, from microprobe analysis, an intergrowth of a manganese bearing titanomagnetite with ilmenite and discrete patches of sphene. The latter phase is probably a metamorphic component formed by the reaction of ilmenite with calcium released in the saussuritisation of the plagioclase. Biotite may occur as a replacement of hornblende and is invariably partially altered to chlorite, with lenses of iron-rich prehnite often developed along its cleavage.

Although most of the basic rocks conform closely to the above description, a few contain remains of hypersthene or augite, or both (eg. BK102 and BK138), and in these rocks the relationships between the primary igneous minerals and the secondary metamorphic assemblage can be elucidated. BK138 is a fine grained metabasite, having a maximum grain size of only 2mm. It is composed of 31% bytownite, An₈₄, 26% poikiloblastic green-brown hornblende, 20% pale green augite, 12% opaque ore, 6% severely corroded hypersthene, and 5% quartz and actinolite.

The poikiloblastic hornblende contains mainly hypersthene inclusions and it is obviously replacing the orthopyroxene which is extremely corroded. The hornblende contains other inclusions of subeuhedral augite and bytownite and also quartz blebs. It appears that in this rock the hornblende is part of the secondary metamorphic assemblage. This view is consistent with the conclusion that the fine grained nature of sample BK138, with its random grain orientation, is a product of rapid cooling upon intrusion, a process which would have allowed little time for corrosion and the replacement of orthopyroxene crystals by hornblende, before subsolidus conditions set in.

Although the augite (analysis in Appendix 2) in sample BK138 is remarkably fresh, a few grains show some alteration to a complex of actinolite studded with quartz blebs.

Titanomagnetite makes up c.65% of the ore grains in this rock with broad exsolution lamellae of ilmenite (33%) and a few patches of sphene (2%), the remainder (analyses in Appendix 2). A recalculated pre-exsolution composition for the whole ore contains c.40% ulvospinel. The ilmenite-titanomagnetite geothermometer of Buddington and Lindsley (1964), however, gives a temperature of only 540° C, indicating that although some exsolution of the ore had probably occurred during solidification and cooling of the basic magma, unmixing of the ore components proceeded almost to completion during subsequent amphibolite facies metamorphism.

Sample BK102 is a medium grained metabasite (max. grain diameter 3-4mm), and contains 25% calcic bytownite, An_{86} , 20% poikiloblastic hornblende, 18% hypersthene, En_{66} , 15% actinolite and quartz, and 8% augite. All of the textural relationships described previously, for sample BK138, are true of sample BK102 but the coarser grain size of the latter enables a more detailed examination of the reaction-relationships involved between the igneous and metamorphic mineral assemblages.

In BK102, corroded cores of hypersthene enclosed in poikiloblastic hornblende are surrounded by a colourless reaction rim which is commonly 100 to 30 microns wide. A microprobe traverse (analysis interval = 20 microns) from the margin of a hypersthene core across such a reaction zone into the adjacent hornblende is listed in Table 2.1 and shows that points in the reaction rim are transitional, in composition, to the orthopyroxene and

TABLE 2.1

Pyroxenes and their metamorphic products.

	HYPERSTHENE	RR1	RR2	REACTION	RIM	RR3	RR4	HORNBLLENDE	AUGITE	ACTINOLITE
	BK102-8/ TRAV.1.8.							BK102-1	BK102-3	BK102-9
SI02	53.17	56.08	50.85		51.96	49.86	47.24	52.69	53.18	
TI02	0.00	0.00	0.80		0.69	0.75	1.64	0.17	0.47	
AL203	1.18	0.70	5.72		6.30	7.25	9.37	1.15	5.03	
TFEO	21.35	18.19	14.41		11.22	12.06	13.42	7.13	10.57	
MND	0.47	0.56	0.23		0.24	0.20	0.00	0.47	0.23	
MGO	23.52	22.98	18.22		16.95	16.44	14.44	14.33	17.15	
CAO	0.52	0.87	8.57		11.56	11.94	11.97	24.42	12.41	
NA2O	0.00	0.42	0.55		0.80	1.03	1.02	0.00	0.72	
K2O	0.00	0.00	0.41		0.27	0.49	0.89	0.00	0.00	
TOTAL	100.21	99.80	99.74		99.29	100.02	99.99	100.36	99.98	
$\frac{MGO}{TFEO}$ RATIO	1.10	1.26	1.26		1.51	1.36	1.07	2.01	1.62	

hornblende. The variations in the concentration of the individual oxides across the zone provide information on the relative mobilities of the major elements in amphibolite facies metamorphism.

It must be emphasised that the conversion of pyroxene to amphibole is primarily a hydration reaction and that a progressive decrease in the analysis total was observed along the traverse, towards the hornblende, corresponding to an increase in the volatile component. However, since the changes in bulk composition across the reaction zone are not simply a dilution effect, all analyses have been recalculated to an anhydrous 100% (approx.) to allow for direct comparison of oxide concentrations.

The major difference between the hypersthene and the first point in the reaction rim (RR1 in Table 2.1) is the large increase in SiO_2 relative to the other major oxides, with both tFeO and MgO decreasing. This is in contrast with the overall reaction of orthopyroxene to hornblende which produces silica as a by-product. The build-up of SiO_2 adjacent to the hypersthene will, therefore, inhibit the overall reaction and the dissolution of SiO_2 away from the reaction zone will be the rate determining step. The trend of increasing SiO_2 is abruptly reversed further away from the hypersthene at the point RR2, although the depletion of tFeO and MgO continues, with tFeO rapidly reaching a steady state concentration. The rate of dissolution of Fe from the reaction zone is much greater than that of Mg, and this is probably due to the ability of Fe to convert to the 3+ state, and presumably increase its solubility, if oxidising conditions prevail. The decrease in SiO_2 , tFeO and MgO , across the reaction zone (RR2-RR4), is compensated by an increase in Al_2O_3 , CaO and to a lesser extent TiO_2 , Na_2O and K_2O . Ca rapidly reaches a steady state value and therefore has a greater mobility than Al, which increases only steadily across the reaction zone.

A closer examination of the adjacent hornblende reveals the presence of many small (c. 20 microns mean diameter) anhedral inclusions of quartz and these are obviously a product of the hydration reaction described above.

Also present in sample BK102 are large (c. 4mm mean diameter) clinopyroxene relicts, composed of irregular patches of pale green augite in an actinolite and quartz bleb mass. The actinolite

clearly replaced the augite as it surrounds and pseudomorphs the latter. However, the mechanism of this reaction appears to be more complex than that of the hypersthene-hornblende reaction. It is seen from microprobe analyses of the augite and adjacent actinolite (in Table 2.1) that both minerals have approximately the same SiO_2 content. Therefore, in order to explain the presence of quartz blebs in the actinolite, it is necessary to have had a Si deficiency at some stage in the reaction, promoting a Si influx from the rest of the rock. The slow rate of dispersion of Si from the immediate reaction zone, as noted in the preceding discussion of the hypersthene-hornblende reaction, may well have generated this Si deficiency in outer parts of the zone.

The sporadic mode of occurrence of the quartz, as blebs in amphibole and as small cusped-edged segregations, in sample BK102 is typical of all the sampled metabasites. It is concluded from the previous discussion, therefore, that the quartz and amphibole present in these rocks is metamorphic in origin and was produced from the hydration of the original igneous pyroxenes, presumably at amphibolite facies temperatures.

2.2 Orthogneisses.

The orthogneisses, previously described by Leake (1970a), are a group of foliated igneous rocks, which, during the D3 deformational episode, were intruded into and through the Cashel metasediments and their associated basic and ultrabasic intrusions.

2.2.1 Field Relations.

At present erosion levels, the orthogneisses constitute some 35% of the intrusive complex and, viewed as a whole, display a wide range in appearance and mineralogy. They are coarse grained rocks with a rough weathering surface which has a moderate to weak F3 foliation, due to the alignment of folia of quartz with feldspar. Although they are mainly leucocratic rocks, melanocratic orthogneiss does occur, notably in the Glinsk district, and may have up to 45% mafic content. The melanocratic varieties contain hornblende and plagioclase in roughly equal proportions, and are distinguished in the field from coarse grained metabasites by their significantly greater quartz content. However, as the orthogneiss becomes more leucocratic, ie. the quartz plus plagioclase proportion

12
increases to approx. 75%, biotite supersedes hornblende as the commoner mafic phase. The most leucocratic rocks contain large (c. 2mm max. grain diameter) phenocrysts of potash feldspar. These kf-bearing granitic gneisses, however, comprise only a small (c. 10%) proportion of the orthogneisses and outcrop over areas usually less than $\frac{1}{2}$ sq.km. They possess the weakest foliation of the orthogneisses and represent the last stages of the intrusion of the orthogneiss magma.

The tonalitic orthogneiss mass that runs from Lough-aunemlagh, in the north-west of the Cashel district, to the south-western flank of Shannavara mountain (Fig. 1.2), is atypical of the tonalitic orthogneiss group in that it is kf-rich and contains many small (2-3m in length) hornblende-bearing aplite veins. The aplite veins are entirely confined to this particular orthogneiss mass and are clearly segregations of the late stage melt residuum. The overall kf-rich nature of this orthogneiss may indicate that the present erosion level exposes the topmost parts of the intrusion, which are enriched in late stage residual melt.

Although showing a wide range in appearance over the whole intrusive complex, the orthogneisses are usually homogeneous in any one area of outcrop ($\frac{1}{2}$ to 1 sq.km) indicating that they are composed of several, if not many, medium sized intrusions. Mapped by Leake (1970a), and Senior (1973), the main orthogneiss masses are elongated parallel to the length of the intrusive complex and enclose areas of paragneiss and metabasite.

Foliated xenoliths of both paragneiss and metabasite, with occasional F3 folds preserved in the former, occur in the orthogneiss indicating that it was intruded during the D3 deformation.

2.2.2 Petrography.

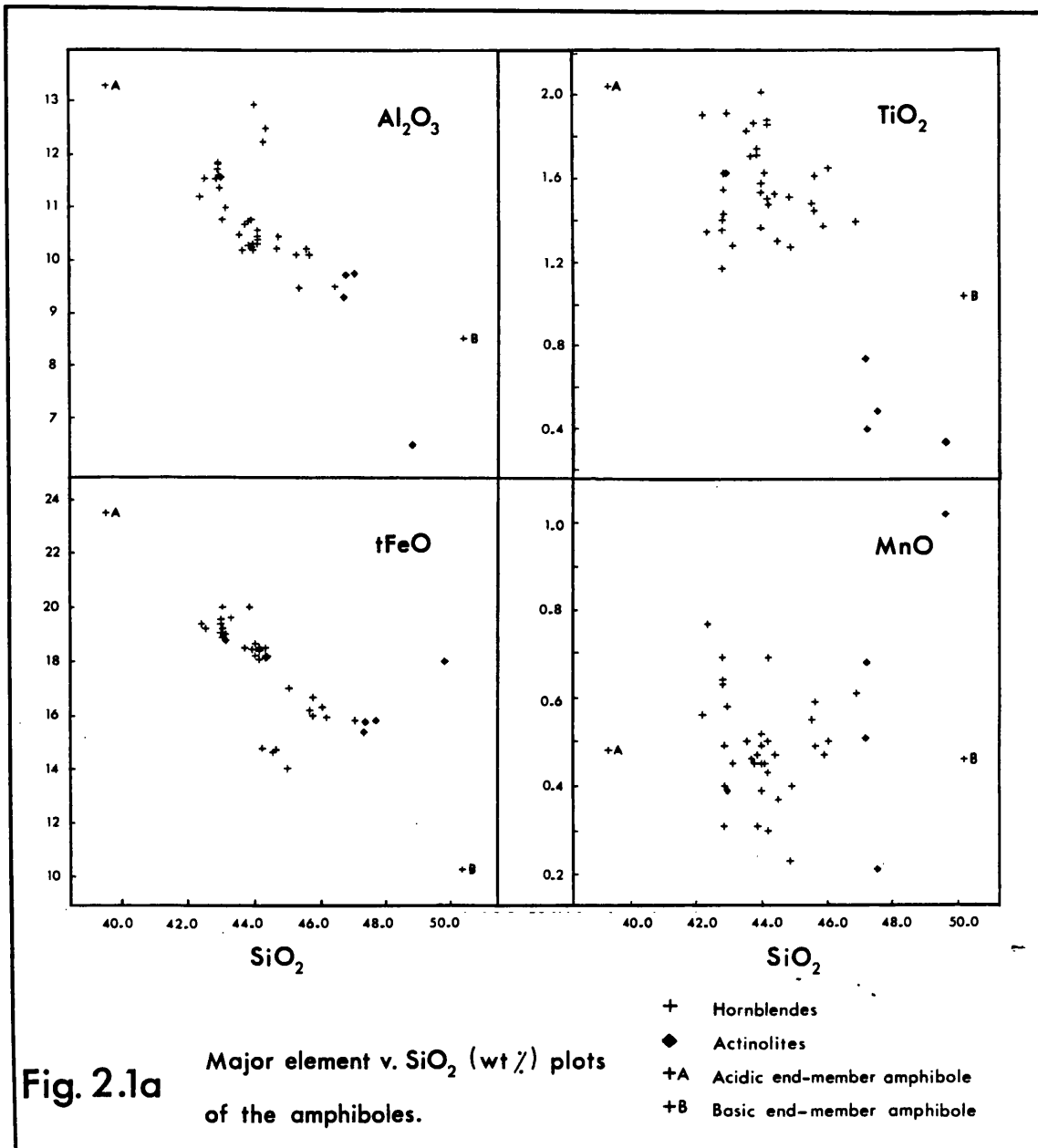
In this study, the orthogneisses will be subdivided and named according to the QAPF classification proposed by the IUGS Subcommission on the Systematics of Igneous Rocks (Strekeisen, 1976).

Modal estimates were calculated for the orthogneisses, from their chemical analyses (Appendix 1), using a least squares fitting computer program, XTLFRAC (Stormer and Nicholls, 1978). Only microprobe analyses of the essential mineral phases of each

rock were used in the modal calculations. If the essential phases of a rock had not been analysed, their compositions were simulated, in the calculations, by the combination of end-member minerals; for example, albite and anorthite analyses were combined to simulate plagioclase. The simulation of hornblende compositions proved much more difficult because of the complexity of solid solution in the amphibole system. Eventually a compromise was decided upon whereby two hypothetical hornblende 'end-members' were selected for the calculations. These are plotted in the major oxide versus SiO_2 variation diagrams of Fig. 2.1a,b together with the hornblendes (and actinolites) analysed in this study (see, also, their plotted position in the CMAS system, Fig. 3.10a,b).

This method of calculating the mode of a rock makes the assumption that all changes to its primary assemblages, ie. the growth of secondary accessory minerals by the partial decomposition of the primary essential ones, occur in a nearly-closed system and that the rock undergoes an isochemical change apart from its H_2O content (H_2O was not used in the calculations, all rocks and phases were recalculated to an anhydrous 100%). Although there are difficulties in modelling precisely the chemistry of mineral phases, nonetheless this method of calculating a mode uses a real and precise characteristic of the rock, its chemical analysis, as its starting point and so in the case of a coarse grained gneissose igneous rock, it is an alternative to point-counting thin sections, which, may be unrepresentative of the bulk modal mineralogy of that rock.

The modal estimates were used to calculate the QAP coordinates (see Fig. 2.2, for explanation and Appendix 1, for listing of the Q%, AF%, PLAG% values). The relevant portion of the QAP diagram with the orthogneisses plotted in it, is shown in Fig. 2.2. The orthogneisses span the range tonalite, granodiorite and granite (N.B. 3 rocks just fall into the quartz diorite field, but for convenience these are included in the tonalitic group). The granitic, granodioritic and quartz-rich tonalitic orthogneisses, however, plot relatively closer to the Q apex than do many analogously named rock types (Streckeisen and Le Maitre, 1979, figs. 3, 4, and 5). Three samples of Kf-bearing tonalitic orthogneiss are also plotted in the QAP diagram and they lie off the Q-P join, in the direction of the A apex.



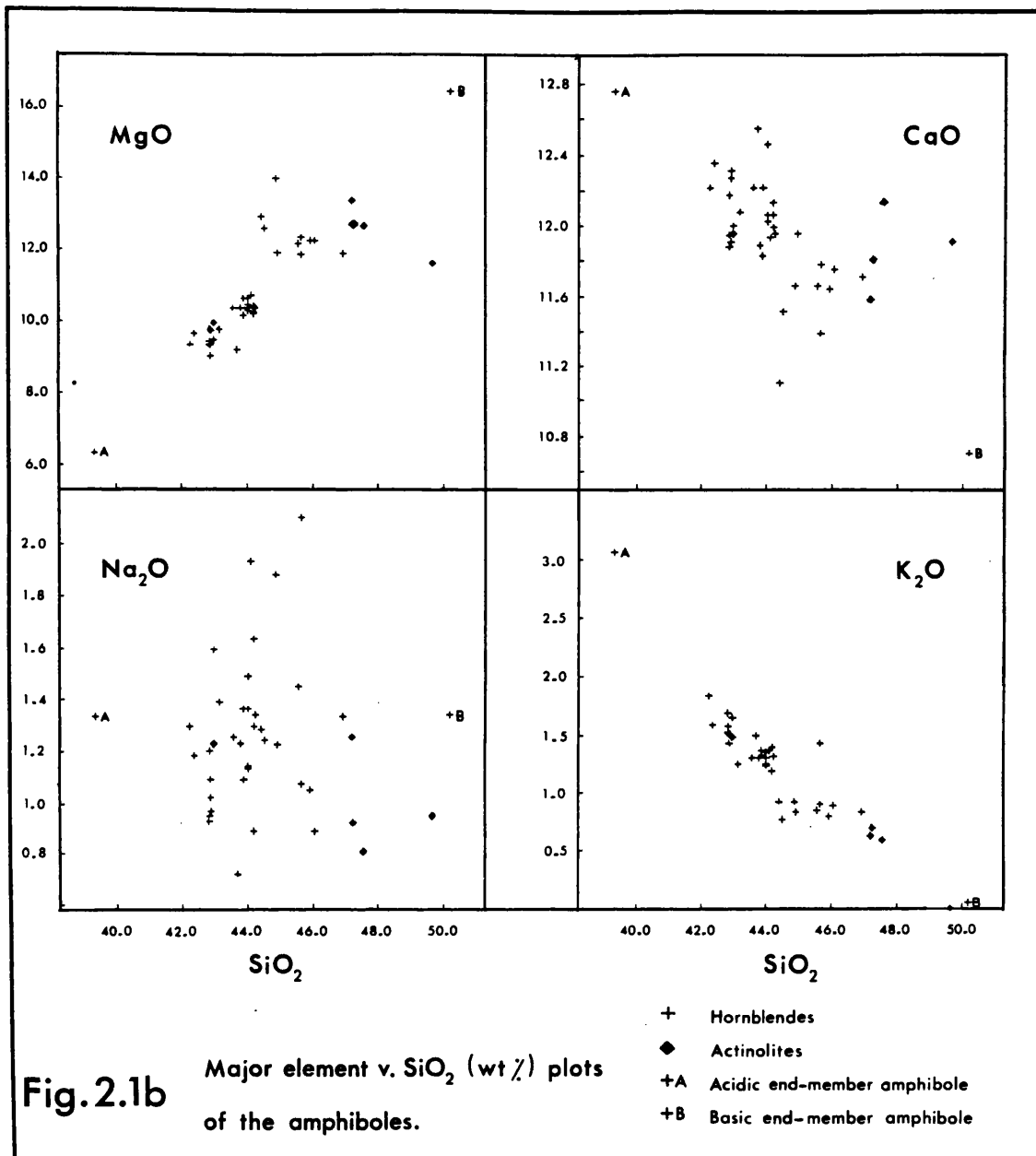


Fig. 2.1b Major element v. SiO₂ (wt%) plots of the amphiboles.

Fig. 2.2 Modal Q-A-P plot (Streckeisen, 1976) of the orthogneisses.

3b. - Granites

4. - Granodiorites

5. - Tonalites

10" - Quartz Diorites

Q = quartz

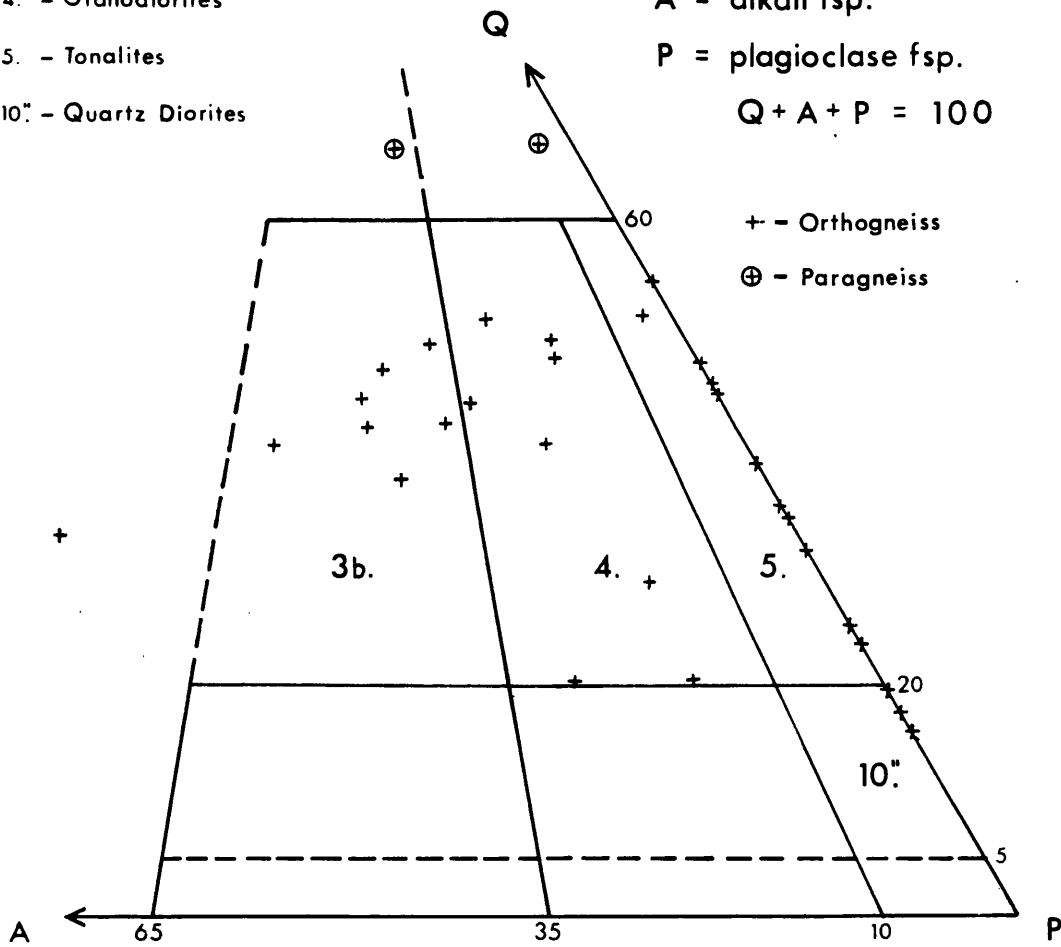
A = alkali fsp.

P = plagioclase fsp.

$$Q + A + P = 100$$

+ - Orthogneiss

⊕ - Paragneiss



14

For the purposes of the description of petrographic details, the orthogneisses will be split into three main groups:-

- a) melanocratic (quartz-poor) tonalitic orthogneiss.
- b) leucocratic (quartz-rich) tonalitic orthogneiss.
- c) granodioritic and granitic orthogneiss.

a) melanocratic tonalitic orthogneiss.

A typical rock has a hypidiomorphic granular texture and contains 40-50% labradorite, An_{55} , 20-40% brown-green hornblende, 10-15% quartz, and up to 4% opaque ore with accessory chlorite, epidote and apatite. The labradorite occurs as large anhedral grains (up to 6mm across) and displays excellent carlsbad-albite twinning where it is not saussuritised and sericitised. Hornblende is present as discrete subeuhedral crystals, up to 1 cm in length, which are often twinned and contain only a few rounded inclusions of quartz and opaque ore. The hornblende in the orthogneisses clearly contrasts with that in the metabasite rocks and is concluded to be igneous in origin. Quartz occurs mainly as irregular multi-grain masses showing strained extinction. The anhedral opaque ore grains have a complex exsolved microstructure and microprobe analyses reveal that this intergrowth mosaic, with irregular 'domains' less than 10 microns across, consists of magnetite, rutile and sphene. A retrogressive origin is suggested for the sphene, in which slowly cooling tonalitic rocks, held at elevated temperatures in the regional metamorphic regime (M3), were partially hydrated, releasing calcium from the alteration of the labradorite which reacts with exsolved rutile in the ore. The original ore was presumably ilmenite.

b) leucocratic tonalitic orthogneiss.

These rocks differ from the melanocratic tonalitic orthogneisses in that they contain less than 20% of a mafic phase, which is either hornblende, or more commonly, chloritised biotite. Where hornblende occurs it is invariably corroded and surrounded by biotite sheafs and chlorite. Andesine, An_{47-50} , and quartz make

up the bulk of the rock with small mafic grains (c.1mm mean diameter) and ore fragments forming interstitial stringers and aggregates. The anhedral ore grains are commonly polymineralic, containing large areas of pure magnetite and other areas of magnetite, rutile and sphene intergrowth.

c) The granodioritic and granitic orthogneiss.

The rocks contain 25-40% andesine, An₄₀₋₄₆, 25-35% quartz, 10-30% phenocrystic microcline, up to 15% chloritised biotite and magnetite fragments, and accessory zircon, common epidote and allanite. These rocks mark the stabilisation of potash feldspar as an essential phase in the orthogneiss series.

The texture is xenomorphic granular, with grains showing slight to moderate alignment in the weak F3 foliation. The grain size is generally coarse with the microcline phenocrysts ranging up to a maximum diameter of c.2cm and matrix grains, a mean diameter of 4mm.

The andesine, an unusually calcic plagioclase for granitic rocks, is strongly saussuritised and corroded and occurs as anhedral grains and also skeletal relics in large microcline grains and quartz folia.

Quartz folia and masses, often containing small grains of microcline and corroded andesine, are composed of numerous strongly sutured sub-grains which exhibit strained extinction. The sub-grains are especially small (c.100 microns) and irregularly shaped in narrow quartz folia extending between large feldspar grains, and are interspersed with the fragmented margins of the feldspars. This indicates that while the quartz simply recrystallised during the formation of the F3 foliation, the feldspar behaved in a rather more brittle fashion.

The anhedral microcline phenocrysts and matrix grains are commonly twinned and contain graphic exsolution lamellae and blebs of quartz as well as cores of andesine. The boundaries between quartz and microcline grains are irregular and this fact, together with the evidence of graphic intergrowth of quartz in microcline, suggests that the two phases crystallised simultaneously.

Thin interstitial clots and stringers of variably chloritised and prehnitised biotite occur throughout, together

with fragments of magnetite.

Light brown coloured bipyramidal zircons are also present, as are dark brown allanite grains (up to 1cm in length), although the latter are much less common.

2.3 Paragneisses.

It is clear from field evidence that the paragneisses are metasediments that have undergone a high temperature partial melting event, which was coincident with the intrusion of the orthogneisses. They consist of a leucogneissic mobilisate, which comprises up to c.75% of their bulk, and various refractory rock types occurring as xenoliths in this leucogneiss.

2.3.1 Field Relations.

Although the paragneisses are the most common rocks of the syntectonic intrusive complex they extend only a short distance (< $\frac{3}{4}$ km) north of it before grading into sillimanite-biotite-schists. There is, therefore, a close spatial correlation between the intrusive complex and the paragneisses. They occur most spectacularly in the central parts of the Shannavara district (Fig 1.2) where they outcrop over several square kilometers, including the whole of Shannavara mountain.

In this district, the paragneisses are heterogeneous rocks consisting of a mobilised component or mobilisate, with xenoliths of alumina-rich melanosome material, semipelite, quartzite and metabasite. Plates 1-9 show the range of xenolith morphologies and also help to demonstrate the chaotic appearance of the paragneisses.

The mobilisate is a strongly foliated, medium grained, quartz-rich leucogneiss which is, in itself, remarkably homogeneous throughout the whole area. However, it contains contrastingly different proportions, shapes and sizes of xenoliths of differing lithologies, from one outcrop to the next, and it is this feature which makes the paragneiss so variable in appearance.

Very commonly dispersed through the mobilisate and aligned with its foliation, are small, ellipsoidal, sillimanite-biotite-opaque ore melanosomes, usually less than 6cm in length. These

Plate 1. This plate illustrates the general features of the paragneiss. A siliceous mobilisate (under the hammer), which has a strong F3 foliation, contains disorientated xenoliths of quartzite (middle right), semipelite (upper centre and upper right), and amphibolite (lower left). The amphibolite is strongly quartz veined. (Hammer length 20cm)

Plate 2. This plate shows the extremely chaotic appearance of the paragneiss.

Plate 3. This plate shows the occurrence of a rounded quartzite xenolith and a slightly folded semipelitic xenolith, in the mobilisate. (Hammer length 20cm)

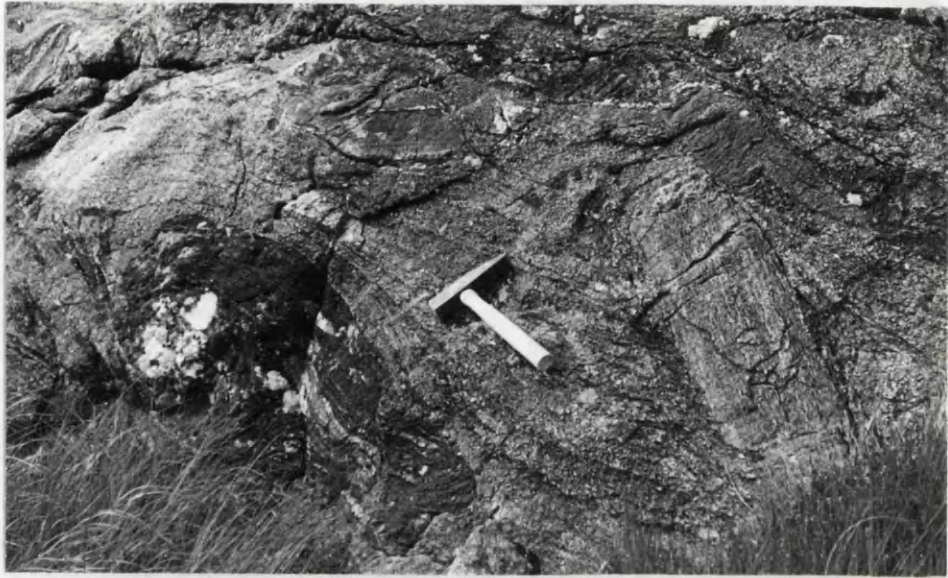


Plate 4. This plate shows a complex outcrop of paragneiss, in which strongly foliated mobilisate contains many small relict semipelitic xenoliths and their siliceous melt. The large light-coloured mass (left-centre) represents the melt envelope which formed around an aggregate of these xenoliths.

Plate 5. This plate shows two semipelitic xenoliths (centre) which are in a moderately advanced state of assimilation. They are surrounded by melting rims which possess "tail-like" extensions at one end of the xenolith. These features may indicate the sense of movement of the mobilisate to that of the xenolith. (Hammer length 20cm)

Plate 6. This plate shows sections of melanosome ellipsoids which are aligned with their long axes parallel to the foliation in the surrounding mobilisate. The melanosomes consist mainly of sillimanite, biotite, ilmenite and andesine.

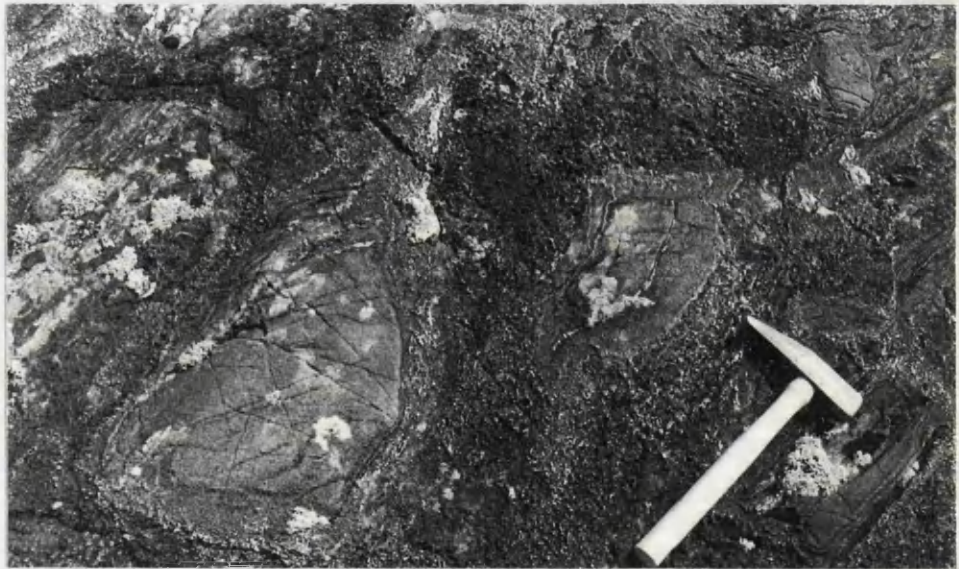
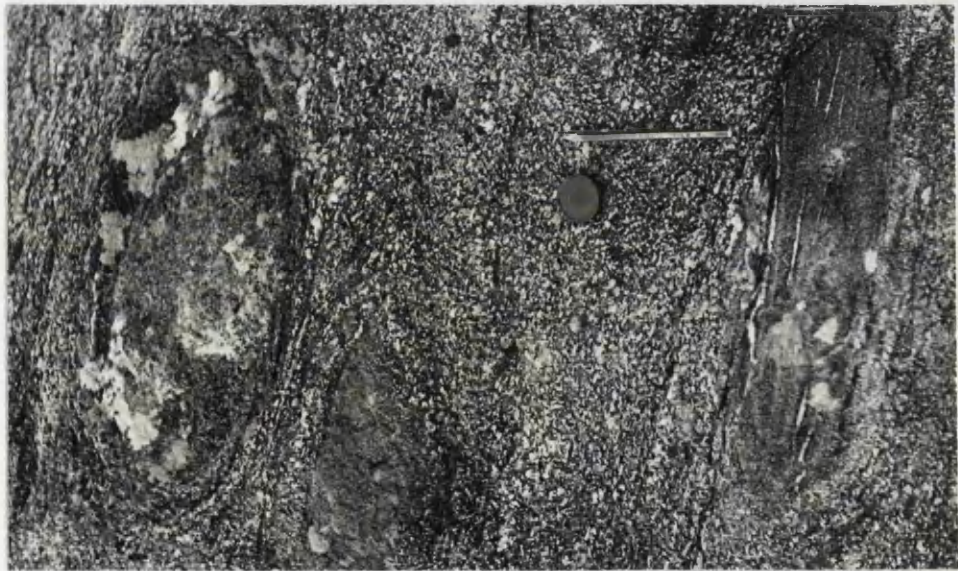


Plate 7. This plate shows an F3 fold in a striped semipelite xenolith. (Hammer length 20cm)

Plate 8. This plate illustrates the siliceous nature of the mobilisate component of the paragneiss. The speckled appearance of the mobilisate is due to the myriads of quartz grains which protrude from the surface after plagioclase has been selectively weathered out. (Pencil length 16cm)

Plate 9. This plate shows a folded siliceous-semipelite xenolith and its melt envelope surrounded by strongly foliated mobilisate.



17

alumina-rich residues also occur as large irregular masses up to one metre across and have a contorted internal structure made up of sillimanite knots and folia, with local concentrations of biotite and opaque ore. Occasionally, large relict megacrysts of cordierite, entirely pinitised, occur in the larger sillimanite masses.

Large (c. 1cm max. diameter) euhedral biotite plates occur in patches, up to 15cm across, lying in embayments in the margins of such residual masses and indicate that the latter provided a useful nucleation surface as the mobilised component began to solidify.

Disorientated psammite and quartzite blocks are extremely common in the mobilisate and exist in all states of assimilation, from well defined rectangular or rounded blocks to "ghost" xenoliths. Siliceous haloes, often with a "tail-like" extension at one end, invariably surround this type of xenolith (Plates 4 and 5). Occasionally, aggregates of psammitic and semipelitic xenoliths occur enveloped in a cloud of siliceous rock (Plate 4), and in these instances no other alternative to the melting explanation can be foreseen. Obviously, the rate of melting of the xenoliths, at least in the final stages of the anatectic event, was greater than the rate of dissipation of the resultant quartz-rich melt into the surrounding melt.

Large ellipsoidal metabasite xenoliths, up to 2 m in length, also occur frequently in the paragneiss but show few features attributable to assimilation. However, they are often sites of prominent quartz veining.

Discounting the metabasite xenoliths, the estimated degree of partial melting of the original metasediments is as high as 80% in places. Such a high level of melting over a wide area is surprising. However, the low ratio of alumina-rich melanosome to mobilisate suggests that the original metasediments were probably rather uniform siliceous semipelitic rocks.

In the Cashel district to the west, the melanosome component makes up a considerably greater proportion of the paragneiss and contains large garnet porphyroblasts, a feature which is rarely seen in the equivalent rocks to the east. One notable outcrop lying $\frac{1}{2}$ km north of Gowla Lodge, shows garnet (c. 2cm max. diameter)-sillimanite-biotite pods, up to 5 metres in length, surrounded by strongly foliated leucogneiss. It would appear that the

original metasediments were rather more pelitic here than in the east.

The contacts of the paragneiss with the tonalitic orthogneiss tend to be relatively sharp and can be distinguished to within 20cm using mineralogical and textural criteria. However, the adjacent orthogneiss, for a distance of up to 5 to 10 metres in from the contact, is generally atypical of the main body of tonalitic orthogneiss, in that it is strongly foliated and in parts is extremely siliceous. It contains abundant numbers of sillimanite lenses (up to 6 cm in length) and also contains xenoliths of corroded quartzite, semipelite and metabasite. The field evidence for assimilation is strong with the orthogneiss margins containing remnants of all the xenoliths found in the paragneiss, and therefore partial melting of the paragneiss did occur in association with the intrusion of the orthogneiss magma. It seems clear that the orthogneiss magmas were the heat source that produced such high degree of partial melting in semipelitic metasediments, to form the paragneisses. It is envisaged that the more refractory siliceous and pelitic units in the original metasedimentary pile, were broken up by the injection of a melt of semipelite origin and that these chaotic melt-xenolith assemblages mantled the rising tonalitic magmas.

Small F3 folds, folding around the main F2 foliation of the Dalradian metasediments, are occasionally preserved in xenoliths of banded semipelite (Plates 7&9). This shows that the anatexis event postdates at least some of the D3 deformation even though the paragneisses and the orthogneisses have both taken up a strong F3 foliation.

2.3.2 Petrography.

A typical example of the leucogneissic mobilisate is medium grained (c.2mm mean grain diameter) with a foliated xenomorphic granular texture and has a mineralogy consisting of 57% quartz, 18% oligoclase, An_{26} , 14% orthoclase, 8% fresh to chloritised biotite, 3% muscovite, and accessory sillimanite clots and associated ilmenite. The constituent grains of this rock show strong alignment to the foliation, especially the quartz which has extensively recrystallised into elongate multi-grain masses with each grain strongly sutured into neighbouring grains,

and also displaying strained extinction under crossed nicols. The feldspars, both plagioclase and orthoclase, show some alteration, with the former being extensively saussuritised. Plagioclase, which microprobe analysis reveals to be oligoclase in composition, occurs as small (c.1mm mean diameter) subeuhedral to anhedral grains often displaying excellent fine lamellar twinning. Orthoclase is present as large (2mm mean diameter) untwinned anhedral grains and microprobe analyses of it reveal an Or component of c.81% and BaO concentrations of up to 0.3 wt.%. Fractured feldspar grains are common in this rock especially those which are slightly disorientated with respect to the foliation. The micas are present as small (c.1mm max. diameter) flakes with biotite much more abundant than muscovite. The biotite is generally variably altered to chlorite, whereas the muscovite is invariably unaltered.

Two examples of mobilisate are plotted in the QAP diagram (Fig2.2) and they lie on the quartz-rich side of the Q60 horizontal, in the field of quartz-rich granitoids. Thus they can easily be distinguished from the more acidic varieties of the orthogneiss which plot across the granite and granodiorite fields.

The alumina rich melanosomes, which occur in the mobilisate, have an extremely variable mineralogy and contain a multitude of textures. Fibrous mats of sillimanite are ubiquitous, often comprising c.50% of the melanosome, with the sillimanite needles forming swirls and knots in the contorted mass. Long trains of ilmenite fragments, in the sillimanite, testify to strong shearing of the melanosome, as do sheared out lenses (c.8mm max. diameter) of porphyroblastic plagioclase. Plagioclase exhibits a wide range of composition in these rocks, with grains ranging from An_{21} - An_{43} in a single rock. Biotite is present as large (0.5 cm max. diameter) flakes, and is often strongly decomposed, containing many needles of sillimanite and becoming colourless towards the margins, where it is mantled by ilmenite. This association probably represents a prograde reaction in which biotite breaks down to ilmenite, sillimanite and a melt component. Garnet occurs as large poikiloblastic grains (up to 2cm in diameter) with included quartz comprising up to 60% of its volume. In many cases garnet possesses a poikilitic core with an inclusion-free rim.

Augen, up to 1cm in length, containing a randomly orientated

fine-grained mosaic of muscovite, quartz, plagioclase and euhedral ilmenite, also occur in the fibrous sillimanite mat and are often surrounded by a chloritic envelope. These augen may represent small pockets of trapped melt, and the chloritic envelope may be due to the retrogressive reaction of the melanosome with H_2O released from the solidifying melt.

2.4 Conclusions.

Much of the primary mineral assemblage of the metabasite rocks was either replaced or modified during the M3 amphibolite facies metamorphism. Original igneous clino- and ortho-pyroxenes have been almost completely replaced by actinolite, hornblende and quartz. Ulvospinel-bearing titanomagnetites re-equilibrated under the metamorphic conditions, leaving ore grains composed of titanomagnetite with exsolved ilmenite lamellae and sphene patches. Plagioclase (bytownite-labradorite) became extensively saussuritised and sericitised.

Primary hornblende is first observed in the melanotonalitic orthogneisses, occurring as discrete subeuhedral grains which are often twinned. Corroded, originally euhedral to subeuhedral, labradorite grains, quartz folia and polymineralic opaque ore grains comprise much of the remaining rock bulk.

The more leucocratic tonalitic orthogneisses contain only minor amounts of hornblende, and its alteration products, biotite and chlorite, and titanomagnetite, and these mafic phases form sinuous interstitial 'stringers' between the felsic grains, andesine and quartz.

The granodioritic and granitic orthogneisses are composed mainly of quartz, microcline and corroded andesine. The andesine is thought to be an early crystallised, higher temperature phase, relative to the quartz and microcline, because it is an unusually calcic plagioclase for granitic rocks.

The metabasite rocks were intruded syn-D2 (Leake, 1970a) and disrupted during the folding of the Dalradian Series in D3. High degrees of partial melting occurred in the Dalradian metasediments which mantled the intruding tonalitic orthogneiss magmas. Magma intrusion was synchronous with the D3 deformation and almost certainly the cause of the M3 metamorphism.

Chapter 3.

Major Element Geochemistry of the Rocks of the Intrusive Complex.

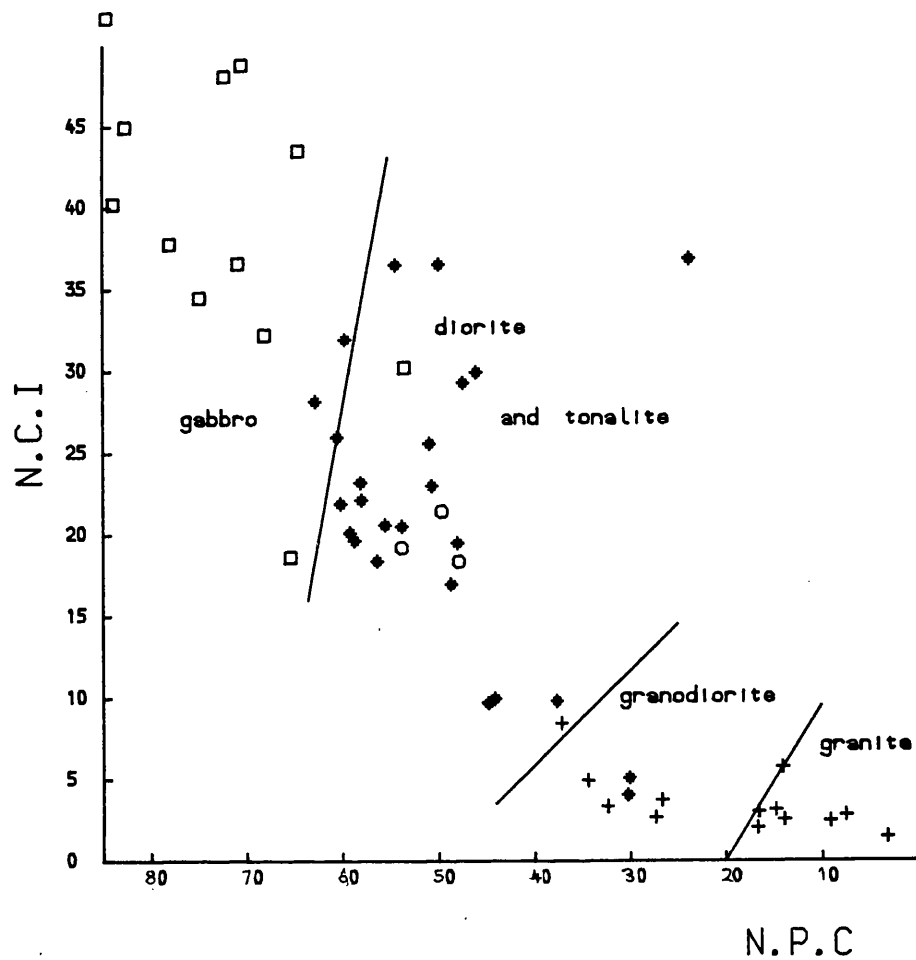
The main aim in this chapter is to present the major element distributions of the whole metabasite-orthogneiss suite, first of all in simple variation diagrams and then in more complex multi-component systems, with a view to forming plausible hypotheses pertaining to the origin of these rocks and to provide explanations for their mineralogical and textural features. These hypotheses and explanations will then be checked for compatibility with the known phase relations of the composition join gabbro-tonalite-granite. The geochemistry of a few paragneiss rocks will also be presented and dealt with in a similar fashion to that of the metabasite-orthogneiss rocks, although the treatment will be much less rigorous because of the small sample population.

In this thesis, all major element data, for both rocks and minerals, have been recalculated on an anhydrous basis. Information on the practicalities of chemical analysis, data reduction, and data plotting carried out during this research is given in Appendices 1, 2, and 3.

Before discussing the geochemical variations of the rocks, a check will first be made to see whether the modal classification adopted in Chapter 2 is compatible with the major element geochemistry. Perhaps the most useful chemical classification scheme is the plot of normative colour index (N.C.I) versus normative plagioclase composition (N.P.C), (Irvine and Baragar, 1971). The formulae for the calculation of these parameters are given beneath fig. 3.1. It can be seen from this plot that the modal classification, ie. the symbols, is indeed compatible with the chemical classification, ie. the fields in the diagram.

3.1 The metabasite and orthogneiss samples - do they represent cumulate or magma compositions?

In this study, the treatment of the chemical data of the metabasite samples will be based on the hypothesis that most of the samples closely approximate to the composition of the magma from which they formed. If this hypothesis is true then it follows that the variations in the major and trace element abundances in the metabasite-orthogneiss rock suite, define the variations which occurred in the compositions of the metabasite and orthogneiss



Symbols represent the modal QAP classification (Strekeisen, 1976)

- - Metabasite.
- * - Tonalitic orthogneiss. (○ = Kf-rich types)
- + - Granodioritic and Granitic orthogneiss.

Labelled fields in the N.C.I. v. N.P.C. plot represent the chemical classification of Irvine and Baragar (1971).

Normative Minerals.

$$\text{Normative Colour Index (N.C.I.)} = \text{OL.} + \text{OPX.} + \text{CPX.} + \text{MT.} + \text{IL.} + \text{HM.}$$

$$\text{Normative Plagioclase Composition (N.P.C.)} = 100 \cdot \text{An} / (\text{An} + \text{Ab} + 5/3\text{Ne})$$

Fig. 3.1 N.C.I. v. N.P.C. plot

magmas.

The pronounced homogeneity of the individual orthogneiss masses indicates that the orthogneiss rocks will have compositions which approximate to the compositions of the orthogneiss magma. The metabasite rocks are the most difficult to reconcile in this problem of whether the rock is cumulate or not, simply because they were extensively amphibolitised in the M3 metamorphism which accompanied the intrusion of the orthogneiss magmas. As the metabasite rocks were also folded during the D3 deformation, it is quite conceivable that some of the metabasite samples are amphibolitised cumulate material.

There are few metabasite outcrops in the field area which display igneous layering, and plagioclase-rich (>65%) metabasites are not found. This suggests that basic cumulate rocks are not prevalent in the field area. There are, however, several masses of very mafic metabasite (Leake, 1970a) and these may represent amphibolitised cumulate pyroxenite and peridotite. Two examples of these mafic rocks, BK408 and BK96, are included in the metabasite samples. The small amount of plagioclase in these two rocks is such that it could easily represent intercumulous material.

The mineralogy of metabasite samples BK102 and BK138 was described in the previous chapter, these rocks being unusual in that they retain much of their primary mineral assemblages, ie. orthopyroxene + clinopyroxene + titanomagnetite + bytownite. If the amphibolitisation of the metabasite rocks was essentially an isochemical change, and if the metabasites are cumulate in origin, then their compositions should be well defined by specific combinations of the four primary phases listed above. It should be theoretically possible to discriminate between the chemical variations of a group of cumulate rocks, each rock consisting of these four phases in random proportions, and the chemical variations of another group of rocks which represent the various compositions of a magma fractionating some combination of these phases.

Two parameters which can be used together to discriminate between groups of rocks with these different characteristics, are $(\text{MgO} + \text{tFeO} - \text{TiO}_2)$ wt% and Al_2O_3 wt%. $(\text{MgO} + \text{tFeO} - \text{TiO}_2)$ wt% is a good indicator of the proportion of pyroxene in the rock, (the Fe component of titanomagnetite being largely removed by subtracting TiO_2 wt% from tFeO wt%). Al_2O_3 does occur in clinopyroxene but in

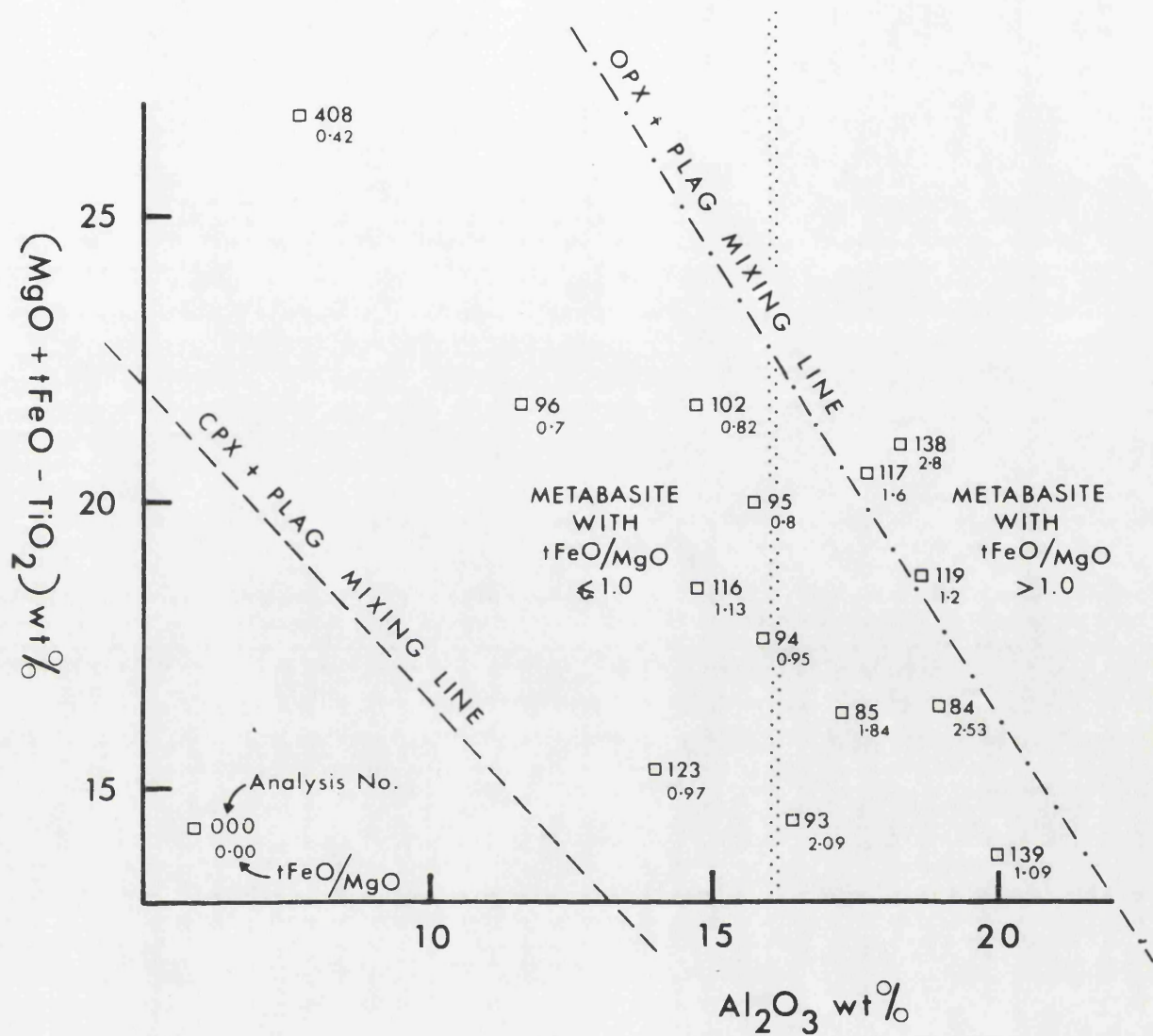


Fig. 3.2. $(\text{MgO} + \text{tFeO} - \text{TiO}_2)$ (wt%) v. Al_2O_3 (wt%) plot of the metabasite rocks.

relatively small amounts compared with calcic plagioclase, and so this parameter is a reliable indicator of plagioclase in the rock.

A plot of $(\text{MgO} + \text{tFeO} - \text{TiO}_2) \text{ v. } \text{Al}_2\text{O}_3$ for the metabasite rocks is shown in fig. 3.2. The plot covers the central section of the field of possible compositions of cumulate rocks formed from the mixing of clinopyroxene, orthopyroxene, and a range of plagioclase from bytownite to labradorite (the approximate boundaries of this field are shown in the plot). Rocks BK408 and BK96, as predicted, plot away from the rest of the metabasite samples in the direction of the mafic, (ie. high $(\text{MgO} + \text{tFeO} - \text{TiO}_2)\text{wt}\%$), end of the plot. The cumulate nature of sample BK408 is confirmed by its extreme position in the plot, relative to the other metabasite rocks, and this origin is also strongly indicated for sample BK96. The other metabasite samples plot within a narrow Al_2O_3 range of only c. 5wt%, and this calculated as a modal percent would represent a total modal plagioclase variation of only c. 15%. The range of modal plagioclase content in a series of pyroxene + plagioclase cumulate rocks would surely be much greater than 15%. Furthermore, a study of the tFeO/MgO ratios of the metabasites shows that there is a systematic increase in tFeO, relative to MgO, with increasing Al_2O_3 . Cumulate rocks consisting of random proportions of clinopyroxene, orthopyroxene, titanomagnetite, and plagioclase, would not be expected to show such a trend. Therefore, it is concluded that the majority of the metabasite samples are more likely to represent magma compositions, rather than cumulate compositions.

3.2 Harker-type diagrams.

After the chemical analysis of the rock samples had been completed it was found that a compositional gap existed between 62 wt% and 70 wt% SiO_2 . However, a study of previous work on the orthogneisses, carried out by Harvey (1967, thss.) and Senior (1973, thss.), shows that this is not a real feature and is due to sampling error. Eight analyses, six from Senior's thesis (those of samples, AS433, AS494, AS527, AS536, AS540, and AS583), and two from Harvey's thesis (G332 and G350), are included in the major element plots and these bridge the apparent compositional gap.

A continuous, though in many cases non-linear, chemical variation exists right through the metabasite-orthogneiss rock suite for all major elements (fig. 3.3a-i) suggesting that the rocks are all comagmatic and related by the process of fractional crystallisation. Of the plots of fig. 3.3, that of MgO wt% v.

SiO_2 is the most significant, in that it highlights the SiO_2 variation in the metabasite rocks. The two samples with the highest MgO content are BK408 and BK96, the suspected cumulate rocks. The other metabasite samples define a scattered but significant trend of decreasing SiO_2 wt%, down to MgO contents of c. 6wt%, and then a trend of increasing SiO_2 wt% until the metabasite trend merges with the tonalitic orthogneiss trend. This non-linear behaviour of SiO_2 in the metabasite rocks explains much of the scatter shown by them in the other major element v. SiO_2 wt% plots. The petrogenetic significance of the chemical variation in the metabasites can be more readily seen in the major element v. SiO_2 (Solidification Index) plots, fig. 3.4.

The orthogneisses define clear trends in all of the major element v. SiO_2 plots (fig. 3.3a-i), though those of P_2O_5 , Na_2O , and K_2O show rather more scatter than the other element trends. Al_2O_3 , MgO, CaO, MnO, tFeO, and TiO_2 all decrease steadily in abundance in the orthogneisses, with increasing SiO_2 wt%, as is the norm in a magmatic differentiation series. The P_2O_5 wt% distribution is puzzling, because the largest amount of scatter occurs in the composition range represented by the analyses of Harvey (1967, thss.) and Senior (1973, thss.). A projection of the trend of those melano-tonalitic orthogneisses analysed in this study, would directly intersect the acidic orthogneisses, also analysed in this study. It would seem that the P_2O_5 analyses of Harvey and Senior are not compatible with those produced in this study, and this difference is probably a function of analytical procedure. The distributions of the alkalis, Na_2O and K_2O , in the orthogneiss rocks, define a distinctive pattern when plotted against SiO_2 . This 'step-like' pattern shows that the tonalitic orthogneisses have fairly constant alkali abundances, while the granodioritic and granitic orthogneiss rocks define a trend of rapid enrichment of the alkalis. The constant K_2O wt% feature of the tonalitic rocks is unusual since potassium is often considered to be a strongly incompatible element in magmatic processes, (ie. it is partitioned into the melt rather than the fractionating phases), and so it should increase continuously throughout the orthogneiss rocks. Na_2O increases rapidly in the granodioritic and granitic orthogneisses and must have acted as an incompatible element in the acidic orthogneiss magma, which supports the hypothesis, that was made in the previous chapter, that sodic plagioclase did not form in the magma. This

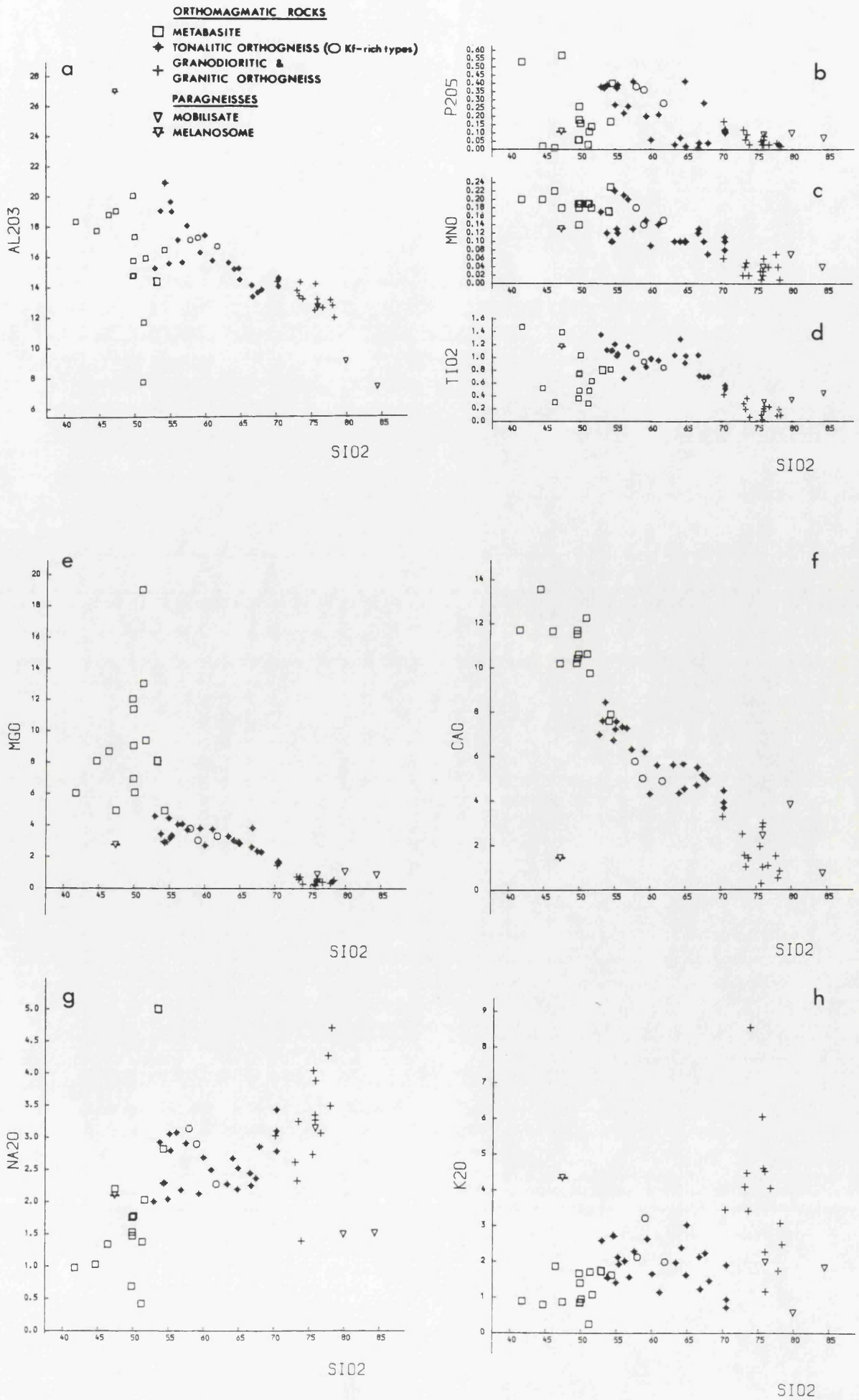


Fig. 3.3a-i Major element (wt%) v. SiO₂ (wt%) plots.

Fig. 3.3 (continued)

- ORTHOMAGMATIC ROCKS
 □ METABASITE
 ◆ TONALITIC ORTHOGNEISS (○ Kf-rich types)
 + GRANODIORITIC & GRANITIC ORTHOGNEISS
- PARAGNEISSES
 ▽ MOBILISATE
 ▾ MELANOSOME

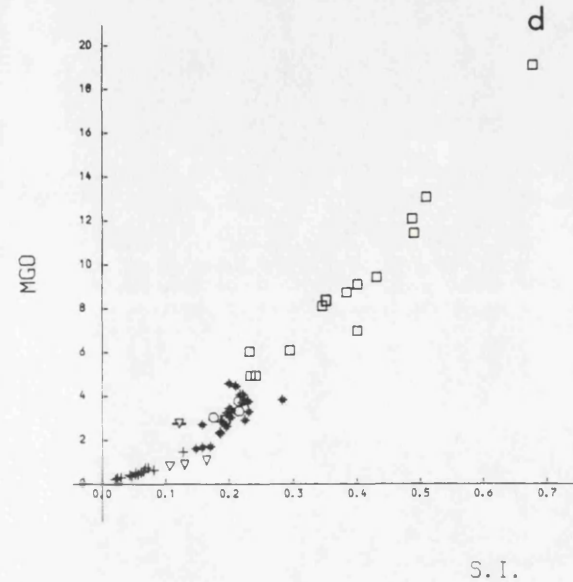
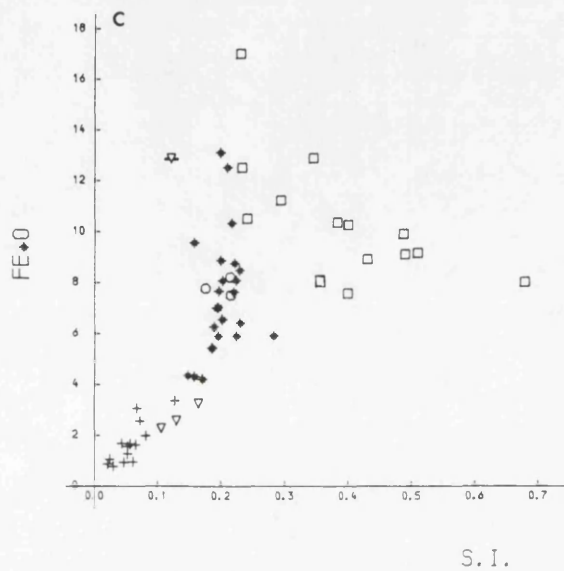
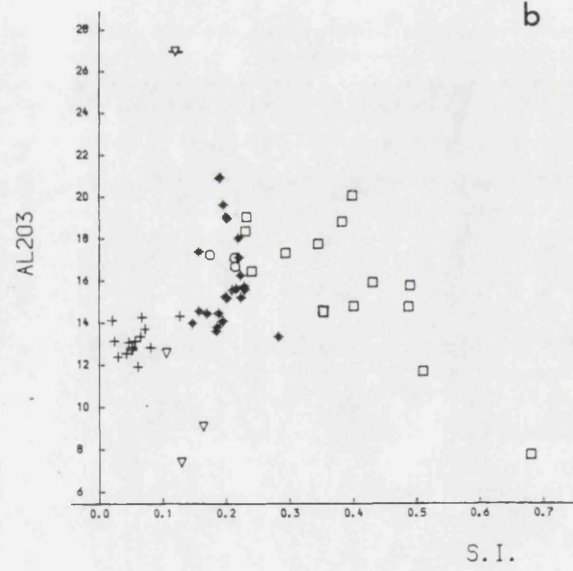
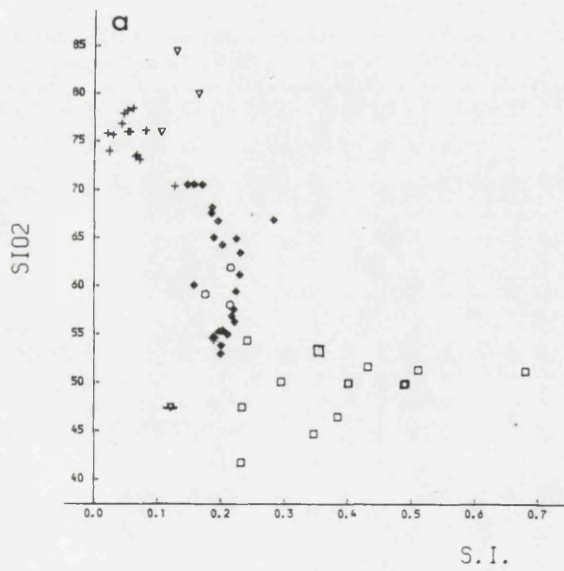
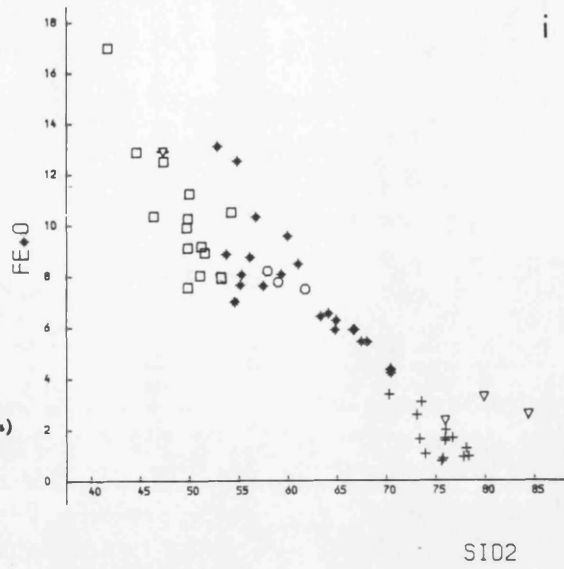


Fig. 3.4a-j Major element (wt%) v. Solidification Index (S.I.) plots.

ORTHOMAGMATIC ROCKS

- METABASITE
- ◆ TONALITIC ORTHOGNEISS (○ Kf-rich types)
- + GRANODIORITIC & GRANITIC ORTHOGNEISS

PARAGNEISSES

- ▽ MOBILISATE
- ▽ MELANOSOME

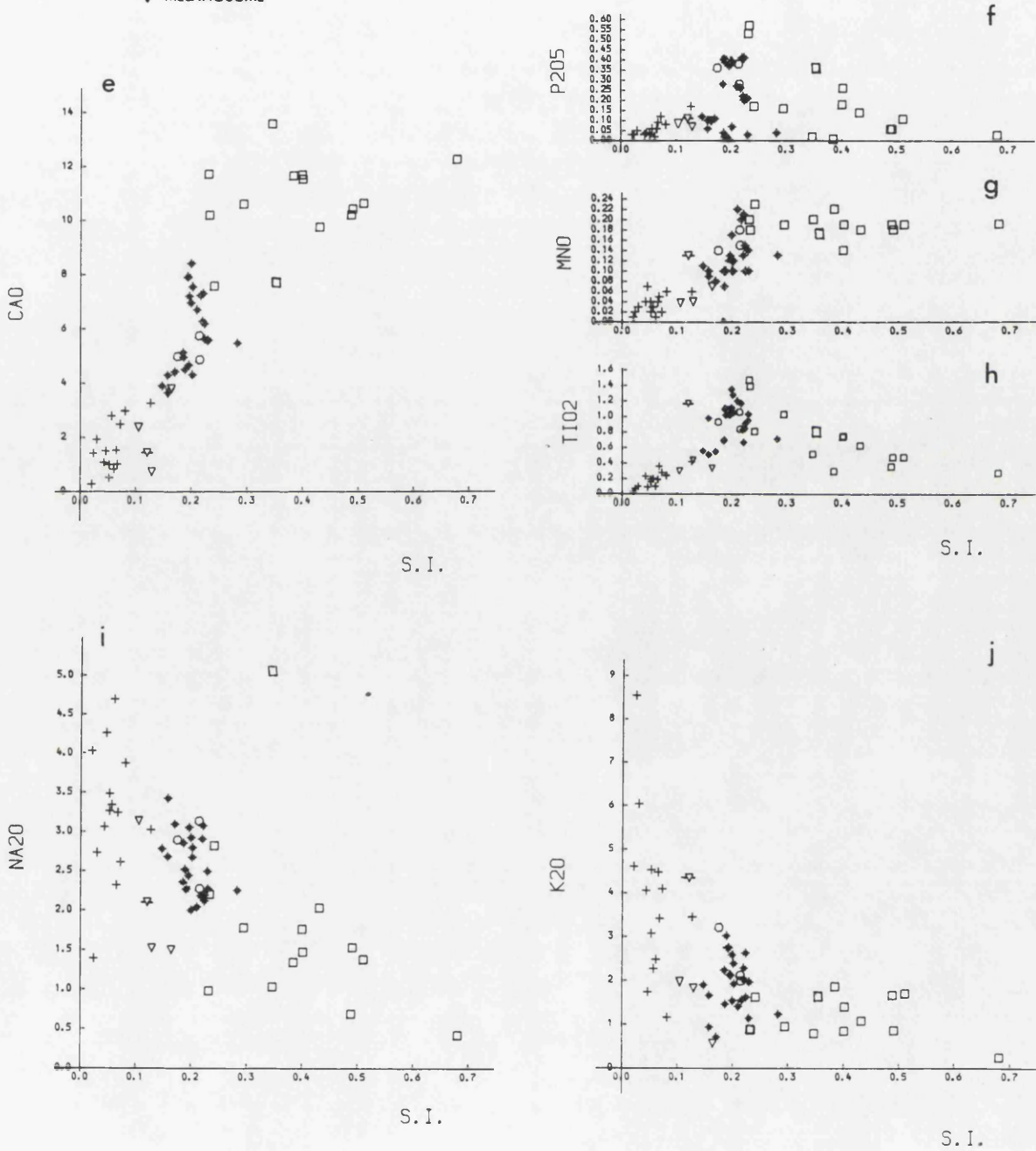


Fig. 3.4 (continued)

implies that much Na_2O is held in the microcline in these rocks, and this is confirmed by the microprobe analyses of this phase (Appendix 2). The high degree of scatter of points about the whole orthogneiss trend indicates that two processes operated to form the alkali distributions of the orthogneiss suite, a magmatic process which produced the overall orthogneiss trend, and a secondary alteration process which produced the scattering. The 'scattering' of potassium may have implications for the distributions of the strongly incompatible trace elements in these rocks.

One example of aluminous melanosome and three of mobilisate represent the paragneiss group in the major element v. SiO_2 wt% plots of fig. 3.3a-i. The higher concentration of K_2O in the melanosome sample (BK409), compared with the mobilisate rocks, is due to the high proportion of residual biotite in the melanosome mineralogy. The low alkali contents of the mobilisate, which is the largest component of the paragneiss, suggests that the relatively constant K_2O and Na_2O abundances in the tonalitic orthogneisses could be due in part to the assimilation of paragneiss by the tonalitic orthogneiss magmas.

Fig. 3.4a-j shows the major element distributions of the metabasite-orthogneiss suite plotted against the so-called Solidification Index, which is the MgO wt% of a rock divided by the sum of its MgO , tFeO , Na_2O and K_2O components. This index was originally formulated without the alkalis, specifically for the comparison of basic rocks. However, Kuno et al., 1957, added these oxides to give the index a wider application. (NB. Their formula for the calculation of Solidification Index (S.I.) involves the multiplication of the index by 100; this step being omitted in this thesis.)

The value of the S.I. decreases from the metabasites through to the granitic orthogneisses. The metabasites have the broadest range of S.I. values with the intermediate rocks and then the granitic rocks having progressively shorter S.I. ranges. This means that the sensitivity of the S.I., towards changes in bulk composition, drops at the acidic end of the spectrum.

The SiO_2 v. S.I. plot, fig. 3.4a, shows the initial trend of SiO_2 depletion in the metabasite rocks. This trend cannot have been caused by the fractional crystallisation of a low- SiO_2 wt% mafic phase, such as hornblende or olivine. Pyroxene would seem to be the only mafic phase capable of producing this feature of the

metabasite group. The orthogneisses define a marked trend of SiO_2 enrichment, which occurs with almost no change in the S.I. value. To produce this trend by fractional crystallisation, the fractionation assemblage as a whole must have had a tFeO/MgO ratio approximately equal to that of the magma, and a low SiO_2 content. Some of the most tFeO -rich metabasite samples have $\text{tFeO}/\text{MgO} = 2.0$ and if they accurately represent the magma composition, then the fractionation of an Fe-rich oxide would seem to be a necessity.

Against S.I., the metabasites define diffuse trends of tFeO and Al_2O_3 enrichment. The tFeO increase is contrary to the trend observed in the tFeO v. SiO_2 wt% plot, fig. 3.3i, and this clearly shows the limitations of simple, two component, variation diagrams in petrogenetic reasoning. The increase in the tFeO content of the metabasite rocks, suggests that clinopyroxene may have been the dominant fractionation phase, if the metabasite magma evolved by pyroxene fractional crystallisation. The diffuse increase in Al_2O_3 would appear to limit the fractionation of plagioclase from the metabasite magma. The excellent correlation between MgO and the S.I., fig. 3.4d, is to be expected because of the very nature of the S.I. parameter. However, the absence of any obvious breaks or discontinuities in the overall metabasite-orthogneiss trend again suggests that all the rocks are genetically linked.

The distributions of P_2O_5 , MnO , and TiO_2 , against S.I., for the metabasite-orthogneiss suite, suggest that a marked change occurred in the nature of the phases fractionating from the most differentiated metabasite magma. The fractionation of a Ti-Fe ore from this magma would be consistent with the TiO_2 data, as well as the tFeO data.

3.3 The AFM diagram and other major element classification diagrams.

The chemical classification system of Irvine and Baragar (1971) makes use of a few selected plots to discriminate between rocks of the three main divisions; Subalkaline, Alkaline, and Peralkaline. The system is also able to discriminate between rocks of the Calc-alkali Series and the Tholeiitic Series which belong to the Subalkaline division.

The $(\text{Na}_2\text{O} + \text{K}_2\text{O})$ versus SiO_2 wt% plot (fig. 3.5) clearly defines the orthomagmatic rocks of the intrusive complex, as rocks of the Subalkaline division. The dividing line in this plot is a modification, proposed by Irvine and Baragar, of MacDonald's (1968)

Fig. 3.6 AFM (wt%) diagram.

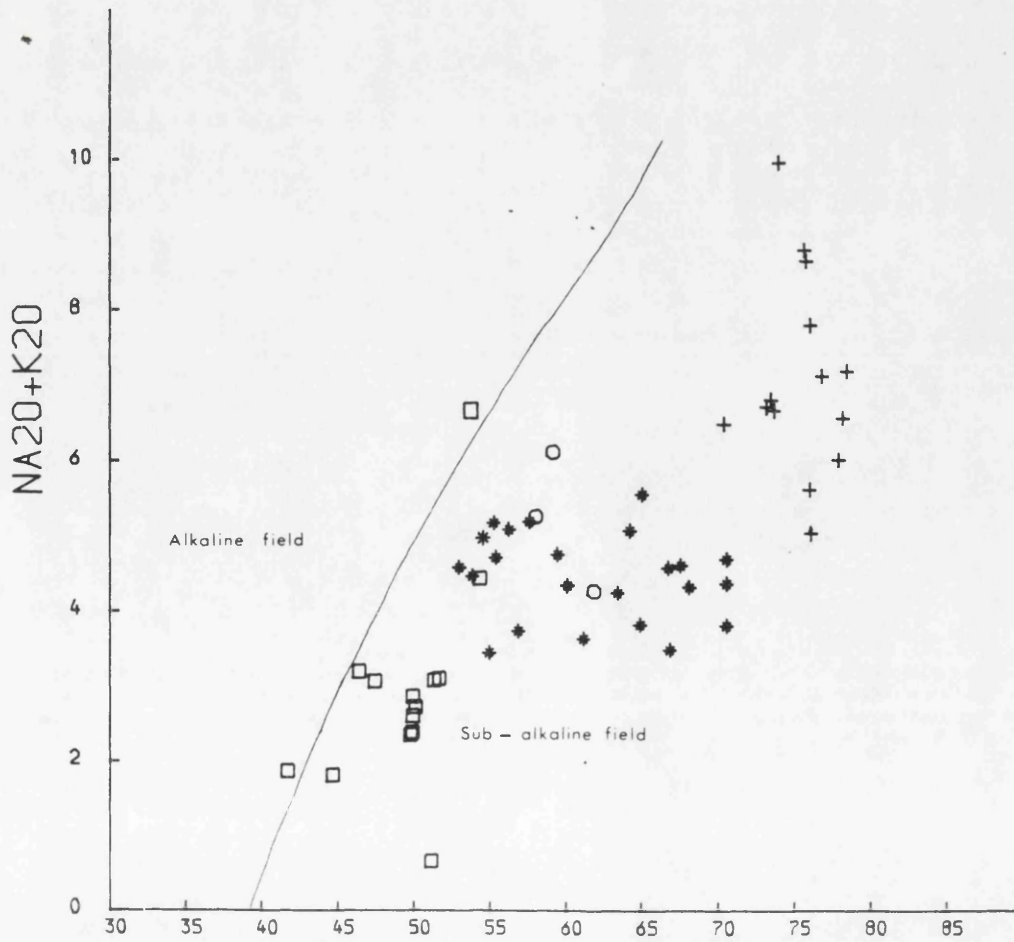
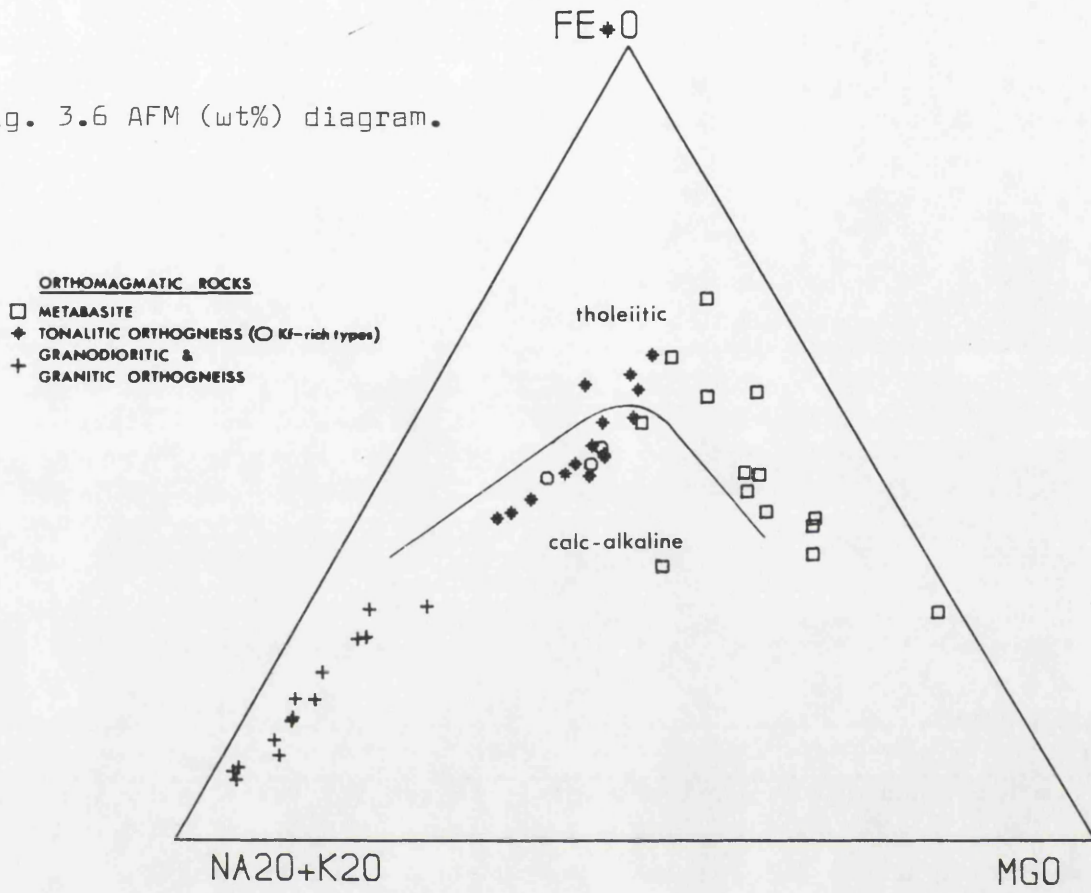


Fig. 3.5 $(Na_2O + K_2O)$ (wt%) v. SiO_2 (wt%) plot.

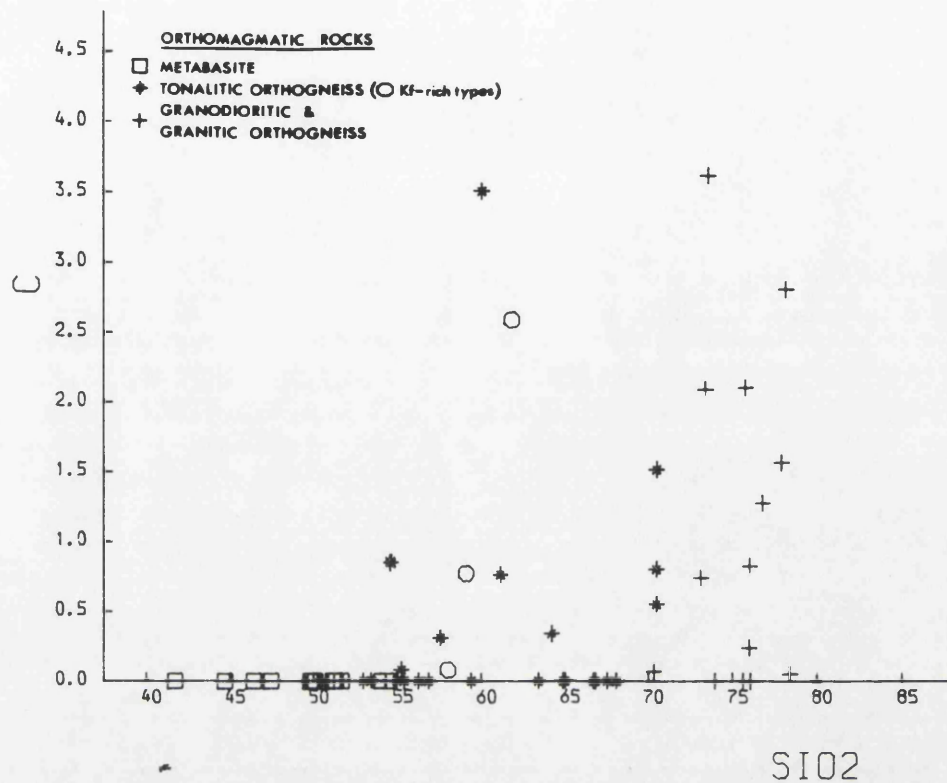


Fig. 3.8 Normative Corundum (C) v. SiO₂ (wt%) plot.

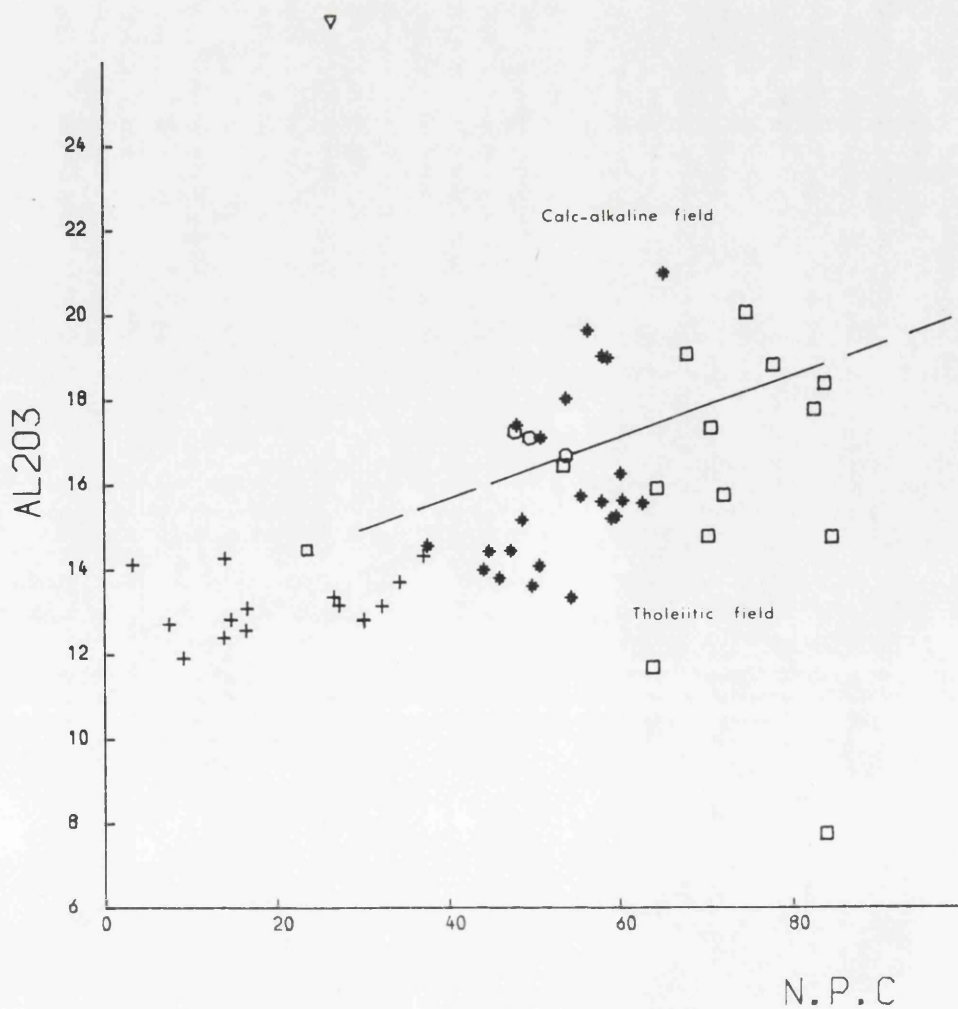


Fig. 3.7 Al₂O₃ (wt%) v. Normative Plagioclase Composition (N.P.C.).

dividing line for Hawaiian tholeiitic and alkaline rocks.

The $(\text{Na}_2\text{O} + \text{K}_2\text{O})$ -tFeO-MgO (AFM) wt% diagram, fig. 3.6, shows that the metabasites define a trend towards iron enrichment, characteristic of tholeiitic rocks. This, as previously stated, is due to the fractionation of high MgO/tFeO phases from the metabasite magma. However, tholeiitic magmas develop extreme iron enrichment, which was not the case with metabasite magma. This moderately Fe-rich magma began to evolve along what is essentially a calc-alkaline trend, ie. constant tFeO/MgO and progressive alkali enrichment. It may be that tholeiitic magma can evolve into typical calc-alkaline magmas, and that the metabasite magma underwent this transition in its latter stages of evolution, or alternatively, the metabasite-orthogneiss rocks may belong to a totally different kind of magmatic series, which has characteristics approximately transitional between the Calc-alkaline and Tholeiitic Series.

The Al_2O_3 wt% versus normative plagioclase composition (N.P.C) plot, fig. 3.7, is another that is used by Irvine and Barager to discriminate between basic to intermediate rocks of calc-alkaline and tholeiitic type. In this instance, the metabasites plot astride the dividing line and overlap each field equally. Whereas, in the previous plot, fig. 3.6, the tonalitic orthogneisses plotted mostly in the calc-alkaline field, in this plot the reverse is true. It is clear that the metabasite and orthogneiss rocks are neither typically calc-alkaline nor typically tholeiitic in their nature.

Cawthorn and Brown (1976), have shown that a trend towards corundum normative compositions occurs, with increasing SiO_2 , in many calc-alkaline rock suites. These authors relate this trend to the fractionation of hornblende from the magma. The rocks of the intrusive complex show such a trend (fig. 3.8), with most of the leucotonalitic orthogneisses and the granodioritic and granitic orthogneisses having corundum in the norm.

3.4 The Ab-An-Or-Q system.

Termed the "Granodiorite System" by von Platen (1965), the synthetic $\text{NaAlSi}_3\text{O}_8$ (Ab)- $\text{CaAl}_2\text{Si}_2\text{O}_8$ (An)- KAlSi_3O_8 (Or)- SiO_2 (Q) system has been used extensively to study the variations of the felsic components in granitoid rocks. The experimental phase relations are schematically presented in fig. 3.9b. The space of the Ab-An-Or-Q system is divided by three cotectic surfaces. A large cotectic surface (g-h-i-j, in fig. 3.9b) separates the principal phase field

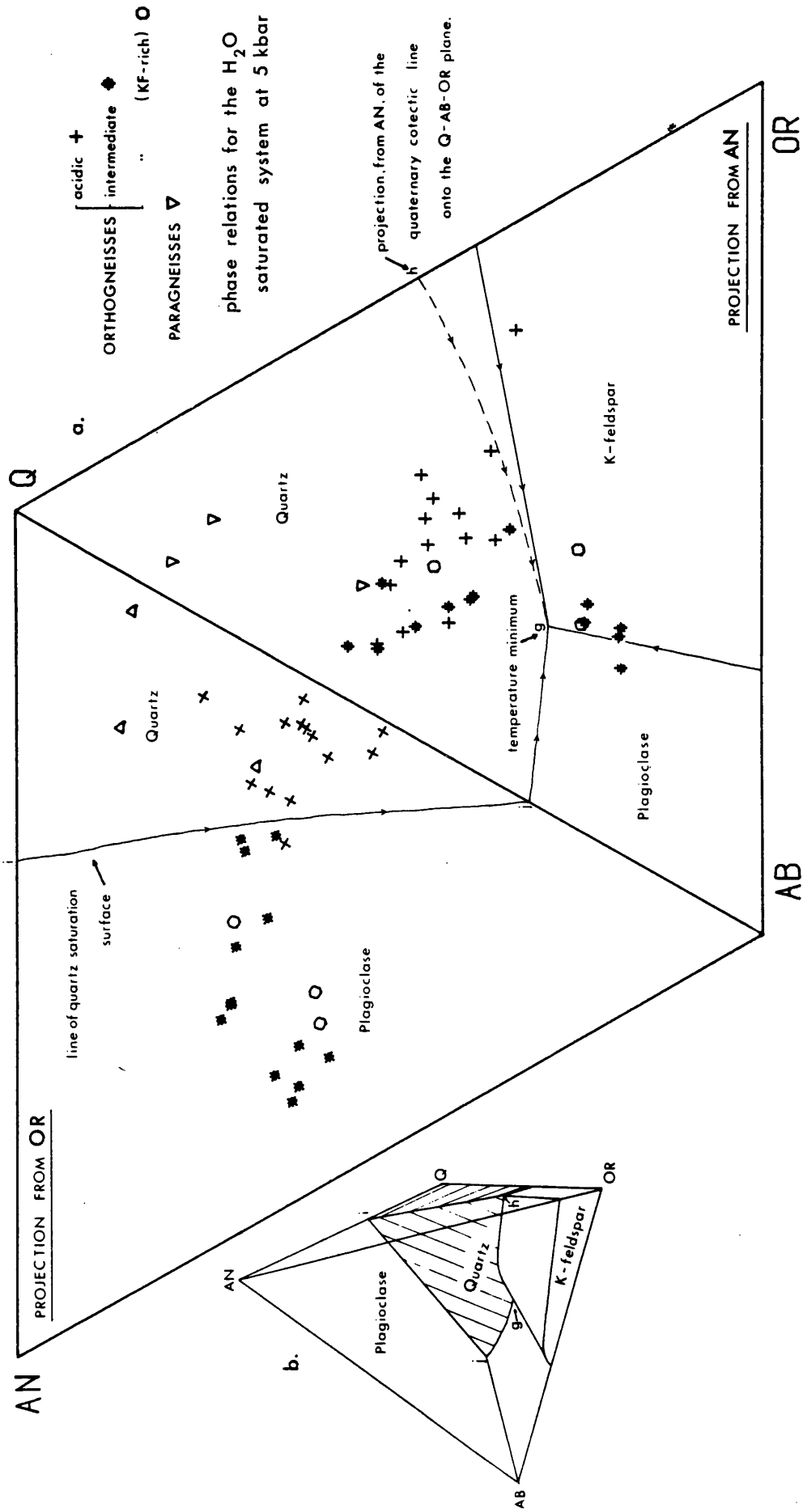


Fig. 3.9 a - Projections of the gneissic rocks in the normative Ab-An-Or-Q system.
 b - Schematic view of phase relations in the normative Ab-An-Or-Q system.

of quartz from that of plagioclase. This surface meets the two other cotectic surfaces, those between the K-feldspar-quartz and K-feldspar-plagioclase fields, at the cotectic line g-h. This cotectic line has a cotectic minimum, or eutectic, at g whose position in the system varies as a function of pressure and also the bulk normative Ab/An ratio (Winkler, 1976), but always remains in the low An part of the system.

The position of the orthogneisses in the Ab-An-Or-Q system are shown in the projections from Or onto the Ab-An-Q face and from An onto the Ab-Or-Q face (fig. 3.9a), together with the phase relations for the synthetic system at 5kbar pressure with excess H₂O (Presnall and Bateman, 1973). The rocks form a continuous array with the tonalitic orthogneisses plotting above the quartz saturation surface, in the field of plagioclase, and the granodioritic and granitic orthogneisses mainly plotting below, in the quartz field. All rocks contain more than 71% normative Ab + An + Or + Q.

The tonalitic orthogneisses, as a whole, define a normative quartz enrichment trend, with this trend being less pronounced in the most quartz normative varieties. The granodioritic and granitic orthogneisses define a rather diffuse trend of normative K-feldspar enrichment.

Mineralogical and textural criteria described in the previous chapter, indicate that, in relation to the Ab-An-Or-Q system, the evolving tonalitic magma moved through the plagioclase phase field crystallising both plagioclase and hornblende. The depletion in these components pushed the magma composition progressively towards the quartz saturation surface and, at some point, intersection of this surface occurred. At this stage the magma's composition was probably similar to that of the leucotonalitic orthogneiss, and the magma began to crystallise quartz in addition to plagioclase and hornblende as it moved along the quartz-plagioclase cotectic surface. The presence of anhedral potash feldspar phenocrysts in the granodioritic and granitic orthogneisses indicates that this magma was now capable of reaching the cotectic line before completely solidifying.

Three mobilisate rocks from the paragneiss are also represented in fig. 3.9a and the plot close to the quartz apex of the tetrahedron. Many granitic rocks have compositions which

cluster in the region of the eutectic point, in the Ab-An-Or-Q system (Winkler, 1976). The melt produced in the extreme anatexis of quartz-rich, plagioclase-mica schists, would evolve, from the region of the eutectic, along the quartz-plagioclase cotectic surface until all of the plagioclase was extracted from the residue. Further melting would involve quartz and biotite, only, and the melt composition would leave the quartz-plagioclase cotectic, in the direction of the Q apex. The mobilisate rock appears to represent the melt which forms at this stage of the anatexis of metasediment. Further discussion on the exact nature of the paragneiss components and the possible temperature of their formation, occurs in section 3.7.

3.5 The CMAS system.

In this study, use is made of O'Hara's (1976) data reduction scheme which converts rock and mineral analyses to four composite components, $XO-YO-R_2O_3-ZO_2$, thereby reducing the complexity of the chemical data so that it may be represented in a single, 3-dimensional, quaternary system. The components are calculated in terms of equivalent weights of CaO, MgO, Al_2O_3 , and SiO_2 , respectively: for example, the YO proportion of the system consists of

$$(\text{mols. of MgO} + \text{MnO} + \text{NiO} + (\text{FeO} - \text{TiO}_2)) \times \text{mol.wt. of MgO}$$

, where FeO, MnO, and NiO all commonly substitute for MgO in mineral structures. TiO_2 is incorporated into the R_2O_3 component as moles of ilmenite, $FeTiO_3$, and this is the reason for the subtraction of an equal number of moles of FeO from the YO component. The complete data reduction with the four components formulated in terms of equivalent weight percentages of the whole system, is as follows:-

$$XO = 100(\text{mols. of CaO} - 3\frac{1}{2}P_2O_5 + 2Na_2O + 2K_2O) \times 56.08 / \text{SUM}$$

$$YO = 100(\text{mols. of MgO} + \text{FeO} + \text{MnO} + \text{NiO} - \text{TiO}_2) \times 40.32 / \text{SUM}$$

$$R_2O_3 = 100(\text{mols. of } Al_2O_3 + Fe_2O_3 + Cr_2O_3 + TiO_2 + Na_2O + K_2O) \times 101.96 / \text{SUM}$$

$$ZO_2 = 100(\text{mols. of } SiO_2 - 2Na_2O - 2K_2O) \times 60.085 / \text{SUM}$$

, where SUM equals the sum of all four components, ie. $XO + YO + R_2O_3 + ZO_2$.

In this thesis, the system components XO, YO, R_2O_3 , and ZO_2 are referred to as C, M, A, and S, respectively, and care should be

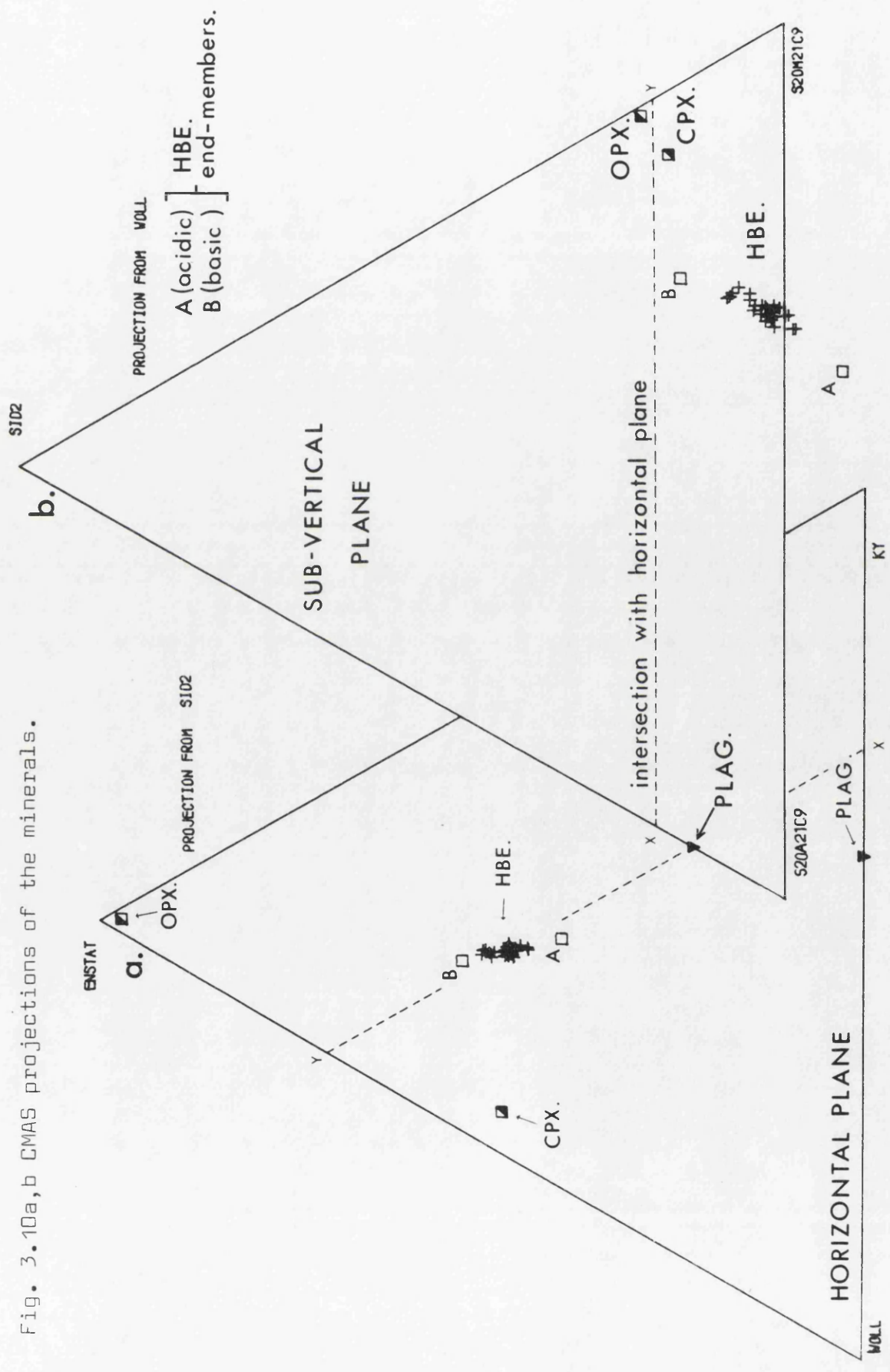
taken not to confuse these CMAS components with the analogous components of the $\text{CaO-MgO-Al}_2\text{O}_3\text{-SiO}_2$ system.

Once the CMAS coordinates of a set of rock, or mineral, analyses have been calculated, those rocks, or minerals, can be plotted in the 3-dimensional space of the CMAS tetrahedron. Those rocks composed of only one of the four components plot at that particular component apex of the tetrahedron, and those composed of only two of the components plot along the edge of the tetrahedron that join these two components. Rocks composed of three of the four components plot in the face of the tetrahedron which has those three components at its three apices, and rocks composed of a combination of all four components plot inside the tetrahedron. Each edge of the tetrahedron is linearly divided into 100 divisions with each division representing one percent of the total C+M+A+S. Therefore, a rock plotting at the point S40A60 would contain 40% S component, 60% A component and none of the C and M components, and consequently would lie on the join S-A, closer to A than S.

3.5.1 Minerals in the CMAS system.

The positions, in the CMAS system, of the 28 hornblendes analysed in this study, and the hypersthene, augite and bytownite from metabasite BK102, are shown by the two projections of fig. 3.10. Also shown, are the positions of the hypothetical hornblende end members, A (= acidic hornblende) and B (= basic hornblende), used earlier to calculate some of the modal estimates. Fig. 3.10a is a projection from the S apex of the tetrahedron, where quartz plots, onto the horizontal median plane, En-Woll-Ky, and fig. 3.10b is a projection from wollastonite onto an almost vertical projection plane, S-S20A21C9-S20M21 (S20A21C9 represents the components S, A, and C in the ratio 20:21:9). These projection planes intersect along the join X-Y, with the S-S20A21C9-S20M21C9 plane extending below the level of the horizontal median plane of the tetrahedron (see fig. 3.13 for a 3-dimensional view of the whole CMAS system). From fig. 3.10b, it is clear that both pyroxenes and also plagioclase feldspar plot close to the level of this horizontal median plane. The hornblendes, however, plot significantly below it and, both igneous and metamorphic varieties, form a single linear array which points down to the centre of the basal C-M-A plane of the tetrahedron. The most SiO_2 deficient hornblendes, ie. those which plot the furthest below the horizontal

Fig. 3.10a,b CMAS projections of the minerals.



median plane, occur in the more acidic rock types. Biotite will not be considered as a fractionation phase since there is very good Rare Earth element evidence (Chapter 4) that hornblende fractionation occurred even in the most acidic orthogneiss magma. In addition, the true nature of the biotite in the acidic orthogneiss rocks, ie. primary or secondary after hornblende, is difficult to ascertain because biotite is invariably associated with alteration products such as chlorite and epidote.

The projection from SiO_2 onto the horizontal median plane, En-Woll-Ky (fig.3.10a), is useful because clinopyroxene and orthopyroxene plot in it at totally different positions. The influence of the two pyroxene types on magmatic differentiation can be assessed from this projection.

3.5.2 Rocks in the CMAS system.

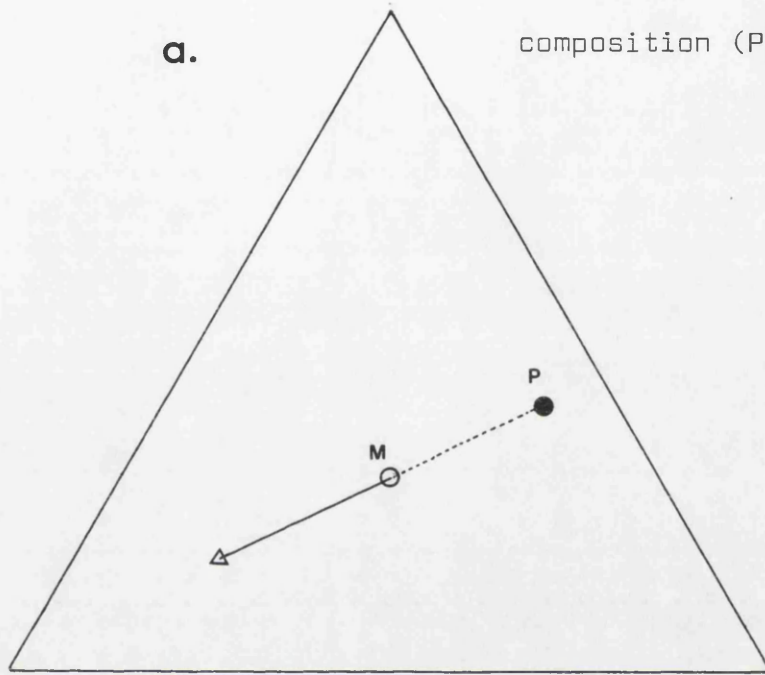
The distribution of the metabasites and the orthogneisses in the CMAS system is shown by the three projections in fig. 3.12. Two of the projections, fig. 3.12a,b, are the same as in fig. 3.10, and the other, fig. 3.12c, is a projection from enstatite onto the plane S-C60S40-A60S40, which is part of the S-C-A face of the tetrahedron. On all three projections, a continuous trend occurs from the metabasite through tonalitic orthogneiss to granitic orthogneiss, although changes in the trend direction are evident at the metabasite-tonalitic orthogneiss junction and in the region of the SiO_2 -rich tonalitic orthogneiss.

This continuous trend is evidence, though not conclusive evidence, that the rocks are all descended from the same basic magma, and it also indicates that they are related by the process of fractional crystallisation. This fractional crystallisation hypothesis will first be examined, and then other possible models will be discussed.

However, to begin with, it is necessary to understand the way in which a magma's composition will change in CMAS space during the fractionation process. A magma, from which a single phase is fractionating, will become progressively depleted in those components which have a phase/magma ratio greater than unity. If, in the CMAS system, the magma had an initial composition represented by a point M and the phase, a fixed composition located at point P, then successive magma differentiates would migrate from M in a direction away from the location of the phase, at P. The

Fractionation from a magma (M)
of a phase of fixed
composition (P).

a.



Fractionation from a magma (M-M3)
of a phase of changing
composition (P-P3).

b.

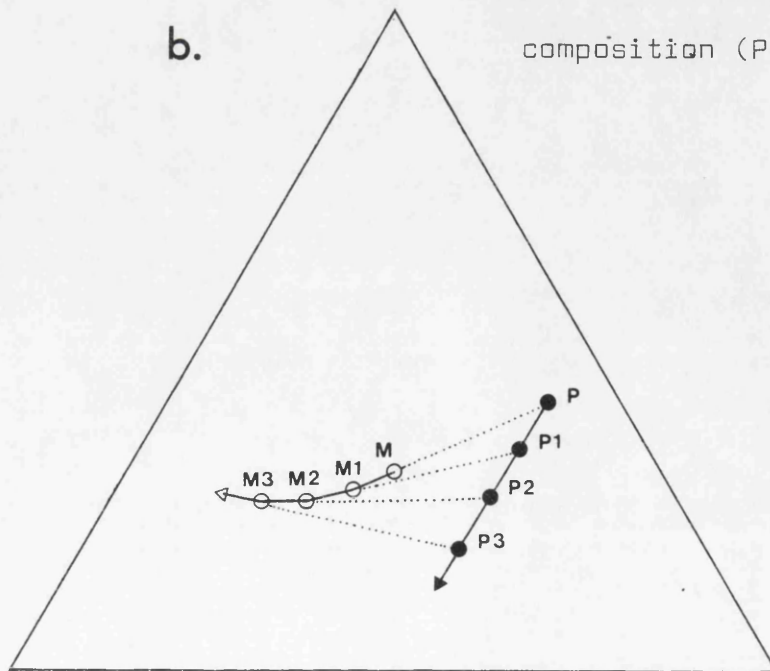


Fig. 3.11a,b Simple magma evolution models.

magmas would form a linear array on the projection of the line PM (fig. 3.11a). Fractionation of a phase whose composition varies linearly in the CMAS space, in response to a changing melt composition, will generate successive magmas which define a curved array (fig. 3.11b). If two phases crystallised from the magma, instead of just one, and if their compositions and the ratio of their relative proportions remained constant, then the total crystal fraction would have a fixed composition. This case is therefore equivalent to the fixed composition, single phase fractionation model, described above.

In natural systems, however, the bulk composition of the crystal fraction will rarely be constant during fractionation, since both phase compositions and proportions will vary continuously, in response to the changing magma composition. Hence, the successive magmas formed by fractional crystallisation in natural systems should define a smooth, but irregular, curve in the CMAS space. Abrupt changes in direction at various points on the curve may be brought about by the stabilisation of a new phase at the liquidus of the magma, or by the disappearance of an existing phase.

The continuous trend of the igneous rocks in the intrusive complex, in CMAS space, can be easily described in terms of three segments corresponding to the three principal rock groups.

The metabasites as shown in fig. 3.12a,b,c plot below the horizontal median plane, En-Woll-Ky, and form an array of points running sub-parallel to the join X-Y. They display a pronounced progressive depletion of the M component and a slight depletion in the S component. Hornblende plots well below the metabasite trend (fig. 3.12b), therefore any fractionation of hornblende would have caused a significant increase in the proportion of the S component in the metabasite magma. This enrichment is not observed, at least not until at the junction of the metabasite and tonalitic orthogneiss trends, and so hornblende fractionation from the metabasite magma is precluded.

Thus, the conclusion, made in the previous chapter, that the hornblende in the metabasites is metamorphic in origin is confirmed in this fractionation model. This same argument also makes it clear that olivine fractionation could not have occurred over the range of magma compositions represented by the metabasite samples (olivine plots midway along the join enstatite-M and if fractionated from the magma would cause a marked SiO_2 enrichment).

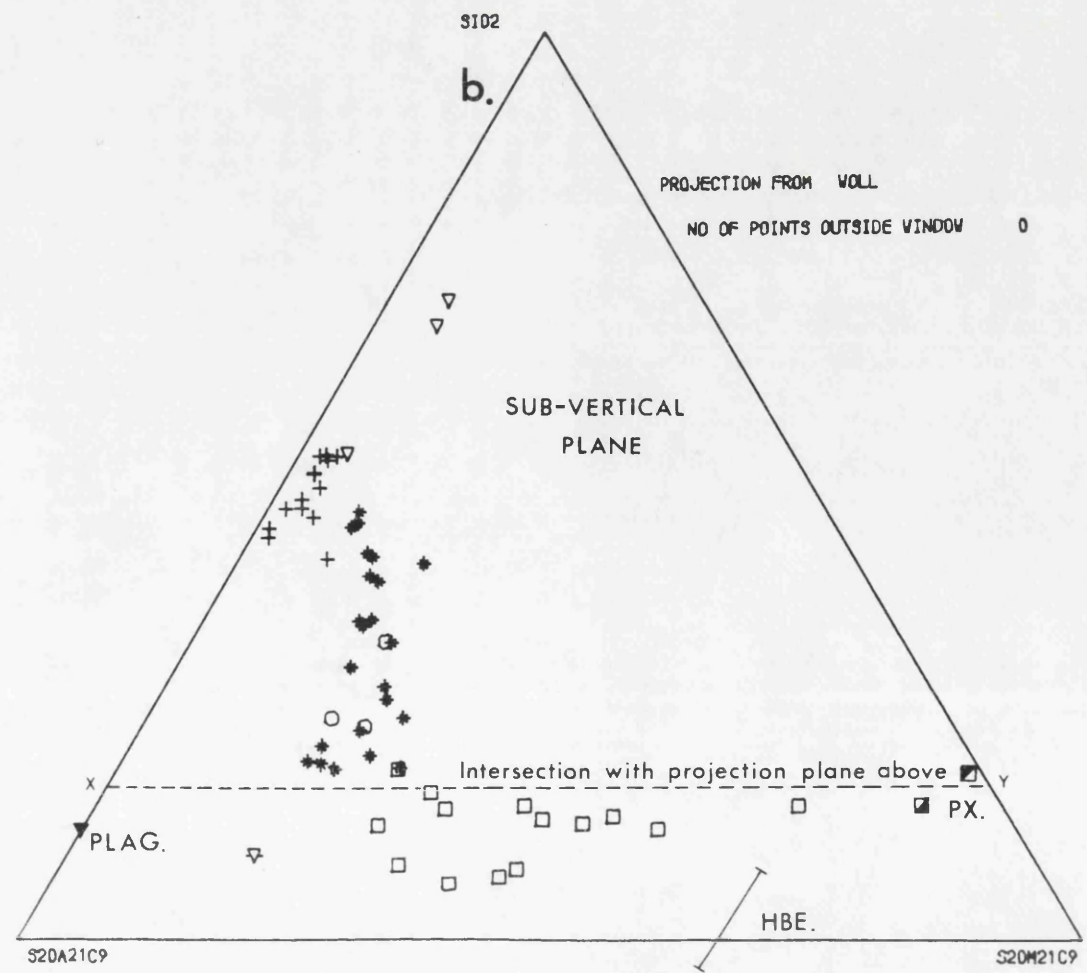
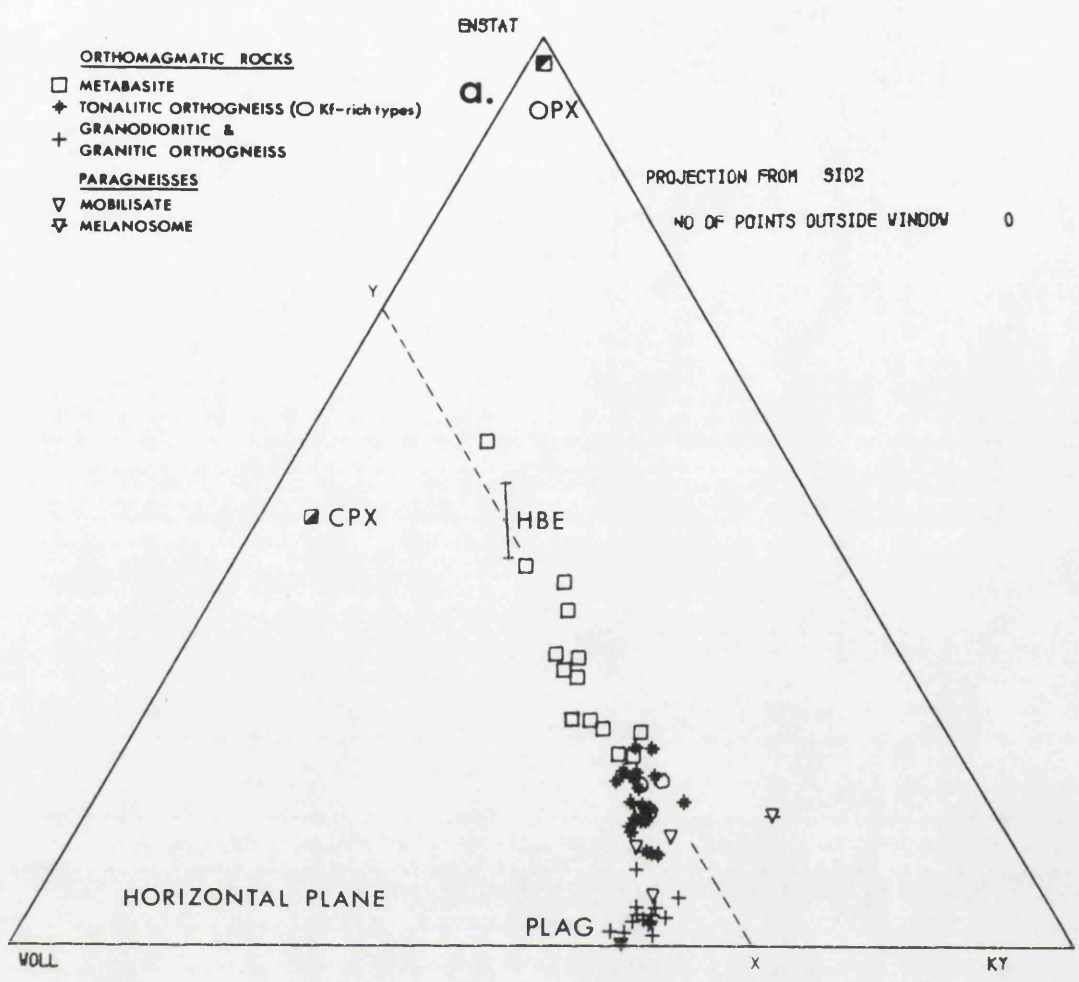


Fig. 3.12a,b,c CMAS projections of the rocks and minerals.

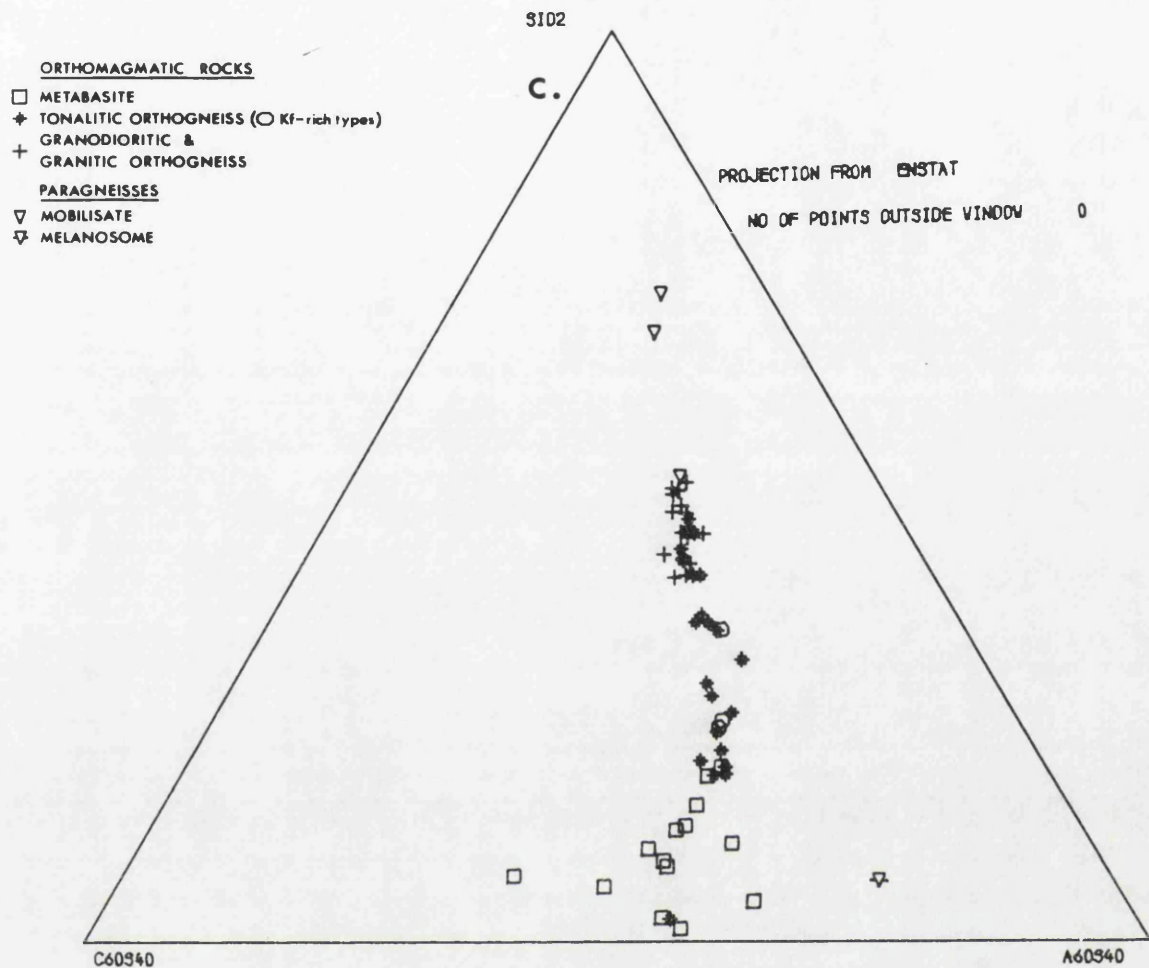


Fig. 3.12 (continued)

The disposition of the projection planes a, b, and c, relative to each other and to the whole CMAS system is shown in the following figure, Fig. 3.13.

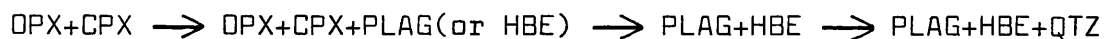
Pyroxene seems to be the only mafic phase able to produce the metabasite trend and fig. 3.12a indicates that both orthopyroxene and clinopyroxene fractionated from the magma in roughly constant proportions, as shown by the linear array of points. The progressive shift of the metabasite rocks towards the location, in the CMAS system, of plagioclase precludes fractionation of this phase.

The trend of the metabasite rocks merges with that of the tonalitic orthogneiss, just above the horizontal median plane, En-Woll-Ky. The slight upturn at the end of the metabasite trend may be due to the stabilisation of plagioclase or hornblende, at the liquidus of the magma.

The tonalitic orthogneisses form an array of points in the CMAS system which define a trend of extreme silica enrichment (fig. 3.12b,c), while the proportions of other components remain constant relative to each other. This rapid concentration of SiO_2 in the magma must be due to a combination of plagioclase and hornblende fractionation and this would agree with the observed presence of primary hornblende in the melanocratic tonalitic orthogneiss.

The most SiO_2 -rich tonalitic rocks define a gentle curve towards the S-C-A face of the CMAS tetrahedron and pass into the granodioritic and granitic orthogneisses. This significant directional change probably represents the incoming of quartz as a stable phase at the liquidus of the magma as is forecast by the previous study of the orthogneiss rocks in relation to the Ab-An-Or-Q system.

Thus the sequence of crystallisation in this fractional crystallisation model is:-

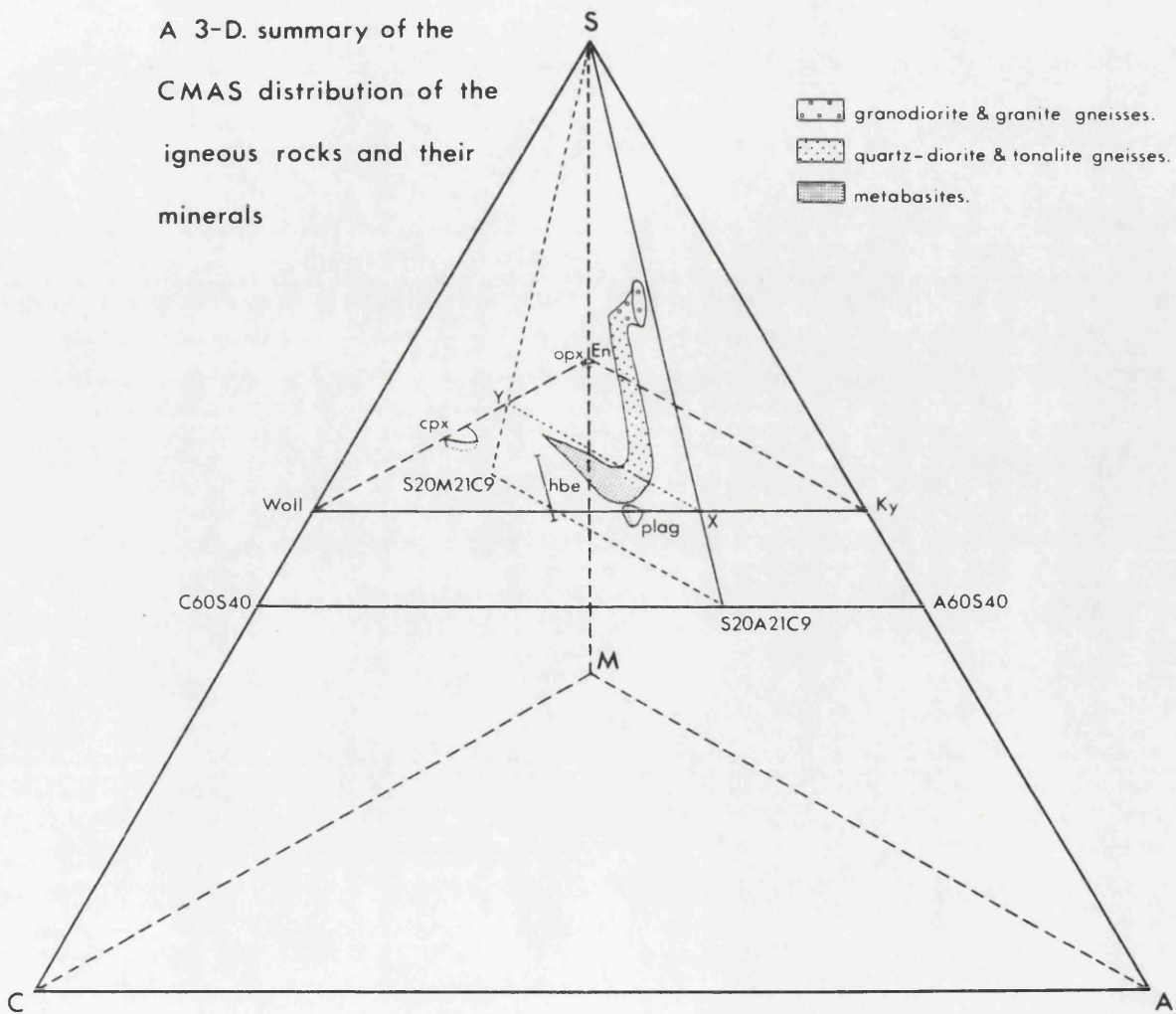


,where the fractionation assemblage PLAG+HBE is stabilised in a magma containing approximately 55 wt% SiO_2 (recalculated without the water content).

Another model which might explain the CMAS trend of these rocks is one of assimilation. As shown in the previous chapter there is compelling evidence for the assimilation of paragneiss by the tonalitic orthogneiss magmas. Three samples of mobilisate and one of melanosome, from the paragneiss, are plotted in the projections of fig. 3.12. A line joining the mobilisate and

Fig. 3.13

A 3-D. summary of the
CMAS distribution of the
igneous rocks and their
minerals



melanosome rocks, in the CMAS system, defines a mixing line near to which the parent metasediment would lie. This line probably also approximates to the array of points representing the various compositions of the mobilisate and melanosome for different degrees of partial melting of the parent metasediment.

It is clear from the lack of significant SiO₂ enrichment along the metabasite trend, that contamination of the more primitive basic magmas, by siliceous paragneiss, was negligible. On the other hand, the wholesale assimilation of paragneiss by the most fractionated Fe-rich metabasite and the melanotonalitic orthogneiss magmas, would certainly contribute to the extreme SiO₂ enrichment trend shown by the tonalitic rocks. The incorporation of siliceous mobilisate similar to that analysed in this study would also deplete the magma in its tFeO content, a feature which is necessary if the metabasite magma evolved into the melanotonalitic orthogneiss magma. Furthermore, it has already been suggested that the alkali distributions in the tonalitic orthogneisses could be partly a product of the assimilation of paragneiss by the tonalitic magmas. Therefore, it is thought that the assimilation of paragneiss may have had an important influence in the petrogenesis of the orthogneiss rocks. This hypothesis will be further discussed in relation to the trace elements, in the following chapter.

Recently, White and Chappell (1977), proposed that some tonalites were the partial products of the ultrametamorphism of andesitic rocks. Their model involves the generation of diapirs of granodiorite partial melt and mobilised restite material, in the form of xenocrysts and xenoliths. Progressive separation of the restite from the partial melt occurs as the diapirs rise through the crust, leaving behind tonalite masses which have never been molten. Conveniently, in the model, the restite continuously re-equilibrates with the surrounding magma, so that geochemically this process is practically indistinguishable from equilibrium partial melting or equilibrium fractional crystallisation. As Chappell and White correctly point out, their model does differ from these two equilibrium processes in one aspect. The temperature of formation of these tonalite masses would be no more than granodiorite liquidus temperatures, ie. 900°C, 8kbar, 8 wt% H₂O, undersaturated melt, (Naney and Swanson, 1980). It is thought that this maximum temperature of emplacement would be too low to fuel

the large scale melting episode which formed the paragneiss rocks, and therefore this model is rejected.

The possibility that the metabasites, tonalitic orthogneisses, and granitic orthogneisses actually represent three unrelated magma types, produced from three different sources, and that they coincidentally form a smooth continuous trend on all major element variation diagrams, is not thought to be likely. However, this hypothesis will be further tested in the following chapters.

3.6 Phase relations across the join gabbro-tonalite-granite.

Phase relations across the join gabbro-tonalite-granite depend to a large extent on the amount of H_2O that is present in the system. This fact was clearly shown by Wyllie (1977, 1979) who, drawing upon the many experimental studies in geological literature, presents an excellent review of the present knowledge on the effects of volatiles on the phase relations of magmas. Unfortunately, however, the amount of H_2O dissolved in a magma at depth is not quantitatively known, and this uncertainty has considerably hampered the formation of concepts of magma genesis and evolution.

The presence of H_2O in a rock considerably lowers the temperature at which it begins to melt and also the temperature at which it is completely molten. It is a widely held view that basic magmas are generated in the mantle from a source which contains a small volatile content, held principally in hydrous phases. The H_2O content in basaltic magma is estimated to be less than 1 wt% for ocean ridge basalts (Moore, 1965), and up to 3 wt% in basalts erupted above subduction zones (Anderson, 1980). A basic magma, rising through the upper mantle and into the lower crust, would crystallise both garnet, at pressures greater than 15 kbar, and clinopyroxene (Stern and Wyllie, 1978). Also, Allen and Boettcher (1978) have shown that amphibole and H_2O undersaturated melt are stable in a bulk basaltic composition at 1050°C, 15 kbar, although amphibole is by no means close to the liquidus of a basaltic magma under these conditions. Orthopyroxene joins clinopyroxene as a liquidus phase at pressures of around 10 kbar and fractionation of these two phases would cause a marked enrichment of Al_2O_3 and the alkalis in the magma but keep its SiO_2 content steady.

Clearly, orthopyroxene-clinopyroxene fractionation does not produce magmas of intermediate composition. If intermediate magmas

are to be formed by fractional crystallisation from a basic magma, then, a low-SiO₂ phase, such as amphibole, must fractionate. This problem has been the subject of much debate, with some workers advocating hornblende fractionation from already highly fractionated basic magmas as the mechanism of producing intermediate calc-alkaline magmas (Cawthorn and O'Hara (1976), Cawthorn and Brown (1976), Allen and Boettcher (1978), Anderson (1980)). Others, including Egglar and Burnham (1973), and Wyllie (1977), dispute that hornblende fractionation is a likely process because of the degree of saturation needed in the parent magma for amphibole to be the primary liquidus phase (ie. the first phase to crystallise) or a 'near primary' liquidus phase.

Egglar and Burnham (1973) determined the phase relations of a Mt. Hood andesite as a function of H₂O concentration up to 10 kbar pressure. They found that amphibole did not become the primary liquidus phase even under saturated conditions. Alternatively, Allen and Boettcher (1978) found that amphibole did exist near to the liquidus of another Mt. Hood andesite, at undersaturated conditions of above 10 kbar pressure. Using field and textural data, Anderson (1980) suggests that amphibole may fractionate, by means of a reaction relationship with olivine, from magmas at least as basic as basaltic andesite, but concedes that experimental work indicates that this cannot happen unless a minimum of 6 wt% H₂O is dissolved in the magma.

Amphibole is further stabilised, at the liquidus, in increasingly acidic bulk compositions. Since the effect of amphibole fractionation is to markedly increase the SiO₂ content of the magma, the process is self perpetuating. Amphibole is the primary liquidus phase of a granodiorite melt containing more than 4 wt% H₂O at 8 kbar pressure (Naney and Swanson, 1980).

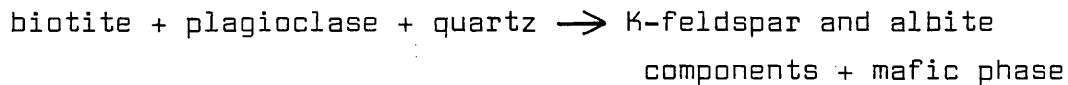
As amphibole is stabilised nearer to the liquidus of a basic magma with increased H₂O content, so plagioclase is destabilised. This effect is added to the, also, destabilising effect of increased pressure, ie. plagioclase is not the primary liquidus phase of any bulk composition at pressures greater than 15 kbar, even under dry conditions (Wyllie (1977), Allen and Boettcher (1978), Wyllie (1980)). Plagioclase is not the primary liquidus phase of basaltic magma at any temperature, pressure or degree of H₂O saturation. However, Allen and Boettcher (1978)

showed that plagioclase is the primary liquidus of a Mt. Hood andesite in undersaturated conditions at pressures of over 10 kbar. Furthermore, Egger and Burnham (1973) discovered that it is the primary liquidus phase of another Mt. Hood andesite, at 5 kbar pressure, even under H_2O saturated conditions. The pronounced stability of plagioclase in Egger and Burnham's experiments on the andesite may well represent the peak of plagioclase stability, in terms of the bulk composition of the system. Naney and Swanson (1980) found that plagioclase was well below the liquidus of a slightly undersaturated (10 wt% H_2O) granodiorite composition at 8 kbar, and was some $300^\circ C$ below the liquidus of a granite composition under exactly the same conditions. In the latter case, alkali feldspar and quartz were both stable to higher temperatures than plagioclase, which was stable only up to a few $^\circ C$ above the solidus. This fact is significant, in terms of the granitic orthogneiss mineralogy, because of the total lack of sodic plagioclase in these rocks. Plagioclase was obviously unstable in the acidic orthogneiss magmas, a theory supported by the presence of corroded remains of andesine. The andesine must then represent an early crystallised phase which has remained suspended in the viscous granitic magma. An estimate of the degree of H_2O saturation of the granitic orthogneiss magma, from these mineralogical relationships would depend, to a large extent, on the depth at which the magma crystallised.

The following fractionation scheme may well apply to the granitic orthogneiss magma. A granodiorite magma, containing 7-8 wt% H_2O , would fractionate hornblende (and/or biotite) and plagioclase at a pressure of 8 kbar (30 km depth), (Naney and Swanson, 1980). If batches of the magma were periodically released, and rose to higher levels (ie. lower pressures) in the crust, then, during the ascent, these magmas would eventually become H_2O saturated, because H_2O is less soluble in magmas at lower pressures. The effect of increased H_2O saturation would be to rapidly lower the temperature of stability of plagioclase and crystallisation of this phase would cease. Plagioclase crystals, carried up in suspension within the magma, would become unstable and would be resorbed. Once the magma becomes completely saturated, any further drop in pressure would lead to rapid solidification (Harris, 1977) with the crystallisation of quartz and potash feldspar.

3.7 Phase relations in the anatexis of metapelitic rocks.

Melting relations of pelitic gneisses have been described by Knabe (1970a,b), Steuhl (1962), and Winkler (1976, Chapter 18). Knabe's experiments, conducted on biotite-plagioclase-quartz rocks at H₂O pressures of 2 kbar, demonstrated that the following biotite degradation reaction controls the rate of melting of the bulk material:-



, where the k-feldspar and albite components combine with quartz to produce melt. The mafic phase formed in this reaction depends on the composition of the biotite. The breakdown of Fe and Ti rich biotite produces ilmenite as the main residual phase.

These experiments confirmed the results of Steuhl who had melted paragneiss consisting of 40% plagioclase, 28% quartz, 22% biotite, and 10% K-feldspar, at 2 kbar pressure with excess H₂O. The first melt to form had a composition on the cotectic line, in the Ab-An-Or-Q system, in equilibrium with all pre-heating phases. At 710°C all of the K-feldspar had melted and the melt had moved on to the melt + plagioclase + quartz cotectic surface. A further increase in temperature melted all the the quartz by 760°C, and by the time 800°C had been reached, 84% of the original gneiss had melted. At this stage in the experiment, the melanosome component was composed of 44% plagioclase, 37% opaque ore and 19% biotite. The melanosome plagioclase was andesine, An₃₇, compared with the oligoclase, An₂₇, in the original gneiss.

These experimental melanosomes bear a strong resemblance to the melanosome of the Connemara paragneiss, which, in many cases, has a mineralogy composed of sillimanite, ilmenite, biotite, and plagioclase, up to An₄₃. There is also evidence for the biotite degradation reaction, forecast by Knabe (1970a,b), in the texture of the natural melanosome (see Chapter 2, section 2.3.3), though this reaction differed from the experimental one, in that it involved the formation of sillimanite, as well as ilmenite and the melt components. This incongruent biotite melting reaction was also identified by Nedelec and Paquet (1981) who studied high-grade paragneisses from the Haut Allier (French Massif Central).

The Dalradian metasediments flanking the intrusive complex,

to the north, typically contain no K-feldspar, even though they are high amphibolite grade rocks (Treloar, 1977, thss.). They have a mineralogy composed of variable proportions of quartz, plagioclase, biotite and muscovite, with accessory garnet and other minor phases. The melting relations of metasediments containing biotite and muscovite, but no K-feldspar, have been discussed by Winkler (1976). In these rocks, anatexis is triggered by the release of K-feldspar component and H_2O in the breakdown of muscovite at temperatures just above the water present granite solidus. With increasing temperature the muscovite breakdown reaction proceeds rapidly, and a correspondingly high rate of melting occurs. However, when the muscovite disappears, at temperatures probably less than $20^\circ C$ above the first melting temperature, the rate of melting drops markedly, and is controlled by the sluggish biotite breakdown reaction. Biotite becomes metastable above $655^\circ C$, at 5 kbar, in the presence of albite + sillimanite + quartz + H_2O (Hoffer, 1978). However, albite is not usually present as a separate phase in paragneisses, rather it is held in solution in plagioclase, usually andesine. If equilibrium is maintained the albite component should diffuse out of the plagioclase structure and react with the biotite to form melt. This happens only to a limited degree, because of the tendency of intermediate plagioclase to react, or melt, almost stoichiometrically (Johannes, 1980). Large temperature increases are needed to produce further, significant, melting in these rocks and the resultant melt becomes H_2O undersaturated.

The temperature required to melt a set proportion of any rock, is much higher for undersaturated conditions ($P_{H_2O} < P_{Total}$), than for saturated conditions ($P_{H_2O} = P_{Total}$), and in rocks with low concentrations (<2 wt%) of H_2O , liquidus temperatures approach those of the dry system. Furthermore, the temperature range, over which undersaturated melting can occur, ie. the difference between the water present and dry liquidus, expands with increasing pressure, due to the enhanced solubility of H_2O in the magma. The temperature range of undersaturated melting may be in excess of $200^\circ C$ for a rock of granitic composition (fig. 2a, Naney and Swanson, 1980).

The mobilisate rocks of the Connemara paragneisses are extremely siliceous (fig. 3.9a) and obviously do not represent minimum melts. White and Chappell (1977), and Winkler and Breitbart (1978), suggest that granitic rocks derived from partial melting of

metasedimentary gneisses may not always represent the actual melt, but the melt plus suspended xenocrystic material carried up from the magma source. In the mobilisate, the suspended xenocrystic material, if there was any, would have been mainly quartz. However, in the field, there are many examples of large xenolithic blocks of siliceous semipelite which are in an advanced state of assimilation, and these suggest that xenocrystic quartz could not have persisted in the melt. The liquidus temperature of such a siliceous^{water-}undersaturated melt would be close to 900°C.

3.8 Conclusions.

Although the rocks of the metabasite-orthogneiss suite belong to the Subalkaline division, they possess chemical features which are neither typically calc-alkaline, nor typically tholeiitic, in nature. The metabasite rocks do, however, show some affinity with tholeiitic rocks, ie. early Fe enrichment, while the orthogneisses have an affinity with calc-alkaline rocks, ie. constant $t\text{FeO}/\text{MgO}$, and SiO_2 enrichment.

The majority of the metabasite and orthogneiss samples do not represent cumulate rocks, having compositions which are probably close approximations to the compositions of the magma from which they formed. These rocks define continuous, often non-linear, trends in all major element plots, which indicates that they are all comagmatic and related by the process of fractional crystallisation.

The metabasite magma evolved by the fractionation of both clino- and ortho-pyroxene, and consequently became progressively Fe enriched and Si depleted. However, at some point, these trends were reversed, possibly by a combination of the additional fractionation of a Fe-Ti ore, and the assimilation of siliceous, Fe-poor, paragneiss. The magma evolved towards melanotonalitic orthogneiss compositions (roughly andesitic), and the two-pyroxene fractionation assemblage was superseded by a plagioclase + hornblende assemblage. The fractionation of the latter assemblage produced the extreme SiO_2 enrichment trend shown by the tonalitic orthogneisses. The H_2O content of the melanotonalitic orthogneiss magma is estimated at 6-8 wt% on the basis that hornblende crystallisation would not occur at levels below this. The H_2O content of the magma built up as fractionation continued, and as a result of this, in the leucotonalitic orthogneiss magma, plagioclase

became unstable near to the liquidus and ceased to fractionate. The last formed plagioclase crystals did not separate completely from the viscous acidic magma and they were partially resorbed. Quartz began to fractionate in addition to hornblende and the magma composition evolved to those of the granodioritic and granitic orthogneisses.

The mineralogy and textures in the melanosome component of the paragneiss are consistent with those observed in the experimental partial melting of quartz-plagioclase-mica schist. The very calcic nature of the plagioclase, An₄₃, indicates that high temperatures were reached during the M3 anatectic event. This is also confirmed by the siliceous nature of the anatectic melt, the mobilisate component of the paragneiss. A peak temperature of c. 900°C is estimated for this event, in the paragneiss.

Chapter 4.

Trace Element Geochemistry of the Rocks of the Intrusive Complex.

In the preceding chapter, the metabasite-orthogneiss samples were treated as though they represent the various compositions of a single evolving magma, even though they have been taken from the many different intrusions and intrusive masses which occur within the field area. This generalisation is justified, in that, although the rocks may be of more than one magma, if these magmas had similar initial compositions, in terms of the major oxides, then intruded into the same environment, ie. the same thermal and tectonic regimes, they should have similar fractionation histories. They should also have magma differentiates which, when taken all together, define the fractionation history of a single composite magma. The studies of the previous chapter indicate that the metabasite-orthogneiss rocks do show such a feature.

Unfortunately, the same generalisation cannot be made with anything like the same confidence for the trace elements. Trace element concentrations are extremely sensitive to even minor variations in a magma's composition and phase relations, its degree of fractionation, and in the amounts of country rock material that it assimilates. Therefore, magmas which are initially similar both in major and trace element composition, may diverge significantly in their trace element compositions during fractionation and intrusion. Thus, in the trace element plots that form the core of this chapter, the trace element distributions should not be expected to define trends that are as well defined as those of the major oxide distributions. Trends that do occur will probably be composite and, in their scatter, they will illustrate the range of variation of the trace element abundances in magmas of the same type.

4.1 Trace element distribution theory.

4.1.1 Trace element mineral-melt distribution coefficients.

The behaviour of trace elements in igneous processes such as fractional crystallisation, or fusion, relies heavily on the mineral-melt distribution coefficient, K_D , which is the ratio of

the equilibrium concentrations of a trace element between a mineral phase and a coexisting melt. K_D 's can be determined directly, either from naturally occurring phenocryst-groundmass pairs or, alternatively, from phenocryst-glass pairs produced in laboratory melting-crystallisation experiments on natural rock systems.

There is no single distribution coefficient to define the behaviour of a trace element throughout an igneous process. Each trace element has a separate K_D for each mineral phase, and the value of the K_D depends, to a large degree, on the ease in which the trace element is accommodated into the structural framework of the phase. Large K_D values mean that the trace element is easily accommodated into the mineral structure.

Trace elements are extremely varied in that they, as a whole, have a broad range in both ionic size and valency. Consequently, mineral groups that possess different basic structural frameworks, will have different trace element affinities. This feature is dramatically shown by the Rare Earth element, (REE), K_D curves of the main mineral groups, (fig. 4.12a,b). Much of the knowledge of K_D variation has come from the experimental studies of Drake and Weill (1975), Watson (1977), Lindstrom and Weill (1978), Mysen (1978b), and Mysen and Virgo (1980). It is recognised, firstly, that mineral-melt K_D 's are inversely correlated with temperature, ie. as the temperature of the melt decreases, K_D 's increase, and, secondly, that mineral-melt K_D 's in basaltic melts are smaller than analogous K_D 's in more acidic melts. There is a strong correlation between these two relationships, because basalts are high temperature melts and, obviously, if the main dependence were on temperature then basalt K_D 's would be expected to be smaller.

Recently, Mysen and Virgo (1980) have shown conclusively that the overwhelming factor that controls the variation of mineral-melt K_D 's is the degree of polymerisation of the coexisting melt, (the degree of polymerisation is expressed in units of 'non-bridging oxygens per silica tetrahedra', (=NBO/T), and ranges from 4.0 in a completely non-polymerised melt to 0.0 in the solid). The authors envisage that trace elements act as network modifiers, having a disordering effect on melt structure. With increasing melt polymerisation, (ie. because of a lower temperature or a more acidic melt composition), the melt becomes increasingly less able to contain these modifying elements and therefore K_D 's increase.

Although melt structure is a function of the other variables listed previously, Mysen and Virgo showed, for selected Rare Earth elements, that the relationship between K_D 's and melt polymerisation is approximately linear, on a log K_D versus NBO/T plot, over the range of melt composition, basalt to andesite. Mysen and Virgo also relate melt composition to melt polymerisation, assigning a value of 0.7 NBO/T to a tholeiitic basalt and values ≤ 0.3 NBO/T to andesite and more acidic magma types.

Much of the presently available K_D data has been obtained from the analysis of naturally-occurring phenocryst-groundmass pairs in a broad range of volcanic rocks (Philpotts and Schnetzler, 1970; Schnetzler and Philpotts, 1970; Arth and Barker, 1976; Schock, 1977; Pearce and Norry, 1979; Luhr and Carmichael, 1980). These data have been criticised most recently by Apter and Boettcher (1981), in that, problems such as incomplete separation, and the demonstration of equilibrium were not shown to have been overcome. However, the data are, on the whole, in good agreement with the conclusions of Mysen and Virgo (1980).

Mineral-melt K_D 's of 14 trace elements for each of the melt types; basalt, andesite, dacite, and rhyodacite, have been selected from the literature and are listed in Table 4.1, together with their source reference. Adjustment of some of the values has been made where discrepancies were thought to exist, in relation to the variations discussed above. In some instances where a trace element K_D was not available for a certain melt type, an estimation was made which was based on that trace element's K_D 's for other melt types and on the K_D 's of other trace elements with similar chemistries.

4.1.2 Trace element variation in terms of bulk distribution coefficients.

At any one instance during crystallisation, or partial melting, a magma may be in equilibrium with a number of phases. The distribution of a single trace element between the magma and these phases is described by its bulk distribution coefficient, D , which is the sum of the products of the individual mineral-melt K_D 's and the phase mass fractions in the total solid. Because it is a function of both the mineral-melt K_D 's and the phase mass fractions, D will vary as they vary with progressive differentiation of the magma. Although abrupt changes in D 's can occur, principally by the rapid appearance, or disappearance, of significant volumes of a low or

Appendage to Table 4.1

Key to Superscripts:-

- K_D^x - value obtained from source reference, x.
- $K_D^{x'}$ - value obtained from source reference, x, and modified slightly, or as is the case for Tb the values were obtained by interpolation methods.
- K_D - value estimated.
- K_D^1 - Arth and Barker, 1976.
- K_D^2 - Philpotts and Schnetzler, 1970.
- K_D^3 - Schnetzler and Philpotts, 1970.
- K_D^4 - Pearce and Norry, 1979.
- K_D^6 - Luhr and Carmichael, 1980.
- K_D^7 - Arth, 1976.

TABLE. 4.1 Mineral-melt distribution coefficients.

Mineral(melt)	Ce	Sm	Eu	Tb	Yb	Lu	Sc	Ti	Ba	Sr	Y	Th	Zr	Nb	Rb	K
HBE.(rhyodacite)	1.520 ⁷	7.770 ⁷	5.140 ⁷	11.800 ⁷	8.380 ⁷	5.500 ⁷	20.000	7.000 ⁴	0.210	0.350	6.000 ⁴	0.200	4.000 ⁴	4.000 ⁴	0.100	0.400
PLG.(")	0.350 ⁷	0.150 ⁷	2.810 ⁷	0.100 ⁷	0.070 ⁷	0.060 ⁷	0.100	0.050 ⁴	0.450 ⁷	4.400 ⁷	0.100 ⁴	0.010	0.100 ⁴	0.600 ⁴	0.041 ⁷	0.300 ⁷
HBE.(dacite)	0.899 ¹	3.990 ¹	3.440 ¹	5.800 ¹	4.890 ¹	4.580 ¹	15.000	5.500	0.150	0.250	4.500	0.200	2.700	3.000	0.080	0.350
PLG.(")	0.241 ³	0.125 ³	2.110 ³	0.088 ³	0.077 ³	0.062 ³	0.050	0.050	0.363 ²	2.840 ²	0.080	0.010	0.070	0.040	0.048 ²	0.263 ²
HBE.(andesite)	0.094 ³	0.336 ³	0.358 ³	0.570 ³	0.463 ³	0.436 ³	10.600 ⁶	3.000 ⁴	0.100 ²	0.198 ²	2.500 ⁴	0.190 ⁶	1.400 ⁴	1.300 ⁴	0.045 ²	0.333 ²
PLG.(")	0.202 ³	0.107 ³	0.732 ³	0.060 ³	0.033 ³	0.034 ³	0.020 ⁶	0.050 ⁴	0.197 ²	1.830 ²	0.060 ⁴	0.008 ⁶	0.030 ⁴	0.025 ⁴	0.051 ²	0.200 ²
CPX.(")	0.420	1.200	0.800	1.350	0.950	0.800	11.500 ⁶	0.400 ⁴	0.050	0.250	1.500 ⁴	0.050 ⁶	0.250 ⁴	0.300 ⁴	0.030	0.033
OPX.(")	0.038 ³	0.100 ³	0.079 ³	0.240 ³	0.671 ³	0.838 ³	3.400 ⁶	0.250 ⁴	0.012 ²	0.024 ²	0.450 ⁴	0.130 ⁶	0.080 ⁴	0.350 ⁴	0.015 ²	0.020 ²
ILM.(")	0.270 ⁶	0.410 ⁶	0.320 ⁶	0.520 ⁶	0.360 ⁶	0.360 ⁶	2.500 ⁶	50.000	0.260 ⁶	0.200	0.800	0.280 ⁶	0.400	1.500	0.200	0.200
PLG.(basalt)	0.023 ³	0.024 ³	0.232 ³	0.017 ³	0.030 ³	0.037 ³	0.010	0.040 ⁴	0.151 ²	1.360 ²	0.030 ⁴	0.003	0.010 ⁴	0.010 ⁴	0.030 ²	0.155 ²
CPX.(")	0.080 ⁷	0.450 ⁷	0.300 ⁷	0.550 ⁷	0.470 ⁷	0.400 ⁷	2.000	0.300 ⁴	0.027 ²	0.093 ²	0.500 ⁴	0.050	0.100 ⁴	0.100 ⁴	0.039 ²	0.027 ²
OPX.(")	0.024 ⁷	0.054 ⁷	0.050 ⁷	0.120 ⁷	0.340 ⁷	0.420 ⁷	1.000	0.100 ⁴	0.013 ²	0.017 ²	0.200 ⁴	0.050	0.030 ⁴	0.150 ⁴	0.022 ⁷	0.140 ⁷
ILM.(")	-	-	-	-	-	-	-	50.000 ⁴	-	-	-	-	0.280 ⁴	0.800 ⁴	-	-

high K_D phase, most variation will be gradational and related to the parameters which influence individual K_D 's. The concentration of a trace element in successive magma differentiates is directly controlled by the variation of its bulk distribution coefficient.

The term 'incompatible element', (synonymous with 'hygro-magmatophile element', or 'large ion lithophile element'), has been applied to trace elements which have very low K_D 's for most of the common magmatic minerals, ie. they are strongly partitioned into the melt relative to the phase. Consequently, these trace elements will usually have low D values for many magma types.

Conventional reasoning assumes that strongly incompatible elements will have D values that remain close to zero throughout most of the differentiation of magmas, and therefore the concentrations of these elements in successive magma differentiates depend almost completely on the degree of fractionation. Thus strongly incompatible trace elements have often been used as fractionation indices, with which to study the distribution of other trace elements. The assumption that $D \approx 0.0$ is certainly a valid one for magmas of basaltic to intermediate composition, but is suspect for more acidic magmas, because of the increased degree of polymerisation and, hence, the higher K_D 's, in the latter. Another factor which detracts from the usefulness of strongly incompatible elements as fractionation indices is one of chemical inhomogeneity. Protracted crystallisation of a magma of any composition will leave a final residual liquid enriched in incompatible elements. Incomplete segregation of this residual liquid would create incompatible element inhomogeneity throughout the crystallised mass.

The alternative to using an incompatible element, as a fractionation index, is to use a strongly compatible one, because if D is sufficiently large the decrease in concentration of the trace element in successive magma differentiates is, also, dependent mainly on the degree of fractionation. However, an element may be compatible with one phase, ie. Ni in olivine, but incompatible with another, ie. Ni in plagioclase, and so D values of these elements can be lowered if the fractionation assemblage is dominated by unreceptive minerals. On the other hand, the D values of an element, which is strongly compatible in basic magmas, are likely to be just as high in granitic magmas simply because mineral-melt K_D 's are higher in magmas of the latter type.

One of the main disadvantages of strongly compatible trace elements as fractionation indices, is that these elements are often present only in extremely small concentrations in granitic rocks, and cannot therefore be determined without relatively large analytical error.

Many trace elements are neither strongly incompatible nor strongly compatible, and across the composition range basalt-rhyolite they can progress from being mildly incompatible ($D < 1.0$) to mildly compatible ($D > 1.0$). This means that during fractionation across this composition range, these elements will usually be enriched in basic magmas, and depending on the nature of the crystallising phases, may become progressively depleted in more acidic magma differentiates. These elements can be called the transitional D group elements.

A few trace elements have distributions which are controlled by just one phase, for example; Sr has large K_D 's for plagioclase but is not compatible with any other common magmatic mineral. The Sr distribution can therefore be useful in assessing the role of plagioclase in a magmatic process.

4.2 Trace element distributions in the rocks of the intrusive complex.

Upto 20 trace elements have been analysed for each rock, 13 by X-ray fluorescence (XRF) analysis, (Cr, Co, Ni, Rb, Sr, Y, Zr, Nb, Ba, La, Ce, Pb, Th), and 9 by instrumental neutron activation analysis (INAA), (La, Ce, Nd, Sm, Eu, Tb, Yb, Lu, Sc). Of these, Cr, Ni, Co, Sc, and Sr are compatible elements and depending on the fractionating phases, should be expected to decrease in concentration from the metabasites to the granitic orthogneisses, whereas Rb, Ba, Pb, and Th are incompatible and should increase. Zr, Y, Nb, and the REE's, including La, Ce, Nd, Sm, Eu, Tb, Yb, and Lu, belong to the transitional D group and together with Sr should provide the most crucial evidence in the assessment of the petrogenetic models put forward in the previous chapter. The REE's are dealt with, as a whole, in section 4.3. All the trace element data are listed in Appendix 1.

4.2.1 Trace element (ppm) versus SiO₂ (wt%) plots of the metabasite - orthogneiss rocks.

The trace element data for the metabasite and orthogneiss rocks analysed in this research are plotted against SiO₂ wt% in

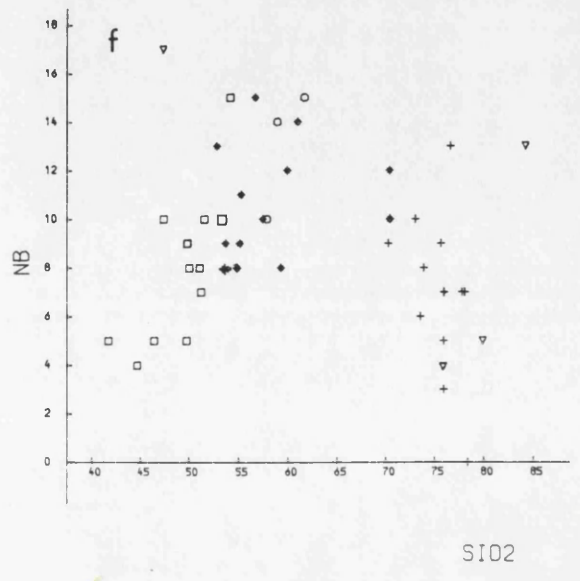
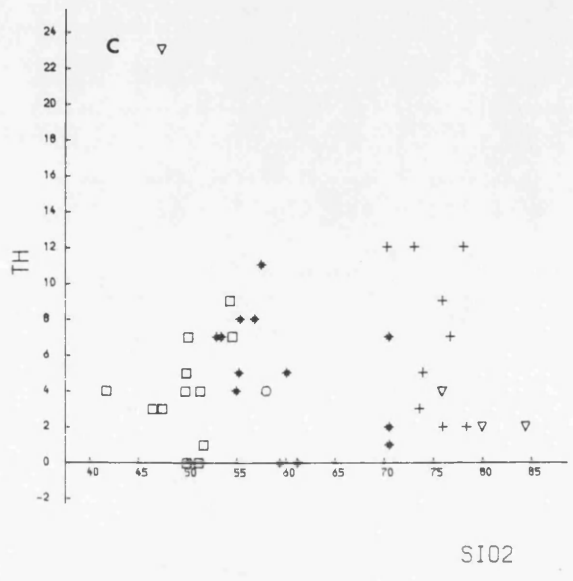
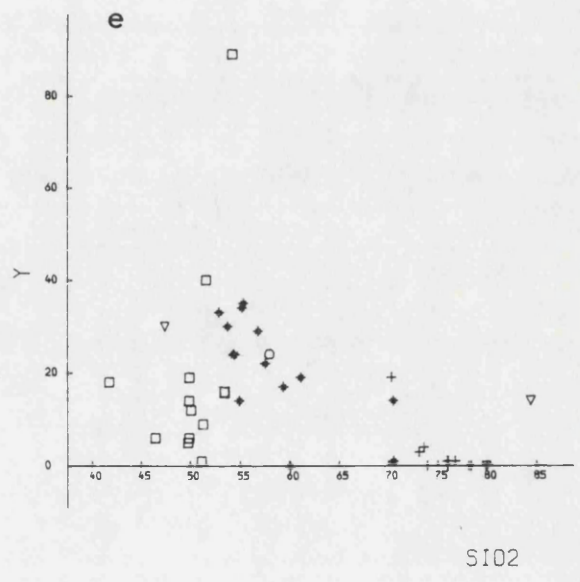
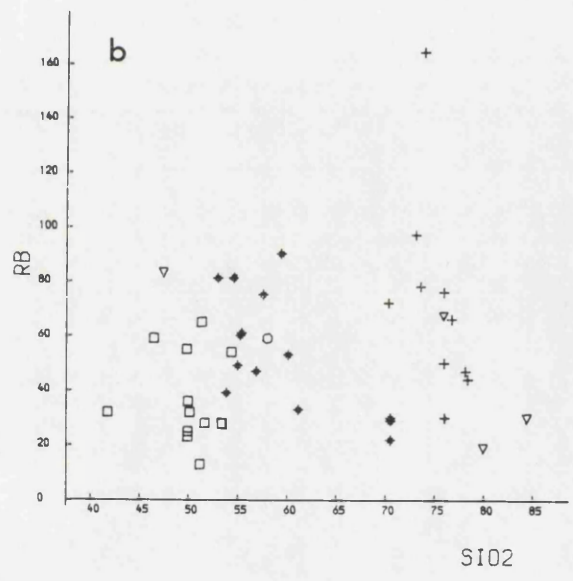
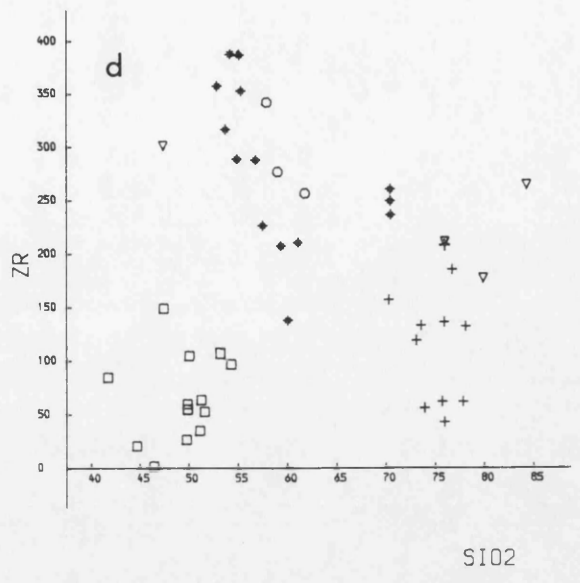
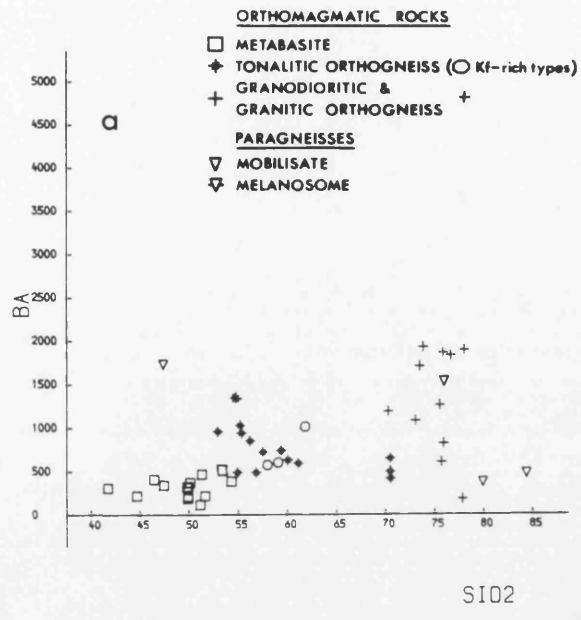


Fig. 4.1a-f Trace element (ppm) v. SiO₂ (wt%) plots.

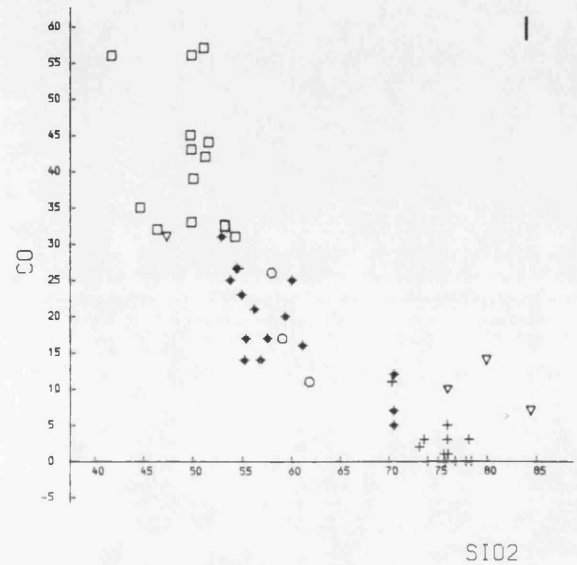
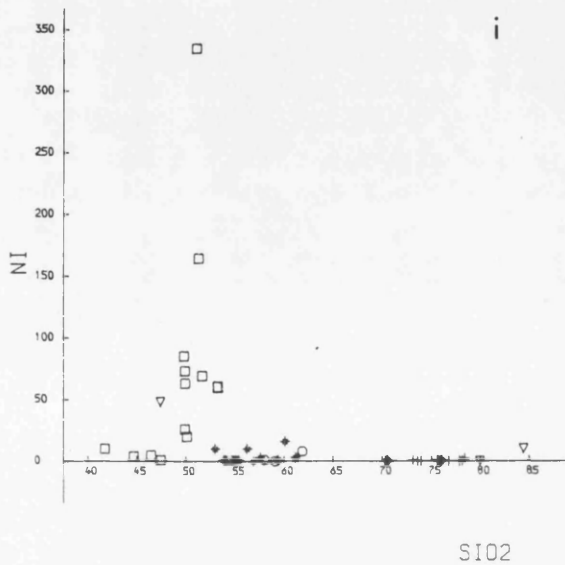
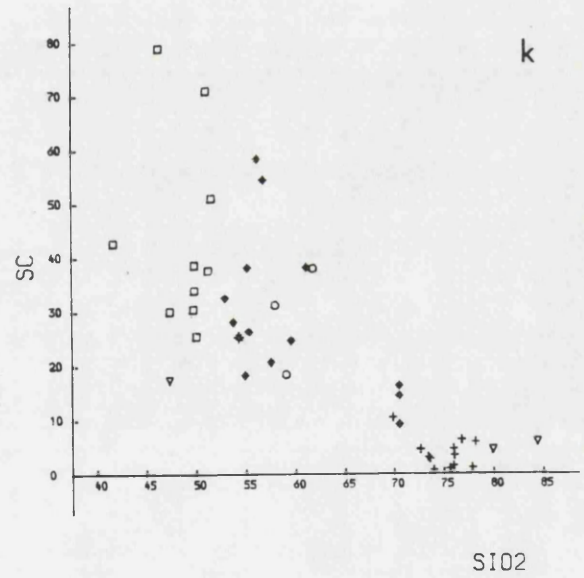
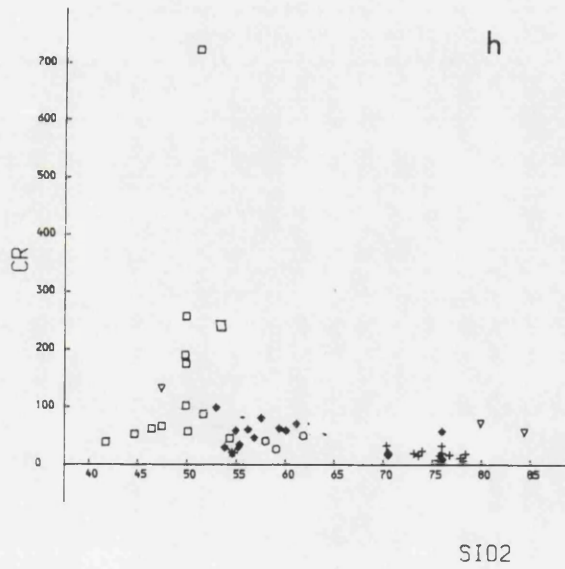
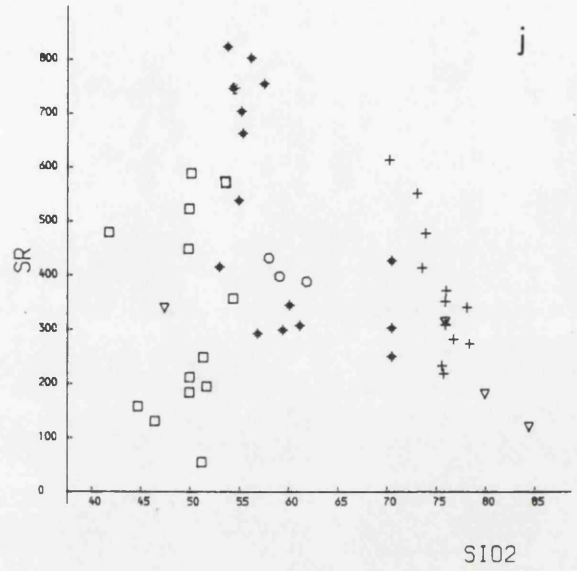
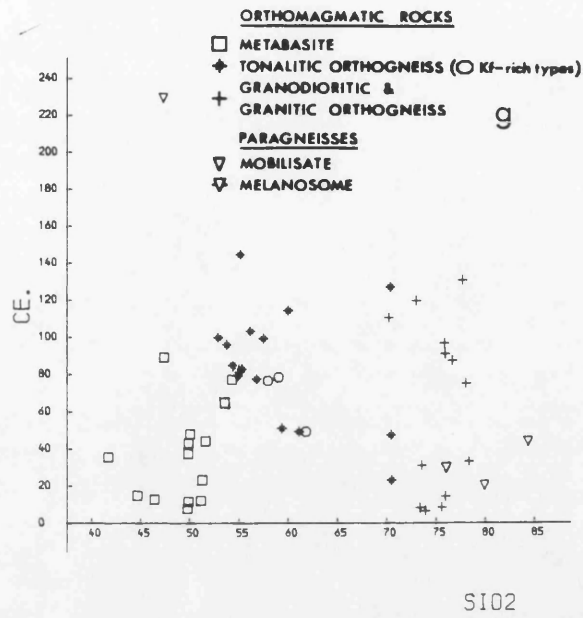


Fig. 4.1g-l Trace element (ppm) v. SiO₂ (wt%) plots.

fig.4.1a-1. In each plot, except that of Zr v. SiO_2 wt%, the data define a continuous trend, (except for the sampling gap, which is discussed in the previous chapter), from the metabasites to the granitic orthogneisses, which in most cases is a strongly non-linear array. This continuous-trend feature reinforces the prior conclusion that these rocks are cogenetic and linked by the process of crystal fractionation.

4.2.1a The incompatible trace elements:- Rb, Ba, Pb, and Th.

As was predicted from the wt% plots of Na_2O , and K_2O , against SiO_2 , the incompatible trace elements, Ba, Rb, Th (fig.4.1a, b, c) and Pb (not shown) display a large degree of scatter over the whole of the metabasite-orthogneiss series. For the metabasites, this scattering may be in part due to variable metasomatic alteration, and this theory can be checked by plotting a ratio of two incompatible elements, say Ba/Rb, against some fractionation index, say Cr. If the metabasites have been variably enriched in both of these incompatible elements, by a metasomatic fluid which had a similar Ba/Rb ratio to that of the premetamorphic basic rocks, then the Ba/Rb ratio of the metabasites would remain approximately constant. The Ba/Rb v. Cr plot (fig.4.2) shows that this is not so, and there is just as much scatter in the Ba/Rb ratio as there is in the individual element data. Therefore, this would suggest that metasomatic alteration was not the prime cause of the scatter in the incompatible element data. However, the Ba/Rb ratio of the metasomatic fluid is not known and so this line of evidence is not strong.

Another possible reason for the scattering of the metabasite incompatible element data, is that some of the metabasite samples represent amphibolitised cumulate rocks, and not magma compositions. This is already the suspected origin of samples BK408 and BK96. The proposed fractionation scheme for the metabasite magma involves the crystal fractionation of clinopyroxene and orthopyroxene only, (Chapter 3, CMAS system). The hypothesis of a cumulate origin for some of the metabasite rocks can be tested in a plot such as Sr v. Cr (fig.4.3). Rocks composed of cumulate pyroxene will have low Sr content because Sr does not enter into the pyroxene structure. BK408, which is probably an amphibolitised pyroxenite has only 55 ppm of Sr. There is a group of 5 metabasite samples with $\text{Sr} < 200$ ppm, in fig.4.3 (which does not include samples BK408 and BK96), and from their low Sr content, these 5 rocks might well represent

ORTHOMAGMATIC ROCKS

- METABASITE
- ◆ TONALITIC ORTHOGNEISS (○ Kf-rich types)
- GRANODIORITIC & GRANITIC ORTHOGNEISS
- ▽ PARAGNEISSES
- ▽ MOBILISATE
- ▽ MELANOSOME

Fig. 4.2 Ba/Rb v. Cr

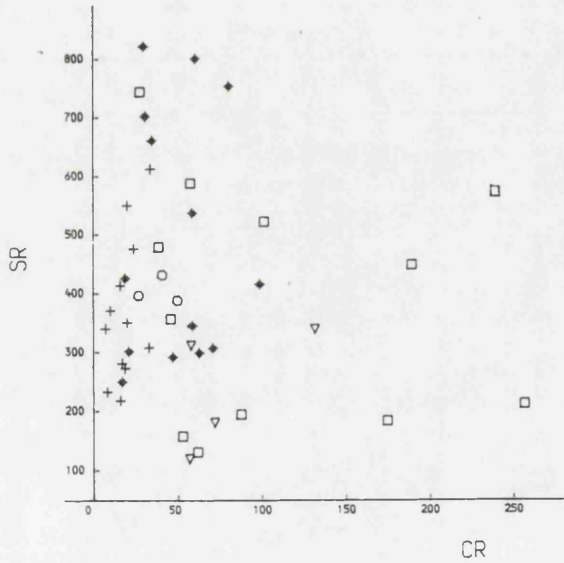
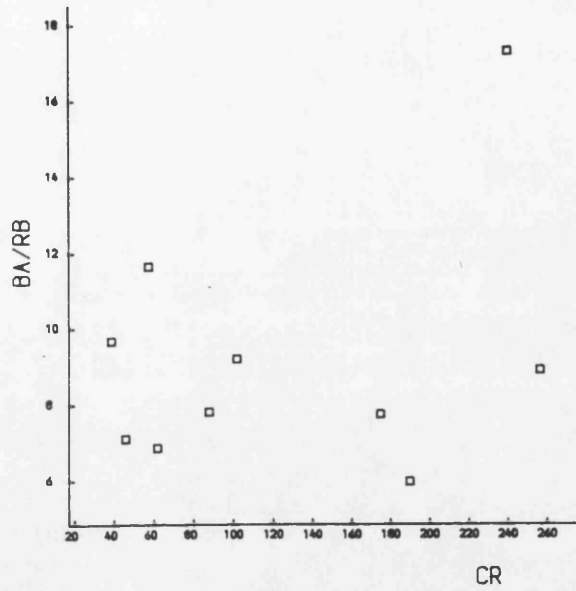
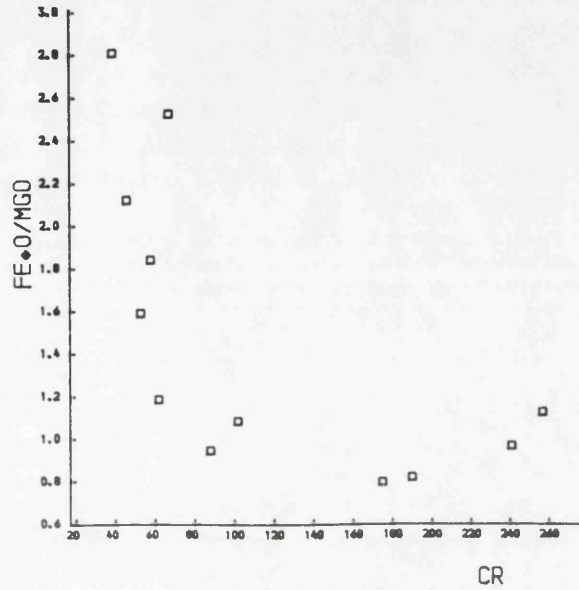


Fig. 4.3 Sr v. Cr

Fig. 4.4 tFeO/MgO v. Cr



pyroxene-rich cumulates. However, three of these rocks contain less than 100 ppm Cr, so this cumulate origin is considered unlikely for them because Cr is strongly partitioned into pyroxene, relative to the magma, and would be present in greater quantities, in pyroxene-rich cumulates, than this. All of the metabasites included in fig. 4.3 have a large modal proportion of plagioclase and therefore the low-Sr group of metabasites cannot be misconstrued as representing pyroxene-rich cumulate rocks. The metabasite rocks with high Sr, ie. BK138 which has 479 ppm, do not contain larger proportions of plagioclase than the low-Sr group. Therefore, it would seem that a large majority of the metabasite samples do not represent cumulate rocks, and therefore, the scatter of the incompatible element data must have been caused by some other phenomenon. Some of this scatter, and certainly most of the scatter in the metabasite Sr data, will be due to leaching of Sr, Ba, and the alkalies, Na and K, during the sericitisation of the plagioclase feldspar. This process will also have affected the orthogneiss rocks, because the plagioclase in these rocks is strongly sericitised too.

The scatter of the incompatible element data for the whole of the metabasite-orthogneiss series may also reflect variations in incompatible element concentrations in different intrusive bodies of the same rock type. This is consistent with the scatter of the Ba/Rb ratio in the metabasite samples (fig.4.2) and would point to differences in incompatible element abundances, and ratios, between the parental metabasite magmas. These differences in the trace element characteristics of the parental magmas of the metabasite-orthogneiss series, could have arisen through processes, (eg. fractional melting (Schilling and Winchester, 1967)), acting at the magma source, which was presumably in the upper mantle. Alternatively, the differences could have arisen during magma intrusion, by the variable assimilation of crustal rocks with different incompatible element characteristics to those of the magmas.

The scatter in the orthogneiss incompatible element data may also reflect the range of inhomogeneity in a single intrusion, caused by the incomplete and inconsistent draining and segregation of incompatible element-rich fluid during the late stages of crystallisation of these rocks. Against this, however, is the distribution of the Kf-rich tonalitic orthogneisses, which do not

plot consistently higher than other tonalitic orthogneisses in the incompatible element v. SiO_2 wt% plots.

Ba displays a clear trend of enrichment with increasing SiO_2 content (fig.4.1a) in the metabasite-orthogneiss series, although this enrichment trend is not as strong in the tonalitic orthogneiss as in the other rock groups. This step-like feature occurs in each of the Ba, Na_2O , and K_2O v. SiO_2 wt% plots and is mainly a function of the rapid increase in SiO_2 in the tonalitic rocks. Therefore, the fractionating phases responsible for such changes in the composition of the tonalitic orthogneiss magmas must have been able to accommodate incompatible elements, like Ba and K, into their structures in significant amounts, and also must have been, in bulk, significantly lower in SiO_2 content, than the magma itself. The tonalitic rocks consist mainly of hornblende and labradorite, and these two phases suitably fulfil the above requirements, in that, hornblende is a low- SiO_2 phase, commonly containing less than 43wt% SiO_2 , and both hornblende and labradorite contain appreciable amounts of Na_2O , and significant amounts of K_2O and Ba.

4.2.1b The transitional D elements:- Zr, Y, Nb, and Ce.

The transitional D elements, Zr, Y, Nb, and Ce all have distributions which define a convex-upwards curve, against SiO_2 , (fig.4.1d,e,f,g), with the maximum concentrations of these elements occurring in the tonalitic orthogneisses.

At first sight, this curved-trend feature appears to be consistent with the hornblende fractionation hypothesis invoked earlier to explain the rapid SiO_2 enrichment trend in the most fractionated metabasites and in the tonalitic orthogneisses. This is because Zr, Y, and Nb have hornblende K_D 's which are greater than unity in magmas of intermediate composition (Pearce and Norry, 1979), and in slightly more acidic magmas Ce also has a hornblende K_D above unity (Arth and Barker, 1976). Thus, if hornblende was the dominant fractionating phase, the transitional D elements would be expected to decrease in concentration from a peak in the tonalitic orthogneisses to a minimum in the granitic orthogneisses. However, certain features of the Zr distribution in the metabasite-orthogneiss rocks, may well prove difficult to explain by this hornblende dominated crystal fractionation hypothesis. There is a gap, in the SiO_2 wt% v. Zr plot (fig.4.1d), of some 150 ppm between the highest Zr concentrations in the metabasite rocks, and the Zr concentrations

of the SiO_2 -poor tonalitic orthogneisses. Apart from the presence of this gap, which is puzzling because it is not apparent in the other transitional D element distributions, the rapid increase (ie. 150 ppm) in the Zr concentration occurs at the point where the fractionation of, predominantly, hornblende is proposed to have been initiated, ie. in the most fractionated metabasite magmas. This Zr distribution is in obvious contradiction with the model, because the Zr bulk distribution coefficient of a hornblende dominated phase assemblage in a strongly fractionated basic magma is probably only slightly lower than unity, and therefore a large increase in the Zr content of this magma, by crystal fractionation means, would be impossible. Thus, it seems that, both hornblende and plagioclase, which has very low K_D 's for Zr, would have had to fractionate from the magma, with enough hornblende separating to cause the magma to become enriched in SiO_2 and yet enough plagioclase separation so that the Zr bulk distribution coefficient was depressed sufficiently, to allow strong Zr enrichment. As is evident in figs.4.1d and 3.3a, the assimilation of paragneissic rocks would also help to enrich the metabasite magma in Zr and SiO_2 .

4.2.1c The compatible elements:- Cr, Ni, Co, Sc, and Sr.

The strongly compatible elements, Cr and Ni, have very low concentrations in the orthogneisses and so they are really only useful in the elucidation of the metabasite petrogenesis. Plotted against SiO_2 wt% (fig.4.1h,i), these two elements have similar distributions, and in both plots the possible cumulate rocks, BK408 and Bk96, are well separated from the rest of the metabasite samples. The metabasites seem to fall into two main groups:- one group with SiO_2 of around 50 wt% and a large range in Cr (c.300-100 ppm) and Ni (100-15 ppm) contents, and another group with SiO_2 between 42-55 wt% and Cr and Ni contents less than 100 ppm and 15 ppm, respectively. The four rocks which have less than 47.5 wt% SiO_2 , plot in similar positions in the Cr and Ni plots, having low concentrations of these elements, and a closer examination reveals that three of them are the most Fe-rich of the metabasite samples. Fe content, and more importantly the Fe/Mg wt% ratio, increases with decreasing compatible element concentrations across the metabasite group, ie. Cr v.tFeo/MgO (fig.4.4). This means that the Fe content and the Fe/Mg ratio both increased with continuing fractionation of the metabasite magmas. The major element variation in the metabasite rocks has been ascribed to two-pyroxene fractionation, ie augite and

hypersthene, from the metabasite magmas (see Chapter 3, Cmas system). Hypersthene contains a large wt% of tFeO (ie. Hypersthene BK102-8 has 21.35 wt% tFeO) whereas augite contains much less tFeO (ie. Augite BK102-3 has 7.15 wt% tFeO) and, clearly, for the tFeO wt% of the metabasite magma to increase as a result of the fractionation of these two phases, augite must predominate over hypersthene. Both pyroxenes, if fractionated from a magma with less than 50 wt% SiO₂, would deplete that magma in SiO₂ and, so, pyroxene fractionation could clearly produce the metabasite tFeO v. S.I. (fig.3.4c), and MgO, Cr, and Ni v. SiO₂ (figs.3.3e, 4.1h, 4.1i) distributions.

The other compatible elements, Co and Sc, are shown plotted against SiO₂ wt% in fig.4.1k,l, and, as expected, the concentrations of both elements decrease steadily through the metabasite-orthogneiss series. In most geological circumstances Sc and Co exist as the ions, Sc³⁺ and Co²⁺, and both elements have large K_D's (>1.0) for the common mafic phases, ie. pyroxene, hornblende (Gill, 1978) and probably biotite. They have very low K_D's for felsic minerals (ie. Sc K_D for plagioclase in alkali basalt = 0.017 (Lindstrom, (1976; in Irving, 1978))).

The Sr distribution in the metabasite rocks has already been described in the discussion on the possible cumulate origin of some of these rocks. As in the metabasite Sr data, the orthogneiss Sr data shows a large scatter (fig.4.1j), and this is undoubtedly due mainly to the strongly seriticised state of the plagioclase feldspar in these rocks. The Sr concentration reaches a peak in the melanotonalitic rocks and steadily decreases to a level of about 300 ppm in the leucotonalitic orthogneisses, presumably because of plagioclase fractionation from the orthogneiss magmas. The granodioritic and granitic orthogneisses show no significant Sr depletion trend, from the level found in the leucotonalitic orthogneisses, and this confirms the previous conclusion, made on the basis of the textures of the acidic orthogneisses, that fractionation of plagioclase had stopped in the most fractionated leucotonalitic orthogneiss magmas.

4.2.2 Trace element variations in the paragneiss rocks.

The small set of data for the paragneisses are also plotted in the trace element versus SiO₂ wt% plots of fig.4.1a,l, and it can be seen that, in each plot, the trace element concentration is greater in the single melanosome sample, BK409 (SiO₂ wt% = 47.39), than in any of the 3 mobilisate samples, (SiO₂ wt% >75.0). This may

, at first, seem at odds with the often supposed behaviour of the trace elements, Ba, Rb, and Th (fig.4.1a,b,c), whereby they preferentially enter into the partial melt, rather than remain in the solid residue. However, the melanosome contains appreciable modal proportions of biotite, which has high K_D 's for these elements. Sr (fig 4.1j) is present in lower concentrations in the mobilisate, than in the melanosome, simply because it is strongly compatible with calcic plagioclase and as progressive melting of the melanosome continued, the melanosome plagioclase became more CaO- and, hence, Sr-rich.

It is difficult to make a quantitative assessment, on the basis of the trace elements, of the amount of paragneissic material assimilated by the metabasite-orthogneiss magmas, during their intrusion, though field evidence suggests that it must have been significant. The step-like feature of the incompatible element distributions, against SiO_2 wt%, may be partly due to the assimilation of siliceous, incompatible element-poor, paragneisses, because in the plots the tonalitic orthogneisses define a trend towards the mobilisate samples, which do have low contents of incompatible elements. As has already been stated, the assimilation of paragneiss rocks may have been significant in the most fractionated metabasite magmas, in helping to reverse the trend of SiO_2 depletion in the magma, and enriching it in Zr.

4.3 The Rare Earth element (REE) distributions in the rocks of the intrusive complex.

4.3.1 The geochemical properties of the REE.

The REE's, often called the Lanthanide elements, are a group of 15 elements, Lanthanum (at.no. 57) to Lutetium (at.no. 71), which occur naturally, in rocks, except for Promethium (at.no. 61) which has no stable isotopes. The REE's with the lower atomic numbers, that is La,Ce,Pr,Nd, and Pm, are known as the light REE's (LREE's), those with the highest atomic numbers, ie. Ho,Er,Tm,Yb, and Lu, as the heavy REE's (HREE's), and those with intermediate atomic numbers, ie. Sm,Eu,Gd,Tb, and Dy, as the middle REE's (MREE's).

The chemistry of the REE's is dominated by the phenomenon known as the Lanthanide Contraction, in which the ionic radii of the individual REE's decrease, with increasing atomic number, across the group. This effect is due to the way in which their outer electron

energy levels are filled and to the increased positive charge on the nucleus for higher atomic numbers. In the ground state, the REE's all have 2 electrons in the 6s energy level, 1 in the 5d energy level, and, depending on the atomic number of the REE, an empty, partly filled, or full 4f energy level. La has no electrons in the 4f energy level and Lu has a full complement of 14 4f electrons. The valence electrons are those of the 6s and 5d levels, which are easily removed, and so the REE's are dominantly trivalent. However, under strongly oxidising conditions, for example in hydrothermal fluids, Ce can oxidise to the Ce^{4+} ion by losing its single 4f electron, in addition to the other 3 valence electrons. Under certain magma conditions, Eu exhibits a divalent state, in addition to the trivalent state. This anomalous behaviour, which is related to the incorporation of the 5d valence electron into the 4f energy level, giving a half-filled 4f energy level and increased stability, sets Eu apart from the rest of the REE's.

Although the REE's are all chemically similar, except Eu, there is a continuous chemical variation across the group, due to the effects of the Lanthanide Contraction. This means that REE's of adjacent atomic number have very similar chemistries, whereas REE's of significantly different atomic number have chemistries which are much less similar.

The REE's belong to the transitional D group, ie. those elements whose bulk distribution coefficients may commonly rise above unity in intermediate to acid magmas. This means that in a magma which differentiates from basic, through intermediate, to acid compositions, the REE concentrations rise and then, depending on the fractionating phases, fall as the REE become more strongly partitioned into the phases, relative to the magma. Because of the decrease in ionic radius across the REE group with increasing atomic number, the heavier the REE then the more easily it is able to fit into the common mafic phases. For this reason, with fractionation, HREE's would be expected to reach the point at which their bulk distribution coefficients exceed unity, sooner than the LREE's. Put in another way, the fractionation of a mafic phase, say hornblende, from a magma of a composition intermediate to andesite and dacite, would deplete the magma in HREE's and enrich it in LREE's. The K_D values of the REE in different minerals from a range of magma types, are listed in Table 4.1.

The metabasite-orthogneiss rocks display clearly this

pattern of enrichment and then depletion of the REE's, with increasingly acidic rock compositions. The highest concentrations of the MREE's and HREE's occur in the melanotonalitic orthogneisses, while the highest LREE concentrations, ie. La, and Ce, occur in the leucotonalitic orthogneisses and the most mafic granodioritic and granitic orthogneisses.

4.3.2 REE mobility during alteration.

Before describing the chondrite-normalised REE patterns of the rocks of the intrusive complex, it is necessary to add a note of caution, in that many of the rocks analysed in this study show the effects of high temperature retrogressive metamorphism. In all rocks, plagioclase feldspar has undergone, often considerable, sericitisation and epidotisation, and in many rocks the mafic phase has been altered to more hydrous forms, such as chlorite.

Recently, there has been much critical discussion on the extent to which the REE concentrations of metamorphosed igneous rocks may have diverged from the primary igneous REE concentrations, because of REE mobility. Unfortunately, because of the lack of definite evidence on the primary REE composition of high-grade meta-igneous rocks, the studies of REE mobility in retrogressive metamorphism have been conducted either on very low-grade rocks (Hellman et al., 1979), or on hydrothermally altered rocks (Alderton et al., 1980, Martin et al., 1978). Hellman et al. studied REE abundances, both in relict-domains and in meta-domains of basic-ultrabasic metavolcanic terrains and put forward four main ways in which the primary REE concentrations of a rock may be modified by REE mobility during low temperature metamorphism. They are:-

1. Gross REE and selected LREE enrichment.
2. REE redistribution about a primary mean.
3. Gross REE depletion.
4. Selective modification of La, Ce, Eu and Yb concentrations.

Alderton et al. measured REE abundances in fresh granite and in associated altered granite, from a number of hydrothermally affected granite localities, in S.W. England, and found that, during sericitisation, where plagioclase is reduced to a mass of fine muscovite, Eu is leached from the rock. They also found that in the chloritisation of biotite, the LREE's become preferentially depleted, relative to the HREE's, in the rock.

The alteration in these granitic rocks, differs from that of the rocks of the intrusive complex in that large amounts of

epidote formed, in the latter, as well as sericite and chlorite. Epidote has a strong affinity for REE's, especially LREE's, and may have acted as a 'sink' into which the REE, released in the alteration of the primary minerals, accumulated, thereby preserving the primary REE abundances in the metabasite-orthogneiss rocks.

4.3.3 Chondrite-normalised REE patterns of the rocks of the intrusive complex.

In order to fully visualise the effects of the systematic chemical variation across the Rare Earth group of elements, it is necessary to incorporate all of the REE data for a rock, or a mineral, into a single graph (for example, see fig.4.5). The type of graph used is essentially a concentration versus atomic number plot, which can easily accommodate several sets of REE data if the Oddo-Harkins effect, which is the occurrence of greater natural abundances of elements with even atomic number, relative to those of odd atomic number, is first eliminated from the data. This is done simply by dividing the REE concentrations in the rock by their respective concentrations in chondritic meteorites. Until recently, all ordinary chondrites, which may be the primaeval material of the solar system, were thought to be identical in composition and so REE data is often normalised using an average of several chondrite compositions. One such average is of 10 ordinary chondrites analysed by Nakamura, 1974, and these are the normalising values used in this thesis (Table 4.2).

The REE's which have been analysed for in this study are La, Ce, Sm, Eu, Tb, Yb, and Lu. A few analyses of Nd were also obtained, but these are not of sufficient quality to be of use in the drawing of the chondrite-normalised REE patterns of figs.4.5-4.9. These chondrite-normalised plots do not include a position along the X-axis for Promethium (ie. atomic no. 61 is omitted), and the gaps in the data, ie. for the elements Pr, Nd, Dy, Ho, Er, and Tm, have been bridged by straight lines joining known data. The element Gd, though not analysed for, has been judged to be the axial element of the REE group and its chondrite-normalised concentration estimated by extending the line from Yb, through Tb, to the Gd position. Eu has different oxidative properties to those of the other REE, and so is often present in concentrations which break the smoothness of the chondrite-normalised REE pattern, producing a *Eu anomaly, (* -signifies a chondrite-normalised value), which may be either positive or negative, ie. above or below the line of the REE*

TABLE. 4.2 REE chondrite normalising values.*

ELEMENT	ABUNDANCE (ppm)
La	0.329
Ce	0.865
Sm	0.203
Eu	0.077
Tb	(0.052)**
Yb	0.220
Lu	0.040

* Average of 10 ordinary chondrites (Nakamura, 1974).

** Interpolated value.

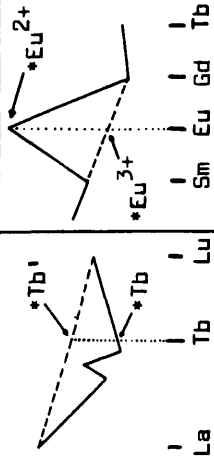
pattern, respectively. In each pattern the *Eu datum is joined by straight lines to the *Sm datum and to the estimated *Gd datum.

Four parameters can be used to categorise a particular REE* pattern and these are:-

1. Σ LREE* - the sum of the chondrite-normalised LREE values, in this thesis Σ LREE* = *La + *Ce .
2. Σ HREE* - the sum of the chondrite-normalised HREE values, in this thesis Σ HREE* = *Yb + *Lu .
3. *Tb'/*Tb - the ratio of a hypothetical chondrite-normalised Terbium value (*Tb') , derived from a hypothetical linear REE* pattern connecting the *La and *Lu values of the real REE* data, and the real chondrite-normalised Terbium value (*Tb) , (for graphical explanation, see Table 4.3).
4. *Eu²⁺/*Eu³⁺ - the ratio of the actual chondrite-normalised Eu value (*Eu²⁺) , and the hypothetical value (*Eu³⁺) , which corresponds to the chondrite-normalised value of the Eu concentration which would be present in the rock, or mineral, if Eu behaved exactly like its nearest neighbour REE's, ie. if it formed only Eu³⁺ ions. (for graphical explanation, see Table 4.3).

The parameters, Σ LREE* and Σ HREE*, can be used together to the proportion of the LREE's to the HREE's, and hence the slope of the overall REE* pattern. The parameter *Tb'/*Tb is a measure of the MREE* depletion, or enrichment, in relation to a hypothetical linear REE* pattern with the same values of *La and *Lu as the real

Table 4.3 REE characteristics of the metabasite-orthogneiss series.

Table 4.3		Σ LREE*	Σ HREE*	*Tb'/*Tb	*Eu ²⁺ /*Eu ³⁺	Comments	
ORTHOgneisses	METABASITES	mean = 70.69 n = 9 range = 129-26	mean = 10.77 n = 9 range = 14.7-7.2	mean = 1.77 n = 8 range = 2.3-1.2	mean = 0.9 n = 8 range = 1.3-0.6	BK84 (Σ LREE*=235) - omitted in mean & range. BK94 (Σ HREE*=30.3) - omitted in mean & range.	
		melano- cratic	mean = 231 n = 9 range = 330-119	mean = 23.6 n = 8 range = 35-14.8	mean = 1.5 n = 9 range = 2-0.9	mean = 0.8 n = 9 range = 1.3-0.4	BK124 (Σ HREE*=73.6) - omitted in mean & range.
		leuco- cratic	mean = 171 n = 4 range = 371-68	mean = 7.9 n = 4 range = 14.5-1.8	mean = 2.36 n = 3 range = 3.2-1.6	mean = 1.4 n = 3 range = 1.9-0.8	
		Granodioritic & Granitic	mean = 339 n = 5 range = 526-236 *Sm(*Eu range = 271-21	mean = 6.7 n = 5 range = 14.2-3.0 range = 5.5-1.6	mean = 3.0 n = 5 range = 4.5-2.0 range = 7.2-2.48	mean = 1.3 n = 5 range = 2.4-0.8 range = 10.3-1.9	BK121 (*Tb'/*Tb=0.9) - omitted in mean & range.
ORTHOgneisses	Kf - rich Tonalitic	mean = 166 n = 3 range = 197-106	mean = 24.2 n = 3 range = 33.2-18.7	mean = 1.6 n = 3 range = 2.0-1.1	mean = 0.8 n = 3 range = 1.0-0.63		
		Σ LREE* = *La*Ce	Σ HREE* = *Yb*Lu				

REE*.curve. *Tb' can be easily measured by graphical methods (Table 4.3). Rocks with *Tb'/*Tb < 1.0 have a convex-upwards REE* pattern, and therefore have MREE* enrichment, whereas rocks with *Tb'/*Tb > 1.0 have concave-upwards REE* patterns and are therefore depleted in the MREE*'s. *Eu²⁺/*Eu³⁺ is simply a measure of the size of the *Eu anomaly, relative to the other MREE*'s.

4.3.3a Metabasite REE* patterns.

The REE* patterns of the metabasite rock are shown in fig. 4.5a,b,c and it can be seen that all are LREE* enriched, relative to the HREE*'s. In terms of Σ REE*'s (ie. the sum of all the REE*'s in a rock), the metabasites fall into two groups; a group of 6 rocks with a high average Σ REE* and a group of 2 rocks, BK102 and BK408, with a low average Σ REE*.

The sample BK408 has a mineralogy containing almost no felsic minerals, and on the basis of its high S.I. value (0.685), and its high concentrations of Cr (2540 ppm) and Ni (334 ppm) it has been suggested that this rock is a cumulate rock. BK96 has also been suggested to be a cumulate rock, having fairly high concentrations of Cr (723 ppm) and Ni (164 ppm), and both it and BK408 have REE* patterns which differ from the other metabasite REE* patterns, in that they have low Σ LREE*/ Σ HREE* ratios (5.54 and 3.43 respectively), compared with an average Σ LREE*/ Σ HREE* value for the other metabasite rocks of 7.06. This large difference in slope between the REE* patterns of BK408 and BK96, and those of the other metabasite rocks, strongly implies that the former have a different petrogenetic origin, ie. cumulate, to the main group of metabasite rocks. The samples BK408 and BK96 also have the most linear REE* patterns (*Tb'/*Tb values of 1.23 and 1.41 respectively) of the metabasites. From the study of the metabasite rocks in the CMAS system in the previous chapter, it was proposed that the magmas, from which they formed, evolved by the fractionation of both orthopyroxene and clinopyroxene, with the latter the most dominant of the two. Do the REE* patterns of the rocks BK408 and BK96 substantiate this hypothesis? The linearity of their REE* patterns certainly does, because the REE K_D 's of pyroxenes (Table 4.1) form a curve, on a concentration v. atomic number plot, which is antipathetic to the REE* patterns of the main metabasite group (compare figs. 4.5a and 4.9a), and thus the REE* patterns of cumulate pyroxenites, crystallised from a basic magma with a REE* pattern

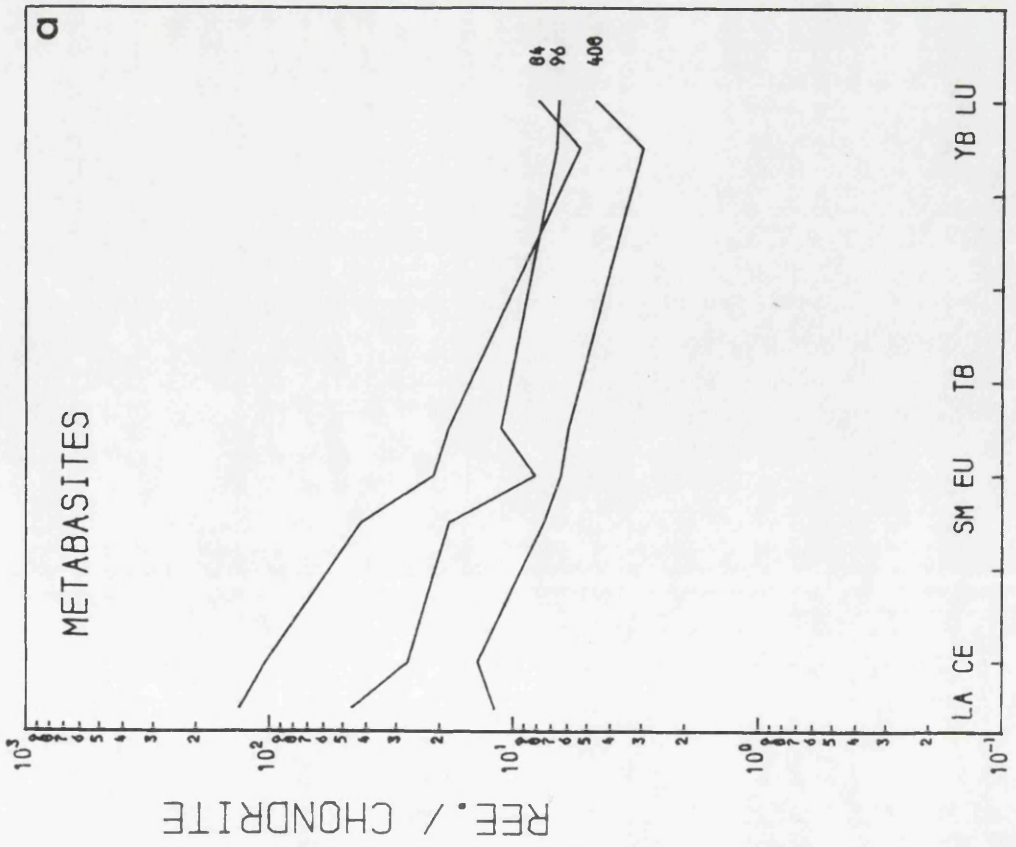
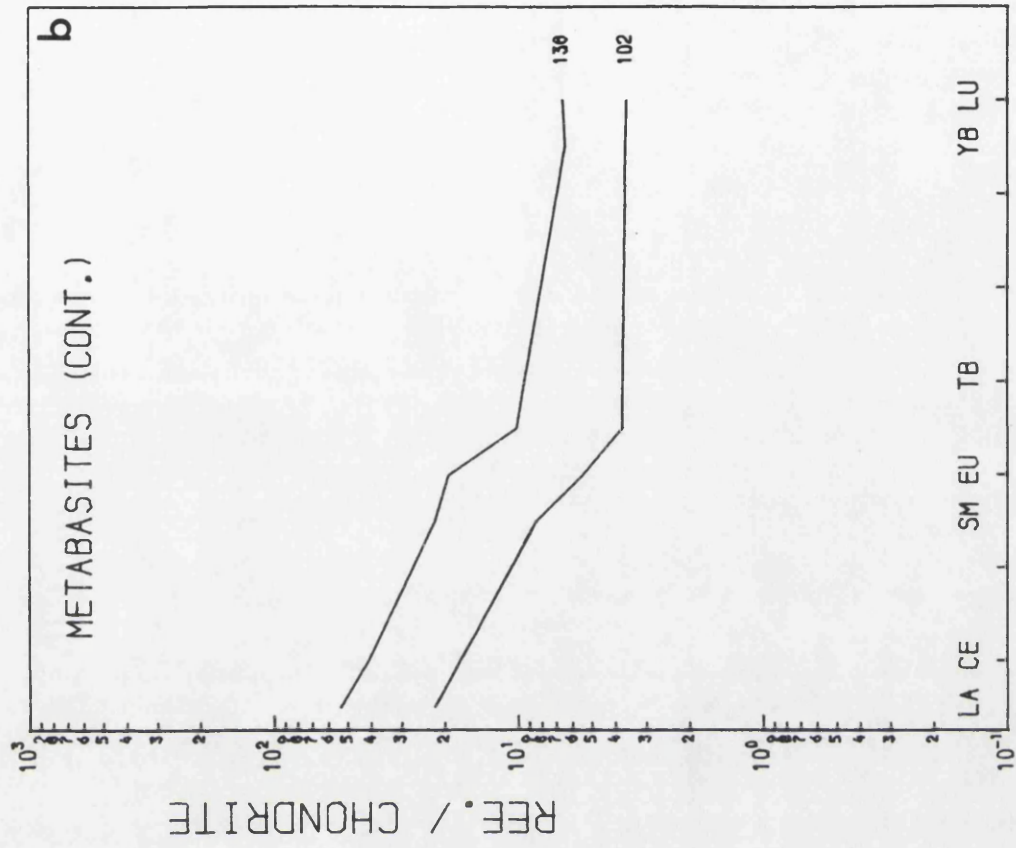


Fig. 4.5a,b Metabasite REE* patterns.

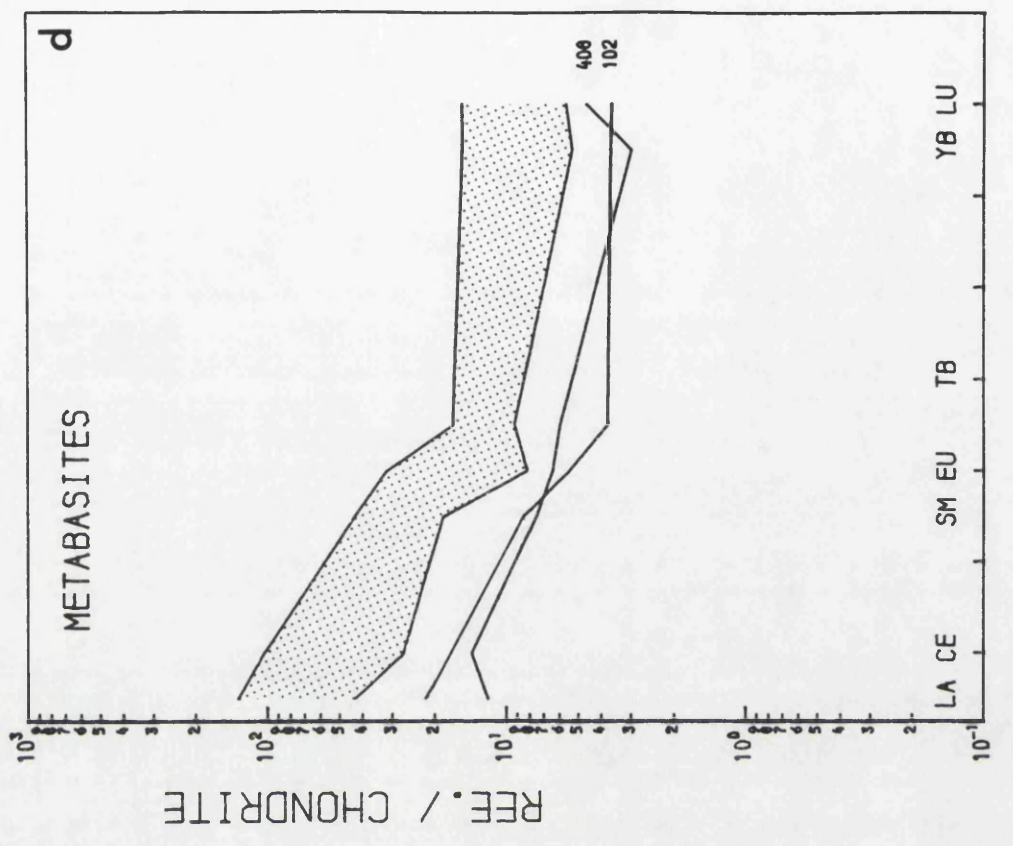
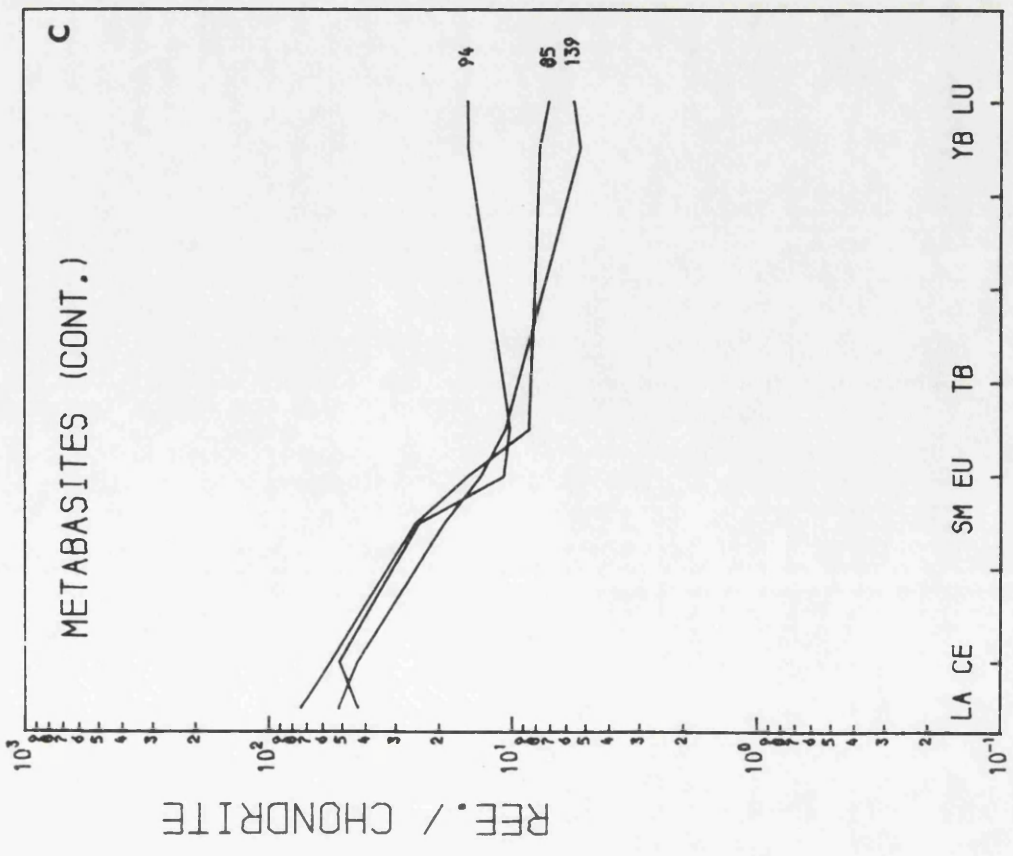


Fig. 4.5c Metabasite REE* patterns, d Metabasite range.

similar to those of the main metabasite group, would be strongly linear. Can cumulate pyroxenite rocks have a REE* pattern which is LREE* enriched, relative to the HREE*'s, even though HREE K_D 's of pyroxenes are greater than those of the LREE's? Cumulate pyroxenite can have a LREE enriched REE* pattern because the absolute concentrations of the REE's in cumulate pyroxene are dependent on the concentrations of the REE's in the magma, as well as on the K_D values. This relationship can clearly be seen in fig.4.8, where a hornblende's REE K_D curve and its REE* pattern are compared. If both BK408 and BK96 represent cumulate pyroxenites then how can the presence of a marked negative anomaly in the REE* pattern of BK96, be reconciled with the lack of one in the REE* pattern of BK408? BK408 is distinctly richer in MgO/(MgO+tFeO) than BK96, (0.7 and 0.59 respectively), and therefore BK408 would have crystallised from a more basic magma than BK96. Morris and Haskin (1974) presented experimental evidence, derived from synthetic melt compositions, that the Eu^{3+} ion has much greater stability, against the divalent ion, in MgO-rich silicate melts, compared with those which are low in MgO and rich in CaO. This is apparently in conflict with the fact that basic magmas are more reducing than acidic ones, which normally would mean that the 2+ ion is more stable, in basic magmas, than the 3+ ion. However, Wood and Fraser (1977) confirm the experimental conclusions by relating them to the interaction, in the melt, of two Eu oxides; Eu_2O_3 , which behaves amphoterically, ie. it has both basic and acidic properties depending on the environment, and EuO , which is a normal basic oxide. This Eu^{3+} stabilisation in MgO-rich melts would increase the affinity of Eu for phases such as pyroxene, and this could account for the lack of a significant negative *Eu anomaly, in terms of the errors on the REE* curve, in the REE* pattern of BK408. The negative *Eu anomaly in the REE* of BK96, would probably be compatible with the Eu K_D for pyroxene in a more fractionated, less MgO-rich magma, and is certainly compatible with the Eu K_D 's of pyroxene in basaltic magma (Table 4.1).

Three hypotheses for the igneous nature of the metabasite samples, apart from BK408 and BK96, are possible; they either represent magma compositions, cumulate rocks, or a collection of both cumulate rocks and rocks of magma compositions. Apart from BK408 and BK96, the metabasites have very similar REE* patterns, which are characterised by either a very small *Eu anomaly or none at all. Metabasite BK138 has a slight positive *Eu anomaly, while

BK94 has a slight negative one, although the latter anomaly may be more of a result of the way the REE* pattern is drawn, in view of the unusually high HREE* content of BK94, than a real feature of the rock. Therefore, it would appear that because the metabasite samples (apart from BK408 and BK96) are so similar, in REE* pattern, they must either be all of cumulate origin or they all represent magma compositions. Pyroxenes crystallising from more fractionated basic magmas than that from which sample BK408 crystallised, will have REE* patterns which contain a significant *Eu anomaly. The metabasite rocks are all thought to have contained primary pyroxenes (Chapter 2). Plagioclase crystallising from the same magmas will have a REE* pattern with a large positive *Eu anomaly. The metabasites, apart from BK408 and BK96, all contain large modal proportions of either labradorite or bytownite, which is almost certainly primary igneous plagioclase. If the metabasites, which do not have significant *Eu anomalies, are cumulate rocks, it would be necessary for each of them to contain both pyroxene and plagioclase in exactly the correct proportions, so that the *Eu anomaly of one phase is exactly cancelled out by that of the other phase. This coincidence does not seem likely and, therefore, it can be concluded that on REE evidence, the metabasite samples, apart from BK408 and BK96, represent magma compositions.

The range of the metabasite REE* patterns is shown graphically in fig.4.5d, with the shaded band representing the range of the high Σ REE* group. The average characteristics of the metabasite REE* patterns are given, in terms of the Σ LREE*, Σ HREE*, *Tb'/*Tb, and *Eu²⁺/*Eu³⁺ parameters, in Table 4.3. The slight concave-upwards shape of most of the metabasite REE* patterns is reflected in a mean *Tb'/*Tb ratio of 1.77, and the general lack of a large *Eu anomaly in the patterns is shown by the *Eu²⁺/*Eu³⁺ ratio, which is close to unity.

There is little evidence for a systematic change in the metabasite REE* patterns, which might be equated with changes due to fractional crystallisation of the metabasite magmas. However, of the metabasites which represent magma compositions, BK102 is probably the least fractionated because of its low REE contents, its fairly high MgO/(MgO+tFeO) ratio (0.55), and its high Cr (190 ppm) and Ni (85 ppm) contents. Of the high Σ REE* group, BK138 has the REE* pattern most similar to that of BK102, and would be a likely representative of a strongly fractionated metabasite magma, which

may have evolved from the BK102 magma composition because of its low $MgO/(MgO+tFeO)$ ratio of 0.26, and its low Cr (39 ppm) and Ni (10 ppm) contents.

If a magma of the composition of BK138 did evolve from the BK102 magma composition, then this involved enrichment, in the magma, of the LREE*'s and MREE*'s relative to the HREE*'s (see fig.4.5b) and also the generation of a slight positive *Eu anomaly, although this anomaly is not present in the other metabasite REE* patterns. At first sight, this appears to be consistent with pyroxene fractionation from the metabasite magmas.

4.3.3b Tonalitic orthogneiss REE* patterns.

The tonalitic orthogneiss REE* patterns are shown in fig. 4.6a,b,c and their range (not including BK1) is shown in fig.4.6d. Of the rocks represented in these plots, BK406, BK405, BK97, BK136, BK105, BK106, BK107, and BK113 are all melanocratic tonalitic orthogneisses (c. >25% mafic content), and BK404, BK403, BK402, and BK1 are leucocratic tonalitic orthogneisses (c. <25% mafic content).

The melanocratic tonalitic orthogneisses all have very similar REE* patterns, except for BK113 which has a low Tb value. These patterns are characterised by a $\Sigma LREE*/\Sigma HREE*$ enrichment of around 10, and a slight to moderate negative *Eu anomaly (mean $*Eu^{2+}/*Eu^{3+} = 0.78$). Compared with the high $\Sigma REE*$ metabasite group, the melanotonalitic orthogneisses have high REE concentrations with an average $\Sigma LREE*$ approximately 3 times greater than the average metabasite value, and an average $\Sigma HREE*$ value more than twice that of the metabasites. The melanocratic tonalitic orthogneiss REE* patterns are generally slightly more linear than those of the metabasites, as illustrated by their smaller average $*Tb'/*Tb$ value (see Table 4.3), and this indicates that although primary hornblende is found in the melanocratic tonalitic orthogneisses, it was pyroxene, together with plagioclase, which controlled the bulk of the REE fractionation from the strongly fractionated, high $\Sigma REE*$, metabasite magmas to the melanocratic tonalitic orthogneiss magmas. This is consistent with the smaller tendency of pyroxene to deplete a magma in the MREE, relative to the HREE depletion, compared with hornblende (Hanson, 1980). Plagioclase is needed as a fractionation phase from the high $\Sigma REE*$ metabasite magma simply to generate the negative *Eu anomaly exhibited by the melanocratic tonalitic orthogneisses.

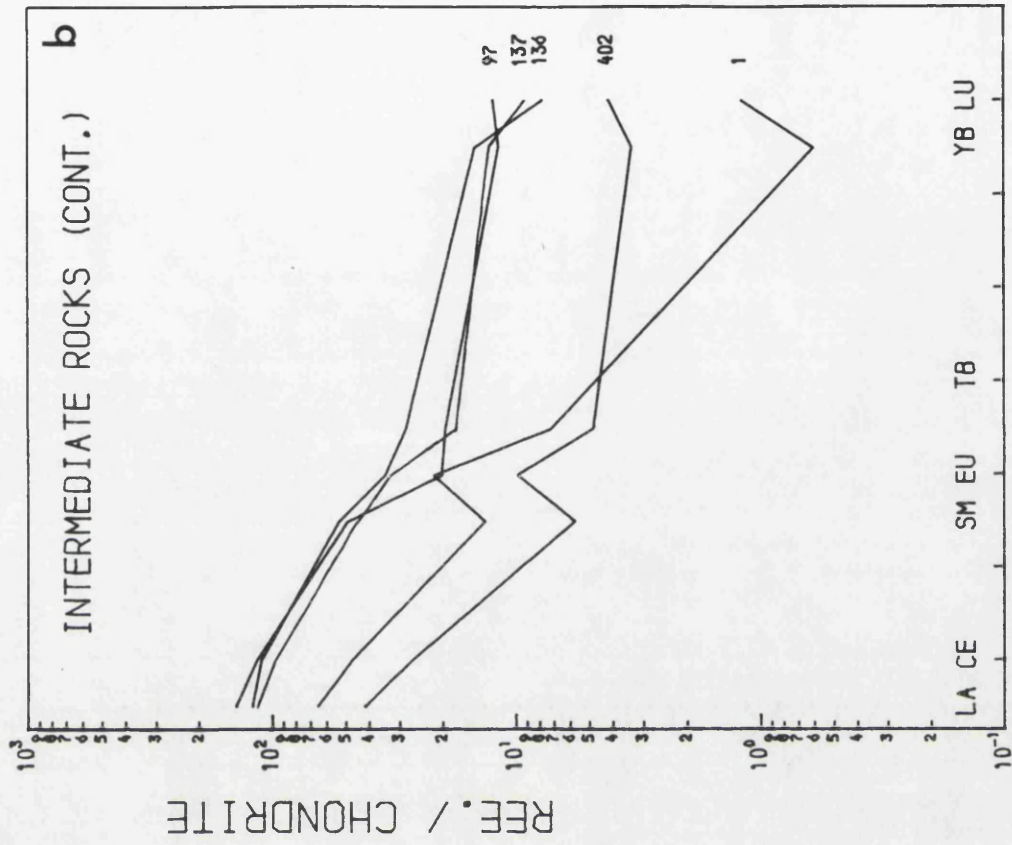
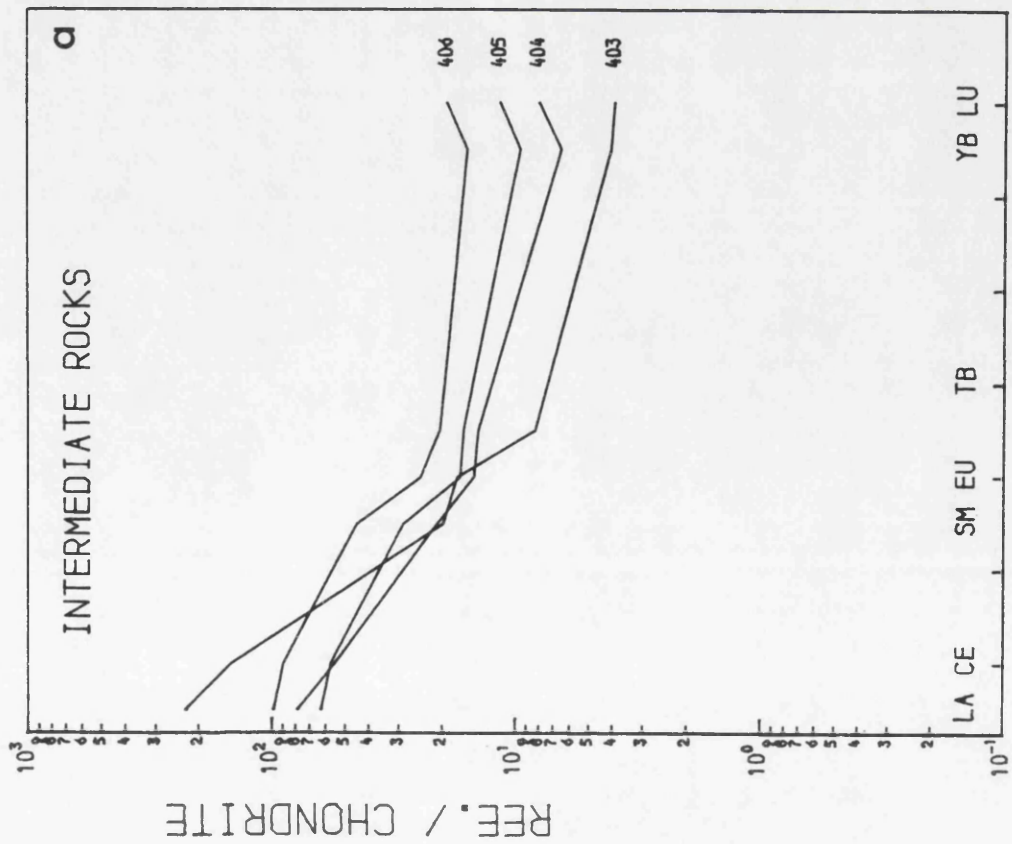


Fig. 4.6a,b Tonalitic orthogneiss REE* patterns.

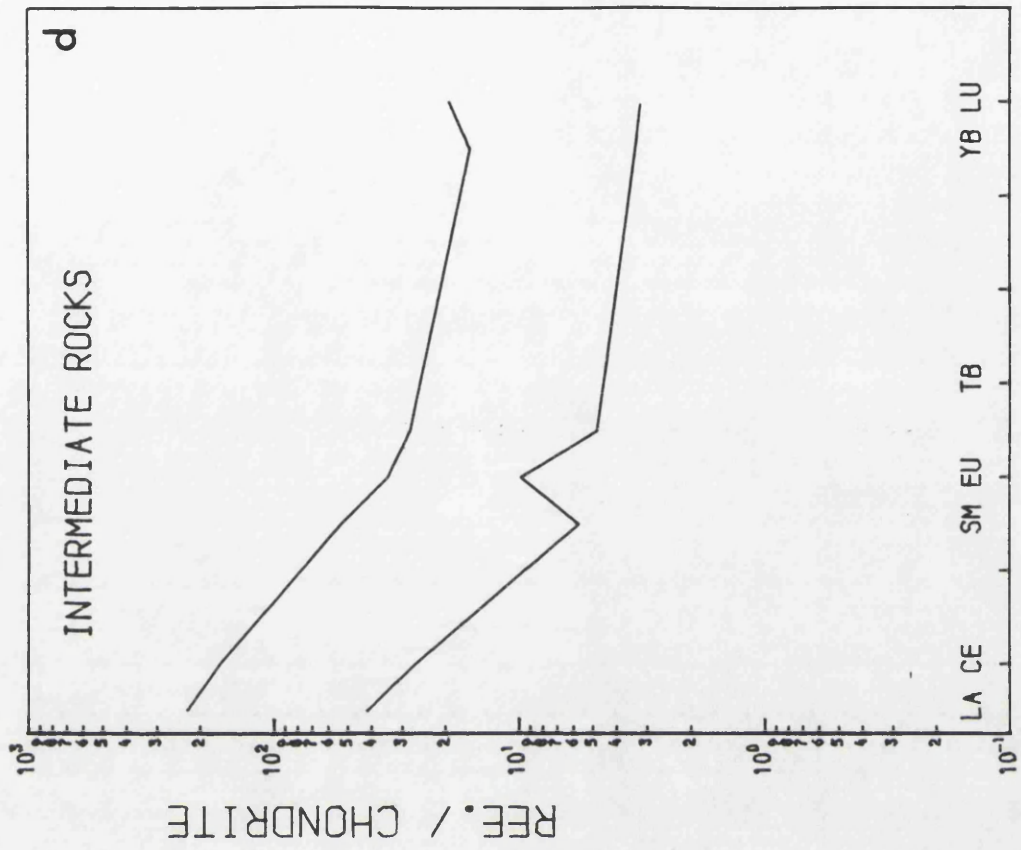
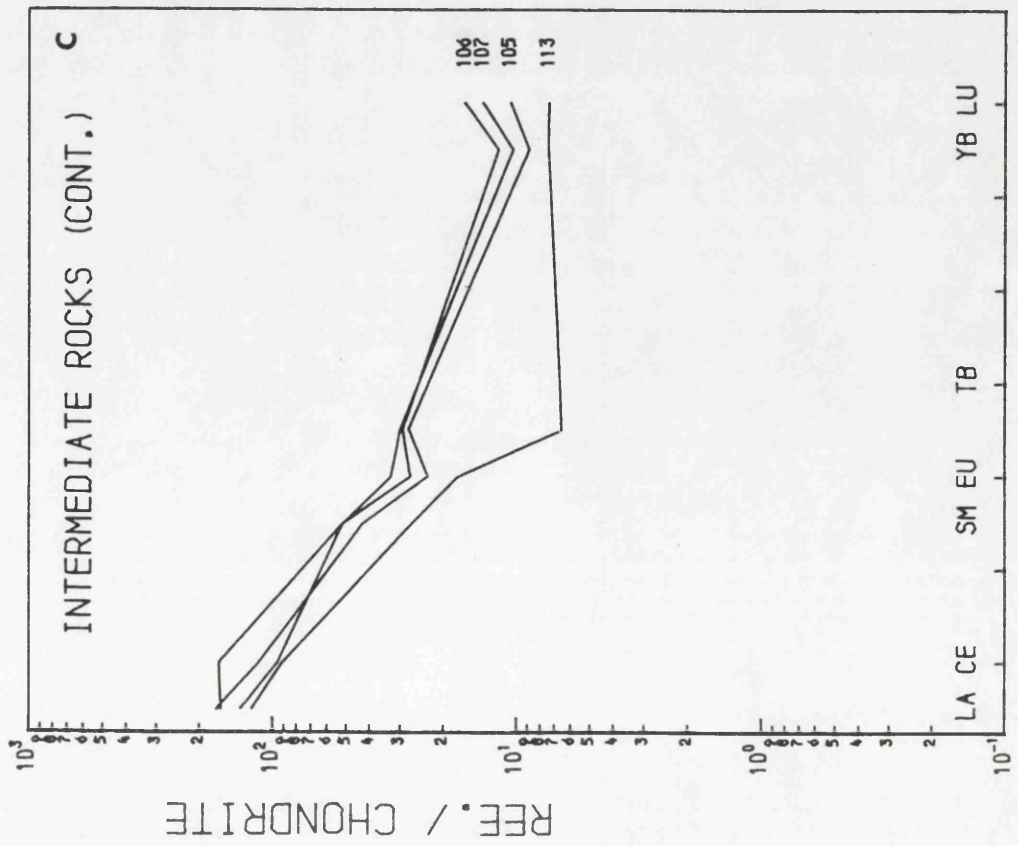


Fig. 4.6c Tonalitic orthogneiss REE* patterns, d range.

As was the case for the metabasites, there seems to be little evidence of a distinct trend of REE fractionation in the melanocratic tonalitic orthogneiss group. Therefore in the modelling of the metabasite-orthogneiss fractionation history (Chapter 5), these rocks will be treated as one magma type, of which sample BK406 is a fairly typical representative.

The Kf-rich tonalitic orthogneiss REE* patterns are shown in fig.4.10 and their numerical characteristics are listed in Table 4.3. It can be seen that these patterns equate with the ordinary melanotonalitic orthogneiss patterns and so the assertion that these Kf-rich rocks are essentially members of the melanotonalitic orthogneiss group, is proved to be correct.

The leucotonalitic orthogneisses differ from the other tonalitic orthogneisses, in that they have a broad spectrum of REE* patterns, ranging from that of BK404, which is similar to that of the average melanotonalitic orthogneiss REE* pattern, to ones with a positive *Eu anomaly and variable Σ LREE* and Σ HREE* values. This latter group is represented by the samples BK403, BK402, and BK1. Compared with the melanotonalitic orthogneissic, the leucotonalitic varieties have low MREE* and HREE* values, and a range of LREE* values which overlaps that of the melanotonalitic rocks. Therefore, the leucotonalitic orthogneisses have a steeper, although not necessarily straighter, REE* pattern than the melanotonalitic rocks, and this is signified by their larger average Σ LREE*/ Σ HREE* ratio (21.63, compared with 9.8). The fact that they show a trend towards significant MREE* depletion, is shown by their average *Tb'/*Tb ratio which is 2.36, compared with 1.46 for the melanotonalitic rocks.

It is difficult to explain the variations of the REE* in the leucotonalitic orthogneisses, if these rocks represent the successive magma compositions of a single parental magma, undergoing crystal fractionation. This is because the REE* variation cannot be fitted into a simple fractionation scheme, without causing some contradiction of the data. For example, if BK404 is taken as the least fractionated magma REE* pattern, then the initiation of a positive *Eu anomaly, and HREE* depletion, in the magma, could be coincident either with a marked enrichment of LREE's, as in BK403. Since the very low values of the HREE*'s, relative to the LREE*'s, in BK1 are atypical of the tonalitic orthogneiss suite, the REE* pattern of this rock will not be

considered in any attempt to explain the overall fractionation of the REE's in the tonalitic rocks. However, the REE* pattern of BK1 is similar to some of the granitic orthogneiss, ie BK104 (fig.4.7), although the absolute REE concentrations in BK1 are much lower than in BK104. This serves to confirm the previous suggestion, (this chapter, introduction), that the orthogneiss rocks are the products of several magmatic sequences, each with a pattern of major element variation closely similar to the others, but with a significantly trace element pattern. Some of the variation in the LREE contents of the leucotonalitic orthogneiss samples possibly may also be due to a strongly anisotropic distribution, in the rock, of late-crystallising orthite. The LREE's can make up to c.23 wt% of orthite (Deer et al., 1966), and thus this anisotropic distribution of orthite could have created LREE inhomogeneity, on a scale of several centimetres, in the leucotonalitic orthogneiss plutons.

BK404 can be considered to be the least fractionated of the group of leucotonalitic orthogneiss samples, because its REE* pattern is similar to the melanotonalitic orthogneiss REE* patterns. A choice has to be made as to which of the two rocks, ie. BK403 and BK402, both of which have REE* patterns with a positive *Eu anomaly, best continues the main trend of fractionation of the orthogneiss rocks, from a REE* distribution similar to that of BK404. Firstly, BK403 has a smaller *Eu anomaly, which suggests that it is closer, in terms of the degree of fractionation, to BK404, than is BK402. Secondly, as discussed previously, the point at which the REE D values become greater than unity, and hence the REE's become depleted in a magma with further fractionation, should occur in the MREE's and HREE's, before the LREE'S. BK403 shows this feature, relative to BK404, whereas BK402 is lower in all the REE's, relative to BK404. Thirdly, the REE* pattern of BK403 is very similar to the least fractionated REE* patterns of the granodioritic and granitic orthogneisses. For these three reasons, BK403 is considered to have the REE* pattern which most readily conforms to a fractionation scheme from a parental melanotonalitic orthogneiss magma (with a REE* distribution similar to that of BK406), to the granodioritic and granitic orthogneiss magmas.

If BK402 has a more fractionated REE* pattern, compared with BK403, as is suggested by the larger positive *Eu anomaly of the former, then it might be expected that REE* patterns similar to that of BK402 would also occur in the granodioritic and granitic

orthogneisses. This is so (fig.4.7b), and this overlap of REE* patterns between the different rock groups again emphasises that the orthogneisses were formed from several magmas.

The steepness of the REE* pattern of BK403 ($\Sigma\text{LREE}^*/\Sigma\text{HREE}^* = 46.9$) compared to that of the melanotonalitic rock BK406, its strong MREE* depletion, ($*\text{Tb}'/*\text{Tb} = 3.15$), and its positive *Eu anomaly, indicate that the magmas from which these rocks crystallised, were related by the fractionation of a mineral assemblage which included hornblende as the dominant phase. This is obvious from the hornblende REE K_D 's for intermediate magmas (Table 4.1), which show that hornblende fractionation can produce all of the features of the BK403 REE* pattern. The presence of plagioclase in the fractionation assemblage can be qualitatively deduced, in the REE data, from the nature and size of the *Eu anomaly (see Table 4.1, plagioclase REE K_D 's), when plagioclase forms a large proportion, say 70% of the fractionating solid. However, in intermediate to acidic magmas, the Eu K_D of hornblende becomes similar to that of plagioclase, and if hornblende dominates the fractionation assemblage then plagioclase fractionation cannot be deduced qualitatively.

4.3.3c Granodioritic and granitic orthogneiss REE* patterns.

The samples of the granodioritic and granitic orthogneiss, including the aplite, BK413, have an extremely broad range of REE* patterns, that define a complete spectrum from those of the least fractionated granodioritic orthogneisses, which are similar to that of the that of the leucotonalitic rock, BK403, right through to that of the aplite. The trend of REE variation in these rocks can be explained more easily once a thorough knowledge of the REE geochemistry of the aplite, BK413, has been obtained.

Sample BK413 was taken from an aplite vein, at least 2 metres in length and up to 18 cm. in width, contained in a Kf-rich tonalitic orthogneiss mass, in the north of the Shannavara district. This orthogneiss mass contains many such aplites, and all are confined entirely within the intrusion itself, so that there can be no doubt that the aplites represent late-stage residual fluid which segregated just prior to the complete solidification of the intrusion. The sampled aplite vein has an interesting mineralogy. It consists, for the main part, of plagioclase, Kf-feldspar, quartz, and minor accessories, this being the mineralogy of BK413, but it also contains patches of hornblende-bearing aplite. The hornblende

occurs as fresh poikilitic phenocrysts, up to 1 cm. in mean diam., and may make up to 50% of the hornblende-aplite patch. The inclusions in the hornblende phenocrysts are invariably large rounded quartz grains, of c. 0.3-0.5 mm. diameter. A sample was taken of the hornblende-aplite immediately adjacent to the BK413 sample location. This sample was crushed into c. 1 mm. sized pieces and the hornblende was separated from it by magnetic separation and picking techniques. The final hornblende extract is estimated to be greater than 98% pure. The hornblende (analysis no. BK414), a microprobe analysis of which is listed in Appendix 2, was analysed ^{for} REE's and some of the other trace elements, and the results are listed in Table 4.4. If the aplite composition (BK413) accurately represents the composition of the final residual fluid, and the hornblende (BK414) and aplite represent an equilibrium assemblage, then the trace element concentrations of the hornblende, divided by those of the aplite, define K_D 's for hornblende in aplitic fluid. These K_D 's and the trace element composition of the aplite, BK413, are also listed in Table 4.4. The REE* patterns of the hornblende (BK414), and the aplite (BK413), and the hornblende REE K_D curve are shown in fig.4.8. The hornblende REE K_D curve has exactly the same shape as other hornblende REE K_D curves, as detailed in the literature (Schnetzler and Philpotts, 1970, Arth and Barker, 1976), although the REE K_D 's determined in this study are much larger than previously published values. To a certain extent, the absolute values of the K_D 's are relatively unimportant, because they are subject to many assumptions, and unknowns. For example, it is quite possible that the hornblende phenocrysts have a strong trace element zonation, even though microprobe analysis has confirmed that this is not the case for the major elements, and this would mean that only the outer rims of the phenocrysts were in equilibrium with the final aplitic fluid. If this is so, then the K_D 's determined from the bulk hornblende would not be true equilibrium values. These apparent K_D 's may be significantly different to the real K_D 's, depending on the variation of the latter during the growth of the hornblende phenocrysts, and on the trace element concentrations in the aplitic fluid. However, what is important is that the hornblende REE K_D curve has the characteristic shape, as this is compatible with the REE composition of the aplite, BK413, being dominantly controlled by the fractionation of the hornblende, BK414.

TABLE. 4.4

Hornblende/ Aplite K_D 's.

	Concentrations in ppm.		$K_D = \frac{414}{413}$
	Hornblende 414	Aplite (liquid) 413	
SC	162.30	0.71	225.00
LA	28.80	4.62	6.23
CE	91.88	6.47	14.20
SM	22.00	0.34	64.70
EU	3.00	0.68	4.38
TB	3.14	0.03	125.60
YB	7.84	0.15	52.26
LU	1.14	0.03	38.00
ZR	251.00	56.00	4.48
NB	28.00	8.00	3.50
Y	39.00	1.00	-
BA	411.00	1918.00	0.21
RB	142.00	164.00	0.87
PB	52.00	31.00	1.68
TH	20.00	5.00	4.00
K	1.65%	8.48%	0.19

For descriptive purposes, the granodioritic and granitic orthogneisses can be split arbitrarily, on the basis of the size of the $^{147}\text{Sm}/^{143}\text{Eu}$ anomaly, into two groups, one with $^{147}\text{Sm}/^{143}\text{Eu} > 1$ and the other with $^{147}\text{Sm}/^{143}\text{Eu} < 1$. The division roughly separates the granodioritic orthogneisses ($^{147}\text{Sm}/^{143}\text{Eu} > 1$, for the most part) from the granitic ones, as defined in the modal Strehkeisen diagram (fig.2.2).

The granodioritic group (fig.4.7a), are characterised by very steep REE patterns, having an average $\Sigma\text{LREE}/\Sigma\text{HREE}$ ratio of 50.8, which may or may not possess a $^{147}\text{Sm}/^{143}\text{Eu}$ anomaly. The range of $^{147}\text{Sm}/^{143}\text{Eu}$, of this group, is from 0.83 to 2.4 and indicates that the significant anomalies are positive ones, which is obvious in fig.4.7a. Of the five samples in the granodioritic group, BK400 has the largest positive $^{147}\text{Sm}/^{143}\text{Eu}$ anomaly and also the greatest MREE depletion, as measured by the $^{149}\text{Sm}/^{147}\text{Sm}$ ratio. The range of this parameter, in the granodioritic orthogneiss group, is 2.05 to 4.51 (Table 4.3), showing that all the samples have significant MREE depletion.

Samples BK98 and BK99 have REE patterns which are very similar to that of the leucotonalitic orthogneiss, BK403, and can be considered to be the least fractionated, in terms of the REE composition, of this group. These samples again illustrate the overlap of REE patterns of rocks from different groups. The granodioritic orthogneiss group has a relatively larger range of HREE and MREE abundances, than LREE abundances (fig.4.7a), and the $^{147}\text{Sm}/^{143}\text{Eu}$ values remain fairly constant throughout. This means that the greater the MREE depletion, measured by the $^{149}\text{Sm}/^{147}\text{Sm}$ ratio, of the REE pattern, then the larger the positive $^{147}\text{Sm}/^{143}\text{Eu}$ anomaly becomes. This REE variation is entirely consistent with a hornblende dominated fractionation hypothesis. Plagioclase may have been a minor fractionation phase from the granodioritic and granitic orthogneiss magmas, although this is not supported by textural, mineralogical, and phase relations, evidence (Chapter 2,3). The role of plagioclase in the evolution of the metabasite-orthogneiss magmas will be assessed by quantitative methods in Chapter 5.

The granitic ($^{147}\text{Sm}/^{143}\text{Eu} < 1$) group of orthogneisses have REE patterns (fig.4.7b,c) which define a clear trend of extreme depletion of all the REE's, except Eu, and which is especially pronounced in the MREE's. This trend culminates in the REE pattern

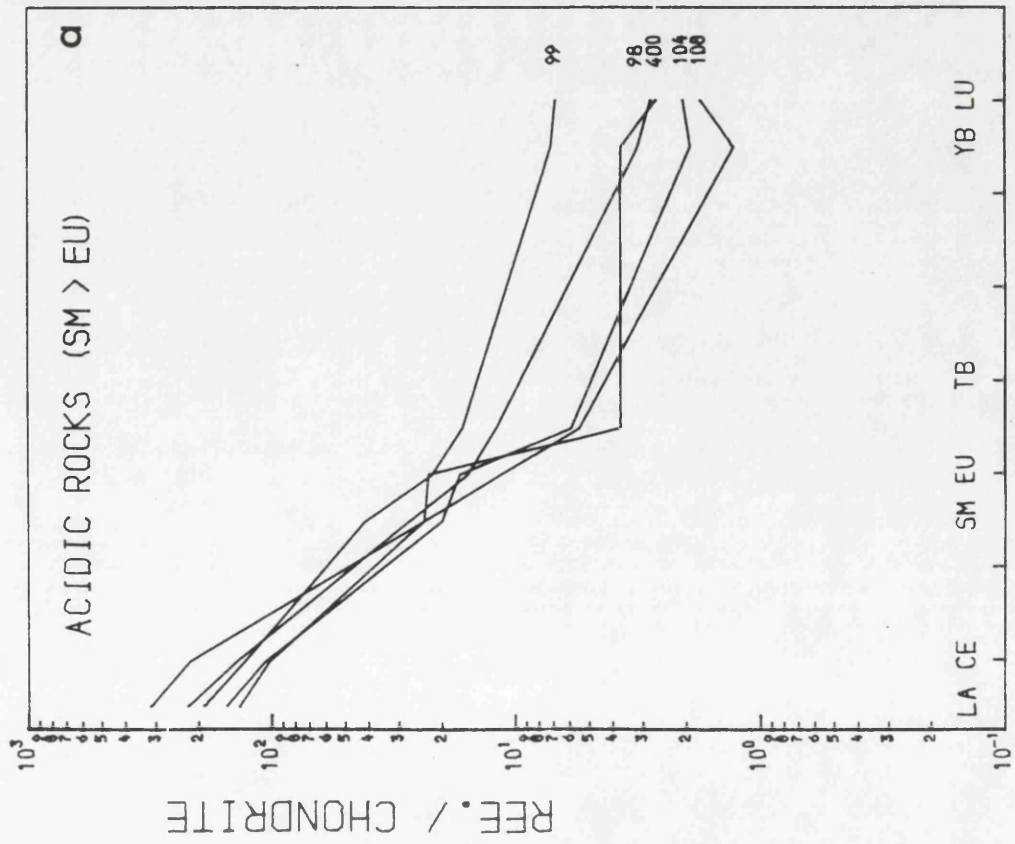
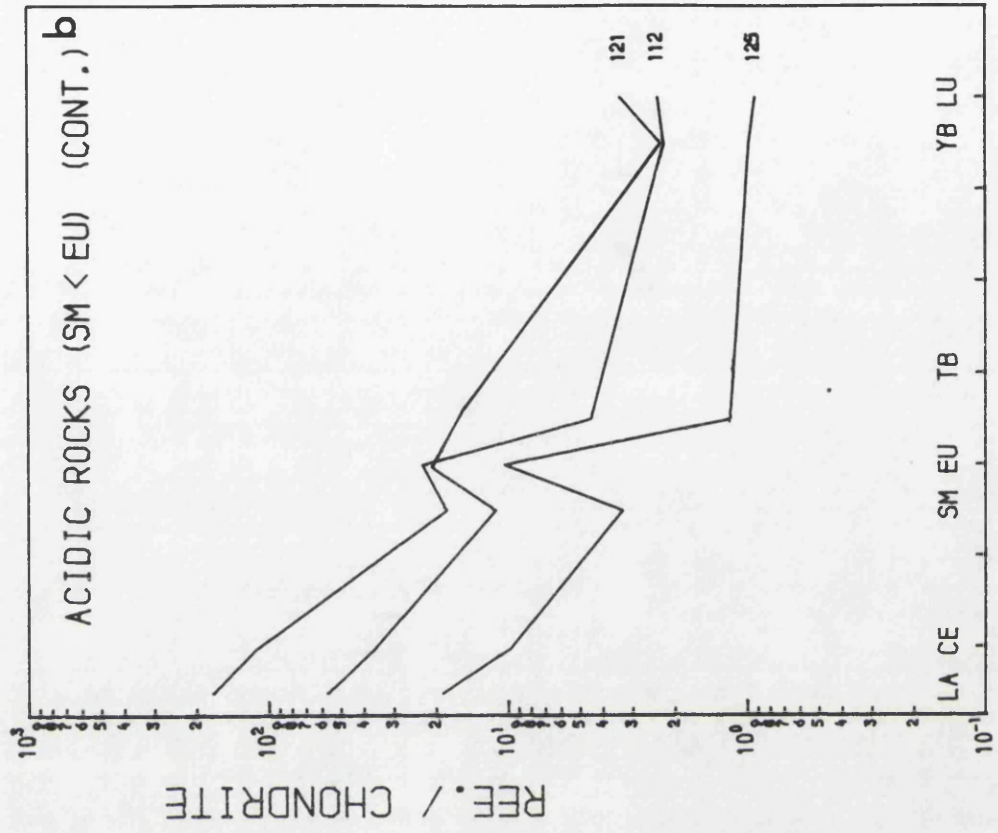


Fig. 4.7a,b Granodioritic and granitic orthogneiss REE* patterns.

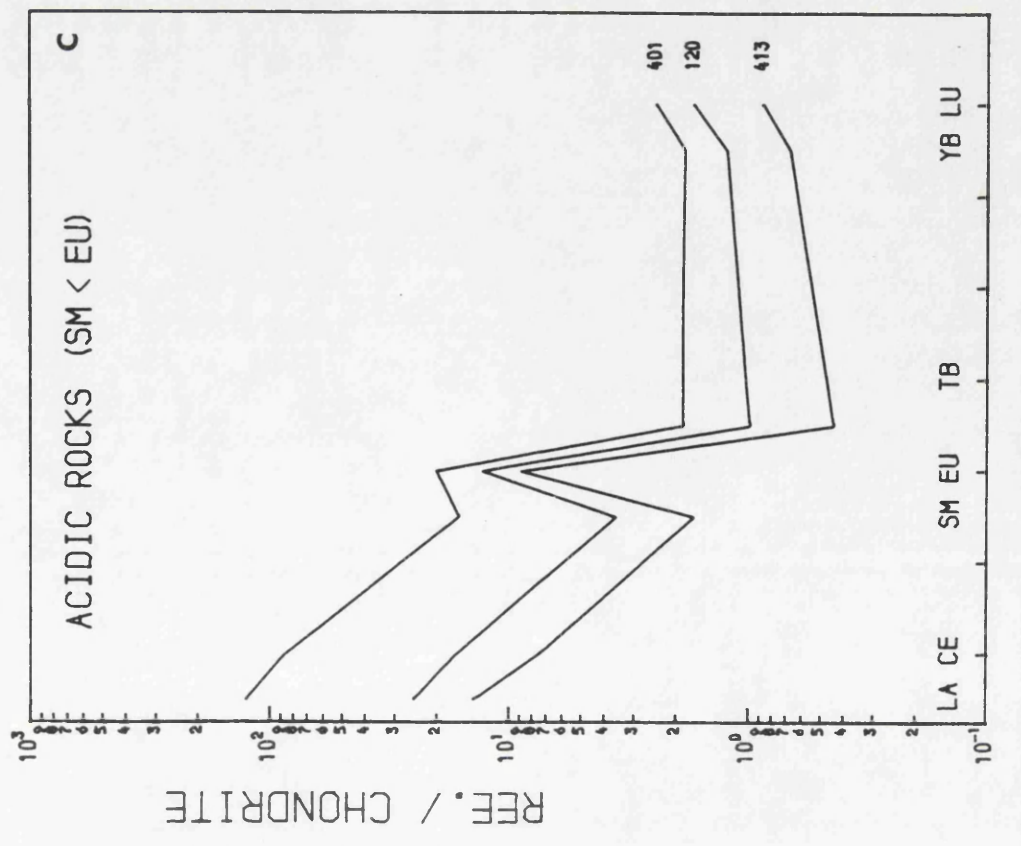
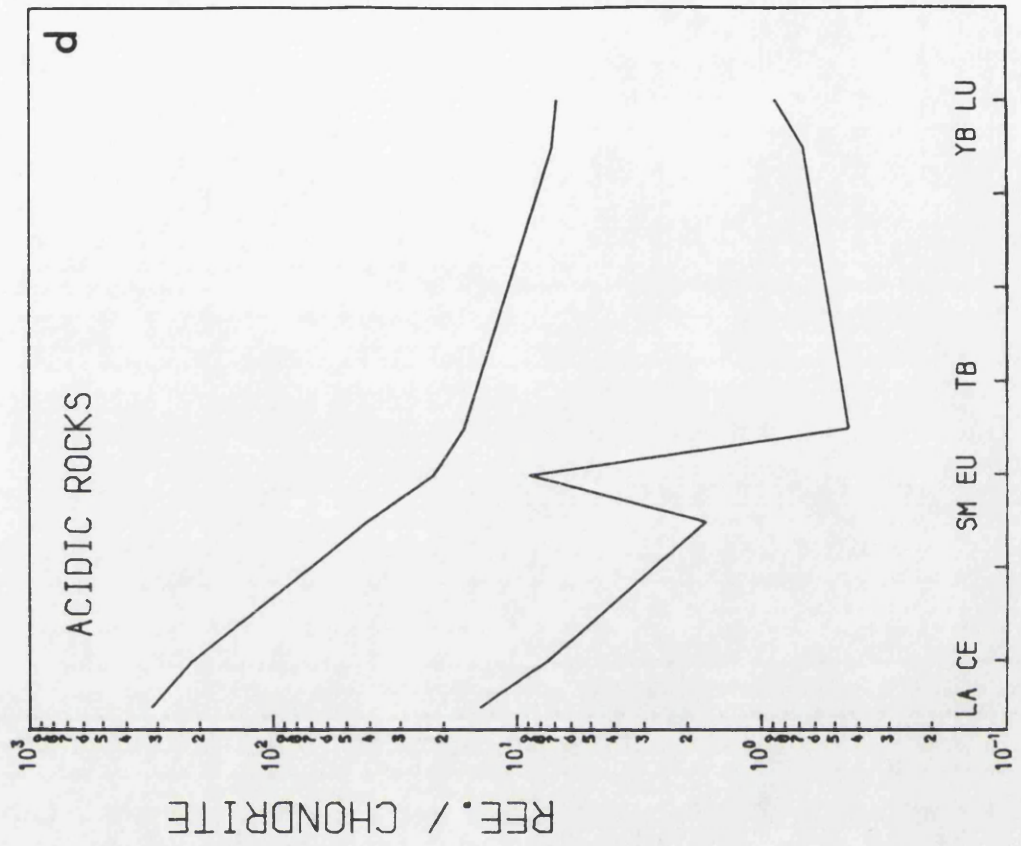


Fig. 4.7c REE* patterns (cont.), d G. & g. orthogneiss range.

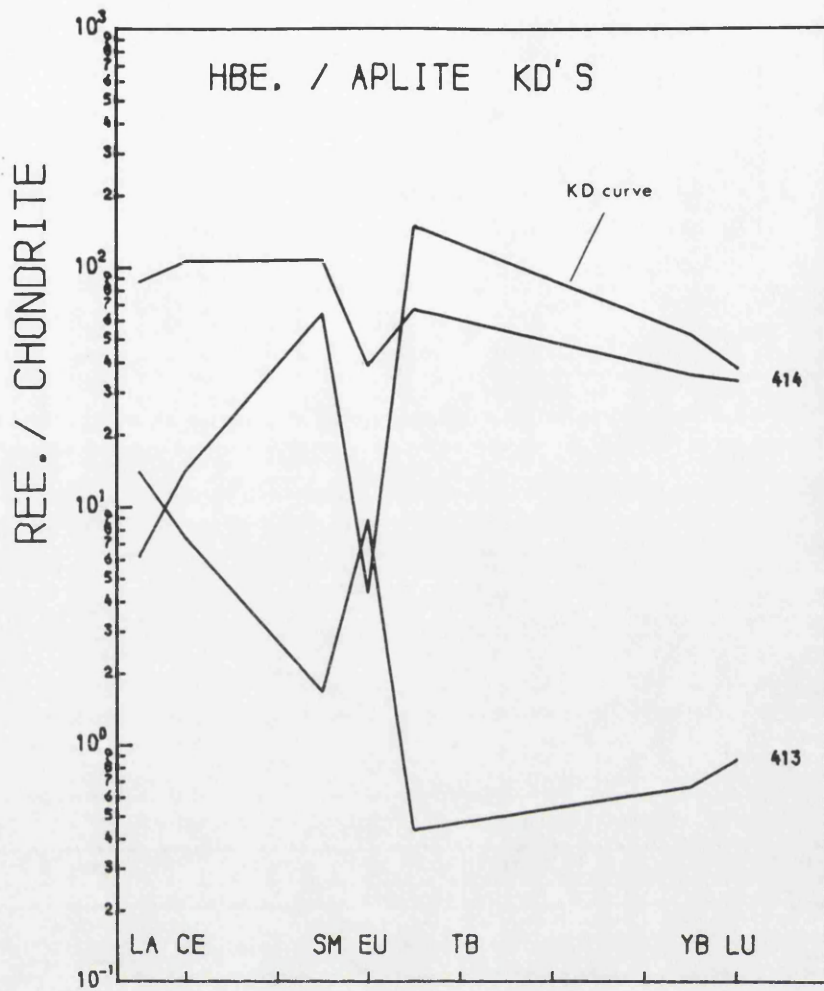


Fig. 4.8 REE geochemistry of a hornblende-aplite.

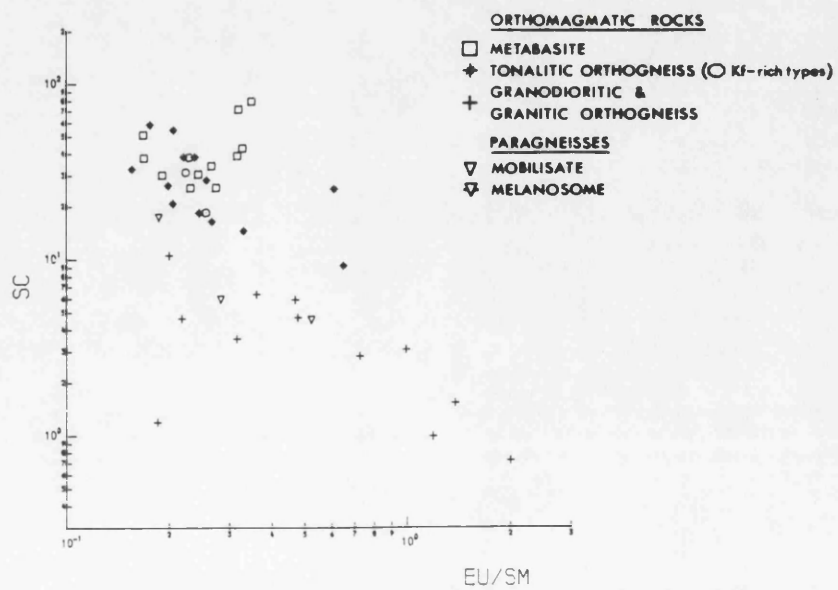


Fig. 4.9 Evolution of the *Eu anomaly.

of the aplite, BK413, which has a $*Tb'/*Tb$ ratio of 7.22 and a $*Eu^{2+}/*Eu^{3+}$ ratio of 10.27. The ranges of these two parameters and of the $\Sigma LREE*$ and $\Sigma HREE*$ parameters are given in Table 4.3. The total range of REE* patterns of the granodioritic and granitic orthogneisses is shown in fig.4.7d.

The REE K_D 's of the hornblende, BK414, in the aplite, BK413, are all much greater than unity, and therefore fractionation of a similar hornblende from the granitic orthogneiss magma would deplete all of the REE's in the magma. However, the LREE K_D 's of the hornblende (Table 4.4) are some 6 to 12 times smaller than those of the MREE's, excluding Eu, and some 4 to 5 times smaller than the HREE K_D 's, yet the granitic orthogneiss REE* patterns show a trend of greater relative depletion in the LREE's than in the HREE's (see fig.4.7b,c,d). This means that although the depletion trend of the MREE's and HREE's in these rocks is entirely consistent with the hornblende fractionation hypothesis, as is the increasing *Eu anomaly, there must be some new phase which is also fractionating from the granitic orthogneiss magma and strongly depleting it in the LREE's. Only one of minerals present in the more acidic orthogneiss rocks is able to do this, and this is orthite. Orthite has K_D 's for the LREE's, in granitic magmas, which are probably in excess of 1000, so only a small amount of orthite fractionation would be required to produce the LREE* depletion in the granitic orthogneiss magmas.

The evolution of the *Eu anomaly, relative to *Sm, throughout the metabasite-orthogneiss series, can be seen in the Sc v. Eu/Sm plot (fig.4.9). The metabasite and melanotonalitic orthogneiss rocks have REE* patterns with either a small *Eu anomaly or none at all. The leucotonalitic, granodioritic, and granitic orthogneisses show the progressive build up of a large positive *Eu anomaly, which is due to the much smaller increase in the Eu K_D of hornblende, compared with that of the other MREE K_D 's, with continuing fractionation of the magma. (N.B. the abscissa index, ie. Eu/Sm, is not a chondrite-normalised value)

4.3.3d Paragneiss REE* patterns.

The mobilisate, BK407, and the melanosome, BK409, were analysed for the REE's, and their REE* patterns are shown in fig.4.11. The two rocks cannot strictly be compared, in terms of their trace element abundances because they were not sampled from

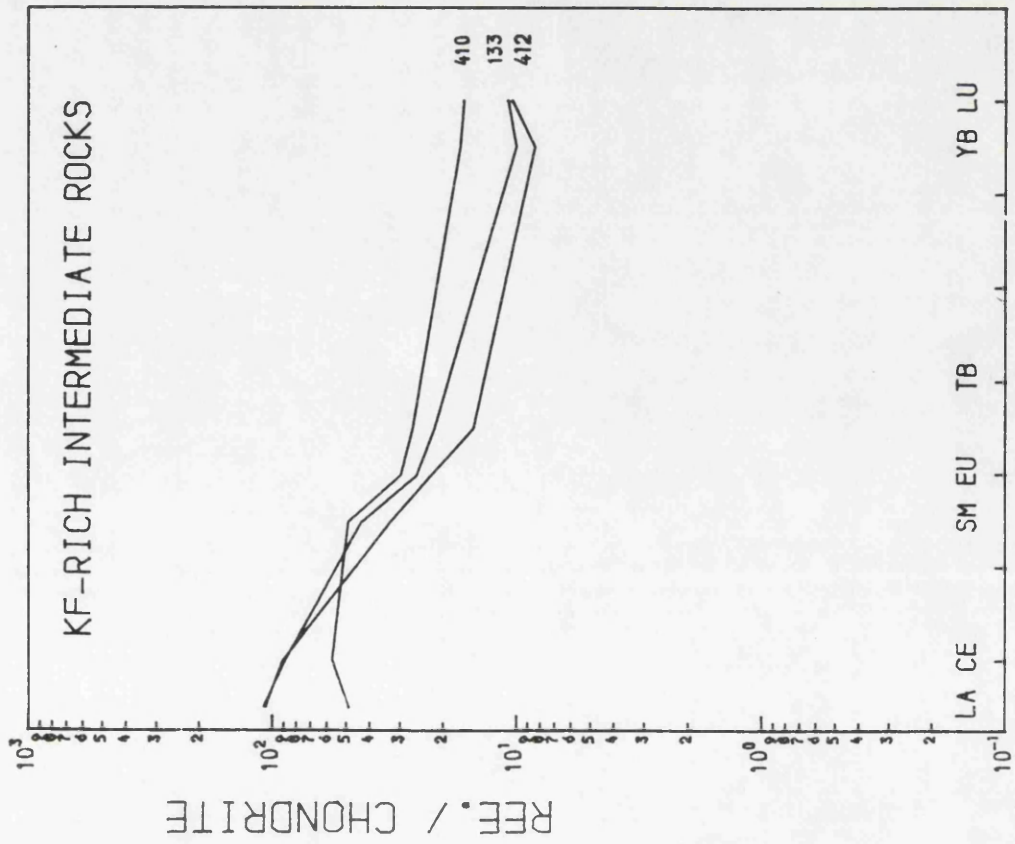


Fig. 4.10 Kf-rich tonalitic orthogneiss REE* patterns.

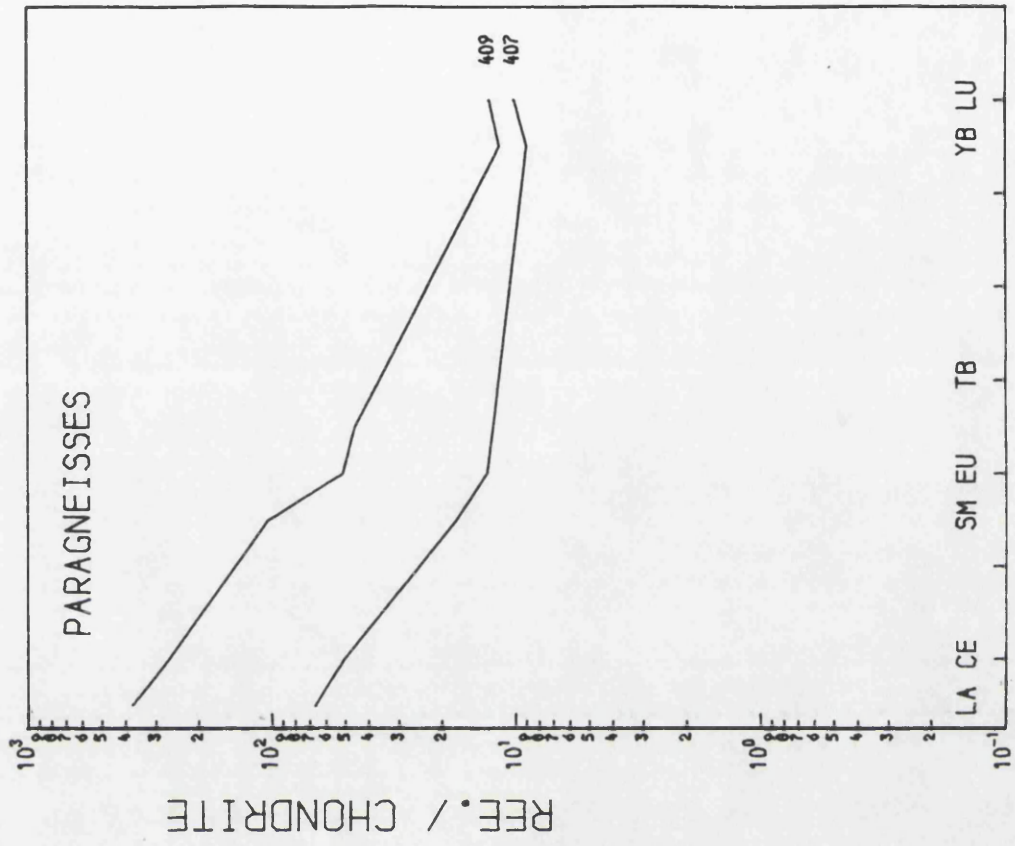


Fig. 4.11 Paragneiss REE* patterns.

adjacent locations. However, on the assumption that the mobilisate magma was fairly homogeneous in trace element composition across a wide area, it can be seen that the REE's are more abundant in the melanosome, than in the mobilisate. The other trace elements also show the same feature (section 4.2.2). The LREE and MREE abundances in the melanosome are more than 5 times those in the mobilisate, while the abundances of the HREE's, ie. Yb and Lu, are very similar in both rocks.

The trace element composition of a solid residue (melanosome), in a partially molten rock, is dependent on the mineralogy of the residue. The mineralogy of the melanosome, BK409, has been described in Chapter 2, and it contains 4 major phases; biotite, sillimanite, plagioclase (An_{42}), and ilmenite. Of these, plagioclase and biotite are thought to be in a state of decay through melting. The plagioclase of the melanosome is considerably more calcic than in the mobilisate, and this is reflected in the strong enrichment of Sr in the melanosome, relative to the mobilisate. Therefore, it was expected that the melanosome would also be suitably enriched in Eu, relative to the other REE's, because Eu, like Sr, tends to substitute for Ca in plagioclase, (Ca and Eu have almost identical ionic radii). However, no positive *Eu anomaly is observed in the REE* pattern of BK409, on the contrary, it has a significant negative *Eu anomaly ($*Eu^{2+}/*Eu^{3+} = 0.75$). This strongly implies that some other phase in the melanosome, with a large Eu K_D , but even larger LREE and MREE K_D 's, is swamping the effect of the Eu K_D of plagioclase. Biotite has low K_D 's for the REE's (Hanson, 1980), and can be disregarded. The REE's are unlikely to substitute for Al, in sillimanite, because of the large difference in ionic radius between them (REE ionic radii = 1.14 to 0.85A) and Al (ionic radius = 0.51A). This leaves ilmenite as the only other alternative. Schock(1977) determined the REE contents of 9 titanomagnetites and their associated rhyodacite-dacite pumice matrices, and calculated the REE K_D 's of this phase. Schock found that the LREE and MREE K_D 's, of titanomagnetite, were significantly greater than the HREE K_D 's, and in most cases, the MREE K_D 's were greater than unity. The REE K_D 's of a titanomagnetite contaminated by ilmenite were very large (La $K_D = 6.0$), with a decrease in K_D occurring from the LREE's, through the MREE's, to the HREE's. The Eu K_D 's of the titanomagnetites were significantly lower than those of the other MREE's. The K_D signature of titanomagnetite,

contaminated with ilmenite, has all of the qualities needed to explain the relative REE distribution between the melanosome and the mobilisate portions of the paragneiss.

The REE* patterns of BK407 and BK409 have a similar shape to those of the metabasite and melanotonalitic orthogneiss rocks. Therefore, the assimilation of these paragneisses, by the metabasite and melanotonalitic magmas, would not greatly alter the overall shape of the REE* patterns of the magmas. In the field, the ratio of mobilisate to melanosome is roughly 4:1, which means that REE* pattern of the bulk paragneiss would be rather more similar to that of BK407, than that of BK409. The assimilation of bulk paragneiss, by the metabasite magma, would enrich it in all REE's, and could therefore be a significant factor in the generation of the melanotonalitic orthogneiss magmas.

4.4 Tectonic setting of the metabasites from their Zr, Ti and Y contents.

The use of the elements, Zr, Ti, and Y, as discriminators in distinguishing the palaeotectonic affinities of basalts, stems from their immobile nature during metamorphism (Cann, 1970). The metabasite rocks are plotted in the Zr-Ti-Y discrimination diagram (fig.4.13), although they are not strictly applicable to this plot since it was designed for basaltic extrusive rocks (Pearce and Cann, 1973). However, it can be seen that the metabasite rocks plot predominantly in the 'within-plate' field, which encompasses both continental and oceanic island basalts. This 'within-plate' field is the best defined of all the fields in the discrimination diagram (Pearce and Cann, 1973). A 'within-plate' hypothesis for the tectonic setting of the metabasite magmas, rather than a volcanic arc hypothesis, is backed up by the conclusion, based on the major element chemistry (section 3.3), that the metabasite, and orthogneiss, rocks do not belong either to the calc-alkali series, or to the tholeiitic series, of volcanic arc magmatic rocks. The metabasite rocks have been shown to be subalkaline (fig.3.5) and they were intruded into the very thick Dalradian sedimentary pile, which was deposited in an ensialic basin (Phillips et al., 1976), and so the metabasite rocks would appear to fit well with the hypothesis that they were intruded into a 'within-continental plate' tectonic environment.

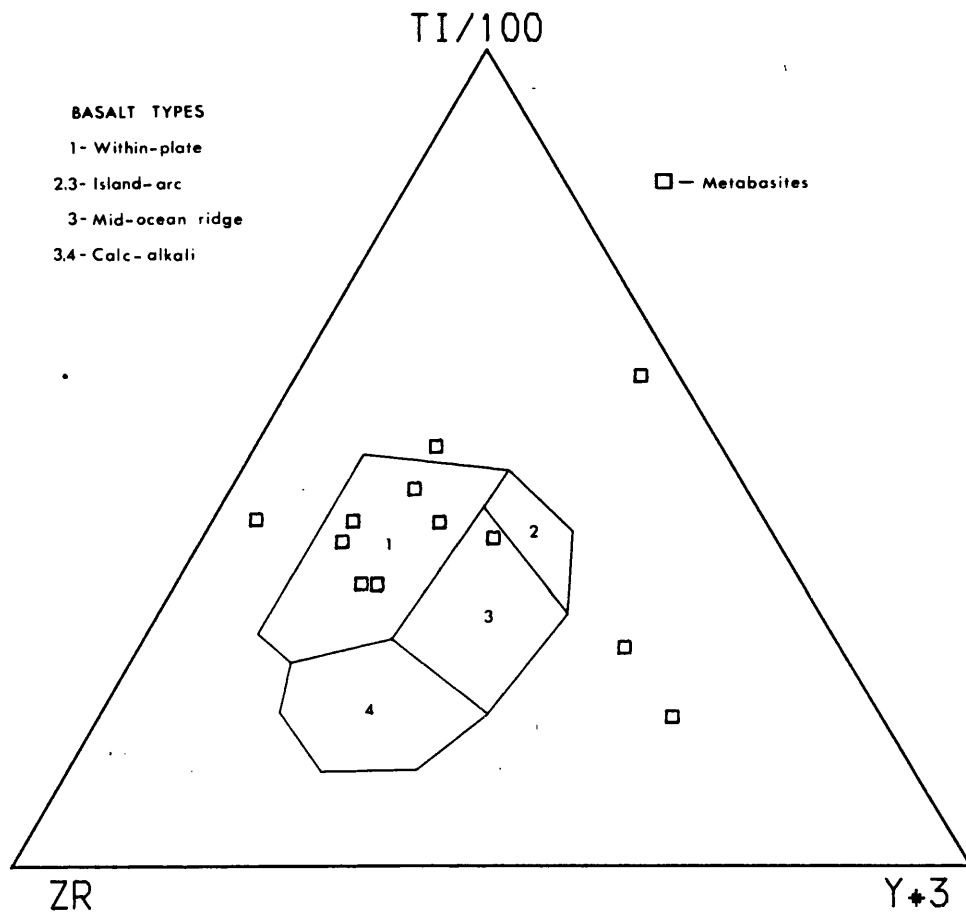
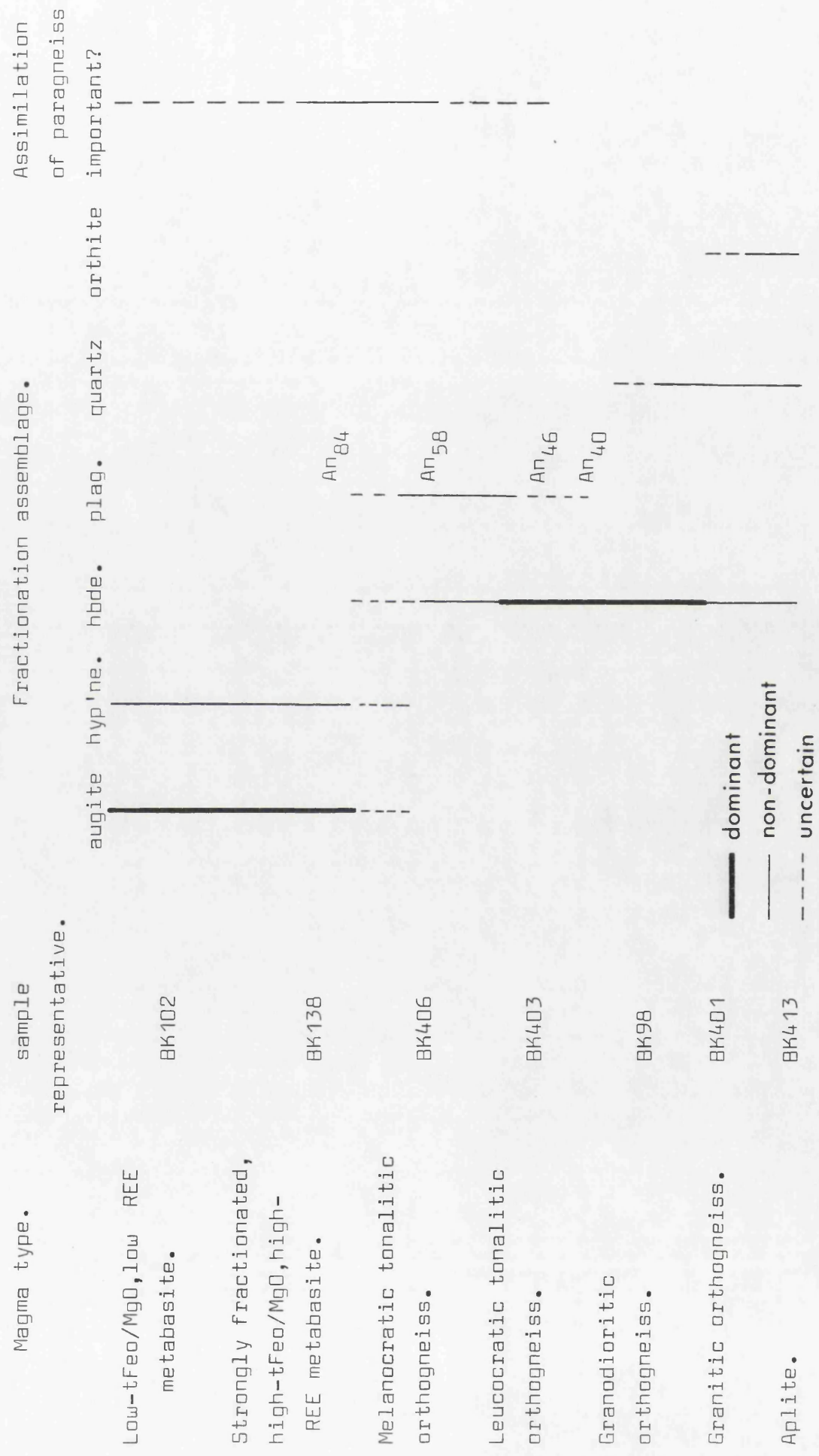


Fig. 4.13 Ti-Zr-Y discrimination diagram (Pearce and Cann, 1973).

Fig. 4.14 A qualitative summary of the differentiation of the metabasite-orthogneiss magmas.



4.5 Conclusions.

The following conclusions were reached, in this chapter, from a qualitative study of the trace element distributions of the rocks of the intrusive complex:-

1. The metabasite and orthogneiss rocks form a continuous trend in almost all the trace element v. SiO_2 plots, which indicates that they are probably comagmatic rocks.

2. The scatter of the incompatible element data, for these rocks, may reflect significant differences in trace element contents between the parental metabasite magmas.

3. From a consideration of the Sr v. Cr plot and from the the REE evidence, it is shown that all but two of the metabasite samples represent magma compositions. The other two samples have REE* patterns compatible with the hypothesis that they were composed of cumulate pyroxene before the amphibolitisation of the metabasite rocks occurred.

4. The reversal of the metabasite magma SiO_2 depletion trend could have been accomplished by the initiation of a hornblende + plagioclase fractionation assemblage, possibly augmented by the assimilation of siliceous paragneiss.

5. The REE* patterns of the orthogneiss samples show that hornblende was a fractionation phase over the whole composition range of the orthogneiss magmas.

6. The Sr distribution, though scattered, supports the conclusion, made in the previous chapter, that plagioclase did not fractionate from the granodioritic and granitic orthogneiss magmas.

7. Orthite fractionation occurred in the granitic orthogneiss magmas and depleted them in the LREE's.

8. The relative trace element distribution in the melanosome and mobilisate components of the paragneiss, is consistent with the expected pattern of trace element partitioning between a siliceous granitic magma and a mineral assemblage containing biotite, plagioclase, and ilmenite.

Most of the conclusions of this and the previous chapter, relate, in a qualitative manner, the metabasite and orthogneiss rocks by a process of crystal fractionation. These conclusions are summarised in fig.4.14.

Chapter 5.

Trace element modelling of the differentiation of the metabasite-orthogneiss magmas.

In this chapter the fractionation scheme for the differentiation of the metabasite magmas, going through to compositions represented by the orthogneiss rocks, will be quantitatively tested using trace element mass balance theory. It is necessary first, to select the most appropriate mathematical model for the fractional crystallisation process acting on a basic magma ascending through plutonic levels in the crust. This study will deal only with closed system fractionation models, ie. those in which the magma is not recharged with new batches of less fractionated magma from the same source.

5.1 Mathematical models of trace element mass balance in a magma undergoing fractional crystallisation.

Mass balance equations were first used to predict the behaviour of trace elements in simple magmatic processes in 1954, when Neumann et al. applied the Rayleigh distillation equations (Rayleigh, 1896) to the problem of magmatic differentiation. Later the equations were refined, first by Greenland (1970) and then by Albarede and Bottinga (1972). The closed system fractional crystallisation process can be considered (for the simplified case of crystallisation of phases in constant proportions, and for constant distribution coefficients) in terms of a binary system defined by the mixing of the two end-member equations:-

1. Surface equilibrium crystal fractionation equation.

$$\frac{C_{\delta L}}{C_{\delta 0}} = F^{(D_{\delta}-1)}$$

where:-

δ = trace element

$C_{\delta L}$ = concentration of δ in the differentiated liquid

$C_{\delta 0}$ = concentration of δ in the parental liquid

F = the fraction of liquid remaining, relative to the initial mass of liquid.

D_{δ} = the bulk distribution coefficient of δ , defined as:-

as:-

$$D_{\delta} = u_A \cdot K_{D_{\delta}}^{A/L} + u_B \cdot K_{D_{\delta}}^{B/L} + \dots$$

where:-

u_A = mass fraction of phase A relative to the total solid.

$K_{D_{\delta}}^{A/L}$ = mineral(A)-melt(L) distribution coefficient of δ .

2. Total equilibrium crystal fractionation equation.

$$\frac{C_{\delta L}}{C_{\delta 0}} = \frac{1}{F + D_{\delta}(1 - F)} \quad \text{equation 2.}$$

(symbols as those in equation 1.)

Equation 1 describes a style of trace element behaviour, in a magma, which is dependent only on the equilibrium reaction between the melt and the surfaces of fractionating crystals. The interiors of crystals growing in the melt do not re-equilibrate with the evolving melt composition by diffusive processes, and furthermore, any cumulate pile still in physical contact with the melt is essentially chemically alienated from it. On the other hand, equation 2 describes a style of trace element behaviour in a magma which is still in physical contact with the sum total of its crystalline products, and where subsolidus diffusion takes place at a sufficient rate to enable the melt and its cumulates to stay in complete chemical equilibrium.

In trying to reconcile these two equations with the actual conditions of crystal fractionation in magmas, Arth (1976) states "the surface equilibrium model may be more applicable to rapidly cooling, shallowly emplaced magmas, whereas the total equilibrium model may better describe plutonic conditions where the cooling of an intruded magma is extremely slow". However, magma intrusion and magma differentiation are closely tied, and so these equations should be reconciled with dynamic magma intrusion, rather than static magma bodies.

The rate of ascent of a magma, to higher levels in the crust, is controlled by the density contrast between it and the surrounding country rocks. This density contrast depends on two variables; the temperature of the magma, ie. the hotter a magma is, the lower is its density, and the relative compositions of the magma and its surrounding country rocks, for example, as basic rocks are much

denser than granitic rocks, then a basic magma will find it difficult to ascend through granitic rocks, even though it will be much hotter than them. In the simple example of a magma with a comparable composition to that of the country rocks, then the density contrast between the magma and the surrounding rocks is controlled mainly by temperature variations in the magma. The magma would cool as it rose through the country rocks, mainly by conductive heat loss across the magma-wall rock boundary, until the temperature fell sufficiently so that the density contrast between it and the surrounding rocks became minimal, at which point the magma would come to rest. The decreasing magma temperature would also promote crystallisation, in the magma, in increasingly larger amounts. Crystallisation would reach a peak at the point at which the magma comes to rest. Latent heat of crystallisation, released in large amounts at this point, would begin to reheat the magma. If the rate of reheating of the magma is greater than the removal of heat by conduction across the magma-wall rock boundary, then the magma could theoretically be heated up almost to its liquidus, but no further. At this point crystallisation would effectively cease and the magma would have already begun to rise upwards again due to its lower density. Using this simplistic cyclic model of magma intrusion it can be seen that the most crystallisation occurs when the magma is static or only slowly rising, and therefore cumulate deposits produced during this period will probably remain in contact and re-equilibrate with the magma. During these periods of increased crystallisation, the total equilibrium fractional crystallisation equation would be a good estimate of the trace element behaviour in the magma. During periods of magma ascent, there may be little crystallisation of the magma, but the very fact that the magma leaves behind its cumulate deposits, would mean that the trace element behaviour in the magma is better described by the surface equilibrium fractional crystallisation equation. If an ascending basic magma intercepted a major density discontinuity in the crust, say the boundary between dense basement rocks and a much less dense siliceous metasedimentary sequence, then the effect of temperature may be insufficient to overcome the density contrast arising from the difference in composition between the magma and the siliceous metasediments. The magma would be forced to remain at the density discontinuity until the composition of the magma became comparable

with that of the overlying rocks, ie. by the process of fractional crystallisation. In this situation, the trace element behaviour in the magma would probably be better described by the total equilibrium equilibrium fractional crystallisation equation.

It is clear that the conditions of equilibrium, between a magma and its cumulates, will vary continuously during the intrusion of that magma into the crust. Therefore, any single trace element fractional crystallisation equation, if applied to a magmatic rock series as a whole, could only hope to describe, at best, an approximation to the fractionation history of that series.

As is stated above, equations 1 and 2 are only valid for the case of crystallisation of phases in constant proportions and of constant distribution coefficients. The former constraint would be extremely improbable in the differentiation of a magma across a broad range of composition, and concerning the latter, much of the discussion of the previous chapter has advocated that distribution coefficients change significantly with fractionation. Therefore, in order to apply these fractional crystallisation equations to a magma series, that series has to be broken down into several units, across which the approximation of constant phase proportions and constant distribution coefficients is not too erroneous.

It is felt that the total equilibrium fractional crystallisation equation is probably the most appropriate of the two equations, to describe the trace element behaviour in a plutonic intruding magma body undergoing fractional crystallisation. Of the two types of fractional crystallisation, the surface equilibrium type is the more effective in depleting the magma of elements with high D values, and enriching it in elements with low D values.

5.2 Simple fractionation vectors and their comparison with the metabasite-orthogneiss trend.

Simple two component fractionation vectors have been calculated for the fractionation of various phases from the three magma types; gabbro, diorite, and granodiorite. These are shown in plots b, d, f in fig.5.1. Fractionation vectors predict the composition path, away from an initial magma composition, taken by a differentiate magma undergoing the fractionation of a certain phase or phase assemblage, in accordance with the trace element fractionation equation selected. The vectors in fig.5.1 were derived from the surface equilibrium fractionation equation (equation 1 in

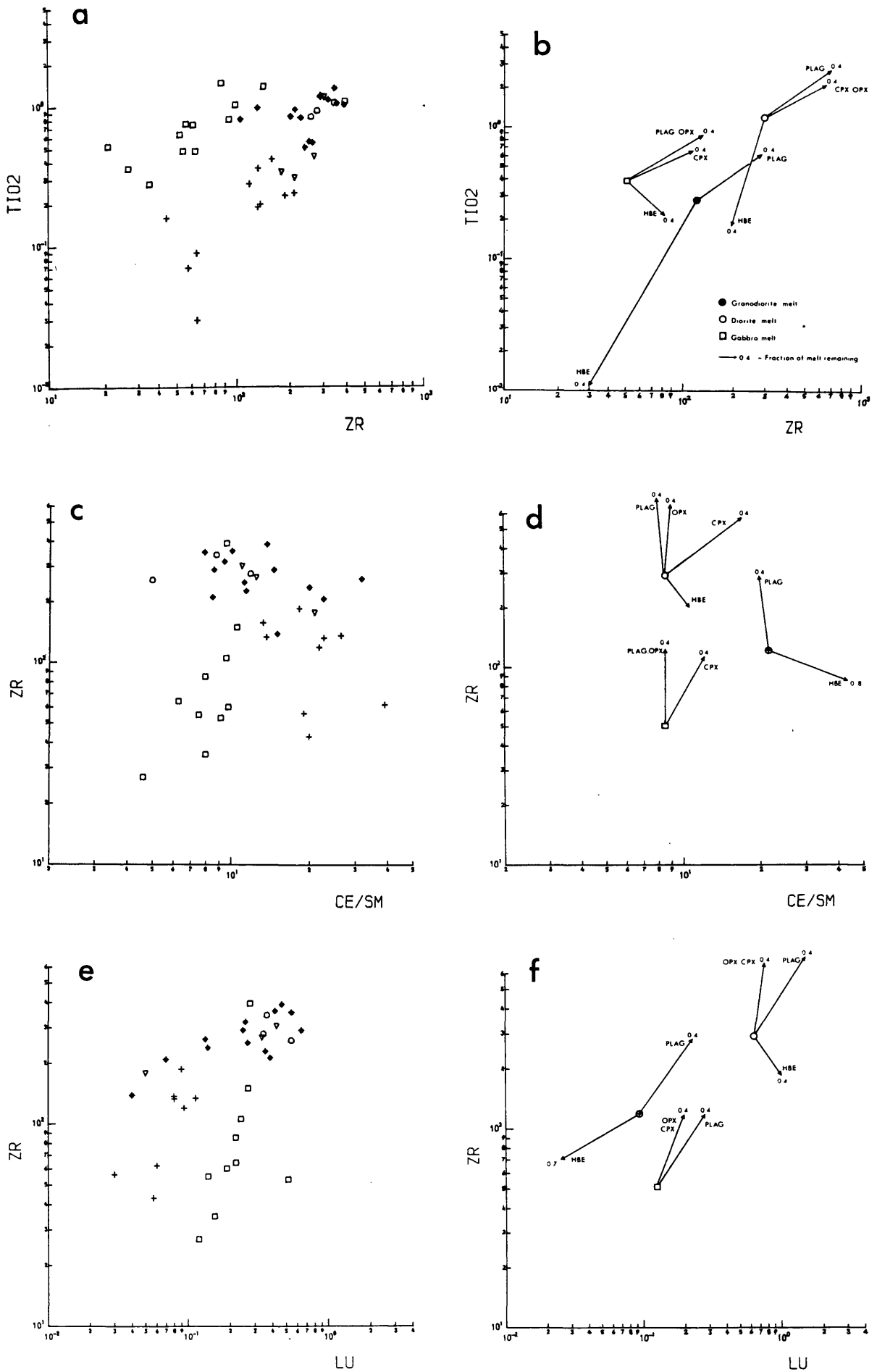


Fig. 5.1 Fractionation vectors applied to the metabasite-orthogneiss series.

section 5.1), using the phase K_D 's of the elements, Ti, Zr, Ce, Sm, and Lu, for the three magma types (Table 4.1). If the total equilibrium fractional crystallisation equation had been used instead, to calculate the fractionation vectors, then the vectors shown in fig.5.1 would be shorter, although their orientations would not differ. The transitional D elements were selected for this study since they have K_D values which are fairly distinctive for each of the phases of interest, ie. hornblende, both pyroxenes, and plagioclase.

The distribution of the metabasite and orthogneiss rocks in the TiO_2 (wt.%) v. Zr (ppm) plot (fig.5.1a), can be compared with the fractionation vectors of the adjacent plot (fig.5.1b). The metabasite rocks and most of the tonalitic orthogneiss rocks follow a trend which would be defined by a magma undergoing the fractionation of one, or a combination, of the following phases; clinopyroxene, orthopyroxene, and plagioclase. A marked change in the direction of the metabasite trend occurs in rocks containing c.350 ppm Zr, and from the fractionation vectors it is clearly due to the initiation of fractionation of a phase assemblage dominated by hornblende. Although the fractionation vectors were calculated using the surface equilibrium equation, which is reckoned to be the least appropriate of the two equations in section 5.1, the correlation between the vector orientations and the metabasite-orthogneiss trend is striking. This substantiates the claim that these rocks were formed from magmas which evolved by fractional crystallisation processes.

K_D 's increase as the melt becomes less basic, and the effect that this has on the Zr and Ti contents of the differentiate magma is shown by the relative lengths of the fractionation vectors emanating from the composition points of the three magma types, gabbro, diorite, and granodiorite. The value at the termination of each vector (fig.5.1b) is the fraction of magma remaining, relative to the initial mass of the magma type.

The distribution of the metabasite-orthogneiss rocks in the Zr (ppm) v. Ce/Sm plot (fig.5.1c) can be compared with the fractionation vectors of the adjacent plot (fig.5.1d). The Ce/Sm ratio, which is a measure of the LREE* enrichment, over the MREE*'s, in the REE* pattern of a rock, is used because it separates the clinopyroxene, and to a lesser extent the orthopyroxene,

75

fractionation vectors from that of plagioclase. The inclined trend of the metabasite rocks indicates that clinopyroxene formed a major part of the fractionation assemblage that crystallised from the metabasite magma. The directional change in the metabasite-orthogneiss trend can again be equated with hornblende fractionation.

The distribution of the metabasite-orthogneiss rocks in the Zr (ppm) v. Lu (ppm) plot (fig.5.1e), compared with the fractionation vectors of fig.5.1f, indicates that the transition between the metabasite and tonalitic orthogneiss magmas involved the fractionation of a plagioclase dominated fractionation assemblage, which was later superseded by the fractionation of an assemblage dominated by hornblende.

5.3 Quantitative modelling of the total equilibrium fractional crystallisation process to the trace element variations in the metabasite-orthogneiss series.

In order to determine, from trace element data, the nature and relative proportions of the phases that precipitated from the various magma types (represented by rock compositions) of a magmatic series, which formed by fractional crystallisation, and also the degree of fractionation of each magma type, relative to an initial magma, it is necessary to define the way in which the trace element concentrations in a fractionating magma can vary. This was carried out in the previous section in a simple semiquantitative manner, by calculating two element fractionation vectors for the fractionation of single phases from a magma and comparing their trends to that of the metabasite-orthogneiss series. A much more complex and quantitative method is to simultaneously apply the appropriate fractionation equation to all of the trace elements in a rock, which represents one magma type, and calculate whether any amount of fractionation of a given phase assemblage will accurately reproduce the trace element distribution in another rock, representative of a more differentiated magma type. The identification of the phase assemblage is an interactive problem, in that the assemblage is first deduced from other considerations, such as petrographic details, and then tested in the model calculation. The calculation derives the relative proportions of the postulated fractionation phases, and also the degree of fractionation, of this assemblage, needed to transform the trace element composition of the parent

magma to that of the magma differentiate. A study of the results should show whether the postulated fractionation assemblage is a valid one for those magma types or whether or not it needs some modification to be more compatible with certain parts of the trace element data.

5.3.1 The computation of the equilibrium fractionation model.

Since the model involves the simultaneous solution of many equations, one for each trace element used, the calculations have to be carried out by computer.

As stated previously, the total equilibrium fractional crystallisation equation is:-

$$\left(\frac{C_{Li}}{C_{Oi}}\right) = \frac{1}{F + D_i^S(1 - F)} \quad \text{equation 1.}$$

where:- F = the fraction of liquid remaining, relative to the initial mass of liquid.

C_{Oi} = the concentration of the i'th trace element in the initial magma.

C_{Li} = the concentration of the i'th trace element in the differentiated magma.

and considering the melt as the m'th phase

$$D_i^S = \sum_{j=1}^{m-1} k_{Dij} \cdot u_j \quad \text{equation 2.}$$

where:-

D_i^S = the bulk distribution coefficient of the i'th trace element for the total solid.

k_{Dij} = mineral/melt distribution coefficient of the i'th trace element for the j'th phase.

u_j = the mass fraction of the j'th phase in the total solid.

by definition,

$$\sum_{j=1}^{m-1} u_j = 1 \quad \text{since } u_m = 0$$

and,

$$\sum_{j=1}^{m-1} u_j(1 - F) + F = 1 \quad \text{equation 3.}$$

Given that the fractionation assemblage is known, it is apparent, from equations 1 and 2 (above), that only two of the five

simple, (ie. non-compound), parameters comprising the equilibrium fractional crystallisation equation are unknown. These are, the fraction of melt remaining, F , relative to the initial magma, and the mass fractions, u_j , of the phases in the bulk solid fractionate. The other parameters can be either measured directly, ie. the trace element concentrations in the initial and final magmas (represented by rock compositions), or can be estimated, ie. the mineral-melt K_D values.

The following text shows the manipulation of equation 1 into a form from which the calculations can be made:-

from mass balance theory,

$$\sum_{j=1}^{m-1} \emptyset_j + \emptyset_m = 1 \quad \text{equation 4.}$$

where:- \emptyset_j = the mass fraction of the j 'th phase in the total system.

\emptyset_m = the mass fraction of the melt in the total system.

by definition,

$$\emptyset_m = F \quad \text{equation 5.}$$

from equations 3 and 4,

$$\emptyset_j = u_j(1 - \emptyset_m) \quad \text{equation 6.}$$

from equations 1, 2, and 5,

$$\left(\frac{C_{Di}}{C_{Li}}\right) = \emptyset_m + \sum_{j=1}^{m-1} K_{Dij} \cdot u_j(1 - \emptyset_m) \quad \text{equation 7.}$$

subs. equation 6 into equation 7,

$$\left(\frac{C_{Di}}{C_{Li}}\right) = \emptyset_m + \sum_{j=1}^{m-1} K_{Dij} \cdot \emptyset_j \quad \text{equation 8.}$$

from equation 4,

$$\emptyset_m = 1 - \sum_{j=1}^{m-1} \emptyset_j \quad \text{equation 9.}$$

subs. equation 9 into equation 8,

$$\left(\frac{C_{Di}}{C_{Li}}\right) = 1 - \sum_{j=1}^{m-1} \emptyset_j + \sum_{j=1}^{m-1} K_{Dij} \cdot \emptyset_j \quad \text{equation 10.}$$

therefore from equation 10,

$$\left(\frac{C_{0i}}{C_{Li}}\right) - 1 = \sum_{j=1}^{m-1} \emptyset_j (K_{Dij} - 1) \quad \text{equation 11.}$$

Equation 11, like equation 1, describes the behaviour of the i'th trace element during the equilibrium fractional crystallisation process. For the n trace elements in the magma, there are n equations of the type of equation 11. These equations may be written in matricial form:-

$$X \cdot \emptyset = Y$$

where:-

$$X = \sum_{j=1}^{m-1} (K_{Dij} - 1) \quad (i = 1 \dots n)$$

X is a n · (m - 1) rectangular matrix, with individual elements, X_{ij} .

$$Y = \left(\frac{C_{0i}}{C_{Li}}\right) - 1 \quad (i = 1 \dots n)$$

Y is a n · 1 row matrix, with individual elements, Y_i .

$$\emptyset = \emptyset_j \quad (j = 1 \dots m-1)$$

\emptyset is a 1 · (m - 1) column matrix, with individual elements, \emptyset_j .

Since the n · (m - 1) + n X_{ij} and Y_i parameters are liable to direct measurement, then the (m - 1) \emptyset_j unknowns can be determined by an iterative least-square calculation, provided that the system is not underdetermined, ie. n < m. Once the (m - 1) \emptyset_j values are known then \emptyset_m can be easily calculated (equation 9.). The algorithm of Albarede and Provost (1977) for least-square fitting, which allows a general error analysis, was employed to solve the $X \cdot \emptyset = Y$ matrix equation. Calculations were carried out by computer using a self-written, interactive computer program, NEWFRAC, which incorporates the algorithm program presented in Albarede and Provost (1977). General details of this program and others used in this study are given in appendix 3.

The least-square algorithm employs a minimisation technique, in which the lowest value for the sum of the squared residuals, S,

(residual = observed - calculated X_{ij} and Y_i data), is sought by varying the values of the individual \emptyset_j elements of the \emptyset column matrix. The value of S as a function of \emptyset is given by the equation;

$$S(\emptyset) = \sum_{i=1}^n \frac{(\sum_{j=1}^{m-1} X_{ij} \cdot \emptyset_j - Y_i)^2}{\sum_{j=1}^{m-1} (\sigma_{ij} \cdot \emptyset_j)^2 - \sigma_i^2} \quad \text{(equation 14, Albarede and Provost, 1977).}$$

where:- σ_{ij} and σ_i are the respective errors on the X_{ij} and Y_i data. For a full explanation of the least-square algorithm and the derivation of equation 14, refer to Albarede and Provost, (1977). The values of the X_{ij} , σ_{ij} , Y_i , and σ_i matrix elements make up the data input to the computer program. The errors on the trace element concentrations of the parent and differentiate magma types were set at an estimated average 10%, and are compounded in the calculation of the Y_i values (C_D/C_L). The errors on the X_{ij} data, (mineral-melt K_D 's, Table 4.1), were estimated using the following rule of thumb;

$$K_D > 0.5 \quad : \quad 0.5 > K_D > 0.05 \quad : \quad 0.05 > K_D$$

$$\sigma_{ij}\% = 20\% \quad \sigma_{ij}\% = 40\% \quad \sigma_{ij}\% = 60\%$$

This is because the errors given for the K_D 's in their source references were thought to be too small for their use in this study, since the K_D 's were not determined from the metabasite-orthogneiss rocks. The errors assigned to estimated K_D 's were double those of actually determined K_D 's.

The elements used in the calculations are Sr, Y, Zr, Nb, Ba, Ce, Sm, Eu, Tb, Yb, Lu, and Sc. Of the trace elements determined but not used, La and Pb have very few published K_D values, the Rb and Th data of the metabasite-orthogneiss rocks is too scattered to be useful, and Cr, Ni, and Co have published K_D 's only for minerals in basic magmas.

5.3.2 Presentation and discussion of the results of the modelling.

Tables 5.1-5.3 list the computer-generated best-fit solutions for the equilibrium fractionation of various postulated phase assemblages from a parental magma type (ie. BK102, in Table 5.1), to produce a more differentiated magma type (ie. BK138, in Table 5.1). The tables consist of a number of columns, each containing the results for a single mineral assemblage (shown at the

top of the column). The data in each column consists of, in descending order;-

1. The C_L/C_L^C ratios of the various trace elements used in the calculations, where C_L and C_L^C are the observed and calculated trace element concentrations of the differentiated magma type. Since the concentration data, input into the computer program, is in the form of the ratio of the parent and differentiated magma types (C_0/C_L), the calculated best-fit concentration results also have the form C_0^C/C_L^C . C_L^C can be derived from these best-fit ratios if it is assumed that the C_0 and C_0^C values are exactly equal. Consequently, the resultant C_L^C values take on the whole of the errors associated with the C_0^C/C_L^C ratios. The C_L/C_L^C ratio is a measure of the goodness of fit of the fractionation model for a particular trace element. The closer the C_L/C_L^C ratio is to unity, the better the fit of the fractionation model to the actual distribution of the particular trace element in the parental and differentiated magma types.
2. The \emptyset_j percentages - These are the phase mass percentages, relative to the initial mass of the parent magma, which must fractionate from the parent magma to produce the best-fit differentiated magma.
3. The \emptyset_m percentage - This is the percentage mass of the best-fit differentiated magma relative to the initial mass of the parental magma.
4. $\sum(R)^2$ - The minimum value of the sum of the squared residuals for the particular solution. The smaller the residuals (ie. observed - calculated X_{ij} and Y_i data), the smaller the $\sum(R)^2$ value, and the better the fit of the model. (N.B. $\sum(R)^2 = S(\emptyset)$)
5. Q - The quality factor of Albarede and Provost (1977), which is equal to:-

$$Q = \frac{S(\emptyset)}{n - m} \quad (\text{equation 38, Albarede and Provost, 1977}).$$

where $n - m$ is the number of degrees of freedom in the calculations. Q should not be much greater than unity if the model is to be accepted as viable.

Table 5.1 Fractionation from BK102 to BK138 (using basaltic K_D 's)

C_L/C_L^C	postulated fractionation assemblages						
	CPX (+ILM)	CPX (+ILM)	OPX (+ILM)	CPX +PLAG (+ILM)	OPX +PLAG (+ILM)	CPX+OPX +PLAG (+ILM)	HBE +PLAG (+ILM)
	1	2	3	4	5	6	7
Ce	0.91	0.77	0.79	1.28	1.31	0.75	1.35
Sm	1.10	1.07	0.90	0.97	0.80	0.88	0.83
Eu	1.15	1.10	1.18	1.19	1.19	1.23	1.17
Tb	1.27	1.22	1.00	0.99	0.86	0.93	0.82
Yb	1.03	1.01	0.98	0.72	0.80	0.81	0.58
Lu	1.02	1.00	1.03	0.72	0.88	0.89	0.61
Sc	1.07	1.03	1.02	1.10	1.07	1.00	0.95
Ti	1.00	1.00	1.00	1.00	1.00	1.00	1.00
Ba	0.31	-	-	0.36	0.33	-	0.41
Sr	0.42	0.36	0.34	1.04	0.89	0.88	1.10
Y	1.10	1.08	1.20	1.17	1.19	1.26	1.31
Zr	1.13	0.99	1.03	0.90	0.92	0.96	1.07
Nb	0.39	-	-	0.29	0.35	-	0.34
$\emptyset_j\%$							
CPX	69.90	76.52		20.51		4.72	
OPX			70.00		36.11	31.84	
HBE							3.30
PLAG (ILM)				53.65	36.26	34.80	68.25
	-0.5	-0.44	-0.2	-0.2	-0.1	-0.2	-0.3
$\emptyset_m\%$	30.63	23.97	30.67	26.05	27.78	28.84	28.77
$\sum(R)^2$	99.90	43.19	32.83	72.79	65.28	18.33	80.78
Q	3.01	2.19	1.91	2.70	2.55	1.62	2.84

5.3.2a Fractionation within the metabasite group (BK102 to BK138).

In the previous chapter, samples BK102 and BK138 were chosen as the parent and most differentiated metabasite magma types, respectively. An initial study of the trace element concentrations in these samples (Appendix 1, Table A) reveals that for all of the trace elements used in the calculations, except Nb, the greater concentrations occur in sample BK138. Nb has an equal abundance in both BK102 and BK138 and this distribution is puzzling since both Zr and Y, which usually behave in a very similar fashion to Nb in magmatic processes, are present in abundances that are c.3 times those in BK102. The Sr abundance in the differentiated magma type (BK138) is only 6.9% greater than that in the parent magma type (BK102). This will limit the amount of fractionation in any fractionation scheme which does not involve plagioclase in the fractionation assemblage, because the Sr abundance in the calculated differentiate magma would tend to rise rapidly with fractionation.

Table 5.1 shows the results of fitting the equilibrium fractionation process to the BK102 and BK138 magma types. The study of the metabasite rocks in the CMAS system (chapter 3.) indicated that the metabasite magma evolved by the fractionation of pyroxenes alone. This hypothesis was tested in the models 1-3 in Table 5.1. Before discussing the results of these fractionation models, it is necessary to explain some of the difficulties of actually gaining sensible results from the computer program. Invariably, where two phases with a closely similar pattern of K_D values form all, or part, of the postulated fractionation assemblage, then the program searches for the lowest $\sum(R)^2$ value simply by proceeding to increase the \emptyset_j of one of these two phases, while producing a complementary decrease in the other phase \emptyset_j . This situation generally leads to a large negative \emptyset_j for the latter phase and a large positive \emptyset_j for the former. As far as was possible, the phases which produce this effect, when used together in the same fractionation assemblage, ie. DPX, CPX, and HBE., were kept apart. Therefore the emphasis, in this section, will be on the comparison of fractionation assemblages which differ only in the nature of the mafic phase. A minor phase was usually added to the postulated fractionation assemblage in order to facilitate the easier convergence of the iterative calculations onto the final solution.

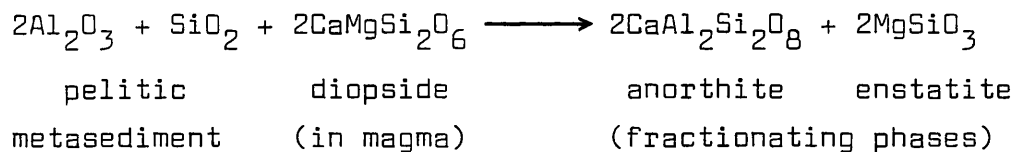
This was usually ilmenite, and its presence in the fractionation assemblage is purely a practical feature of running the program. This addition of a minor phase does not alter the solution significantly when the main fractionation phases have a markedly different K_D pattern, ie plagioclase + clinopyroxene. However, if two phases of like trace element affinities are present in the postulated fractionation assemblage, then the presence of a minor phase could produce a strongly misleading shift in the relative proportions of these two phases, in the final solution. Since the inclusion of like phases in the same fractionation assemblage has been mostly avoided in this study, this latter effect can be largely largely ignored.

Models 1, 2, and 3 are concerned only with the equilibrium fractionation of pyroxene from the parent BK102 magma type. Clinopyroxene is the sole fractionation phase in model 1, producing a best-fit differentiate magma which closely resembles, in terms of trace element contents, the BK138 magma type, except for the three elements, Ba, Sr, and Nb. The Nb anomaly between BK102 and BK138 has already been discussed, and can probably be put down to analytical error, especially since the Nb content of the rocks is so low (≈ 5 ppm). As was forecast above, the Sr concentration is not sufficiently high in BK138, compared with BK102, to allow a large amount of fractionation of a phase assemblage not involving plagioclase feldspar. Since this model requires around 70% fractionation of clinopyroxene from the parent magma to produce the best-fit differentiate magma, and because Sr has a low K_D for pyroxene, the latter magma will have a much larger Sr content than BK138, giving rise to the low C_L/C_L^C value of 0.42. It is difficult to know what to ascribe this Sr deficiency in BK138 to, whether it can be put down to the scatter in the Sr data (fig.4.3), whether plagioclase did form part of the fractionation assemblage after all, or even that the equilibrium model is inadequate to describe the fractionation of the metabasite magmas. The CMAS evidence would point to the absence of plagioclase as a fractionation phase from the metabasite magmas, however, the possible presence of this phase will be considered further in models 4, 5, 6, and 7. Ba also has a very low C_L/C_L^C ratio, in the results of model 1, and this could be due to the previously described strong scatter in the incompatible element data, or it may be due to the inadequacy of the equilibrium

fractional crystallisation model to explain the incompatible element variations, if these variations are entirely igneous in origin. The REE concentrations in the best-fit magma differentiate closely resemble those of the BK138 magma type, as is shown by the C_L/C_L^C ratios which are all fairly close to unity.

In model 2, the elements Ba and Nb have been omitted and the fractionation assemblage is the same as in model 1, ie. CPX (+ ILM). This drastically reduces the $\sum(R)^2$ value (99.9 in model 1, 43.2 in model 2), and also reduces the quality factor, Q, (from 3.01 to 2.19). The amount of clinopyroxene fractionation from the BK102 magma type is slightly greater in model 2, compared with the previous model, and this has the effect of lowering all of the C_L/C_L^C ratios. This latter feature could well be related to the increase in K_D values in the evolving metabasite magma, compared with the K_D 's in the calculations, which are held constant for the range of the metabasite rocks. With the increasing K_D 's, in the metabasite magma, the transitional D elements will increase less rapidly in the magma with fractionation, whereas the concentrations of these elements in the calculated differentiate magma would be governed by the initially set K_D values. Thus with large degrees of fractionation the C_L/C_L^C ratios of the transitional elements might be expected to become less than unity. Orthopyroxene replaces clinopyroxene as the fractionation phase in model 3, yet produces an almost identical result as the latter phase did in model 2. From models 1-3 it appears that c.70% of the mass of the BK102 magma type must crystallise as a clinopyroxene-orthopyroxene assemblage in order to produce most of the trace element characteristics of BK138.

Models 4 and 5 show the results of pyroxene and plagioclase fractionation from the BK102 magma type. These two models bring the Sr C_L/C_L^C ratio to around unity yet they produce low HREE C_L/C_L^C ratios. The Ba C_L/C_L^C ratio is unaffected. Plagioclase is required as the major fractionation phase in these two models, a feature that the CMAS evidence certainly would not allow. The question arises as to whether there is some way that plagioclase fractionation could have occurred without leaving a signature in the major element data? Bowen's (1928) proposed reaction for the assimilation of aluminous metasediments by a basic magma, and its effects on the crystallisation of the magma, is:-



O'Hara (1980) considers this reaction, stating that much of the assimilated material would be immediately precipitated as plagioclase and a calcium-poor pyroxene. The melt will therefore accommodate only part of the assimilated material, ie the alkalis and some SiO_2 . Since much of the material needed to produce the plagioclase is derived from the assimilated material, the evolving major element composition of the magma would hardly show the effects of plagioclase fractionation, whereas, the Sr content of the magma would be strongly affected. If this is the mechanism which caused the distribution of Sr in the BK102 and BK138 magma types, then the results of models 4 and 5 could give a reasonable estimate of the amount of metasedimentary material assimilated by the metabasite magma. On the other hand, the fact that none of the high REE metabasite REE* patterns possess a significant Eu* anomaly, limits the fractionation of plagioclase to a relatively minor occurrence, given that Eu^{2+} was the predominant state of Eu in the metabasite magma. This latter qualification has to be made since the formation of Eu^{3+} is more favourable in basic magmas than in acidic ones (see earlier discussion, chapter 4, section 4.3.3a), and it may also be favoured by the presence of dissolved H_2O in the magma (Wood and Fraser, 1977). However, Schnetzler and Philpotts (1970) found that the REE K_D patterns of plagioclase possess a marked positive Eu* anomaly even in basic magmas (ie. Eu^{2+} was present in the magma). Also, most basic magmas contain only small amounts (<4%) of dissolved H_2O (Anderson, 1980). Possible inferences on the oxidising potential (ie. H_2O content) of the metabasite magma could be drawn from the work of Evans (1964) who studied some extremely desilicated, corundum-spinel-magnetite-biotite bearing, xenoliths in the metabasite rocks from the Toombeola area to the east of Cashel Hill, and showed them to be strongly oxidised with $(\text{Fe}^{3+}/(\text{Fe}^{3+} + \text{Fe}^{2+})) \cdot 100 > 60\%$. This oxidisation might have been caused by the infiltration of H_2O from the magma into the xenoliths, but it equally might have been caused by H_2O released, inside the xenoliths, from the breakdown of biotite to corundum + spinel + magnetite. The latter explanation was the one considered by Evans to be the more likely.

Therefore, it appears that Eu^{2+} would have been present in the metabasite magma and hence, if plagioclase fractionation did occur from the magma, as the Sr data may suggest, the REE* patterns of some of the high REE metabasite rocks should possess a significant Eu* anomaly. This is not so and therefore, plagioclase fractionation is not thought to have been a major feature of the evolution of the metabasite magmas. The Sr distribution in BK102 and BK138 is probably primarily a function of the scatter of the Sr data in the metabasite rocks, presumably caused by secondary alteration processes.

Model 6 is essentially a combination of the two previous models, and it too requires plagioclase as the dominant fractionation phase. The model strongly favours the fractionation of orthopyroxene over that of clinopyroxene (31.84%, compared with 4.72%), however, from the earlier discussion, there is likely to be a large error on this orthopyroxene-clinopyroxene ratio, and anyway the tFeO data suggests that the fractionation of the metabasite magma was controlled by a clinopyroxene dominated fractionation assemblage.

Model 7 consists of the fractionation of a hornblende and plagioclase assemblage from the BK102 magma type. The model is not strictly valid since the hornblende K_D 's are those of hornblende in an andesitic matrix (Table 4.1), no REE K_D 's for hornblende from a basaltic liquid being available. This may be the reason for the model requiring so little hornblende fractionation to arrive at the best-fit solution. However, the results do show up the effects of the greater K_D values of the elements, Zr and Y, relative to the REE's, in hornblende compared with pyroxene. In model 7, the REE's are enriched in the calculated differentiate magma to a greater extent than either Zr or Y, and the resulting best-fit differentiate magma has REE contents which are higher than those of BK138 (ie. $C_L/C_L^C < 1.0$), and Zr and Y contents which are lower (ie. $C_L/C_L^C > 1.0$). This effect would probably have been seen if K_D 's of hornblende from basaltic liquid had been used instead of those for hornblende from andesitic liquid. This effect rules out hornblende fractionation, in the metabasite magma over the composition range represented by the rocks BK102 and BK138, in favour of pyroxene fractionation, which is in agreement with the CMAS evidence (chapter 3).

The results of modelling the equilibrium fractional

crystallisation process from an initial magma type (BK102) to reproduce the more differentiated magma type represented by sample BK138 have been fairly successful for most of the trace elements selected. Ba and Nb did not fit any model, though this can probably be ascribed to analysis error for the latter. From a consideration of the models and previous trace element evidence, plagioclase is again rejected as a major fractionation phase although a small amount (estimated at less than 15% in order to avoid creating a significant negative Eu anomaly in the magmas REE pattern) may have fractionated in response to the assimilation of metasedimentary material by the metabasite magma. The degree of fractionation needed to produce the best-fit solution is surprisingly similar in all of the models in Table 5.1, and considering models 1 and 3 as the most appropriate to the fractionation of the metabasite magma, then the differentiated magma type (BK138) has 30% of the mass of the initial magma type (BK102).

5.3.2b Fractionation from a highly fractionated metabasite magma type (BK138) to a melanotonalitic orthogneiss magma type (BK406).

In the previous chapter, sample BK406 was chosen as being representative of the melanotonalitic orthogneisses, and therefore representative of the melanotonalitic orthogneiss magma. Table 5.2 lists the results of modelling the equilibrium fractional crystallisation process in an initial magma of type BK138, to obtain a differentiate magma of type BK406. However, before discussing the four models listed in Table 5.2, it is necessary to make an initial study of the trace element concentrations in BK138 and BK406 (see Appendix 1, Tables A and B), to point out possible anomalies which may produce misleading results in the models. For all of the trace selected, except Ti and Sr, the greater concentration occurs in BK406, compared with BK138. The most marked differences between the two rocks are in their Zr and Sr contents, with BK138 containing 85 ppm of Zr and 479 ppm of Sr, while BK406 contains 287 ppm of Zr and 292 ppm of Sr. These differences forecast that plagioclase will be a prominent phase in the fractionation assemblage.

Models 1-3 all contain plagioclase as part of the postulated fractionation assemblage and each one of the three mafic phases; clinopyroxene, orthopyroxene, and hornblende. These three models produce results in which the best-fit differentiate magma

Table 5.2 Fractionation from BK138 to BK406 (using andesitic K_D 's)

C_L/C_L^C	postulated fractionation assemblages				
	CPX +PLAG (+ILM)	OPX +PLAG	HBE +PLAG (+ILM)	PLAG (+ILM)	
	1	2	3	4	
Ce	1.00	1.00	0.99	1.04	Fractionation assemblages, HBE + ILM and PX's + HBE, were not successful .
Sm	0.91	0.85	0.84	0.89	
Eu	1.02	0.98	1.00	1.02	
Tb	0.98	0.83	0.80	0.84	
Yb	0.94	1.03	0.89	0.94	
Lu	1.11	1.25	1.05	1.13	
Sc	1.06	0.89	0.96	0.54	
Ti	0.99	0.32	0.99	1.02	
Ba	0.76	0.77	0.77	0.82	
Sr	0.95	0.91	0.95	0.96	
Y	0.70	0.68	0.74	0.66	
Zr	1.16	1.22	1.28	1.27	
Nb	1.10	1.15	1.19	1.19	
$\emptyset_j\%$					
CPX	4.67				
OPX		8.78			
HBE			3.42		
PLAG	62.40	57.03	63.35	62.48	
(ILM)	1.75		1.52	1.86	
$\emptyset_m\%$	31.16	34.18	31.65	35.66	
$\sum(R)^2$	13.00	43.75	17.92	28.18	
Q	1.14	1.99	1.33	1.60	

correlates excellently with the BK406 magma type. The models require only small amounts of fractionation of the mafic phase, and around 60% fractionation of plagioclase, from the initial BK138 magma type to produce the best-fit differentiate magma. Ilmenite, which was only included as an aid to encourage convergence of the calculations onto the final solution, may be a viable minor fractionation phase since the Ti content of BK138 is significantly greater than that of BK406. This might be supported by the phase relations study of Egger (1972a ; in Egger and Burnham, fig 4, 1973) which shows that ilmenite is within c.50°C of the liquidus of a Mt. Hood andesite containing c.5 wt% H₂O at 5Kb pressure. As already stated (chapter 3), plagioclase has its highest stability in andesitic compositions and is often the first phase to crystallise out of this type of magma. Thus the phase relations agree well with the model results. A comparison of the C_L/C_L^C ratios of the REE's for the three different models show that the fractionation of clinopyroxene produces the best match with the BK406 magma type, but the difference between the models is negligible. Since BK406 does not contain any relict pyroxene, whereas this phase does occur in BK138, it is reasonable to expect the transition from pyroxene to hornblende fractionation to have occurred in the period of fractionation between these two magma types. However, crystallisation of the mafic phase was clearly a minor feature during this fractionation step.

Model 4, in Table 5.2, consists of a fractionation assemblage of only plagioclase and ilmenite. Since plagioclase is by far the most dominant phase of the other three models, the fit of model 4 to the magma types BK138 and BK406 is a good one. However, the need for one of mafic phases, used in the previous models, to be present in the fractionation assemblage is shown by the low Sc C_L/C_L^C ratio.

The percentage mass of the BK406 differentiate magma remaining, relative to an initial mass of BK138 magma, is c.32%, and as a percentage mass of the parent BK102 magma, the BK406 differentiate magma represents c.9.6%.

Models 1-4 indicate that hornblende fractionation was not important in driving the metabasite magma towards tonalitic compositions. However, from fig 3.12b it is clear that plagioclase fractionation alone cannot sufficiently enrich the magma in SiO₂. In

section 4.2.1b it was noted that assimilation of siliceous paragneiss could equally well have fuelled the initial trend towards SiO_2 enrichment in the high Fe/Mg metabasite magma. The introduction of Al_2O_3 , from assimilated metasediment, into the metabasite magma would buffer the anorthite content of the fractionating plagioclase at a high level, thereby keeping the SiO_2 content of this phase relatively low (c.48 wt%). Thus once the magma became richer in SiO_2 than the plagioclase fractionating from it, the SiO_2 enrichment trend would escalate due to a combination of assimilation and fractionation. The amount of paragneiss assimilated by the high Fe/Mg metabasite magma is unknown, but if it were significantly greater than about 20% of the magma mass the equilibrium fractional crystallisation equation would obviously be inadequate in modelling the trace element variations in this magma. The very fact that the models 1-4 fit so well with the observed trace element concentrations in the representative rock types, may be fortuitous or may reflect that assimilation did not overshadow fractional crystallisation during the evolution of the metabasite and melanotonalitic orthogneiss magmas.

5.3.2c Fractionation from the melanotonalitic orthogneiss magma type (BK406) to the leucotonalitic orthogneiss magma type (BK403).

The results of fitting the equilibrium fractionation process to the magma types represented by rock samples BK406 and BK403 (parent and differentiate magma types, respectively) are listed in Table 5.3 (models 1-4). An initial study of the trace element compositions of samples BK406 and BK403 (Appendix 1, Table B), reveals that they have almost identical Ba, Sr, and Zr contents. Ba is an incompatible element and should be present in a greater abundance in the differentiate magma (BK403), though this observed discrepancy may well be a result of the scatter of the Ba data. The similar Sr and Zr contents of the two rocks forecast that both plagioclase and hornblende occurred in significant amounts in the fractionation assemblage, since their bulk distribution coefficients must have been close to unity. A comparison of the relative concentrations of the elements, Zr, Nb, and Y, in the two rocks indicates that both Zr and Y may cause erroneous results in the modelling calculations. The XRF analysis of Y in BK403 gives a concentration of only 1 ppm, which is well below the detection

Table 5.3 Fractionation from BK406 to BK403 (ie. 1-4)(using dacitic K_D 's) and from BK403 to BK401 (5)(using rhyodacitic K_D 's).

C_L/C_L^c	postulated fractionation assemblage					
	HBE +PLAG	HBE +PLAG	HBE (+ILM)	HBE (+ILM)	HBE +QTZ	
	1	2	3	4	5	
Ce	0.91	0.91	0.94	0.94	0.79	
Sm	0.92	0.90	0.93	0.92	1.14	
Eu	1.14	1.13	1.13	1.12	1.15	
Tb	0.98	0.96	0.99	0.98	0.95	
Yb	0.69	0.67	0.71	0.69	1.06	
Lu	0.53	0.51	0.54	0.53	1.04	
Sc	1.11	1.10	1.11	1.11	1.06	
Ti	1.07	1.06	0.98	0.98	0.90	
Ba	0.71	0.72	0.74	0.75	1.15	
Sr	0.83	0.83	0.74	0.75	0.47	
Y	0.08	-	0.08	-	1.01	
Zr	1.18	1.18	1.20	1.20	0.84	
Nb	1.04	1.03	1.06	1.05	1.00	
$\emptyset_j\%$						
HBE	32.58	31.00	33.37	31.80	29.56	
PLAG	4.40	4.40				
QTZ					45.50	
(ILM)			1.00	-0.80		
$\emptyset_m\%$	63.04	64.65	67.64	69.05	24.94	
$\sum(R)^2$	78.33	35.40	77.74	35.02	44.27	
Q	2.67	1.88	2.65	1.87	2.00	

limits of Y for this analysis technique (Appendix 1), and so this value is likely to be erroneous. Both Y and Nb have considerably smaller abundances in BK403, relative to BK406, while the Zr contents of the samples are very similar. These elements generally behave in a similar fashion in magmatic processes (Pearce and Norry, 1979), and so should have roughly the same pattern of distribution between the two samples. All other elements, except Ce, occur in greater abundance in the parent magma type (BK406) compared with the differentiate magma type (BK403).

Two fractionation assemblages are modelled in the calculations; hornblende + plagioclase (models 1 and 2), and hornblende + (ilmenite) (models 3 and 4). As predicted, the results of models 1 and 3 show that the abundance of Y in magma type BK403 cannot be explained by the fractionation of either of these assemblages from a parent magma of the composition of BK406. Models 2 and 4 differ from models 1 and 3 in that they omit the Y data. Model 2 involves the fitting of the equilibrium fractionation equation to these two magma types, using hornblende and plagioclase as fractionation phases and the corresponding K_D values determined from dacitic rocks (see Table 4.1). The best-fit differentiate magma composition differs from that of the BK403 magma type mainly in its HREE contents, with the abundances of Yb and Lu in the former, being 1.5 to 2 times those in sample BK403. However, the C_L/C_L^C ratios of the REE group, as a whole, show a pattern of deviations from unity which suggest that the hornblende REE K_D values, used in the model, are inappropriate to this fractionation stage of the orthogneiss magmas. All of the REE C_L/C_L^C values, except that of Eu, are less than unity, ie. in each case the calculated best-fit value is greater than the BK403 value. This implies that the hornblende REE K_D values are too small, provided that the equilibrium fractional crystallisation equation is relevant to the evolution of the tonalitic orthogneiss magmas. Ba and Sr fit reasonably well with the model after considering the degree of scatter in the data of these two elements (see previous chapter). The inconsistency between the relative distributions of Zr and Nb in the parental (BK406) and differentiate (BK403) magma types, is borne out by the fairly high Zr C_L/C_L^C value of 1.18, showing that the model requires greater depletion of this element in the magma than is observed.

The best-fit fractionation assemblage, of model 2, is dominated by hornblende (31.0% of the mass of the parental liquid), with only 4.4% of plagioclase fractionation being required. This calculated best-fit assemblage is in agreement with the petrographic evidence which indicates that plagioclase fractionation had probably slowed and then finally ceased by the formation of the leucotonalitic orthogneiss magma. Model 4, involving the fractionation of a hornblende + (ilmenite) assemblage produces very similar results to those of model 2.

The mass of the best-fit differentiate magma (ϕ_m), relative to the mass of the BK406 parent magma, is c.65%, and its mass relative to the mass of the initial BK102 magma is c.6.24%.

5.3.2d Fractionation from the leucotonalitic orthogneiss magma type (BK403) to the granitic orthogneiss magma type (BK401).

The results of one fractionation model (model 5) are given in Table 5.3. This model involves the fitting of the equilibrium fractionation of hornblende and quartz to a parent magma type (BK403) and a differentiate magma type (BK401). An initial study of the relative abundances of those trace elements in samples BK403 and BK401 used in the calculations, reveals that all of the elements, except Sr, Ba, and Eu, are present in greater abundance in the parent magma type (BK403). The Eu distribution is important in that the hornblende K_D in granite magma is significantly greater than 1.0 (c.5.0 in Table 4.1), and, therefore, the fractionation of hornblende alone could not produce the observed enrichment of Eu in the fractionating magma. Neither would the presence of plagioclase, together with hornblende, explain this feature, since the plagioclase K_D in granitic magmas is also greater than 1.0. The fractionation of quartz in significant quantities would dilute the effects of the large hornblende REE K_D 's. Since, in hornblende, the K_D value is smaller than the other MREE K_D values, it is possible for the D^{Eu} value to be selectively lowered below unity. However, the hornblende K_D 's of La and Ce, in granitic magmas, are even lower than the K_D , and so any lowering of the D^{Eu} value, through quartz fractionation, will produce values of D^{La} and D^{Ce} which are much smaller than unity. La and Ce are both strongly depleted in the differentiate magma type (BK401), compared to the parent magma type (BK403), and so if hornblende and quartz are retained in the postulated fractionation assemblage, they must be accompanied by a

91
phase which has large K_D 's for the LREE's. This phase must be orthite. Unfortunately, absolute values of the orthite K_D 's for the elements used in the calculations, are not known and so, the assemblage hornblende + quartz, only, was used in model 5. K_D 's for quartz were estimated at 0.01.

The calculated best-fit differentiate magma of model 5 is very similar to the BK401 magma type, for all elements except Ce and Sr. The low C_L/C_L^C value of Ce can be reconciled with the omission of orthite from the fractionation assemblage. Sr also has a low C_L/C_L^C value (0.47) and this is undoubtedly related to the slow separation from the magma of the corroded plagioclase crystals observed in the granodioritic and granitic rocks (see chapter 2). Equilibration of the magma with these corroded plagioclase crystals during separation could have produced the observed Sr distribution in the two magma types.

It is not thought that the calculated \emptyset_j % values of hornblende (29.56%) and quartz (45.50%), required to produce the best-fit differentiate magma, from the parent (BK403) magma type, will be greatly affected by the introduction of orthite as a fractionation phase. The degree of plagioclase separation must be fairly small since Sr increases significantly in abundance in the fractionating magma. The estimated mass of the best-fit differentiate magma remaining, relative to the mass of the parent BK403 magma type, is c.20% and its mass relative to the initial BK102 magma type is c.1.25%.

5.4 Conclusions of the trace element modelling.

The magma types selected in the previous chapter (see fig. 4.14), which span the whole composition range of the metabasite-orthogneiss series, can be adequately described as samples of a single magma that evolved by a combination of closed-system, sub-total equilibrium, fractional crystallisation and subordinate assimilation. The differentiation scheme formulated from conclusions made in chapters 2, 3, and 4, and depicted in fig. 4.14, has been modified and to some extent quantified. This refined differentiation model is depicted in fig. 6.1, and summarised below.

In the initial stages, the metabasite magma evolved by the fractionation of clinopyroxene and orthopyroxene. This led to Fe enrichment and slight SiO_2 depletion in the magma. At some point, the magma began to assimilate paragneissic country rocks and this

resulted in an increase in its SiO_2 content. The change in composition was sufficient to cause plagioclase to supersede pyroxene as the primary liquidus phase (ie. the highest temperature phase). The fractionation of calcic plagioclase and the subordinate assimilation of paragneiss drove the magma to an andesitic composition (ie. the melanotonalitic orthogneiss), at which point, hornblende replaced pyroxene as the fractionating mafic phase. This produced an even more rapid SiO_2 enrichment in the magma, which resulted in the destabilisation of plagioclase at the liquidus and the fractionation of a hornblende dominated assemblage. Plagioclase crystallisation finally ceased by the formation of the leucotonalitic orthogneiss magma. However, the last formed plagioclase, with a composition of c. An_{40} , did not separate fully as the magma evolved to a granitic composition through the fractionation of quartz + hornblende + orthite.

Chapter 6.

Discussion of the results, and general conclusions.

The aim of this work has been partially fulfilled, in that some plausible origins for the various component rock groups of the intrusive complex have been determined.

6.1 Discussion of the results.

The results of this thesis show that the metabasite and orthogneiss rocks can be reconciled with a derivation from a single metabasite magma type, and so in this sense this work agrees with Leake (1970a). However, both studies are subject to the constraint that the intrusion of the metabasite magmas, into the Dalradian rocks of southern Connemara, was followed by the intrusion of the orthogneiss magmas within a geologically-reasonable period of time, ie. one which corresponds to the length of time taken for a plutonic magma to differentiate from basaltic to tonalitic composition, say 5 Ma. The metabasite rocks were intruded during the D2 deformation of the Dalradian rocks (Leake, 1970a), while the intrusion of the orthogneiss occurred during the D3 deformation (Leake (1970a), and this study). The intrusion of the metabasite rocks has been dated at 510 ± 10 Ma, based on U-Pb isotopes in zircons (Pidgeon, 1969), and therefore this dates the D2 deformation also. The orthogneisses predate the Dughterard Granite, which outcrops to the east of the Shannavara district, and which has a cooling date of 469 ± 7 Ma (Leggo *et al.*, 1966). The M3 metamorphism in the Scottish Dalradian has been dated at 496 ± 17 Ma by Pankhurst (1970) and this presumably dates the D3 deformation, the two being thought to be synchronous. Therefore, the time period between the D2 and D3 deformational events was probably sufficiently short as to not invalidate the conclusions of this thesis and Leake (1970a).

The presence of two amphibole types, brown amphibole and green actinolitic amphibole, in the metabasite rocks led Leake (1970a) and Bremner and Leake (1981) to conclude that the brown hornblende was an early crystallising igneous hornblende, and Bremner (*thss.*, 1977) states that hornblende fractionation controlled the crystallisation of the Roundstone metabasite mass. However, the microtextural evidence in Chapter 2 of this study

indicates that, apart from plagioclase, the mineralogy of the metabasite rocks is invariably metamorphic in origin, with only occasional remnants of an igneous mafic assemblage being preserved. Amphibole, both types, and quartz are the breakdown products of clino- and ortho-pyroxene, with metamorphic reaction rims surrounding the pyroxene relics. Titaniferous ore grains, in the metabasite rocks, equilibrated extensively during the M3 metamorphism, producing an unmixing of the Ti-rich (ilmenite) and Ti-poor (titanomagnetite) components. A subsequent reaction partially converted this ilmenite to sphene during the amphibolitisation process. This latter reaction is confirmed by Spear (1981) who found that sphene formation in amphibolite is favoured by low temperatures (c. 550°C), and high oxygen fugacity.

The results of the analysis of the geochemical data of the metabasite rocks, in this thesis, are not compatible with the fractionation of hornblende from the metabasite magma, and so this thesis disagrees with the conclusion of Leake (1970a) and Bremner and Leake (1981) on this subject. On the other hand, the results do agree with the conclusion of Egglar and Burnham (1973), i.e. that melts of andesitic composition are not generated by the fractionation of hornblende from melts of basaltic composition. The fractionation of hornblende probably cannot occur in melts with less than 55 wt% SiO₂ (recalculated without H₂O), except perhaps in instances where the magma is abnormally H₂O-rich.

Primary hornblende is first recognised in the melano-tonalitic orthogneisses and continues to be present right through to the granitic orthogneiss rocks, although in the latter it is commonly altered to biotite and chlorite. Plagioclase ranges from An₈₆ to An₄₀, in the metabasite and orthogneiss rocks, with plagioclase of the latter composition occurring in the leucotonalitic, granodioritic and granitic orthogneisses. However, the plagioclase in the latter two rock groups is invariably strongly corroded at its margins and is thought to represent earlier crystallised plagioclase, which probably formed in the leucotonalitic orthogneiss magma and did not segregate from it.

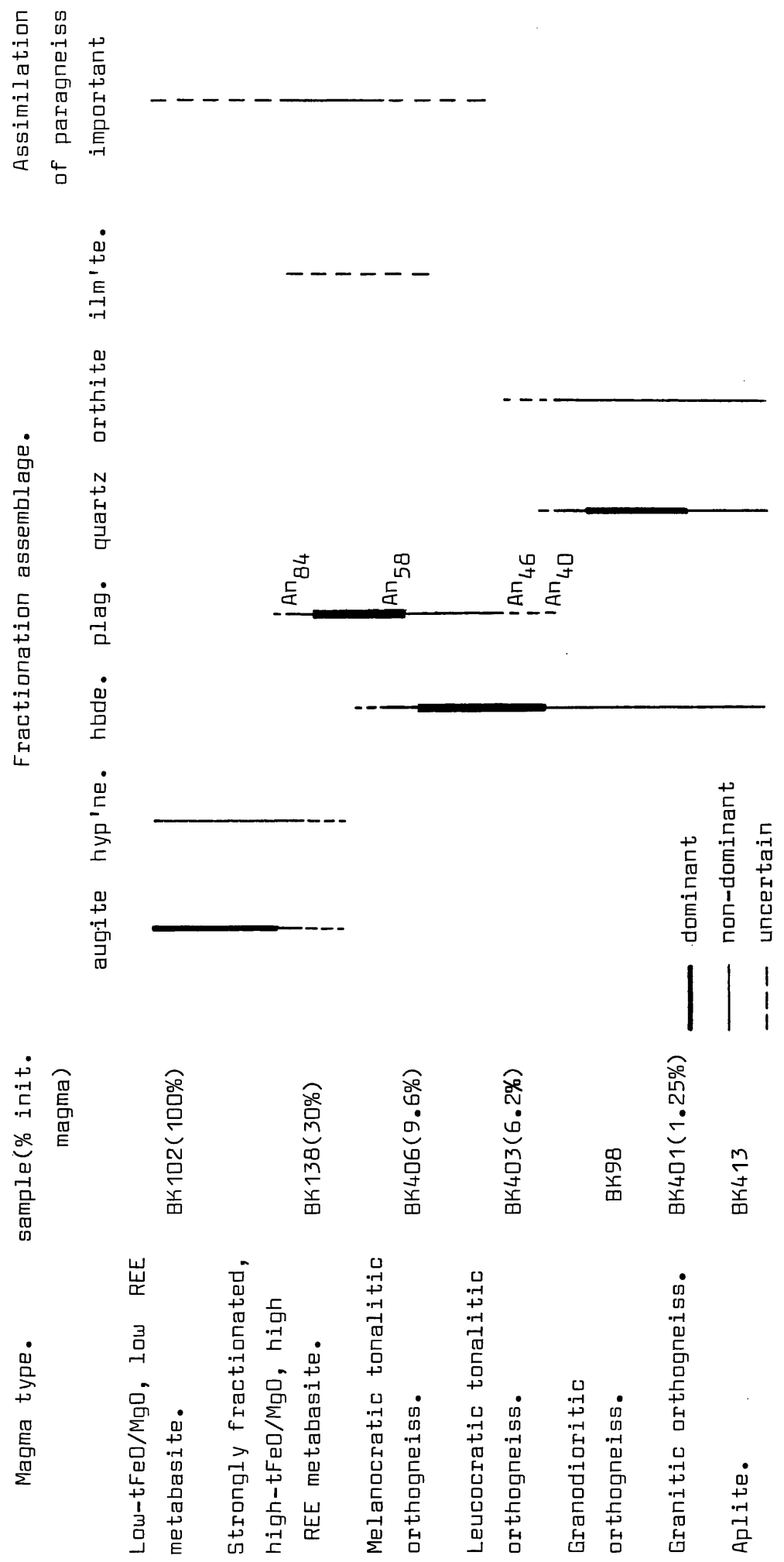
There is strong field evidence for the assimilation of paragneiss by the metabasite magmas (Leake and Skirrow (1960), Evans (1964)), and by the tonalitic orthogneiss magmas (Senior (1973), and this study). The paragneiss which mantles the tonalitic

orthogneiss intrusions in the Shannavara district is a chaotic rock, composed of a siliceous leucogneissic mobilisate, with a strong F3 foliation, containing disorientated xenoliths of quartzite, semipelite and residual melanosome, all in various states of assimilation, and also pods of metabasite. All of these xenoliths can be found in the orthogneiss, near to the contact with the paragneiss. The morphology of the quartzitic and semipelitic xenoliths, which are often rectangular and presumably represent refractory layers in the metasedimentary pile, indicates that these lithologies have been disrupted by the injection of mobilisate, induced by the continued upward intrusion of the tonalitic orthogneiss magmas.

Although the metabasite and orthogneiss rocks still exhibit a well defined igneous chemistry, their incompatible element and Sr abundances have been strongly modified by the amphibolitisation process which these rocks underwent. The comagmatic nature of the metabasite and orthogneiss rocks is shown by their continuous chemical variations in both the major and trace element data. Almost all of the samples have compositions which to a close approximation represent magma compositions. The various metabasite and orthogneiss magma types that occur at the presently exposed level of the intrusive complex are thought to represent batches of magma periodically released to higher levels from a main magma stock at depth. The main body of magma was itself moving upwards through the crust and differentiating by fractional crystallisation. The release of batches of magma may have been caused by tectonic squeezing of the main magma body. (Leake, 1970a).

The results of the trace element modelling (Chapter 5) show that the bulk the variation in the trace element abundances of the metabasite-orthogneiss rock series can be adequately described by a process intermediate to the two types of closed-system fractional crystallisation, total equilibrium and surface equilibrium fractionation. They also indicate that the assimilation of paragneiss is extremely important in producing the fractionation link between the metabasite and melanotonalitic orthogneiss magmas. The sequence of fractionation from the metabasite and orthogneiss magmas, and their calculated masses, relative to the initial magma mass (magma type BK102), are given in fig. 6.1. The sequence of fractionation proposed in fig. 6.1 agrees extremely well with the

Fig. 6.1 A quantitative summary of the differentiation of the metabasite-orthogneiss magmas.



experimental phase relations of the basalt-andesite-rhyolite system, which are summarised in Chapter 3. The calculated masses of the various metabasite and orthogneiss magma types, relative to the BK102 metabasite magma type, fit reasonably well with the observed proportions of the various rock groups in the intrusive complex, though the orthogneisses are slightly more abundant at the present erosion level than the model forecasts. The model confirms the relatively minor importance of the granitic orthogneiss in the series, and therefore predicts that the intrusive complex did not form the root of a granitic batholith which has since been stripped away by erosion.

The metabasite magmas are presumed to have originated in the mantle (Senior and Leake, manuscript) and since the metabasites are fairly similar to tholeiitic rocks (ie. they plot in the tholeiitic part of the AFM diagram, exhibit an Fe enrichment trend, and are subalkaline), they have a probable source in the upper mantle (Allegre et al., 1981). The low- Σ REE magma type BK102 has a REE* pattern which is remarkably LREE* enriched, and therefore this magma type is obviously strongly fractionated. Similar REE* patterns, though not so extreme in their LREE* enrichment, have been determined in basalts from the Tyrrhenian Sea, a small marginal basin floored by oceanic crust of a transitional nature (ie. between oceanic and continental crust), in the western Mediterranean Sea (Hamelin, 1979). It seems likely that as the width of the marginal basin increases, the new crust forming in it is increasingly like true oceanic crust (Hawkins, 1977). The metabasite REE* patterns are very different to typical MORB (mid-ocean ridge basalt) REE* patterns, which are often LREE* depleted. Therefore, the BK102 metabasite REE* pattern may suggest that the metabasite magmas were intruded into a very transitional type of marginal basin (ie. floored by crust intermediate to true oceanic and true continental crust) which contained the Dalradian metasedimentary pile. Claims that the Dalradian rocks were deposited in an ensialic basin (Phillips et al., 1976) are therefore supported by the metabasite REE data.

The metabasite magma initially fractionated an assemblage of clinopyroxene and orthopyroxene, with the former phase being the more dominant of the two. This led to an Fe enrichment trend, similar to that observed in tholeiitic rock series, and also to

a trend of SiO_2 depletion, in the magma. However, at some point after the magma had differentiated to the BK138 magma type, these two trends were reversed and this is attributed in this thesis to the assimilation of siliceous paragneiss. The assimilation of sedimentary material would have caused the fractionation of plagioclase in the magma and would have quickly driven the magma to more siliceous compositions. At these new, roughly andesitic compositions, the fractionation of plagioclase, from the magma, could proceed without the need of further assimilation of paragneiss. The sudden reversal of the Fe enrichment and the SiO_2 depletion trends, may suggest that the metabasite magma broke through into the Dalradian cover at this point, after passing through relatively refractory basement. If this assimilation of paragneiss had not occurred it is probable that the metabasite magma would have continued to follow a tholeiitic crystallisation sequence ending with the crystallisation of fayalite + quartz.

The proposed development of the metabasite magma composition may throw light onto the problem of the derivation of granitic magmas which have a significant mantle component. It may be that granite magmas cannot form from mantle-derived magma by fractional crystallisation processes, without some incorporation of a siliceous crustal component, by assimilation. This is also suggested by Allegre and Ben Othman (1980), and DePaolo (1980, 1981) on the basis of Nd isotopic evidence from young (<1.8 Ma) granitoid rocks, ie. the Sierra Nevada batholithic granitoids. In this study, the leucotonalitic, granodioritic and granitic orthogneisses have been calculated to represent only 6% of the mass of the initial BK102 magma type. Clearly, much larger amounts of assimilation than that involved in the generation of the acidic orthogneisses, are needed to form, say, the granitoid batholiths of the Sierra Nevada. Furthermore, the assimilation of siliceous paragneiss, by the metabasite magma, caused the fractionation of dominant plagioclase over a wide magma composition interval. This indicates that large volumes of plagioclase-rich cumulates underly the batholithic granitoid intrusions, at depth, and therefore, this may explain the origin of anorthosite massifs. Wiebe (1980), and Duchesne and Demaiffe (1978) point out that anorthosite massifs are invariably surrounded by amphibolite to granulite grade paragneisses, which often contain granite intrusions, thought to be

anatectic melts that were derived from the surrounding crust at the time of emplacement of the anorthosite mass (Buddington, 1972). Wiebe (1980) advocates that anorthosites are formed as cumulates from an extremely feldspathic parental magma, and indicates that this magma may be derived by the prolonged fractionation of pyroxene from a tholeiitic magma. Wiebe does not consider the assimilation of the partially molten country rocks by this fractionating tholeiitic magma, which would initiate plagioclase fractionation without the need for an extremely feldspathic parental magma.

6.2 General conclusions of this work.

The following conclusions have been reached in this study of the rocks of the Connemara syntectonic intrusive complex:-

1. The metabasite and orthogneiss rocks are comagmatic and represent the sequence of compositions attained by an initial magma type evolving from basaltic composition (ie. the metabasites), through andesitic composition (ie. the tonalitic orthogneisses), to dacitic and rhyolitic compositions (ie. the granodioritic and granitic orthogneisses).
2. The main magmatic process operating on the magma throughout this sequence was fractional crystallisation. Assimilation of paragneiss by the magma was important during the transitional stage of differentiation between the metabasite and melano-tonalitic orthogneiss magma types.
3. The magma initially crystallised clinopyroxene and orthopyroxene and its composition progressed along a tholeiitic trend. However, the assimilation of paragneiss caused the stabilisation of plagioclase as a primary liquidus phase, as well as enriching the magma in SiO_2 and depleting it in Fe. The fractionation of a plagioclase dominated phase assemblage drove the magma through andesitic compositions to more siliceous ones. Hornblende superseded plagioclase as the primary liquidus phase and these two phases fractionated from the magma to produce the leucotonalitic orthogneiss magma type. Due to the build up of H_2O in the magma, the stability field of plagioclase dropped well below the magma liquidus and fractionation of plagioclase ceased. Further fractionation of hornblende with quartz produced the granodioritic and granitic

orthogneiss magma types.

4. In the trace element modelling of the fractionation process, the orthogneiss corresponds to only c. 10% of the total mass of the initial magma (see fig.6.1). Therefore it is clear that the intrusive complex did not form the root of a granitoid batholith which has since been stripped away.
5. High temperatures (c. 900°C) were reached in the Dalradian country rocks which mantled the rising melanotonalitic orthogneiss magmas and this caused large degrees of partial melting across a broad aureole zone.
6. It is suggested that large granitoid batholiths containing a significant mantle-derived component, may be formed from broadly tholeiitic magma, perhaps initially containing a few percent H₂O, which interacts with, and assimilates, a relatively siliceous crustal component, early on its evolution. This would prevent a significant trend of Fe enrichment like the one shown by the metabasite rocks, and it would also produce much larger volumes of granitoid magma than observed in this study. From this hypothesis it can be predicted that large volumes of granitoid magmas will form where mantle magmas interact with thick continental crust, ie. at cordilleran plate margins, and this is in fact where granitoid rocks are most voluminous.

6.3 Suggestions for further research.

Further work is needed to substantiate evidence gathered in this thesis that hornblende fractionation was not the dominant influence in the production of the orthogneiss rocks from the strongly fractionated, Fe-rich metabasite magma type (represented by sample BK138). It is suggested that the effects of H₂O content on the phase relations of a rock composition similar to that of sample BK138 should be determined experimentally. This study would also require the determination of H₂O dependent phase relations of a melanotonalitic orthogneiss composition (ie. that of sample BK406). Presumably, the H₂O levels needed to promote dominant hornblende fractionation in the melt, from the BK138 and BK406 magma types, would inhibit the fractionation of plagioclase. The effects of assimilation on the phase relations of the BK138

100
magma type could be determined by adding various quantities of the mobilisable component of the paragneiss to the experimental charge.

REFERENCES

- ALBAREDE, F. & BOTTINGA, Y. 1972. Kinetic disequilibrium in trace element partitioning between phenocrysts and host lava. Geochim.Cosmochim.Acta. 36, 141-56.
- ALBAREDE, F. & PROVOST, A. 1977. Petrological and geochemical mass-balance equations: an algorithm for least-square fitting and general error analysis. Comput.Geosci. 3, 309-326.
- ALDERTON, D. H. M., PEARCE, J. A. & POTTS, P. J. 1980. Rare earth element mobility during granite alteration: evidence from southwest England. Earth planet.Sci.Lett. 49, 149-65.
- ALLEGRE, C. J. & BEN OTHMAN, D. 1980. Nd-Sr isotopic relationship in granitoid rocks and continental crust development: a chemical approach to orogenesis. Nature.London. 286, 335-342.
- ALLEGRE, C. J., DUPRE, B., LAMPRET, B. & RICHARD, P. 1981. The subcontinental debate, I. Lead-neodymium-strontium isotopes in primary alkali basalts from a shield area: the Ahaggar volcanic suite. Earth planet.Sci.Lett. 52, 85-92.
- ALLEN, J. C. & BOETTCHER, A. L. 1978. Amphiboles in andesite and basalt: stability as a function of P - T - f_{H_2O} - f_{O_2} . Am.Mineral. 63, 1074-87.
- ANDERSON, A. T. 1980. Significance of hornblende in calc-alkaline andesites and basalts. Am.Mineral. 65, 837-51.
- APTED, M. J. & BOETTCHER, A. L. 1981. Partitioning of rare earth elements between garnet and andesite melt: an autoradiographic study of P - T - X effects. Geochim.Cosmochim.Acta. 45, 827-37.
- ARTH, J. G. 1976. Behaviour of trace elements during magmatic processes- a summary of theoretical models and their applications. J.Res.U.S.geol.Surv. 4, 41-47.
- ARTH, J. G. & BARKER, F. 1976. Rare-earth partitioning between hornblende and dacitic liquid and implications for the genesis of trondhjemitic-tonalitic magmas. Geology. 4, 534-536.

- BADLEY, M. E. 1972. The geology of the Maumturk Valleys and Inagh Valley, Connemara. Ph.D. Thesis. Univ. Nottingham.
- BADLEY, M. E. 1976. Stratigraphy, structure and metamorphism of Dalradian rocks of the Maumturk Mountains, Connemara, Ireland. J.geol.Soc.London. 132, 509-20.
- BOWEN, N. L. 1928. The evolution of the igneous rocks. Princeton Univ. Press, Princeton, N.J.
- BREMNER, D. L. 1977. The Roundstone ultrabasic complex, Connemara, Ireland. Ph.D. Thesis. Univ. Glasgow.
- BREMNER, D. L. & LEAKE, B. E. 1981. The geology of the Roundstone ultrabasic complex, Connemara. Proc.R.Irish Acad. 80(B), 395-433.
- BUDDINGTON, A. F. 1972. Differentiation trends and parental magmas for anorthositic and quartz mangerite series, Adirondacks, New York. Geol.Soc.Am.Mem. 132, 477.
- BUDDINGTON, A. F. & LINDSLEY, D. M. 1964. Iron-titanium oxide minerals and synthesised equivalents. J.Petrol. 5, 310-57.
- CANN, J. R. 1970. Rb, Sr, Y, Zr and Nb in some ocean-floor basaltic rocks. Earth planet.Sci.Lett. 19, 7-11.
- CAWTHORN, R. G. & BROWN, P. A. 1976. A model for the formation and crystallization of corundum-normative calc-alkaline magmas through amphibole fractionation. J.Geol.Chicago. 84, 467-476.
- CAWTHORN, R. G. & O'HARA, M. J. 1976. Amphibole fractionation and calc-alkaline magma genesis. Am.J.Sci. 276, 309-29.
- COBBING, E. J. 1969. The geology of the district north-west of Clifden, Co. Galway. Proc.R.Irish Acad. 67(B), 303-25.
- CRUSE, M. J. B. & LEAKE, B. E. 1968. The geology of Renvyle, Inishbofin and Inishshark, north-west Connemara, Co. Galway. Proc.R.Irish Acad. 67(B), 517-28.
- DEER, W. A., HOWIE, R. A. & ZUSSMAN, J. 1966. An introduction to the rock-forming minerals. Longman, London.
- DEPAOLO, D. J. 1980. The sources of continental crust: Nd isotope evidence from the Sierra Nevada and Peninsula Ranges. Science. 209, 684-.

- DEPAOLO, D. J. 1981. Trace element and isotopic effects of combined wallrock assimilation and fractional crystallization. Earth planet.Sci.Lett. 53, 189-202.
- DRAKE, M. J. & WEILL, D. F. 1975. The partition of Sr, Ba, Ca, Y, Eu^{2+} , Eu^{3+} and other REE between plagioclase feldspar and magmatic silicate liquid: an experimental study. Geochim.Cosmochim.Acta. 39, 689-712.
- DUCHESNE, J-C. & DEMAIFFE, D. 1978. Trace elements and anorthosite genesis. Earth planet.Sci.Lett. 38, 249-72.
- EDMUNDS, W. M. & THOMAS, P. R. 1966. The stratigraphy and structure of the Dalradian rocks north of Recess, Connemara, Co. Galway. Proc.R.Irish Acad. 64(B), 317-28.
- EGGLER, D. H. 1972A. Water-saturated and undersaturated melting relations in a Paracutin andesite and an estimate of water content in the natural magma. Contrib.Mineral.Petrol. 34, 261-71.
- EGGLER, D. H. & BURNHAM, C. W. 1973. Crystallization and fractionation trends in the system Andesite- H_2O - CO_2 - O_2 at pressures to 10 kbar. Bull.geol.Soc.Am. 84, 2517-32.
- EVANS, B. W. 1959. The geology of the Toombeola district, Connemara, Eire. Ph.D. Thesis. Univ. Oxford.
- EVANS, B. W. 1964. Fractionation of elements in the pelitic hornfelses of the Cashel-Lough Wheelaun intrusion, Connemara, Eire. Geochim.Cosmochim.Acta. 28, 127-56.
- GILL, J. B. 1978. Role of trace element partition coefficients in models of andesite genesis. Geochim.Cosmochim.Acta. 42(6A), 709-24.
- GREENLAND, L. P. 1970. An equation for trace element distribution during magmatic crystallization. Am.Mineral. 55, 455-65.
- HAMELIN, B., LAMPRET, B., JORON, J-L., TREUIL, M. & ALLEGRE, C. J. 1979. Geochemistry of basalts from the Tyrrhenian Sea. Nature.London. 278, 832-34.
- HANSON, G. N. 1980. Rare earth elements in petrogenetic studies of igneous systems. Ann.Rev.Earth planet.Sci. 8, 371-406.

- HARRIS, D. M. 1977. Ascent and crystallization of albite and granitic melts saturated with H₂O. J.Geol.Chicago. 85, 451-59.
- HARVEY, P. K. 1967. The geology of the Glinsk district, Connemara, Eire. Ph.D. Thesis. Univ. Bristol.
- HAWKINS, J. W. 1977. Petrologic and geochemical characteristics of marginal basin basalts. In: TALWANI, M. & PITMAN III, W. C. (EDS.). Island arcs, deep sea trenches and back-arc basins. pp. 355-65. Am.Geophys.Union., Series 1.
- HELLMAN, P. L., SMITH, R. E. & HENDERSON, P. 1979. The mobility of the rare earth elements: evidence and implications from selected terrains affected by burial metamorphism. Contrib.Mineral.Petrol. 71, 23-44.
- HOFFER, E. 1978. Melting reactions in aluminous metapelites: stability limits of biotite+sillimanite+quartz in the presence of albite. Neues.Jahrb.Mineral. Monatshefte., 396-407.
- IRVINE, A. J. 1978. A review of experimental studies of crystal/liquid trace element partitioning. Geochim.Cosmochim.Acta. 42(6A), 743-70.
- IRVINE, T. N. & BARAGAR, W. R. A. 1971. A guide to the chemical classification of the common volcanic rocks. Can.J.Earth Sci. 8, 523-48.
- JOHANNES, W. 1980. Metastable melting in the Granite System Qz-Or-Ab-An-H₂O. Contrib.Mineral.Petrol. 72, 73-80.
- KILBURN, C., PITCHER, W. S. & SHACKLETON, R. M. 1965. The stratigraphy and origin of the Portaskaig Boulder Bed Series (Dalradian). Geol.J. 4, 343-60.
- KNABE, W. 1970A. Reaktionen der biotits bei der anatexis. Geol.Jahrb. 88, 355-72.
- KNABE, W. 1970B. Anatexis von quarz-plagioklas-biotit-metamorphiten. Geol.Jahrb. 89, 1-31.
- KUNO, H., YAMASAKI, K., IIDA, C. & NAGASHIMA, K. 1957. Differentiation of Hawaiian magmas. Jpn.J.Geol.Geogr. 28, 179-218.

- LEAKE, B. E. 1958A. The Cashel-Lough Wheelaun intrusion, Co. Galway. Proc.R.Irish Acad. 59(B), 155-203.
- LEAKE, B. E. 1970A. The origin of the Connemara migmatites of the Cashel district, Connemara, Ireland. Q.J.geol.Soc.London. 125, 219-76.
- SENIOR, A. & LEAKE, B. E. The geology of the Shannavara district, Connemara, and the origin of the Connemara gneisses (manuscript).
- LEAKE, B. E. & SKIRROW, G. 1960. The pelitic hornfelses of the Cashel-Lough Wheelaun intrusion, County Galway, Eire. J.geol.Soc.London. 68, 23-40.
- LEGGO, P. J., COMPSTON, W. & LEAKE, B. E. 1966. The geochronology of the Connemara granites and its bearing on the antiquity of the Dalradian Series. Q.J.geol.Soc.London. 122, 91-118.
- LINDSTROM, D. J. 1976. Experimental study of the partitioning of the transition metals between clinopyroxene and coexisting silicate liquids. Ph.D. Thesis. Univ. Oregon.
- LINDSTROM, D. J. & WEILL, D. F. 1978. Partitioning of transition metals between diopside and coexisting silicate liquids. I. Nickel, cobalt and manganese. Geochim.Cosmochim.Acta. 42(6A), 817-31.
- LUHR, J. F. & CARMICHAEL, I. S. E. 1980. The Colima volcanic complex, Mexico. 1. Post-caldera andesites from Volcan Colima. Contrib.Mineral.Petrol. 71, 343-72.
- MACDONALD, G. A. 1968. Composition and origin of Hawaiian lavas. Geol.Soc.Am.Mem. 116, 477-522.
- MARTIN, R. F., WHITLEY, J. E. & WOODLEY, A. R. 1978. An investigation of rare-earth mobility: fenetised quartzites, Borralan Complex, N.W. Scotland. Contrib.Mineral.Petrol. 66, 69-73.
- MOORE, J. G. 1965. Petrology of deep-sea basalt near Hawaii. Am.J.Sci. 263, 40-52.
- MORRIS, R. V. & HASKIN, L. A. 1974. EPR measurements of the effect of glass composition on the oxidation state of europium. Geochim.Cosmochim.Acta. 38, 1435-45.

- MORRIS, W. A. & TANNER, P. W. G. 1977. The use of palaeomagnetic data to delineate the history of the development of the Connemara Antiform. Can.J.Earth Sci. 14, 2601-13.
- MORTON, W. H. 1964. The petrology and structure of the basic igneous complex at Roundstone, Co. Galway, Eire. Ph.D. Thesis. Univ. Manchester.
- MYSEN, B. O. 1978B. Experimental determination of rare earth element partitioning between hydrous silicate melt, amphibole and garnet peridotite minerals at upper mantle pressures and temperatures. Geochim.Cosmochim.Acta. 42, 1253-63.
- MYSEN, B. O. & VIRGO, D. 1980. trace element partitioning and melt structure: an experimental study at 1 atm. pressure. Geochim.Cosmochim.Acta. 44, 1917-30.
- NAKAMURA, N. 1974. Determination of REE, Ba, Fe, Mg, Na and K in carbonaceous and ordinary chondrites. Geochim.Cosmochim.Acta. 38, 757-75.
- NANEY, M. T. & SWANSON, S. E. 1980. The effect of Fe and Mg on crystallization in granitic systems. Am.Mineral. 65,639-53.
- NEDELEC, A. & PAQUET, J. 1981. Biotite melting in high-grade metamorphic gneisses from the Haut Allier(French Massif Central). Contrib.Mineral.Petrol. 77, 1-10.
- NEUMANN, H., MEAD, J. & VITALIANO, C. J. 1954. Trace element variation during fractional crystallization as calculated from the distribution law. Geochim.Cosmochim.Acta. 6, 90-9.
- O'HARA, M. J. 1976. Data reduction and projection schemes for complex compositions. In: Third progress report of research supported by NERC at Edinburgh and Manchester Universities (1972-1975). Publications Series D, No. 6. pp.103-126.
- O'HARA, M. J. 1980. Non-linear nature of the unavoidable long-lived isotopic, trace and major element contamination of a developing magma chamber. Philos.Trans.R.Soc.London. 297(A), 215-27.
- PANKHURST, R. J. 1970. The geochronology of the basic igneous complexes (of north east Scotland). Scott.J.Geol. 6, 83-107.

- PATRICK, D. 1967. The structural and metamorphic geology of the Corcogemore Mountains area, Connemara, Eire. Ph.D. Thesis. Univ. Bristol.
- PEARCE, J. A. & CANN, J. R. 1973. Tectonic setting of basic volcanic rocks determined using trace element analyses. Earth planet.Sci.Lett. 19, 290-300.
- PEARCE, J. A. & NORRY, M. J. 1979. Petrogenetic implications of Ti, Zr, Y, and Nb variations in volcanic rocks. Contrib.Mineral.Petrol. 69, 33-47.
- PHILLIPS, W. E. A., STILLMAN, C. J. & MURPHY, T. 1976. A Caledonian plate tectonic model. J.geol.Soc.London. 132, 579-609.
- PHILPOTTS, J. A. & SCHNETZLER, C. C. 1970. Phenocryst-matrix partition coefficients for K, Rb, Sr and Ba, with applications to anorthosite and basalt genesis. Geochim.Cosmochim.Acta. 34, 307-22.
- PIDGEON, R. T. 1969. Zircon U-Pb ages from the Galway granite and the Dalradian, Connemara, Ireland. Scott.J.Geol. 5, 375-92.
- PRESNALL, D. C. & BATEMAN, P. C. 1973. Fusion relations in the system $\text{NaAlSi}_3\text{O}_8$ - $\text{CaAl}_2\text{Si}_2\text{O}_8$ - KAlSi_3O_8 - SiO_2 - H_2O and generation of granite magmas in the Sierra Nevada batholith. Bull.Geol.Soc.Am. 84, 3181-202.
- RAYLEIGH, J. W. S. 1896. Theoretical considerations respecting the separation of gases by diffusion and similar processes. Philos.Mag. 42, 77-102.
- SCHILLING, J. G. & WINCHESTER, J. W. 1967. Rare-earth fractionation and magmatic processes. In: RUNCORN, S. K. (ED.). Mantles of the Earth and terrestrial planets. pp. 267-83. Interscience Publishers, London and New York.
- SCHNETZLER, C. C. & PHILPOTTS, J. A. 1970. Partition coefficients of rare-earth elements between igneous matrix material and rock-forming mineral phenocrysts - II. Geochim.Cosmochim.Acta. 34, 331-340.
- SCHOCK, H. H. 1977. Trace element partitioning between phenocrysts of plagioclase, pyroxenes and magnetite and the host pyroclastic matrix. J.Radioanalytical Chem. 38, 327-40.

- SENIOR, A. 1973. The geology of the Shannavara district, Connemara, Eire. Ph.D. Thesis. Univ. Bristol.
- SPEAR, F. S. 1981. An experimental study of hornblende stability and compositional variability in amphibolite. Am.J.Sci. 281, 697-734.
- STERN, C. R. & WYLLIE, P. J. 1978. Phase compositions through crystallization intervals in basalt-andesite-H₂O at 30 kbar with implications for subduction zone magmas. Am.Mineral. 63, 641-63.
- STEUHL, H. H. 1962. Die experimentelle metamorphose und anatexis eines para-biotitgneises aus dem Schwarzwald. Chem.Erde. 21, 413-449.
- STORMER, J. C. & NICHOLLS, J. 1978. XTLFRAC: a program for the interactive testing of magmatic differentiation models. Comput.Geosci. 4, 143-59.
- STRECKEISEN, A. 1976. To each plutonic rock its proper name. Earth Sci.Rev. 12, 1-33.
- STRECKEISEN, A. & LE MAITRE, R. W. 1979. A chemical approximation to the modal QAPF classification. Neues.Jahrb.Mineral. Abhandlungen. 136(2), 169-206.
- TANNER, P. W. G. 1967. The Dalradian of Connemara. In: Ins. African geol. Univ. Leeds 11th Annual Report, 26-28.
- TANNER, P. W. G. & SHACKLETON, R. M. 1979. Structure and stratigraphy of the Dalradian rocks of the Bennabeola area, Connemara, Eire. In: HARRIS, A. L., HOLLAND, C. H. & LEAKE, B. E. (EDS.). The Caledonides of the British Isles-reviewed. Spec.Publ.geol.Soc.London. 8.
- TRELOAR, P. J. 1977. The stratigraphy, geochemistry, and metamorphism of the rocks of the Recess area, Connemara, Eire. Ph.D. Thesis. Univ. Glasgow.
- VON PLATEN, H. 1965A. Experimental anatexis and genesis of migmatites. In: PITCHER, W. S. & FLYNN, G. W. (EDS.). Controls of metamorphism. Oliver & Boyd, London.
- WATSON, E. B. 1977. Partitioning of manganese between forsterite and silicate liquid. Geochim.Cosmochim.Acta. 41, 1363-74.

- WHITE, A. J. R. & CHAPPELL, B. W. 1977. Ultrametamorphism and granitoid genesis. Tectonophysics. 43, 7-22.
- WIEBE, R. A. 1980. Anorthositic magmas and the origin of Proterozoic anorthosite massifs. Nature.London. 286, 564-67.
- WINKLER, H. G. F. 1976. Petrogenesis of metamorphic rocks. 4th Edition. Springer, New York.
- WINKLER, H. G. F. & BREITBART, R. 1978. New aspects of granitic magmas. Neues.Jahrb.Mineral. Monatshefte. pp 463-480.
- WOOD, B. J. & FRASER, D. G. 1977. Elementary thermodynamics for geologists. Oxford Univ. Press.
- WYLLIE, P. J. 1977. Crustal anatexis: an experimental review. Tectonophysics. 43, 41-71.
- WYLLIE, P. J. 1979. Magmas and volatile components. Am.Mineral. 64, 469-500.
- YARDLEY, B. W. D. 1974. The deformation, metamorphism and metasomatism of the rocks of the Cur area, Connemara, Eire. Ph.D. Thesis, Univ. Bristol.
- YARDLEY, B. W. D. 1976. Deformation and metamorphism of Dalradian rocks and the evolution of the Connemara cordillera. J.geol.Soc.London. 132, 521-42.

Appendix 1.

Rock Analyses.

This appendix lists the analyses of 50 rocks from the Cashel, Shannavara, and Glinsk districts of S.Connemara.

All major element analysis, apart from that for FeO, was carried out on fused beads (Harvey et al., 1972), using a Phillips PW1450 sequential automatic X-ray fluorescence spectrometer which is driven by a Phillips P/852M minicomputer. FeO was analysed by titration. All trace element analysis, except for that of Sc and the REE's, was carried out on pressed powder pellets (Leake et al., 1969), using a Phillips PW1220 X-ray fluorescence spectrometer. The XRF data, output on punched paper tape, was processed by a Data General Nova 2 minicomputer with 16K core storage using programs written by Dr G.M.Farrow of the Dept. of Geology, Glasgow University.

The REE's and Sc were determined by instrumental neutron activation analysis (INAA), using a method similar to that of Moyes and Whitley, (1977). Four batches of rocks were analysed, each batch consisting of between 8 and 13 rock samples, 3 samples of the U.S.G.S. Standard Basalt, BCR-1, and one pure Eu standard. In all, 41 rock samples were analysed for the REE's and Sc, and the data for 37 of these is sufficient to draw satisfactory chondrite-normalised REE patterns. The elements La, Sm, Yb, Lu, Eu, Tb and Sc were analysed using an 80 cm³ coaxial Ge(Li) gamma ray detector, with a resolution of 2.2 KeV. at 1.332 MeV., which, for the first two sample batches, was linked to a Nova 1210 minicomputer programmed to operate as a 4096 channel analyser. The elements Ce and Nd were analysed using a 0.5 cm² planar Ge(Li) gamma-ray detector, with a resolution of 623 eV at 122 KeV, which for the first two sample batches, was linked to a Digital PDP8/E minicomputer utilising 2048 channels. For the third and fourth sample batches, the two Ge(Li) detectors were linked to an E. & EG. Ortec 7032 Data Acquisition and Analysis System, which has four independent 4096 channel analysers all interfaced to an LSI-11 minicomputer. The radio-isotopes, and their photopeaks, used in the analysis of the REE's and Sc are:-
¹⁴⁰La (1596 KeV), ¹⁴¹Ce (145 KeV), ¹⁴⁷Nd (91 KeV), ¹⁵³Sm (103 KeV),
¹⁵²Eu (1408 KeV), ¹⁶⁰Tb (966-963 KeV, pair peak), ¹⁷⁵Yb (283,396),
¹⁷⁷Lu (208 KeV) and ⁴⁶Sc (889 KeV). The concentration of an element

in the sample, can be calculated from the size of the photopeaks of its radio-isotopes. Photopeak areas, for the first three sample batches, were calculated on a Nova 3 minicomputer using a computer program, Covell. This program calculates the peak area above a smoothed background. Photopeak areas for the fourth batch of samples were calculated using the 'Gamma II' spectrum analysis program provided in the software package associated with the LSI-11 minicomputer. The REE and Sc contents of the samples were calculated from the sample photopeak areas, using the average photopeak areas of the basalt BCR-1 as a standard reference. The recommended REE and Sc contents of BCR-1 are given in Flanagan, 1969.

The analysis and data processing, involved in the determination of the REE's and Sc, were carried out at the Scottish Universities Research and Reactor Centre, East Kilbride. All of the other trace element data and the major element data was determined in the Geochemistry Unit at the Dept. of Geology, Glasgow University.

The limit of detection of the trace elements analysed by XRF methods is shown below:-

Cr	1 ppm	Y	3 ppm	* La	6 ppm
Co	10	Zr	6	* Ce	2
Ni	4	Nb	2	Pb	14.5
Rb	3	Ba	7	Th	9
Sr	3				

(* La and Ce were determined by XRF analysis for those rocks not subjected to INAA analysis.)

Accuracy is a function of concentration, and so any accuracy estimate must be accompanied by some approximate concentration level, at which the accuracy estimate is valid. The accuracy of the REE and Sc analyses are given below:-

La-	less than 3%	error on concentrations greater than 10 ppm.
Ce-	" 10%	" " 10 ppm.
Sm-	" 5%	" " 1 ppm.
Eu-	" 6%	" " .1 ppm.
** Tb-	" 10%	" " 0.4 ppm.
Lu-	" 5%	" " 0.2 ppm.
Yb-	" 10%	" " 0.5 ppm.
Sc-	" 3%	" " 10 ppm.

**-estimated error.

The accuracy of determination of the major elements is estimated below:-

SiO ₂	0.5%	MgO	0.5%
TiO ₂	0.05%	CaO	0.5%
Al ₂ O ₃	0.5%	Na ₂ O	0.5%
tFe ₂ O ₃	0.5%	K ₂ O	0.3%
MnO	0.05%	P ₂ O ₅	0.05%

In the following data tables the format consists of, in descending order, major elements, trace elements, REE's and Sc, selected CIPW normative minerals, N.P.C. and N.C.I. (see fig.3.1 , for explanation), and the QAP parameters (see fig.2.2 , Strekeisen modal classification diagram). The calculation of the CIPW norms and the N.P.C. and N.C.I. parameters, was carried out using a CIPW norm computer program integrated with the Glasgow Geochemical Unit's Data Retrieval System, which is available on the Glasgow University ICL 2976 mainframe computer. The Data Retrieval System was set up by Mr I.W.Ferguson. The calculation of the QAP parameters has already been described (Chapter 2).

The rock samples are grouped into the main rock types, and in each group they are ordered according to their SiO₂ content. All major element analyses have been recalculated on an anhydrous basis. The list of analyses is comprised of:-

Table A - Metabasites.

Table B Tonalitic orthogneisses.

Table C - Granodioritic and granitic orthogneisses.

Table D - Kf-bearing tonalitic orthogneisses and paragneisses.

Missing values are indicated by a dash (-), and these values have either not been analytically determined, or not calculated.

References.

HARVEY, P. K., TAYLOR, D. M., HENDRY, R. & BANCROFT, F. 1972. An accurate fusion method for the analysis of rocks and chemically related materials by X-ray fluorescence spectrometry.

X-ray Spectrometry. 2, 33-44.

LEAKE, B. E., HENDRY, G. L., KEMP, A., PLANT, A. G., HARVEY, P. K., WILSON, J. R., COATS, J. S., AUCOTT, J. W., LUNEL, T., & HOWARTH, R. J. 1969. The chemical analysis of rock powders by automatic X-ray fluorescence. Chem.Geol. 5, 7-86.

MOYES, A. B. & WHITLEY, J. E. 1977. Determination of Rare Earth elements in igneous rocks by neutron activation with group separation. SURRC Report No. 59.

TABLE. A

Metabasites.

	138	117	119	84	102	95	139	116
SiO2	41.75	44.71	46.45	47.48	49.81	49.92	49.93	49.94
TiO2	1.47	0.52	0.30	1.39	0.36	0.48	0.74	0.75
Al2O3	18.34	17.73	18.77	19.03	14.74	15.73	20.01	14.76
Fe2O3	10.91	4.91	3.68	6.33	3.00	2.74	2.07	3.49
FeO	7.18	8.46	7.03	6.81	7.20	6.64	5.69	7.11
MnO	0.20	0.20	0.22	0.18	0.19	0.18	0.14	0.19
MgO	6.04	8.07	8.70	4.94	12.04	11.39	6.95	9.07
CaO	11.70	13.56	11.64	10.19	10.20	10.42	11.67	11.51
Na2O	0.98	1.03	1.34	2.20	0.69	1.53	1.76	1.47
K2O	0.89	0.79	1.86	0.87	1.67	0.86	0.85	1.40
P2O3	0.53	0.02	0.01	0.57	0.06	0.06	0.18	0.26
TOTAL	100.00	100.00	100.00	100.00	100.00	100.00	100.00	100.00
tFeO	16.99	12.87	10.34	12.50	9.90	9.10	7.55	10.25
CR	39.00	53.00	62.00	67.00	190.00	175.00	102.00	257.00
NI	10.00	4.00	5.00	1.00	85.00	73.00	26.00	63.00
CO	56.00	35.00	32.00	-	45.00	43.00	33.00	56.00
RB	32.00	-	59.00	-	55.00	25.00	23.00	36.00
SR	479.00	158.00	131.00	-	448.00	184.00	522.00	212.00
Y	18.00	-	6.00	-	5.00	6.00	14.00	19.00
ZR	85.00	21.00	2.00	149.00	27.00	55.00	60.00	55.00
NB	5.00	4.00	5.00	10.00	5.00	9.00	9.00	9.00
BA	310.00	221.00	405.00	342.00	329.00	194.00	212.00	321.00
PB	12.00	-	21.00	24.00	14.00	21.00	14.00	86.00
TH	4.00	-	3.00	3.00	4.00	5.00	5.00	0.00
LA	17.57	15.00	11.55	43.56	7.15	7.54	17.04	9.00
CE	35.50	-	12.77	89.00	14.51	11.71	37.30	43.00
ND	13.70	-	2.23	-	-	3.29	23.00	-
SM	4.46	-	1.16	8.47	1.71	1.56	3.83	-
EU	1.48	-	0.41	1.63	0.42	0.50	1.03	-
TB	0.49	-	-	0.78	0.19	-	0.49	-
YB	1.41	-	0.80	1.18	0.80	0.99	1.16	-
LU	0.22	-	0.17	0.27	0.12	0.14	0.19	-
SC	42.70	-	79.00	30.10	30.50	38.64	33.95	-
AP	1.23	0.05	0.02	1.32	0.14	0.14	0.42	0.60
IL	2.79	0.99	0.57	2.64	0.68	0.91	1.41	1.42
OR	5.26	4.67	10.99	5.14	9.87	5.08	5.02	8.27
AB	8.29	8.71	11.21	18.61	5.84	12.94	14.89	12.44
AN	43.02	41.42	39.71	39.48	32.19	33.51	44.19	29.54
C	0.00	0.00	0.00	0.00	0.00	0.00	0.00	0.00
MT	15.82	7.12	5.34	9.18	4.35	3.97	3.00	5.06
HM	0.00	0.00	0.00	0.00	0.00	0.00	0.00	0.00
DIWO	4.83	10.74	7.50	3.07	7.52	7.43	5.23	10.80
DIEN	3.84	6.62	4.88	2.03	5.17	5.16	3.40	7.17
DIFS	0.44	3.50	2.11	0.82	1.75	1.66	1.48	2.84
HYEN	11.21	2.47	0.00	10.28	22.27	18.57	13.91	15.41
HYFS	1.30	1.31	0.00	4.16	7.54	5.58	6.04	6.10
Q	1.77	0.00	0.00	3.08	0.00	0.00	0.86	0.10
QLFO	0.00	7.71	11.76	0.00	1.78	3.25	0.00	0.00
QLFA	0.00	4.49	5.61	0.00	0.67	1.15	0.00	0.00
NE	0.00	0.00	0.07	0.00	0.00	0.00	0.00	0.00
N.P.C	83.84	82.63	77.91	67.96	84.64	72.14	74.79	70.37
N.C.I	40.22	44.94	37.76	32.18	51.72	48.07	34.46	48.79
KF%	-	-	-	0.00	0.00	0.00	0.00	0.00
Q%	-	-	-	0.00	0.00	0.00	0.00	0.00
PLAG%	-	-	-	100.00	100.00	100.00	100.00	100.00

TABLE A

Metabasites. (Cont.)

	85	408	96	94	93	123
SI02	50.11	51.17	51.33	51.67	54.36	53.44
TI02	1.03	0.28	0.48	0.63	0.81	0.81
AL203	17.30	7.74	11.68	15.89	16.43	14.49
FE203	5.62	2.29	1.86	3.20	5.28	3.04
FEO	6.17	5.95	7.48	6.02	5.75	5.22
MNO	0.19	0.19	0.19	0.18	0.23	0.17
MGO	6.08	19.03	13.03	9.39	4.94	8.20
CAO	10.60	12.24	10.62	9.97	7.58	7.58
NA2O	1.78	0.42	1.38	2.03	2.82	5.02
K2O	0.95	0.25	1.71	1.08	1.62	1.61
P2O3	0.16	0.03	0.11	0.14	0.17	0.37
TOTAL	100.00	100.00	100.00	100.00	100.00	100.00
tFEO	11.22	8.01	9.15	8.90	10.50	7.95
CR	58.00	2540.00	723.00	88.00	46.00	241.00
NI	20.00	334.00	164.00	69.00	1.00	60.00
CO	39.00	57.00	42.00	44.00	31.00	32.00
RB	32.00	13.00	65.00	28.00	54.00	28.00
SR	588.00	55.00	249.00	195.00	357.00	570.00
Y	12.00	1.00	9.00	40.00	89.00	16.00
ZR	105.00	35.00	64.00	53.00	97.00	107.00
NB	8.00	8.00	7.00	10.00	15.00	10.00
BA	373.00	117.00	468.00	219.00	384.00	486.00
PB	20.00	0.00	44.00	20.00	24.00	67.00
TH	7.00	0.00	4.00	1.00	9.00	7.00
LA	24.29	3.94	15.10	14.12	23.00	32.00
CE	48.00	12.10	23.29	44.20	77.00	64.00
ND	-	-	-	23.60	-	-
SM	5.02	1.51	3.71	4.85	-	-
EU	1.17	0.49	0.63	0.82	-	-
TB	0.43	0.27	0.54	0.57	-	-
YB	1.69	0.65	1.47	3.33	-	-
LU	0.24	0.16	0.22	0.52	-	-
SC	25.51	71.06	37.66	51.12	-	-
AP	0.37	0.07	0.26	0.33	0.40	0.86
IL	1.96	0.53	0.91	1.20	1.54	1.54
OR	5.61	1.48	10.11	6.38	9.57	9.51
AB	15.06	3.55	11.67	17.17	23.86	37.97
AN	35.41	18.50	20.63	31.06	27.39	12.25
C	0.00	0.00	0.00	0.00	0.00	0.00
MT	8.15	3.32	2.70	4.64	7.66	4.41
HM	0.00	0.00	0.00	0.00	0.00	0.00
DIWO	6.32	17.55	13.09	6.85	3.80	9.58
DIEN	4.37	13.33	8.92	4.77	2.53	6.82
DIFS	1.44	2.41	3.14	1.50	1.00	1.92
HYEN	10.77	29.47	14.20	18.61	9.78	0.00
HYFS	3.55	5.33	4.99	5.87	3.86	0.00
Q	5.79	0.00	0.00	1.42	8.38	0.00
OLFO	0.00	3.22	6.53	0.00	0.00	9.53
QLFA	0.00	0.64	2.53	0.00	0.00	2.95
NE	0.00	0.00	0.00	0.00	0.00	2.44
N.P.C	70.74	83.90	63.87	64.39	53.44	23.63
N.C.I	36.56	75.79	57.00	43.43	30.17	36.75
KF%	0.00	-	-	0.00	0.00	-
Q%	0.00	-	-	0.00	6.17	-
PLAG%	100.00	-	-	100.00	93.83	-

TABLE. 8

Tonalitic orthogneisses.

	97	137	136	113	107	106	124	406
SI02	52.98	54.59	53.83	54.95	55.22	55.38	56.24	56.84
TI02	1.35	1.09	1.11	1.20	1.02	1.05	0.67	1.17
AL203	15.23	20.91	18.99	15.54	19.60	18.95	17.08	15.60
FE203	6.96	1.63	3.94	7.04	3.93	4.27	3.97	5.75
FEO	7.07	5.47	5.31	6.17	4.12	4.21	5.16	5.13
MNO	0.17	0.10	0.12	0.22	0.13	0.12	0.21	0.20
MGO	4.58	2.92	3.44	4.45	3.24	3.36	4.05	4.06
CAO	6.96	7.88	8.41	6.70	7.20	7.55	7.31	7.24
NA2O	2.00	2.29	2.92	2.04	3.05	2.79	3.07	2.18
K2O	2.58	2.72	1.54	1.41	2.12	1.92	2.01	1.56
P2O3	0.38	0.40	0.39	0.27	0.37	0.39	0.22	0.26
TOTAL	100.00	100.00	100.00	100.00	100.00	100.00	100.00	100.00
tFEO	13.09	6.94	8.85	12.50	7.65	8.05	8.73	10.30
CR	99.00	28.00	30.00	59.00	31.00	35.00	61.00	47.00
NI	10.00	3.00	1.00	2.00	0.00	1.00	10.00	0.00
CO	31.00	27.00	25.00	23.00	14.00	17.00	21.00	14.00
RB	81.00	81.00	39.00	49.00	60.00	61.00	-	47.00
SR	415.00	744.00	822.00	537.00	702.00	661.00	801.00	292.00
Y	33.00	24.00	30.00	14.00	34.00	35.00	-	29.00
ZR	357.00	390.00	316.00	288.00	386.00	352.00	-	287.00
NB	13.00	8.00	9.00	8.00	9.00	11.00	-	15.00
BA	957.00	1361.00	-	489.00	1027.00	938.00	849.00	487.00
PB	22.00	13.00	-	19.00	41.00	16.00	-	8.00
TH	7.00	7.00	-	4.00	5.00	8.00	-	8.00
LA	46.20	37.90	39.61	40.00	53.60	44.50	36.14	32.16
CE	99.70	83.50	95.70	79.00	144.00	82.60	103.00	77.34
ND	-	50.60	52.50	-	54.40	38.50	74.50	-
SM	9.92	8.73	10.18	5.43	10.50	10.50	15.50	9.02
EU	1.55	2.42	2.64	1.34	2.52	2.10	2.74	1.87
TB	0.93	0.85	1.31	0.35	1.31	1.31	3.70	1.01
YB	2.58	2.74	3.27	1.64	2.27	2.61	7.89	3.46
LU	0.42	0.28	0.26	0.25	0.47	0.55	1.28	0.65
SC	32.63	25.52	28.11	18.32	38.20	26.33	58.44	54.52
AP	0.88	0.93	0.91	0.63	0.86	0.91	0.51	0.60
IL	2.56	2.07	2.11	2.28	1.94	1.99	1.27	2.22
OR	15.25	16.07	9.10	8.33	12.53	11.35	11.88	9.22
AB	16.92	19.37	24.70	17.26	25.80	23.60	25.97	18.44
AN	24.96	36.48	34.16	29.08	33.30	33.51	26.89	28.17
C	0.00	0.83	0.00	0.00	0.08	0.00	0.00	0.00
MT	9.70	2.36	5.71	10.21	5.70	6.19	5.76	8.34
HM	0.00	0.00	0.00	0.00	0.00	0.00	0.00	0.00
DIWD	2.96	0.00	2.09	1.00	0.00	0.58	3.32	2.52
DIEN	1.90	0.00	1.28	0.70	0.00	0.41	2.07	1.81
DIFS	0.87	0.00	0.70	0.22	0.00	0.12	1.04	0.49
HYEN	9.51	7.27	7.29	10.39	8.07	7.96	8.02	8.30
HYFS	4.36	6.90	3.97	3.31	2.63	2.35	4.04	2.25
Q	9.95	7.61	7.86	16.37	8.95	10.89	9.01	17.41
OLFO	0.00	0.00	0.00	0.00	0.00	0.00	0.00	0.00
OLFA	0.00	0.00	0.00	0.00	0.00	0.00	0.00	0.00
NE	0.00	0.00	0.00	0.00	0.00	0.00	0.00	0.00
N.P.C	55.59	65.31	58.03	62.75	56.34	58.68	50.87	60.44
N.C.I	31.86	18.59	23.15	28.10	18.34	19.59	25.52	25.92
KF%	0.00	0.00	0.00	0.00	0.00	0.00	0.00	0.00
Q%	2.36	5.32	3.66	9.98	4.16	7.25	10.56	18.65
PLAG%	97.64	94.67	96.34	90.02	95.84	92.75	89.43	81.35

TABLE. B

Tonalitic orthogneisses. (Cont.)

	105	91	1	405	403	404	402
SI02	57.55	59.40	60.07	61.14	70.50	70.50	70.51
TI02	0.83	0.85	0.98	0.95	0.55	0.56	0.51
AL203	18.00	16.24	17.38	15.71	14.42	13.98	14.55
FE203	2.83	3.50	4.96	4.40	2.33	2.08	2.37
FEO	5.07	4.91	5.10	4.50	2.09	2.47	2.17
MNO	0.13	0.15	0.09	0.14	0.08	0.11	0.10
MGO	3.70	3.80	2.71	3.74	1.70	1.60	1.68
CAO	6.29	6.19	4.30	5.57	4.42	3.90	3.65
NA2O	2.90	2.12	2.68	2.49	3.09	2.78	3.42
K2O	2.28	2.63	1.66	1.14	0.71	1.90	0.94
P2O3	0.41	0.20	0.06	0.21	0.11	0.12	0.10
TOTAL	100.00	100.00	100.00	100.00	100.00	100.00	100.00
tFED	7.61	8.06	9.56	8.46	4.19	4.34	4.30
CR	81.00	63.00	59.00	71.00	21.00	17.00	19.00
NI	3.00	1.00	16.00	3.00	0.00	0.00	1.00
CO	17.00	20.00	25.00	16.00	5.00	7.00	12.00
RB	75.00	90.00	53.00	33.00	22.00	30.00	29.00
SR	753.00	299.00	345.00	307.00	302.00	250.00	426.00
Y	22.00	17.00	0.00	19.00	1.00	14.00	1.00
ZR	226.00	207.00	138.00	210.00	260.00	249.00	236.00
NB	10.00	8.00	12.00	14.00	10.00	12.00	10.00
BA	721.00	735.00	627.00	587.00	492.00	643.00	414.00
PB	26.00	34.00	16.00	7.00	0.00	11.00	4.00
TH	11.00	0.00	5.00	0.00	7.00	2.00	1.00
LA	55.90	17.00	21.30	20.53	74.10	25.62	13.73
CE	98.70	51.00	40.70	49.21	126.50	47.35	23.07
ND	37.00	-	11.30	-	-	-	-
SM	8.67	-	2.71	5.81	4.00	4.23	1.16
EU	1.79	-	1.67	1.29	1.33	1.13	0.76
TB	1.20	-	-	0.78	0.38	0.65	0.23
YB	1.95	-	0.13	2.10	0.90	1.43	0.74
LU	0.36	-	0.04	0.39	0.13	0.27	0.14
SC	20.77	-	24.80	38.24	14.47	16.35	9.15
AP	0.95	0.46	0.14	0.49	0.26	0.28	0.23
IL	1.58	1.61	1.86	1.80	1.04	1.06	0.97
OR	13.47	15.54	9.81	6.74	4.20	11.23	5.56
AB	24.53	17.93	22.67	21.06	26.14	23.52	28.93
AN	28.53	27.03	20.94	26.26	21.21	18.56	17.45
C	0.31	0.00	3.50	0.76	0.80	0.55	1.51
MT	4.10	5.07	7.19	6.38	3.38	3.02	3.44
HM	0.00	0.00	0.00	0.00	0.00	0.00	0.00
DIWO	0.00	0.99	0.00	0.00	0.00	0.00	0.00
DIEN	0.00	0.62	0.00	0.00	0.00	0.00	0.00
DIFS	0.00	0.31	0.00	0.00	0.00	0.00	0.00
HYEN	9.21	8.84	6.75	9.31	4.23	3.98	4.18
HYFS	5.60	4.41	3.65	3.06	1.00	1.89	1.18
Q	11.57	17.00	23.38	23.98	37.66	35.79	36.43
OLFO	0.00	0.00	0.00	0.00	0.00	0.00	0.00
OLFA	0.00	0.00	0.00	0.00	0.00	0.00	0.00
NE	0.00	0.00	0.00	0.00	0.00	0.00	0.00
N.P.C	53.76	60.12	48.02	55.49	44.79	44.10	37.62
N.C.I	20.49	21.85	19.45	20.55	9.65	9.95	9.77
KF%	0.00	0.00	0.00	0.00	0.00	0.00	0.00
Q%	11.31	22.44		24.98	44.93	47.59	45.78
PLAG%	88.69	77.56		75.02	55.04	52.41	54.12

TABLE. C

Granodioritic and Granitic orthogneisses.

	99	98	135	121	125	112	120	104
SiO2	70.33	73.15	73.43	73.60	75.64	75.98	76.01	76.07
TiO2	0.42	0.26	0.19	0.36	0.10	0.20	0.16	0.24
Al2O3	14.31	13.70	13.35	14.26	12.39	13.14	12.82	12.82
Fe2O3	1.48	2.28	0.74	1.74	0.48	0.86	1.12	1.21
FeO	2.03	0.52	0.95	1.51	0.33	0.68	0.54	0.89
MnO	0.06	0.02	0.04	0.05	0.03	0.03	0.02	0.06
MgO	1.46	0.74	0.59	0.72	0.29	0.44	0.52	0.63
CaO	3.27	2.49	1.52	1.02	1.92	2.80	1.00	2.97
Na2O	3.02	2.61	2.32	3.24	2.73	3.34	3.26	3.87
K2O	3.45	4.09	4.47	3.41	6.04	2.27	4.52	1.16
P2O3	0.17	0.12	0.06	0.09	0.05	0.06	0.03	0.08
TOTAL	100.00	100.00	100.00	100.00	100.00	100.00	100.00	100.00
tFeO	3.36	2.57	1.62	3.07	0.76	1.65	1.55	1.98
CR	34.00	20.00	-	16.00	8.00	33.00	20.00	10.00
NI	0.00	1.00	-	0.00	1.00	0.00	0.00	1.00
CO	11.00	2.00	-	3.00	1.00	3.00	5.00	1.00
RB	72.00	97.00	-	78.00	-	50.00	76.00	30.00
SR	612.00	550.00	-	413.00	233.00	308.00	351.00	371.00
Y	19.00	3.00	-	4.00	-	0.00	0.00	1.00
ZR	157.00	119.00	-	133.00	-	136.00	43.00	207.00
NB	9.00	10.00	-	6.00	-	5.00	3.00	7.00
BA	1184.00	1079.00	-	1698.00	1256.00	816.00	1853.00	-
PB	25.00	14.00	-	14.00	-	43.00	42.00	-
TH	12.00	12.00	-	3.00	-	9.00	2.00	-
LA	62.20	72.50	12.01	18.68	6.18	52.60	8.19	50.24
CE	110.00	119.00	8.26	30.93	8.40	96.40	14.34	90.70
ND	-	-	1.15	12.12	3.88	32.30	1.25	-
SM	8.31	5.48	1.44	2.27	0.67	3.66	0.72	4.02
EU	1.67	1.20	1.44	1.66	0.80	1.76	1.00	1.28
TB	0.74	0.49	-	0.58	0.06	0.21	0.05	0.25
YB	1.56	0.69	0.14	0.50	0.22	0.49	0.27	0.42
LU	-	0.09	0.04	0.11	0.03	0.08	0.06	0.07
SC	10.55	4.63	3.07	2.81	0.99	4.66	1.53	3.54
AP	0.40	0.28	0.14	0.21	0.12	0.14	0.07	0.19
IL	0.80	0.53	0.36	0.68	0.19	0.38	0.30	0.46
OR	20.39	24.17	26.42	20.15	35.69	13.42	26.71	32.74
AB	25.55	22.08	19.63	27.41	23.09	28.25	27.58	32.74
AN	15.11	11.57	7.15	4.47	3.72	13.50	4.77	14.18
C	0.07	0.74	2.08	3.60	0.00	0.24	0.82	0.00
MT	2.15	0.86	1.07	2.52	0.70	1.25	1.28	1.75
HM	0.00	1.68	0.00	0.00	0.00	0.00	0.24	0.00
DIWO	0.00	0.00	0.00	0.00	0.87	0.00	0.00	0.01
DIEN	0.00	0.00	0.00	0.00	0.72	0.00	0.00	0.01
DIFS	0.00	0.00	0.00	0.00	0.04	0.00	0.00	0.00
HYEN	3.64	1.84	1.47	1.79	0.00	1.10	1.29	1.56
HYFS	1.81	0.00	0.82	0.74	0.00	0.58	0.00	0.24
Q	30.03	36.21	38.49	38.36	33.40	41.11	36.91	41.94
OLFO	0.00	0.00	0.00	0.00	0.00	0.00	0.00	0.00
OLFA	0.00	0.00	0.00	0.00	0.00	0.00	0.00	0.00
NE	0.00	0.00	0.00	0.00	0.00	0.00	0.00	0.00
N.P.C	37.16	34.38	26.69	14.02	13.88	32.34	14.74	30.22
N.C.I	8.40	4.91	3.72	5.73	2.52	3.31	3.11	4.03
KF%	14.96	21.72	27.72	18.71	35.39	10.68	26.89	2.10
Q%	40.54	42.30	41.94	43.56	40.40	47.98	44.41	48.99
PLAG%	44.50	35.97	30.32	36.56	24.03	41.33	28.66	43.77

TABLE C

Granodioritic and Granitic orthogneisses (Cont.), and Aplites.

	400	108	401	122	413	411
SI02	76.79	77.90	78.19	78.42	73.99	75.78
TI02	0.23	0.09	0.19	0.10	0.07	0.03
AL203	12.56	13.08	12.71	11.91	13.15	14.12
FE203	1.10	0.54	0.65	0.66	0.82	0.69
FEO	0.67	0.44	0.68	0.35	0.31	0.24
MNO	0.04	0.07	0.04	0.01	0.02	0.01
MGO	0.40	0.34	0.44	0.53	0.27	0.20
CAO	1.07	1.50	0.52	0.83	1.41	0.27
NA2O	3.06	4.26	3.48	4.69	1.39	4.03
K2O	4.05	1.74	3.07	2.48	8.54	4.60
P2O3	0.03	0.04	0.03	0.02	0.03	0.03
TOTAL	100.00	100.00	100.00	100.00	100.00	100.00
tFEO	1.66	0.93	1.26	0.94	1.05	0.86
CR	17.00	12.00	7.00	19.00	24.00	16.00
NI	0.00	0.00	0.00	2.00	0.00	0.00
CO	0.00	0.00	3.00	0.00	0.00	0.00
RB	66.00	-	47.00	44.00	164.00	-
SR	281.00	-	340.00	273.00	476.00	218.00
Y	1.00	-	0.00	0.00	0.00	-
ZR	185.00	62.00	132.00	-	56.00	62.00
NB	13.00	7.00	7.00	0.00	8.00	9.00
BA	1824.00	181.00	1883.00	4875.00	1918.00	600.00
PB	15.00	-	14.00	25.00	31.00	-
TH	7.00	-	12.00	2.00	5.00	-
LA	44.52	103.00	41.35	-	4.62	-
CE	87.10	185.00	74.70	33.00	6.47	-
ND	-	-	-	-	-	-
SM	4.78	4.75	3.30	-	0.34	-
EU	1.74	0.88	1.56	-	0.68	-
TB	0.19	0.22	0.09	-	0.02	-
YB	0.81	0.28	0.40	-	0.15	-
LU	0.09	0.06	0.08	-	0.03	-
SC	6.33	1.19	5.87	-	0.72	-
AP	0.07	0.09	0.07	0.05	0.07	0.07
IL	0.44	0.17	0.36	0.19	0.13	0.06
OR	23.93	10.28	18.14	14.66	50.47	27.18
AB	25.89	36.04	29.44	39.68	11.76	34.09
AN	5.11	7.18	2.38	3.99	4.42	1.14
C	1.27	1.56	2.79	0.05	0.00	2.09
MT	1.49	0.78	0.94	0.64	0.80	0.69
HM	0.07	0.00	0.00	0.08	0.27	0.22
DIWO	0.00	0.00	0.00	0.00	0.78	0.00
DIEN	0.00	0.00	0.00	0.00	0.67	0.00
DIFS	0.00	0.00	0.00	0.00	0.00	0.00
HYEN	1.00	0.85	1.10	1.32	0.00	0.50
HYFS	0.00	0.21	0.40	0.00	0.00	0.00
Q	40.68	42.75	44.33	39.13	30.39	33.94
OLFO	0.00	0.00	0.00	0.00	0.00	0.00
OLFA	0.00	0.00	0.00	0.00	0.00	0.00
NE	0.00	0.00	0.00	0.00	0.00	0.00
N.P.C	16.48	16.61	7.48	9.14	27.32	3.24
N.C.I	3.00	2.01	2.80	2.43	2.65	1.47
KF%	23.87	10.12	19.30	14.04	-	30.78
Q%	46.96	49.59	49.13	51.35	-	29.02
PLAG%	29.12	40.29	31.48	34.60	-	40.19

TABLE. D

Kf-bearing Tonalitic orthogneisses, and Paragneisses (3 mobilisate, 1 melanosome).

	133	412	410	109	11E	407	409
SI02	58.02	59.11	61.86	75.99	79.96	84.41	47.39
TI02	1.06	0.93	0.84	0.31	0.34	0.44	1.17
AL203	17.07	17.21	16.65	12.53	9.09	7.40	26.96
FE203	3.22	3.61	2.92	1.49	1.94	0.71	7.05
FEO	5.29	4.51	4.85	0.99	1.52	1.94	6.52
MNO	0.18	0.14	0.15	0.04	0.07	0.04	0.13
MGO	3.77	3.04	3.31	0.90	1.09	0.89	2.76
CAO	5.75	4.99	4.87	2.42	3.81	0.74	1.44
NA2O	3.13	2.89	2.27	3.14	1.50	1.52	2.10
K2O	2.12	3.21	1.99	1.99	0.57	1.83	4.34
P2O3	0.38	0.36	0.28	0.09	0.10	0.07	0.11
TOTAL	100.00	100.00	100.00	100.00	100.00	100.00	100.00
tFED	8.19	7.76	7.48	2.33	3.26	2.58	12.87
CR	41.00	27.00	50.00	58.00	72.00	57.00	132.00
NI	1.00	0.00	2.00	0.00	0.00	10.00	48.00
CO	26.00	17.00	11.00	10.00	14.00	7.00	31.00
RB	59.00	-	-	68.00	19.00	30.00	83.00
SR	431.00	397.00	388.00	312.00	161.00	120.00	339.00
Y	24.00	-	-	1.00	0.00	14.00	30.00
ZR	341.00	276.00	256.00	208.00	177.00	264.00	301.00
NB	10.00	14.00	15.00	4.00	5.00	13.00	17.00
BA	572.00	596.00	1010.00	1538.00	370.00	470.00	1728.00
PB	10.00	-	-	21.00	50.00	11.00	10.00
TH	4.00	-	-	4.00	2.00	2.00	23.00
LA	35.50	34.96	16.11	17.00	13.75	21.57	122.90
CE	76.40	76.29	49.26	30.00	20.20	43.54	229.07
ND	43.50	-	-	-	-	-	-
SM	8.73	6.61	9.91	-	-	3.51	20.92
EU	1.97	1.71	2.29	-	-	1.00	3.92
TB	0.99	0.70	1.28	-	-	0.61	1.88
YB	2.20	1.85	3.73	-	-	1.97	2.55
LU	0.36	0.35	0.55	-	-	0.34	0.43
SC	31.23	18.44	38.03	-	-	5.95	17.38
AP	0.88	0.84	0.65	0.21	0.23	0.16	0.26
IL	2.01	1.77	1.60	0.59	0.65	0.84	2.22
OR	12.53	18.97	11.76	11.76	3.37	10.61	25.65
AB	26.48	24.45	19.20	26.56	12.69	12.86	17.76
AN	25.04	22.40	22.33	11.42	16.39	3.21	6.43
C	0.08	0.77	2.58	1.13	0.00	1.74	16.45
MT	4.67	5.23	4.23	2.16	2.81	1.03	10.24
HM	0.00	0.00	0.00	0.00	0.00	0.00	0.00
DIWO	0.00	0.00	0.00	0.00	0.78	0.00	0.00
DIEN	0.00	0.00	0.00	0.00	0.57	0.00	0.00
DIFS	0.00	0.00	0.00	0.00	0.13	0.00	0.00
HYEN	9.39	7.57	8.24	2.24	2.14	2.22	6.87
HYFS	5.30	3.75	5.11	0.08	0.50	2.25	4.21
Q	12.41	14.09	24.13	43.80	59.66	64.82	9.76
OLFO	0.00	0.00	0.00	0.00	0.00	0.00	0.00
OLFA	0.00	0.00	0.00	0.00	0.00	0.00	0.00
NE	0.00	0.00	0.00	0.00	0.00	0.00	0.00
N.P.C	49.58	47.81	53.76	30.07	56.36	19.97	26.56
N.C.I	21.37	18.33	19.18	5.07	7.58	6.34	23.54
KF%	19.75	29.10	16.59	0.00	2.67	13.58	-
Q%	12.74	6.56	19.05	54.64	66.32	55.94	-
PLAG%	67.50	64.33	61.96	45.35	31.01	20.48	-

Appendix 2.

Mineral Analyses.

This appendix lists the analyses of 60 mineral grains from rocks listed in Appendix 1. The analysis was carried out in the Geochemistry Unit of the Geology Dept., Glasgow University, using a Cambridge Instruments Microscan 5 X-Ray microanalyser (microprobe) fitted with a Link Systems Energy Dispersive Analyser.

The analysis procedure has the following specifications:-
Analysis method: Energy Dispersive System (EDS).

Operating conditions:

Accelerating potential = 20 kV.

Probe current = 3×10^{-9} amps.

Count time = 50-200 secs (automatically corrected for dead time).

Processing: Peak areas of the elements of interests are obtained from each spectrum using an iterative stripping technique (Statham, 1976), with a reference Cobalt spectrum. Elemental concentrations are then obtained by calibrating against pure metal or simple mineral standards, followed by a full atomic number, absorption and fluorescence correction (ZAF) as described by Sweatman and Long (1969).

Detection limits:

CaO and K₂O 0.03%

All other oxides 0.02%

The list of analyses is comprised of:-

Table E - Amphiboles

Table F - Pyroxenes, micas, and K-feldspars

Table G - Plagioclases

Table H - Ore components.

The analysis identifier (eg. BK407-3) gives the rock no., and the no. of the analysis selected from the sequence of analyses made on the phase, in the specified rock. Analyses are recalculated to 100%.

References.

STATHAM, P. J. 1976. A comparative study of techniques for Quantitative analysis of the X-Ray spectra obtained with a Si(Li) detector. X-Ray Spectrometry. 5, 16-28.

SWEATMAN, T. R. & LONG. J. V. 1969. Quantitative electron-probe microanalysis of rock forming minerals. J.Petrol. 10, 332-79.

TABLE. E

Amphibole analyses.

	HBE.516	HBE.517	HBE.518	HBE.520	HBE.521	HBE.522	HBE.523	HBE.524	HBE.525
	BK134-1	BK134-2	BK134-3	BK134-5	BK134-6	BK134-7	BK134-8	BK134-9	BK134-10
SI02	44.16	44.01	43.97	43.87	43.11	42.86	44.19	43.55	44.17
TI02	1.50	1.53	2.01	1.71	1.28	1.43	1.85	1.82	1.87
AL203	10.31	10.20	10.25	10.28	10.99	11.58	10.56	10.47	10.38
TFE0	18.50	18.44	18.07	18.25	19.61	19.99	18.13	18.49	18.22
MNO	0.43	0.39	0.52	0.31	0.45	0.31	0.30	0.50	0.50
MGO	10.28	10.66	10.49	10.66	9.82	9.05	10.23	10.38	10.45
CAO	11.99	12.03	12.03	12.22	12.08	12.31	12.06	12.22	12.13
NA2O	1.63	1.49	1.36	1.36	1.39	0.97	1.29	1.25	0.89
K2O	1.19	1.24	1.30	1.33	1.26	1.51	1.40	1.31	1.39
TOTAL	100.00	100.00	100.00	100.00	100.00	100.00	100.00	100.00	100.00
MG FE	RATIO	0.56	0.58	0.58	0.50	0.45	0.56	0.56	0.57

TABLE. E Amphibole analyses. (Cont.)

	HBE.526	HBE.527	HBE.528	HBE.529	HBE.530	HBE.531	HBE.532	HBE.533	HBE.534
	BK134-11	BK406-1	BK406-2	BK406-3	BK406-4	BK414-1	BK414-2	BK414-3	BK410-1
SiO2	44.00	46.89	45.63	45.64	45.53	42.22	43.67	42.97	46.02
TiO2	1.57	1.39	1.61	1.44	1.48	1.90	1.70	1.91	1.64
Al2O3	10.31	9.51	9.49	9.49	10.12	11.18	10.19	10.76	10.11
TFE0	18.41	15.82	16.67	16.00	16.19	19.42	20.00	19.01	10.11
MNO	0.45	0.61	0.49	0.59	0.55	0.56	0.46	0.58	0.50
MGO	10.30	11.92	12.35	11.90	12.17	9.38	9.21	9.53	12.28
CAO	12.46	11.71	11.78	11.39	11.66	12.22	12.54	12.00	11.75
NA2O	1.14	1.33	1.07	2.10	1.45	1.29	0.72	1.59	0.89
K2O	1.36	0.83	0.90	1.44	0.85	1.83	1.50	1.65	0.88
TOTAL	100.00	100.00	100.00	100.00	100.00	100.00	100.00	100.00	100.00
MG FE	RATIO	0.75	0.74	0.74	0.75	0.48	0.46	0.50	0.77

TABLE. E Amphibole analyses. (Cont.)

	HBE.548	HBE.549	ACT.519	ACT.541	ACT.542	ACT.543	ACT.546	HBE.500	HBE.501
	BK124-4	BK124-5	BK134-4	BK119-1	BK119-2	BK119-3	BK124-1	A	B
SiO2	42.37	42.80	42.94	47.53	47.19	47.23	49.60	38.93	51.35
TiO2	1.34	1.17	1.62	0.48	0.74	0.39	0.32	1.97	1.00
Al2O3	11.52	11.53	11.56	9.76	9.35	9.74	6.49	13.30	8.55
TFE0	19.21	19.42	18.82	15.81	15.39	15.78	18.02	22.79	10.39
MNO	0.77	0.63	0.39	0.21	0.51	0.68	1.02	0.46	0.48
MGO	9.67	9.40	9.99	12.69	13.39	12.75	11.69	6.15	15.58
CAO	12.35	12.17	11.96	12.13	11.58	11.81	11.91	12.62	11.08
NA2O	1.18	1.20	1.23	0.81	1.25	0.92	0.95	1.33	1.36
K2O	1.59	1.69	1.48	0.59	0.63	0.69	0.00	2.44	0.20
TOTAL	100.00	100.00	100.00	100.00	100.00	100.00	100.00	100.00	100.00
MG FE	RATIO	0.50	0.48	0.53	0.77	0.81	0.65	0.27	1.49

TABLE. G. Plagioclase analyses.

	BYT'ITE.	BYT'ITE.	LAB'ITE.	AND'INE.	AND'INE.	OLIG'SE.	AND'INE.	AND'INE.	OLIG'SE.
	BK102-2	BK138-1	BK406-1	BK403-1	BK121-3	BK407-3	BK409-2	BK409-3	BK409-4
SI02	45.66	46.70	53.67	57.32	58.36	61.53	56.78	58.85	63.21
TI02	0.00	0.00	0.22	0.00	0.00	0.00	0.00	0.00	0.00
AL203	34.47	33.85	29.56	27.28	26.16	23.86	27.32	25.66	23.52
TFE0	0.21	0.65	0.00	0.20	0.25	0.00	0.00	0.20	0.00
MNO	0.00	0.00	0.00	0.00	0.00	0.00	0.00	0.00	0.00
MGO	0.00	0.00	0.00	0.00	0.00	0.00	0.00	0.00	0.00
CA0	18.02	16.92	11.83	9.24	8.07	5.59	9.06	7.51	4.31
NA20	1.54	1.88	4.71	5.91	6.63	8.72	6.75	7.61	8.95
K20	0.00	0.00	0.00	0.00	0.25	0.30	0.10	0.15	0.00
TOTAL	100.00	100.00	100.00	100.00	100.00	100.00	100.00	100.00	100.00
AN%	86.60	83.26	58.12	46.30	40.20	26.16	42.60	35.30	21.00

Appendix 3.

Details of Computing Used in This Study.

The following computer programs and subprograms were used in this study (* - denotes that the routine was written by myself);

Subroutine PLOT (*) - Plots data for two components on to a two axis linear plot.

Subroutine LOG2PLT (*) - Plots data for two components on to a two axis logarithmic plot.

Program REEPLT (*) - Using chondrite-normalised data, REEPLT draws REE* patterns on to a log/lin plot.

Program TRIPLET (*) - Plots data for three components on to a triangular plot.

Program PLOTVECTORS (*) - Using K_D data, PLOTVECTORS calculates and draws Rayleigh or equilibrium fractional crystallisation vectors on to a two axis logarithmic plot.

Program NEWFRAC (*, in part) - Trace element modelling program, used extensively in Chapter 5. The program tests a fractional crystallisation hypothesis on a parental and a differentiate magma pair.

Program CIPW7 - Calculates an analysis in terms of normative minerals.

Program GPP3 - Generalised projections program: this program has been used in this thesis to generate the CMAS projections. (The program was incorporated into the Glasgow Geochemistry Unit's computer library by Dr. M. R. Giles).

Programs CIPW7 and GPP3, along with a number of data manipulation and calculation programs, are now integrated in the Geochemistry Unit's Data Retrieval System which has been set up by Mr I. W. Fergusson. The plotting routines PLOT, LOG2PLT and REEPLT have also been incorporated into the System, for general use. All plotting routines make use of the GHOST GRAPHICAL OUTPUT SYSTEM (Calderbank and Prior, 1978). All of the programs listed above are written in FORTRAN 4 computer language.

The program NEWFRAC calls on 13 subroutines:-

INPT (*) INTERACT (*) MAIN (*) PRINTMT (*) HISTO (*)
MATINV SING VPSYM1 VVPSYM XFY XFYØ XFY1 XFY2

Those subroutines not marked with (*) were kindly supplied by

Dr. F. Albarede. These eight routines contain the algorithm for least-square fitting of over-determined linear systems (Albarede and Provost, 1977). However, because they were originally written for an IBM computer, these subroutines were incompatible with the Glasgow University ICL 2976 mainframe computer. Mr. D. A. Fildes of the university computer advisory service converted the language structure to one that was compatible with the FORTRANF1 compiler. The program involved approximately 4 months additional work by myself before it became fully operational.

References.

CALDERBANK, V. J. & PRIOR, W. A. J. 1978. The Ghost Graphical Output System. User Manual; Part 1: The User Image. H.M. Stationary. (GLM-R177(Part 1)).

ALBAREDE, F. & PROVOST, A. 1977. Petrological and geochemical mass-balance equations: an algorithm for least-square fitting and general error analysis. Comput. Geosci. 3, 309-326.

Appendix 4.

List of Sample Localities.

1. Samples from the Cashel District.

- BK1 - 135 ft. east of the Gowla road, along a bearing of 120° from the eastern tip of Red Island, south of Cashel.
- BK84 - 110 ft. along a bearing of 315° from the summit of Cashel Hill.
- BK85 - 440 ft. along a bearing of 335° from the summit of Cashel Hill.
- BK91 - roadside exposure, at crossroad to the north-east of lough Alurgan.
- BK93 - 210 ft. along a bearing of 200° from the southern tip of lough Alurgan.
- BK94, BK95 - 2000 ft. along a bearing of 330° from the small island in the north-western corner of Loughaunillaun.
- BK96 - 580 ft. along a bearing of 294° from the north-western corner of Loughaunanny.
- BK97 - 325 ft. due west of the north-western corner of Loughaunanny.
- BK98 - 920 ft. along a bearing of 082° from the northern-most tip of Lough Nambrakmore.
- BK99 - 720 ft. along a bearing of 075° from the southern-most tip of Lough Nambrakmore.
- BK102 - summit of hill (264 ft.) midway between Loughs Achuss and Minnaun.
- BK104 - 150 ft. along a bearing of 265° from the southern-most tip of Lough Minnaun.
- BK105 - 1110 ft. along a bearing of 294° from the north-western corner of Loughaunanny.
- BK106 - 920 ft. along a bearing of 075° from the southern-most tip of Lough Nambrakkeagh.
- BK107 - 1540 ft. along a bearing of 096° from the southern-most tip of Lough Nambrakkeagh.
- BK108 - 1320 ft. along a bearing of 105° from the southern-most tip of Lough Nambrakkeagh.
- BK109 - road cutting, opposite the southern-most tip of Lough Nambrakkeagh.
- BK112 - 550 ft. due south of the southern most tip of Lough Nambrakkeagh.

- BK113 - 790 ft. along a bearing of 155° from the southern-most tip of Lough Nambrakkeagh.
- BK116, BK117, BK118, BK119 - 670 ft. along a bearing of 190° from the western tip of Beaghgivereen Lough.
- BK120 - 2530 ft. along a bearing of 275° from the E in Glenturkan Lough(as written on the Cashel 6-in sheet Co. Galway 51).
- BK121 - 2360 ft. along a bearing of 287° from the E in Glenturkan Lough.
- BK122 - 2800 ft. along a bearing of 271° from the E in Glenturkan Lough.
- BK123 - 2800 ft. along a bearing of 281° from the E in Glenturkan Lough.
- BK124 - 2640 ft. along a bearing of 287° from the E in Glenturkan Lough.
- BK125 - 1210 ft. along a bearing of 202° from the south-western tip of Lough Nambrakkeagh.
- BK133 - 450 ft. around northern shore from the eastern corner of Lough Navreaghoge.
- BK134 - the promontory running out towards the small island in the eastern corner of Lough Navreaghoge.
- BK135 - 495 ft. around the southern shore from the eastern corner of Lough Navreaghoge.
- BK136 - the eastern corner of Lough Navreaghoge.
- BK137 - 530 ft. due west of the southern shore promontory in the western part of Lough Navreaghoge.
- BK138 - 650 ft. due west of the northern-most shore of Lough Navreaghoge.
- BK139 - 630 ft. along a bearing of 290° from the northern-most shore of Lough Navreaghoge.

2. Samples from the Glinsk District.

- BK400 - 993 ft. along a bearing of 277° from the centre of the island in Callerherick Lough.
- BK401 - 1249 ft. along a bearing 263° from the centre of the island in Callerherick Lough.
- BK402 - 2119 ft. along a bearing of 054° from the eastern end of Callerherick Lough.
- BK403 - 594 ft. along a bearing of 032° from the eastern end of Callerherick Lough.

BK404 - 370 ft. along a bearing of 101° from the eastern end of
Callerherick Lough.

BK405 - 190 ft. along a bearing of 066° from the eastern end of
Callerherick Lough.

BK406 - 225 ft. along a bearing of 327° from the eastern end of
Callerherick Lough.

3. Samples from the Shannavara District.

BK407 - 90 ft. along a bearing of 235° from the summit of Shannavara
Hill.

BK408 - 2800 ft. along a bearing of 188° from the southern tip of
Loughaunillaun.

BK409 - 258 ft. along a bearing of 248° from the southern most tip
of Lough Fannanagrau.

BK410, BK411 - north-western corner of shoreline of ruffnaconneelagh
Lough.

BK412, BK413 - the promontory into the north-west sector of Lough
Dwran.